Universitat Politècnica de València
Departamento de Máquinas y Motores Térmicos

Assessment and optimization of the indicated cycle with a 0D thermodynamic model

Doctoral Thesis
Presented by:
Diego Blanco Cavero
Supervised by:
Dr. Jaime Martín Díaz

Valencia, December 2018

DOCTORAL THESIS

Assessment and optimization of the indicated cycle with a 0D thermodynamic model

presented by

DIEGO BLANCO CAVERO

submitted to

DEPARTAMENTO DE MÁQUINAS Y MOTORES TÉRMICOS of the UNIVERSITAT POLITÈCNICA DE VALÈNCIA

in fulfilment of the requirements for the degree of

Doctor of Philosophy

Valencia, December 2018

Doctoral Thesis

Assessment and optimization of the indicated cycle with a 0D thermodynamic model

Presented by: Diego Blanco Cavero
Supervised by: Dr. Jaime Martín Díaz

Examining Board:

President: Prof. Dr. Antonio Torregrosa
Secretary: Prof. Dr. Octavio Armas
Examiner: Dr. Antonio Arpaia

Reviewing Board:

Dr. Antonio Arpaia
Dr. María del Carmen Mata Montes
Dr. Bart Degraeuwe

Valencia, December 2018

Abstract

Issues affecting internal combustion engines, such as pollutant emissions, oil depletion and the raising of alternative powertrains (full electric vehicle), link the future of vehicles powered by this type of powertrain to its improvement in terms of fuel consumption and pollutant emissions. Additionally, the high stringency of the current and upcoming legislation is forcing automotive manufacturers to focus on developing innovative engine strategies aimed to increase the efficiency with low penalty in emissions. A first step to tackle this issue is to focus on the processes occurring in the combustion chamber, which is the core of the engine.

Taking into account this scenario, the main objective of the present work is to assess and optimize the indicated cycle of an internal combustion engine based on a zero-dimensional thermodynamic tool. The coupling of this tool, previously developed in the work group, with a NO_x emissions model and an optimization tool allows evaluating the impact on gross indicated efficiency of several operational limits and real processes taking place in the combustion chamber.

Thus, the first step was the assessment of the indicated efficiency of some ideal cycles in the engines studied in the work. Since the difference between ideal and real cycles is due to the existence of some imperfections, a sensitivity study of these imperfections is carried out to determine the ones with the highest impact on gross indicated efficiency. Later on, the optimum theoretical cycles have been searched for, now taking into account the main phenomena occurring in the cylinder, to get the combustion profile that maximizes the indicated efficiency while keeping some mechanical restrictions and emission limits. In this analysis, the combustion velocity raised as the most important parameter to take into account.

In order to assess some experimental techniques commonly used to enhance the combustion velocity, key parameter as commented, different approaches such as Global Energy Balance, split of losses and the use of design of experiments have been conducted. The conclusions extracted from these analysis have been used to optimize experimentally the combustion law. The comparison between this experimental optimization and the theoretical one provides the impact on gross indicated efficiency of the combustion velocity limitation imposed by the engine hardware. This methodology acts as a benchmarking tool between different hardware architectures, setting the efficiency ceiling of the considered operating point, and thus the maximum gain achievable by implementing an hypothetical perfect hardware.

Resumen

Las amenazas a las que se enfrentan los motores de combustión interna, tales como emisiones contaminantes, agotamiento del petróleo o el auge de otros tipos de motores (vehículo eléctrico), vinculan el futuro de los vehículos propulsados por este tipo de motor a la mejora del mismo en cuanto a consumo de combustible y a emisiones contaminantes se refiere. Adicionalmente, la alta exigencia de la normativa actual y venidera está forzando a las empresas de automoción a centrarse en el desarrollo de estrategias innovadoras dirigidas a aumentar el rendimiento del motor con baja repercusión en emisiones contaminantes. Un primer paso para atajar esta problemática es centrarse en los procesos que ocurren en la cámara de combustión, que es la base del motor.

Teniendo en cuenta este escenario, el objetivo principal del presente trabajo es evaluar y optimizar el ciclo indicado de un motor de combustión interna por medio de una herramienta termodinámica 0D. El acoplamiento de esta herramienta, previamente desarrollada en el grupo de trabajo, con un modelo de emisiones de NO_x y una herramienta de optimización, permite la evaluación del impacto sobre el rendimiento indicado de varios límites operacionales y procesos reales que tienen lugar en la cámara de combustión.

En primer lugar, se ha evaluado el rendimiento indicado de diferentes ciclos ideales en los motores estudiados en el trabajo. Debido a que la diferencia entre ciclos ideales y reales es resultado de la existencia de varias imperfecciones, se ha realizado un estudio de sensibilidad de dichas imperfecciones para determinar cuáles son las que tienen mayor impacto sobre el rendimiento indicado. A continuación, se han buscado los ciclos teóricos óptimos, en este caso ya teniendo en cuenta los principales fenómenos que ocurren en el cilindro, para obtener la ley de combustión que maximiza el rendimiento indicado a la vez que cumple con diferentes restricciones mecánicas y límites de emisiones. En este análisis se concluye que la velocidad de combustión es el parámetro más importante a tener en cuenta.

Con el fin de evaluar algunas técnicas experimentales comúnmente usadas para aumentar la velocidad de combustión, parámetro clave como se ha comentado, se han utilizado diferentes enfoques tales como balances globales de energía, división de pérdidas y diseños de experimentos. Las conclusiones extraídas de dichos análisis han sido usadas para optimizar experimentalmente la ley de combustión. La comparación entre esta optimización experimental y la teórica proporciona el impacto en el rendimiento indicado que supone la limitación en la velocidad de combustión impuesta por el motor analizado. Esta metodología actúa como una herramienta de análisis comparativo entre diferentes arquitecturas del motor, estableciendo el techo de eficiencia bajo las condiciones de operación consideradas, y con ello la ganancia máxima alcanzable por un hipotético motor perfecto.

Resum

Les amenaces a què s'enfronten els motors de combustió interna, com ara emissions contaminants, esgotament del petroli o motors alternatius (vehicle elèctric), vinculen el futur dels vehicles propulsats per aquest tipus de motor a la millora del mateix quant a consum de combustible i a emissions contaminants es refereix. Addicionalment, l'alta exigència de la normativa actual i venidora està forçant a les empreses d'automoció a centrar-se en el desenrotllament d'estratègies innovadores dirigides a augmentar el rendiment del motor amb baixa repercussió en emissions contaminants. Un primer pas per a atallar esta problemàtica és centrar-se en els processos que ocorren en la cambra de combustió, que és la base del motor.

Tenint en compte aquest escenari, l'objectiu principal del present treball és avaluar i optimitzar el cicle indicat d'un motor de combustió interna per mitjà d'una ferramenta termodinàmica 0D. L'adaptament d'esta ferramenta, prèviament desenrotllada en el grup de treball, amb un model d'emissions de NO_x i una ferramenta d'optimització, permet l'avaluació de l'impacte sobre el rendiment indicat d'uns quants límits operacionals i processos reals que tenen lloc en la cambra de combustió.

En primer lloc, s'ha avaluat el rendiment indicat de diferents cicles ideals en els motors estudiats en el treball. Pel fet que la diferència entre cicles ideals i reals és resultat de l'existència de diverses imperfeccions, s'ha realitzat un estudi de sensibilitat de les dites imperfeccions per a determinar quines són les que tenen major impacte sobre el rendiment indicat. A continuació, s'han buscat els cicles teòrics òptims, en aquest cas ja tenint en compte els principals fenòmens que ocorren en el cilindre, per a obtindre la llei de combustió que maximitza el rendiment indicat al mateix temps que compleix amb diferents restriccions mecàniques i límits d'emissions. En aquest anàlisi es conclou que la velocitat de combustió és el paràmetre més important a tindre en compte.

A fi d'avaluar algunes tècniques experimentals comunament usades per a augmentar la velocitat de combustió, paràmetre clau com s'ha comentat, s'han utilitzat diferents enfocaments com ara balanços globals d'energia, divisió de pèrdues i dissenys d'experiments. Les conclusions extretes d'aquest anàlisi han sigut usades per a optimitzar experimentalment la llei de combustió. La comparació entre esta optimització experimental i la teòrica proporciona l'impacte en el rendiment indicat que suposa la limitació en la velocitat de combustió imposada pel motor analitzat. Esta metodologia actua com una ferramenta d'anàlisi comparativa entre diferents arquitectures del motor, establint el sostre d'eficiència davall les condicions d'operació considerades, i amb això el guany màxim abastable per un hipotètic motor perfecte.

A mis abuelos

Agradecimientos

No me gustaría finalizar esta tesis sin agradecer a todas las personas que, de una manera u otra, han contribuido a que haya llegado hasta aquí. En primer lugar me gustaría agradecer al CMT por haberme brindado la oportunidad de realizar esta etapa durante los últimos 4 años. En especial, gracias a tí, Jaime, por confiar en mí desde el primer día (aunque los *"panchos siempre mentimos"*) y guiarme durante este período ayudándome a crecer como investigador y ofreciéndome tu consejo cuando lo necesitaba. Has sido un director magnífico del que he aprendido casi todo lo que sé de motores, pero has sido un mejor amigo aún.

Me gustaría también agradecer a todos los profesores que me han ayudado cuando he acudido a ellos. En especial a Ricardo Novella, por sus consejos y por ser un agitador de ideas (muchas de ellas plasmadas en este trabajo); a Pablo Olmeda, por ayudarme en todas mis consultas y por su amistad fuera del trabajo; y a Antonio García, del que además de sus conocimientos, he aprendido de su practicidad. También quisiera darles las gracias a Javi López, Jose M. García y Jose Manuel Pastor por la ayuda que me han brindado cuando les he planteado alguna consulta.

Muchas gracias también a Norma y Xavi por ayudarme y aguantarme con todas las consultas y desarrollos relacionados con Calmec y SiCiclo. No se me olvida Víctor, que a pesar de no haber compartido trabajo con él, ha pasado demasiadas veces por mi cabeza en estos 4 años. También me gustaría darles las gracias a todas las personas que realizaron su PFC-TFG-TFM conmigo durante estos 4 años. Gracias a Dani Navarro, Carlos, José Luis, Corentin, Juan, César, Sonia, Andreu, Dani Verdú, Paco, José Miguel, Narin, Thomas, Iván, Jose Manuel, Juan Carlos y Julio porque, a pesar de que era yo el que guiaba vuestro trabajo, yo he sido también el que más me he llevado de todos vosotros.

Todo el trabajo experimental que se ve reflejado en esta tesis (y algún otro que no aparece aquí) ha sido posible gracias al trabajo de muchas personas en las salas de ensayo. Gracias a Toni, Marron, Dani y Juanan por su ayuda y compañía durante las largas semanas de medida en sala y gracias también a Sergi y Ali, que no han dudado en ayudarme cuando la electricidad y/o la electrónica no estaban de mi parte.

I would also like to express my most sincere gratitude to GM-Global Propulsion Systems Turin, specially to the advanced engineering group. Thank you for giving me the opportunity to work with you and supporting me during my period in Torino. In particolare, grazie a Fra, Edu, Anto, Andrés e Manuel (spero tu sappia già l'italiano) per il vostro sostegno durante quei 3 mesi e per la vostra amicizia per sempre.

Durante estos 4 años he conocido a mucha gente, pero hay personas que se quedan marcadas. Entre ellas se encuentra el grupo de incógnito, que me acogió recién llegado a Valencia como si de uno más se tratara. Gracias Ricardo, Marcos, Estepa, Vaquerizo y Jordi por todos los momentos y experiencias que vivimos juntos. Otra de esas personas es David, con el que he compartido estos 4 años desde el primer día hasta el último y cuya amistad no quiero perder nunca. También agradezco a Samuel que me engañara para que viviera en su piso porque ese día gané uno de mis mejores amigos.

También me gustaría agradecer a mis amigos de Zamora que llevan en mi vida mucho más que 4 años. Especialmente a Astu y Brezmes por sus visitas y por los viajes de fin de semana donde quiera que estuviéramos en los que tanto nos hemos divertido. ¡El próximo toca Liverpool!

Todo esto no hubiera sido posible sin el apoyo y amor incondicional por parte de mis padres. Todo lo que soy os lo debo a vosotros y nunca os agradeceré lo suficiente todo lo que habéis luchado para que yo llegue hasta aquí. ¡GRACIAS!. También, me gustaría tener un recuerdo especial para mis abuelos, de los que tanto he aprendido a pesar de que a alguno no lo conocí, algunos no pudieron llegar hasta aquí y alguna está mas fuerte que nunca. Espero que estéis la mitad de orgullosos de mí de lo que yo estoy de vosotros. No me puedo olvidar tampoco de mi tío José María, luchador incansable que ha dejado una huella imborrable en mí.

Finalmente, gracias a mi compañera de viaje desde hace 7 años, Belén. Gracias por tu amor, tus ánimos, tu comprensión y todo el apoyo que me has dado en esta etapa. Tú me has dado alas para llegar hasta aquí, me has puesto los pies en el suelo cuando lo necesitaba y has hecho que este camino de 4 años haya sido mucho más llevadero. Por suerte, nos queda toda una vida juntos por delante para seguir agradeciéndote.

A todos vosotros, gracias.

Funding acknowledgments

Diego Blanco Cavero has been partially supported through contract FPI-S2-2016-1356 of "Programa de Apoyo para la Investigación y Desarrollo (PAID)" of Universitat Politècnica de València. The support of GM Global R&D and the Spanish Ministry of Economy and Competitiveness through projects TRA2013-41348-R and TRA2017-89894-R is also greatly acknowledged.

¿Cómo podemos conocer los límites
si no tratamos de sobrepasarlos?
Gilles Villeneuve

Table of Contents

Index of Figures

Index of Tables

Nomenclature

$CA50$	Crank angle in which 50% of the total fuel is burnt
c_v	Heat capacity at constant volume
m	Mass
n	Engine speed
N	Engine load
p	Pressure
Q	Heat transfer to engine walls
R	Universal gas constant
R^2	Coefficient of determination
T	Temperature
V	Combustion chamber volume

Subscripts

0	Motoring conditions
bb	Referred to blow-by
def	Referred to deformation model
f	Referred to fuel
IVC	At Intake Valve Closing
ref	Reference conditions
TDC	At Top Dead Centre

Initials and acronyms

AFR	Air to Fuel Ratio
$ATDC$	After Top Dead Centre
BDC	Bottom Dead Centre
$BSFC$	Brake Specific Fuel Consumption
$BTDC$	Before Top Dead Centre

BTE	Brake Thermal Efficiency
CAD	Crank Angle Degree
CDC	Conventional Diesel Combustion
CFD	Computational Fluid Dynamics
CGC	Conventional Gasoline Combustion
CI	Compression Ignition
CR	Compression Ratio
DI	Direct Injection
DOC	Diesel Oxidation Catalyst
DoE	Design of Experiments
DPF	Diesel Particulate Filter
ECU	Electronic Control Unit
EOC	End Of Combustion
EV	Full Electric Vehicle
EVO	Exhaust Valve Opening
EGR	Exhaust Gas Recirculation
GA	Genetic algorithm
GDI	Gasoline Direct Injection
GEB	Global Energy Balance
GIE	Gross Indicated Efficiency
GPF	Gasoline Particulate Filter
HEV	Hybrid Electric Vehicle
HC	Hydrocarbon
$HCCI$	Homogeneous Charge Compression Ignition
HRL	Cumulative Heat Release Law
HRR	Heat Release Rate
$HSDI$	High Speed Direct Injection
HT	Heat Transfer
ICE	Internal Combustion Engine
IEA	International Energy Agency
IGR	Internal Gas Recirculation
$ISFC$	Indicated Specific Fuel Consumption
IVC	Intake Valve Closing
IVO	Intake Valve Opening

LNT	Lean NO_x Trap
LTC	Low Temperature Combustion
$NEDC$	New European Driving Cycle
OEM	Original Equipment Manufacturer
$PCCI$	Premixed Charge Compression Ignition
$PEMS$	Portable Emissions Measurement System
$PHEV$	Plug-in Hybrid Electric Vehicle
PM	Particulate Matter
PP	Peak Pressure
PPC	Partially Premixed Combustion
PRR	Pressure Rise Rate
$RCCI$	Reactivity Controlled Compression Ignited
SCR	Selective Catalytic Reduction
SI	Spark Ignition
SOC	Start Of Combustion
SOE	Start Of Energizing time
SOI	Start Of Injection
SR	Swirl Ratio
TBC	Thermal Barrier Coating
TDC	Top Dead Centre
VVT	Variable Valve Timing
$WLTP$	Worldwide harmonized Light-duty vehicles Test Procedure

Chapter 1

Introduction

Contents

1.1 Background

Reciprocating Internal Combustion Engines (ICEs) are by far the most used powertrains in the transportation sector. The amount of vehicles using this technology has been continuously increasing since its invention and, even though nowadays they are in their worst days in terms of popularity and public acceptance, they continue being the main powertrains and it is likely to remain so in the foreseeable future [1]. As an example, Figure 1.1 shows the transportation sector energy consumption in USA in 2018 in percentage. As can be observed, both gasoline and Diesel powered vehicles represent around 84% of the total energy consumption by transports in USA and only jet fuel, used in gas turbines for air transport, has also an important market share (10%), while electric motors only represent 0.1%. Additionally, ICEs are also used, although to a lesser extent, for backup power and for providing electricity to areas not connected to an electrical grid.

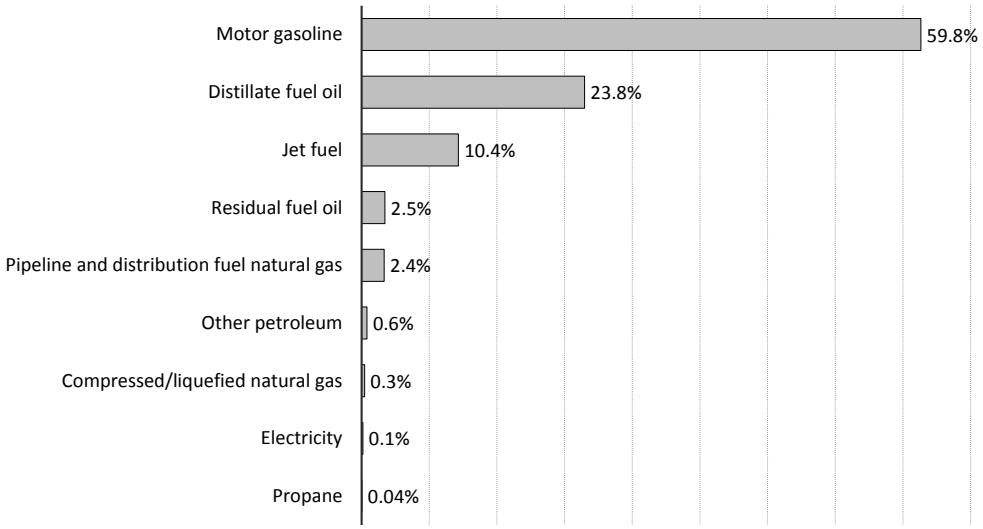

Figure 1.1. *U.S. transportation sector energy consumption in 2018, by energy source. Source: [2].*

However, despite its undeniable contribution to the economic progress, there have always been 2 principal issues concerning this type of powertrains:

1. ICEs convert chemical energy to mechanical energy through a combustion process that produces different types of pollutant emissions. On the one hand, CO_2 emissions are directly related to the quantity and type of fuel burned. As known, CO_2 is a green house gas that contributes to the global warming. Additionally, there are other pollutant emissions, importance of which depends on the combustion mode. Main issues of Compression Ignition (CI) engines are NO_x and Particulate Matter (PM) emissions, while Spark Ignition (SI) engines have major problems with CO and HC emissions [3], although NO_x and PM are becoming also important due to the new technologies implemented in these engines. These pollutants have harmful effects on human health [4–6] and this problem is even more important in cities, where the high density of vehicles propelled by ICEs causes dangerous concentrations of these pollutant emissions.

2. As commented, fossil fuels are the main source of energy for ICE. The problem is that, as pointed out by some authors [7], global oil peak

production has already been reached and, even though there is still oil for several decades, its price will start to rise soon. Around 100 oil fields produce half of the global production of crude oil and most of them are well past their peak of production and the rest will begin to decline soon [8]. According to the IEA oil production forecast in 2014 shown in Figure 1.2, weight of oil production beyond 2020 will shift from producing fields to fields that are not still fully developed or that have not even been found [9]. In these new fields, more aggressive extraction methods for the environment are used (for example *fracking*[1] [10–12] or *tar sands*[2] [13, 14]). Such harmful methods have deep environmental impacts ranging from the potential to cause earthquakes to the contamination of water supplies.

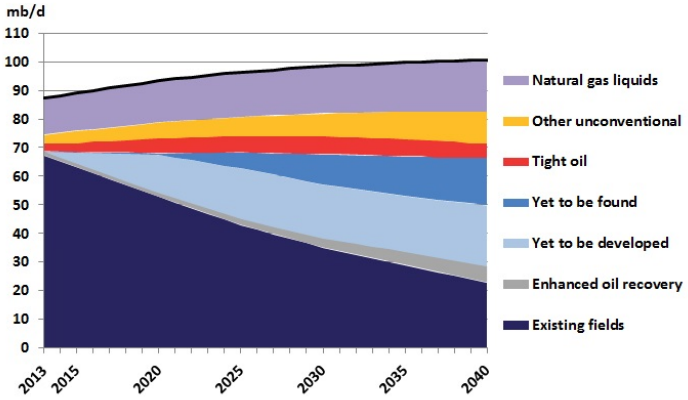

Figure 1.2. *IEA forecast of global all-oil production to 2040. Source: [9].*

Apart from these two main problems, recently, full Electric Vehicles (EV) are also becoming a concern affecting the future of ICE due to their zero local emissions, low noise and, so far, low operating cost. Nonetheless, they still present important challenges [15], such as limited operating range, higher cost than conventional vehicles, battery pack replacement cost, battery pack life and long recharging time. Furthermore, the existent electric infrastructure would not be able to cope with the demand if an important percentage of the vehicle fleet were electric, and the upgrading of this infrastructure would be costly in terms of money and time. Therefore, rather than a

[1] *Fracking* consists on the hydraulic fracturing of rocks by means of a pressurized liquid.
[2] *Tar sands* are a mixture of mostly sand, clay, water, and a thick, molasses-like substance called bitumen.

threat, electrification should be considered as an opportunity to improve ICE performance by means of hybridization. Several approaches from a low grade of hybridization (48V systems [16, 17] or mild hybrid systems [18, 19]) up to a more aggressive scenario (full hybrid (HEV) [20, 21] or Plug-in Hybrid Electric Vehicles (PHEV) [22, 23]) could be adopted taking advantage of the benefits provided by both technologies.

All these challenges link the ICE's future to its improvement in terms of consumption and pollutant emissions. In fact, different legislations have been introduced during past years to force automotive Original Equipment Manufacturers (OEMs) to cut down their engines' emissions. The USA and Europe were the first ones to adopt this kind of legislation with *Tier* and *Euro* directives in 1987 and 1992 respectively. Later on, Japan, China, India and Brazil have also applied their own legislation to tackle the exhaust emissions issue.

From their introduction on, these legislations have evolved imposing increasingly restrictive limits to different pollutant species and trying to reflect driving conditions taking place in a real vehicle. Figure 1.3 shows the evolution of the European norms and limits for Diesel cars from Euro 1 to Euro 6. There, it can be seen that the NO_x limit has been reduced about 84%, PM about 96% and HC and CO more than 80% with respect to Euro 1 limits.

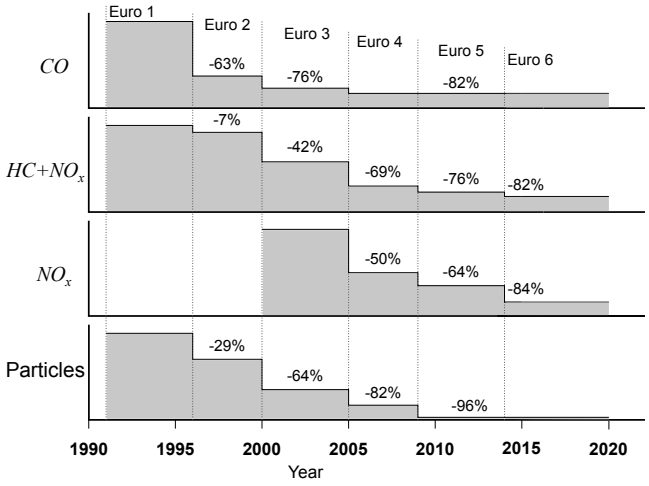

Figure 1.3. *Euro normative evolution.*

In 2015, the dieselgate scandal [24] damaged the reputation of ICE, particularly the Diesel one, putting the spotlight on the procedure used

to measure these emissions. From Euro 1 to Euro 6c, the New European Driving Cycle (NEDC) was the chosen procedure to check ICE pollutant emissions. This driving cycle has been severely criticized for not being representative of real-world vehicle operation [25–27]. On board tests using Portable Emissions Measurement Systems (PEMS) have shown that ICE powered cars, in particular Diesel, emitted much more NO_x [28] and consumed more fuel [25, 26, 29] on the road than during type approval on the NEDC in the lab. However, some authors [30] have recently pointed out that emissions certification with the NEDC might be robust and future legislation may likewise only be robust if backed by in-use conformity testing and comprehensive market surveillance.

To tackle this issue, the certification cycle has been substituted in Euro 6d TEMP (2017) by the Worldwide harmonized Light vehicles Test Procedure (WLTP). The WLTP cycle reaches higher speeds (131.3 km/h instead of 120 km/h), has stronger acceleration and there are fewer stop phases than in the NEDC (12.6% vs 23.7%) [31]. In a further step, an on road test, the Real Driving Emissions (RDE) procedure, will be introduced from 2019 onwards. This procedure, unlike NEDC and WLTP, assesses NO_x, PM and CO emissions on board using special testing equipment and following certain trip requirements [32], making this procedure much more realistic than the previous ones. Besides, this new procedure also introduces the novelty that independent organizations will be allowed to test the compliance of any vehicle during its whole service life.

This increasing stringent of the emissions limits along with the new procedures to certificate them have pushed OEMs during the past two decades to work hard in order to cut down pollutant emissions. In the beginning, just active techniques oriented to limit their formation during the combustion process were investigated. But now this is not enough, leading to the generalization of additional equipment to mitigate these emissions. These aftertreatment systems range from Lean NO_x trap (LNT) and Selective Catalytic Reactor (SCR) for NO_x emissions; particulate filters (DPF or GPF) to trap particulates; and catalytic converters to reduce HC and CO (DOC in CI engines) and also NO_x (3-way catalyst in SI engines). Such systems are very efficient in cutting down pollutant emissions but they imply a penalty on fuel consumption due to the gas flow restriction through the exhaust, which increases the pumping work. In addition, some of these systems often require regeneration processes that are achieved through inefficient post injection strategies.

Therefore, since the reduction of NO_x, CO, HC and PM emissions are mainly entrusted to aftertreatment systems, CO_2 emissions, directly related to fuel consumption, have become the key topic. Additionally, according to upcoming EU legislation [33], the fleet average CO_2 emissions of every OEM will be limited to 95 grams of CO_2 per kilometre in 2020, which means a fuel consumption of around 3.6l/100km for a Diesel car and represents a reduction of 27% in comparison with 2015 target. These reasons along with the decrease of fossil fuel storages commented above, have led researchers to focus on developing innovative engine strategies aimed to increase the efficiency with low penalty in emissions.

Regarding this point, it is interesting to take into account that, according to Helmers *et al.* [29], there has not been climate benefit in the European Union in terms of CO_2 equivalent emissions (CO_2 and black carbon) between 1995 and 2015. Even though during that period there was an improvement in the vehicles fuel consumption, this was not translated into a reduction of the equivalent CO_2 emissions due to a combination of increased annual vehicle registrations and a stagnation in real-world CO_2 emission values for all types of vehicles. However, rather than deterrent, these are incentive factors to further improve the ICE efficiency to achieve a significant reduction in their CO_2 equivalent emissions.

An important issue to address the future research lines intended to reduce fuel consumption of ICE is to know what the most important sources of losses are. With this aim, Figure 1.4 shows a schema in which several indicated cycles are plotted starting from the chemical energy of the fuel (1^{st} level) up to the mechanical energy available at the crankshaft (7^{th} level). Starting from the total amount of energy available in the fuel, the first step is the application of a thermodynamic cycle in order to transform part of this energy into useful work. The ideal cycle with the highest indicated efficiency is the Carnot cycle (2^{nd} level), however, since this cycle is not suitable for ICE operation, the Otto cycle (3^{rd} level), also known as constant volume cycle, raises as the highest efficiency ideal cycle with processes close to an ICE operation (with some differences, of course). Ideal cycles make some assumptions that lead to higher indicated efficiencies than the achievable ones under realistic conditions. Thus, there are some efficiency losses that separate the optimum real cycle (6^{th} level) from the Otto cycle. In order to evaluate the efficiency reduction between these two extremes, it is interesting to consider two intermediate cycles:

- Optimum theoretical cycle (4^{th} level): even though no technical limitation is yet considered (mechanical resistance, emissions or the real injection system), there are some other efficiency losses related to the

non ideal combustion development, heat transfer, working with ideal instead of perfect gas, blow-by leakages and the shortening of the closed cycle when delaying the intake and/or advancing the exhaust processes. Taking into account these efficiency losses, this is the theoretical cycle with the maximum efficiency Heat Release Law (HRL).

- Optimum theoretical constrained cycle (5^{th} level): this cycle takes into account some pressure limits, intended to keep the engine integrity, and some emissions concerns, aimed to meet the applicable legislation, that have a certain impact on indicated efficiency. Thus, after considering these restrictions, the optimum constrained cycle still with a theoretical combustion that maximizes the indicated efficiency, is obtained. As commented, this cycle is still theoretical and therefore it is far from real cycles taking place in the engine, specially regarding its combustion velocity.

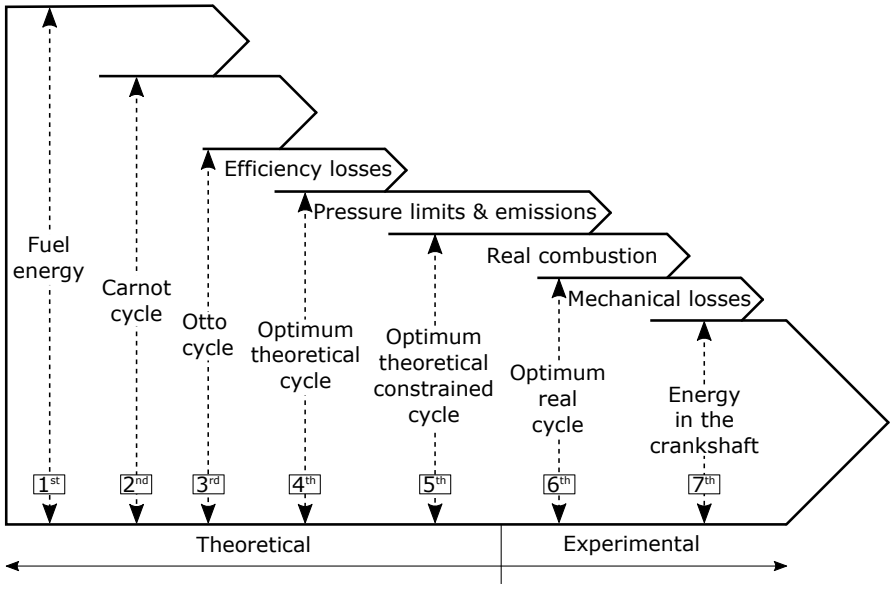

Figure 1.4. *Maximum efficiency cycles from fuel energy to crank energy.*

The following step is the cycle taking place in a real engine (6^{th} level), which differs from the optimum theoretical constrained one in the limited combustion velocity imposed by the existent engine hardware. Finally, the last step is aimed to transfer this energy available in the combustion chamber to the crankshaft (7^{th} level), with the consequent mechanical losses.

Taking into account this energy degradation, this work is focused on the analysis of the impact on Gross Indicated Efficiency (GIE) of the different efficiency losses stated in the upper part of Figure 1.4 starting from the Otto cycle up to the real indicated cycle (6^{th} level). Even though fuel consumption optimization would require to go further up to the energy available at the crankshaft, this work only deals with the indicated cycle because it is considered that any optimization of this cycle will also have a positive effect on fuel consumption. To analyse the efficiency degradation presented in the figure, a combination of different analysis based on a 0D thermodynamic model is used in this work.

Additionally, pollutant emissions are also considered by coupling a predictive NO_x model to the thermodynamic model. Although there are more pollutants than NO_x, it is considered that, unlike other pollutants (out of the scope), its formation mechanisms are well known and thus, predicting its emissions accurately is a feasible task with a 0D model. The combination of the thermodynamic and NO_x model will make the assessment of the indicated cycles with the highest efficiency as well as the most important sources of efficiency losses possible.

Firstly, the indicated efficiency of some ideal cycles, including Carnot and Otto cycles, is assessed in the engines presented in Section 3.2. Then, a sensitivity study, in which all efficiency losses commented are evaluated to determine the ones with the highest impact on GIE, is carried out. Later on, the optimum cycles under constrained and non constrained conditions presented in the 4^{th} and 5^{th} levels of Figure 1.4 are searched for. In this step, all processes occurring in the combustion chamber are taking into account. Similarly, some studies [34–36], that evaluated the optimum shape of the HRL imposing several constraints to pressure and NO_x emissions, were already carried out. However, these works used simple 0D models that did not take into account important phenomena such as the heat capacity ratio change due to temperature and composition variations, deformations (volume change), injected fuel mass and blow-by leakages (Eriksson *et al.* [34, 35] do consider mass trapped in the crevice volume). Skipping these processes has an effect on the determination of the optimum shape of HRL and it is important when assessing the efficiency of the cycle.

In this work an optimization tool based on genetic algorithms has been coupled to an in-house developed 0D model to obtain the optimum combustion law. This model takes into account all phenomena involved in the combustion process, thus allowing to obtain the optimum HRL along with the cycle efficiency under different constrained conditions. This approach is used at

different operating conditions to get the combustion profile that maximizes the indicated efficiency while keeping some mechanical and performing restrictions, such as maximum peak pressure, maximum pressure rise rate and NO_x emissions limits. In this analysis, the combustion velocity rises as the most important parameter to take into account when optimizing the indicated cycle.

Then, different approaches such as Global Energy Balance [37, 38], split of losses [39, 40] and the use of design of experiments are conducted in order to assess some experimental techniques (swirl and injection pattern) commonly used to enhance the combustion velocity (key parameter as commented). After that, some operating conditions are optimized experimentally using the conclusions extracted from previous analysis. The last step of the work is the comparison of optimum HRLs derived from this experimental optimization with the best ones obtained theoretically. Differences in these 2 approaches should be mainly attributed to the combustion velocity limit derived from the use of a certain hardware. This comparison is useful as a tool to perform a benchmarking between different hardware architectures.

1.2 Previous works

The works presented in this doctoral thesis have made use of a thermodynamic model along with some sub-models and methodologies developed in previous theses. Following, the timeline of these works and a brief description of their main subject is presented:

- 1986: Tinaut [41] established the basis of the 0D thermodynamic model used to perform the combustion diagnosis of Direct Injection (DI) Diesel engines.

- 1998: Armas [42] implemented the combustion diagnosis model (Calmec) including several sub-models necessary to accurately determine the heat release. This thesis presented a comprehensive sensitivity analysis of different terms involved in the combustion diagnosis and a methodology for adjusting the uncertainties of the approach.

- 2007: Degraeuwe [43] developed a lumped conductance model for DI Diesel engines, which was able to determine the specific heat rejection to different engine components and sub-systems (i.e. cooling and lubricating).

- 2007: Martín [44] updated the model proposed by Armas [42] by improving some models such as the heat transfer and the filling and emptying ones. This work set the basis for a general engine thermal characterization, including information of the complete cycle. Furthermore, he upgraded the predictive approach of the 0D model (SiCiclo).
- 2016: Carreño [45] presented a comprehensive methodology to perform and analyse the energy repartition in an ICE. This work deals with the improvement and calibration of several sub-models presented in previous works and with the development and application of Global Energy Balances in ICE.

These works established the basis for an integral engine thermal characterization aimed at performing either an accurate combustion diagnosis (Calmec) or an in-cylinder predictive approach (SiCiclo). The present thesis is not intended to improve the thermodynamic model, but it takes advantage of the potential of both tools.

1.3 Objectives

The main objective of this work is **to assess and optimize the indicated cycle of an ICE**. To comply with the main objective, some particular objectives have to be satisfied:

1. *To identify and assess the efficiency losses affecting a real cycle, unlike an ideal one.* Using this approach, allows to point out the main responsible for the efficiency loss experimented by a real cycle compared to an ideal one.
2. *To determine the efficiency boundaries of an ICE restricted to different operational limits.* Given a certain architecture and operating conditions, this approach provides the optimum HRL along with its respective efficiency under different operational limits such as maximum peak pressure, maximum pressure rise rate or NO_x emissions.
3. *To evaluate various techniques to enhance combustion velocity.* Being the combustion velocity the main issue controlling engine efficiency and emissions, two approaches used to enhance it are assessed (swirl and injection settings). Conclusions extracted from this analysis will be used to optimize experimentally some operating conditions.

4. *To assess the impact on GIE of the real combustion velocity, limited by the engine hardware.* The theoretical optimization will act as a benchmark when comparing with the experimental one obtained using a certain hardware.

The fulfilment of all these objectives will lead to the complete identification and assessment of efficiency losses derived from both operational limits and hardware performance. To achieve these objectives, the methodology explained below will be applied.

1.4 Methodology

The methodology followed to achieve the objectives is shown in Figure 1.5 and explained in the next paragraphs.

Chapter 2 deals with the literature survey of strategies aimed to optimize the indicated cycle along with the most common methodologies carried out to analyse them. In this sense, a comprehensive review of the state of the art engine research is performed to understand the current situation of ICE.

Chapter 3 explains thoroughly both the experimental installations and the theoretical models used in this work, including:

- Details of the instrumentation required to perform the experimental work.
- A description of the thermodynamic and NO_x models and the optimization tool as well as their specific calibration and validation.

In **Chapter 4**, starting from the assessment of the main ideal cycles in the studied engines, efficiency losses taking place in a real ICE are evaluated separately. Then, the optimum cycle taking into account several operational limits inherent to ICE operation (maximum in-cylinder pressure, maximum pressure rise rate and NO_x emissions) is searched for at different operating conditions covering the whole operating map of a DI Diesel engine.

In **Chapter 5**, a study to characterize two techniques (swirl and injection strategy) used to experimentally improve the combustion velocity is carried on. After that, two different experimental points are optimized using conclusions extracted in this study. Finally, both modelled and experimental optimums are compared to obtain the impact of the real combustion process on indicated efficiency.

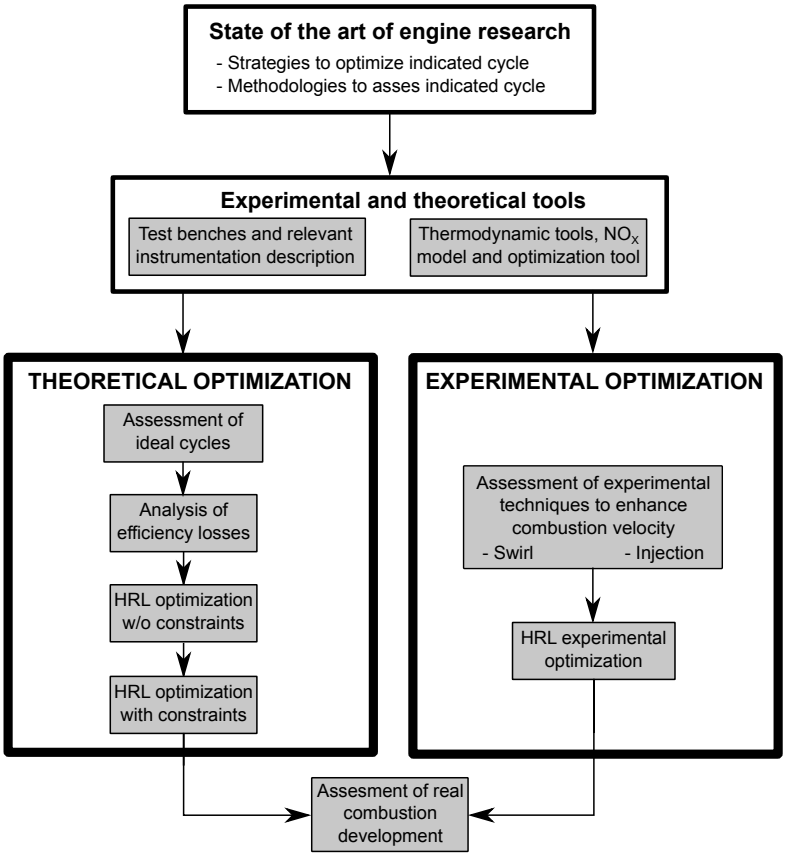

Figure 1.5. *Thesis methodology.*

Finally, the main conclusions extracted from the works presented in the work is collected in **Chapter 6**. Additionally, some interesting future works are discussed in this section.

For convenience, besides each chapter bibliography, at the end of this document all the references cited are organized in alphabetic order, indicating the pages where they are cited.

Bibliography

[1] Kalghatgi G. "The outlook for fuels for internal combustion engines". *International Journal of Engine Research*, Vol. 15 n^o 4, pp. 383–398, 2014.

[2] US Energy Information Administration. "U.S. transportation sector energy consumption in 2018, by energy source". *Statista - The Statistics Portal, Statista*, 2018.

[3] Heywood J.B. *Internal Combustion Engines Fundamentals*. McGraw-Hill, ISBN 978-0-07-028637-5, New York, 1988.

[4] Health Effects Institute. "Diesel Exhaust: A Critical Analysis of Emissions, Exposure, and Health Effects". *A Special Report of the Institute's Diesel Working Group*, 1995.

[5] Pope C. and Dockery D. "Health Effects of Fine Particulate Air Pollution: Lines that Connect". *Journal of the Air & Waste Management Association*, Vol. 56 n^o 6, pp. 709–742, 2006.

[6] Oberdörster G. and Utell M.J. "Ultrafine particles in the urban air: to the respiratory tract–and beyond?". *Environmental health perspectives*, Vol. 110 n^o 8, pp. A440–A441, 2002.

[7] Chapman I. "The end of Peak Oil? Why this topic is still relevant despite recent denials". *Energy Policy*, Vol. 64, pp. 93–101, 2014.

[8] Sorrell S., Speirs J., Bentley R., Miller R. and Thompson E. "Shaping the global oil peak: A review of the evidence on field sizes, reserve growth, decline rates and depletion rates". *Energy*, Vol. 37 n^o 1, pp. 709–724, 2012.

[9] IEA. *World Energy Outlook 2008*. International Energy Agency, Paris, France, 2014.

[10] United Nation Environment Programe (UNEP), Global Environmental Alert Service (GEAS). "Gas fracking: can we safely squeeze the rocks?". *Environmental Development*, Vol. 6, pp. 86–99, apr 2013.

[11] Davies R., Foulger G., Bindley A. and Styles P. "Induced seismicity and hydraulic fracturing for the recovery of hydrocarbons". *Marine and Petroleum Geology*, Vol. 45, pp. 171–185, aug 2013.

[12] Goodman P., Galatioto F., Thorpe N., Namdeo A., Davies R. and Bird R. "Investigating the traffic-related environmental impacts of hydraulic-fracturing (fracking) operations.". *Environment international*, Vol. 89, pp. 248–260, feb 2016.

[13] Nikiforuk A. *Tar sands: Dirty oil and the future of a continent*. Greystone Books Ltd, Barcelona, 2010.

[14] Westman C. "Social Impact Assessment and the Anthropology of the Future in Canada's Tar Sands". *Human Organization*, Vol. 72 n^o 2, pp. 111–120, 2013.

[15] Rajashekara K. "Present status and future trends in electric vehicle propulsion technologies". *IEEE Journal of Emerging and Selected Topics in Power Electronics*, Vol. 1 n^o 1, pp. 3–10, 2013.

[16] Milton G., Blore P., Tufail K., Coates B., Newbigging I., Cooper A. and Shayler P. "CO2 reduction through low cost electrification of the diesel powertrain at 48V". *SAE Technical Paper Series*, 2017.

[17] Timmann M., Inderka R. and Eder T. "Development of 48V powertrain systems at Mercedes-Benz". In *Internationales Stuttgarter Symposium. Proceedings. Springer Vieweg, Wiesbaden*, 2018.

[18] Bao R., Avila V. and Baxter J. "Effect of 48 V Mild Hybrid System Layout on Powertrain System Efficiency and Its Potential of Fuel Economy Improvement". *WCX 17: SAE World Congress Experience*, mar 2017.

[19] Yoon K., Hong J. and Shim J. "A Study on Front End Auxiliary Drive (FEAD) System of 48V Mild Hybrid Engine". *WCX World Congress Experience*, apr 2018.

[20] Nitz L. "General Motors' Innovative Hybrid and T̈wo-Mode HybridS̈ystems". *2006 FISITA World Automotive Congress*, oct 2006.

[21] Fontaras G., Pistikopoulos P. and Samaras Z. "Experimental evaluation of hybrid vehicle fuel economy and pollutant emissions over real-world simulation driving cycles". *Atmospheric Environment*, Vol. 42 n^o 18, pp. 4023–4035, 2008.

[22] Elgowainy A., Burnham A., Wang M., Molburg J. and Rousseau A. "Well-To-Wheels Energy Use and Greenhouse Gas Emissions of Plug-in Hybrid Electric Vehicles". *SAE International Journal of Fuels and Lubricants*, Vol. 2 n^o 1, pp. 627–644, apr 2009.

[23] Lin Z. "Optimizing and Diversifying the Electric Range of Plug-in Hybrid Electric Vehicles for U.S. Drivers". *SAE International Journal of Alternative Powertrains*, Vol. 1 n^o 1, pp. 180–194, apr 2012.

[24] Schmidt C. "Beyond a One-Time Scandal. Europe's Ongoing Diesel Pollution Problem". *Environmental Health Perspectives*, Vol. 124 n^o 1, pp. 19–22, 2016.

[25] Dings J. "Mind the gap! Why official car fuel enconomy figures don't match up reality". *Transport and Environment*, pp. 1–47, 2013.

[26] Mock P., German J., Bandivadekar A., Riemersma I., Ligterink N. and Lambrecht U. "From laboratory to road. A comparison of official and real-world fuel consumption and CO2 values for cars in Europe and the United States". *International Council on Clean Transportation*, n^o May, pp. 77, 2013.

[27] Marotta A., Pavlovic J., Ciuffo B., Serra S. and Fontaras G. "Gaseous Emissions from Light-Duty Vehicles: Moving from NEDC to the New WLTP Test Procedure". *Environmental Science and Technology*, Vol. 49 n^o 14, pp. 8315–8322, 2015.

[28] Giakoumis E. and Zachiotis A. "Investigation of a Diesel-Engined Vehicle's Performance and Emissions during the WLTC Driving Cycle - Comparison with the NEDC". *Energies*, 2017.

[29] Helmers E., Leitão J., Tietge U. and Butler T. "CO_2 -equivalent emissions from European passenger vehicles in the years 1995 - 2015 based on real-world use : Assessing the climate benefit of the European "diesel boom ", url = https://doi.org/10.1016/j.atmosenv.2018.10.039, volume = 198, year = 2019". *Atmospheric Environment*, n^o October 2018, pp. 122–132.

[30] Degraeuwe B. and Weiss M. "Does the New European Driving Cycle (NEDC) really fail to capture the NOX emissions of diesel cars in Europe?". *Environmental Pollution*, Vol. 222 n^o X, pp. 234–241, 2017.

[31] Mock P., Kühlwein J., Tietge U., Franco V., Bandivadekar A. and German J. "The WLTP: How a new test procedure for cars will affect fuel consumption values in the EU". *ICCT White Paper*, Vol. 1 n^o 9, pp. 1–20, 2014.

[32] European Parliament. "Commission regulation (EU) No 64/2012 of 23 January 2012 amending Regulation (EU) No 582/2011 implementing and amending Regulation (EC) No 595/2009 of the European Parliament and of the Council with respect to emissions from heavy duty vehicles (Euro". *Official Journal of the European Union*, pp. 1–23, 2012.

[33] European Parliament. "Commision regulation (EU) No 333/2014 OF the European Parliament and of the Council of 11 March 2014 amending Regulation (EC) No 443/2009 to define the modalities for reaching the 2020 target to reduce CO2 emissions from new passenger cars". *Official Journal of the European Union*, Vol. 103 n^o 333, pp. 15–21, 2014.

[34] Eriksson L. and Sivertsson M. "Computing Optimal Heat Release Rates in Combustion Engines". *SAE International Journal of Engines*, Vol. 8 n^o 3, pp. 2015–01–0882, 2015.

[35] Eriksson L. and Sivertsson M. "Calculation of Optimal Heat Release Rates under Constrained Conditions". *SAE Int. J. Engines*, 2016.

[36] Guardiola C., Climent H., Pla B. and Reig A. "Optimal Control as a method for Diesel engine efficiency assessment including pressure and NOx constraints". *Applied Thermal Engineering*, Vol. 117, pp. 452–461, 2017.

[37] Payri F., Olmeda P., Martín J. and Carreño R. "A New Tool to Perform Global Energy Balances in DI Diesel Engines". *SAE Int. J. Engines*, Vol. 7 n^o 1, pp. 43–59, 2014.

[38] Benajes J., Olmeda P., Martín J., Blanco-Cavero D. and Warey A. "Evaluation of swirl effect on the Global Energy Balance of a HSDI Diesel engine". *Energy*, Vol. 122, pp. 168–181, 2017.

[39] Weberbauer F., Rauscher M., Kulzer A., Knopf M. and Bargende M. "Generally applicate split of losses for new combustion concepts". *MTZ worldwide*, Vol. 66 n^o 2, pp. 17–19, 2005.

[40] Thirouard M., Knop V. and Pacaud P. "Downsizing or cylinder number reduction in Diesel engines : effect of unit displacement on efficiency and emissions". In *THIESEL 2012 Conference on Thermo- and Fluid Dynamic Processes in Diesel Engines*, pp. 1–19, 2012.

[41] Tinaut F. *Contribución al estudio del proceso de combustión en motores de encendido por compresión de inyección directa.* Doctoral Thesis, Universidad Politécnica de Valencia, 1986.

[42] Armas O. *Diagnóstico experimental del proceso de combustión en motores Diesel de inyección directa.* Servicio de Publicaciones UPV, ISBN 84-7721-772-X, Valencia, 1999.

[43] Degraeuwe B. *Contribution to the thermal management of DI Diesel engines.* Doctoral Thesis, Universidad Politécnica de Valencia, 2007.

[44] Martín J. *Diagnóstico de la combustión en motores de Diesel de inyección directa.* Reverté, ISBN 978-84-291-4717-9, Barcelona, 2012.

[45] Carreño R. *A comprehensive methodology to analyse the Global Energy Balance in Reciprocating Internal Combustion Engines.* Doctoral Thesis, 2016.

Chapter 2

Techniques to assess and optimize the indicated cycle

Contents

2.1 Introduction

Since ICE invention, researchers' efforts have been addressed to improve its performance from different points of view. In its early days, the focus was only on increasing its power due to its low development. Then, once reasonable

power levels were reached, the next step was to improve its fuel economy. Later on, the introduction of new legislation put the spotlight on pollutant emissions reduction. In fact, during the last years the importance of these 2 issues has clearly shifted leading to the current situation where pollutant emissions are the key issue when designing an engine. However, this situation is nearly to change due to the upcoming legislation where, as commented in Chapter 1, CO_2 emissions will have to be reduced by 27% by 2020 compared to 2015 legislation [1].

Taking into account the current and future scenarios, nowadays the improvement of the engine performance involves both fuel economy and pollutant emissions issues. As commented in Section 1.1, even though the improvement of fuel consumption would require to analyse the brake efficiency, since this work is intended to provide a better understanding of the processes inside the combustion chamber, the focus is on the assessment and optimization of the indicated cycle. In any case, any improvement of the indicated cycle is transferred into a gain on brake efficiency, and thus on fuel consumption. Additionally, the present work also takes into account the pollutant emissions issue by considering NO_x emissions when optimizing the indicated cycle.

In this chapter, a comprehensive review of the state of the art research regarding the assessment and optimization of the indicated cycle of ICE is carried out in two different parts. In the first part of the chapter, the most common technologies and strategies used nowadays to improve the indicated cycle of an ICE along with new approaches currently under investigation are outlined. Afterwards, some methodologies followed to assess and optimize the impact of all these strategies on indicated efficiency or the potential of a certain ICE architecture, are presented in the second part of the chapter.

2.2 Strategies to optimize the indicated cycle

This section collects the most common strategies used nowadays in the state of the art ICEs, along with new ideas that are under investigation, to optimize the indicated cycle of an ICE. For the sake of clarity and according to their importance level, they are grouped in two main topics, depending on the efficiency loss over which they have a direct impact: combustion development and heat transfer.

2.2.1 Combustion development

As it will be shown along the work, combustion development is one of the most important limitations when optimizing the indicated cycle of an ICE. Thus, this section presents the state of the art research focusing on the main contributors to the combustion development performance, namely: fuel injection and air management.

2.2.1.1 Fuel injection

Fuel injection is the controlling factor of combustion in CI engines and it is also gaining importance in SI engines due to the use of direct injection. Therefore, it is important to investigate all possible techniques that could lead to an improvement of the indicated cycle by varying the fuel injection strategy. Thus, an experimental investigation of the effects of varying the injection settings of a CI engine has been carried out in Section 5.2.2. Before that, in this section the most common strategies, dealing with fuel injection, used to optimize the indicated efficiency and emissions trade-off are going to be briefly described.

Increasing the injection pressure improves the spray mixing properties, important in CI engines to determine the fuel-air mixing rate and the air utilization [2]. Nowadays, the highest injection pressure used in production Diesel engines reaches 2500 bar, although the benefits of increasing it over 3000 bar have been also evaluated [3, 4]. Increasing the injection pressure leads to a quicker delivery of the same fuel quantity that also implies a faster combustion, with a subsequent increase in the indicated and brake efficiencies along with a reduction in the PM formation [5]. However, the drawback is that this faster combustion enhances the NO_x formation [6] due to the increase of the gas temperature. Additionally, increasing the injection pressure means an increment of the power required by the injection pump leading to a penalty on Brake Specific Fuel Consumption (BSFC) [7]. SI engines equipped with DI systems are increasing also this injection pressure although its maximum pressure is usually lower than 10% of the previously described in CI engines (reaching pressures up to 250 bar [8] in engines currently in production).

In CI engines, the injection timing affects the air-fuel mixing process resulting in a different Heat Release Rate (HRR) shape, due to the change in the premixed/diffusion repartition. On the one hand, in CI engines the ignition delay changes when the injection timing is varied due to different pressure and temperature in the chamber near TDC. Advancing the Start of Injection (SOI) up to a certain point leads to higher in-cylinder pressure

evolution, thus increasing the indicated efficiency [9] and reducing the PM formation [10]. However, as in the previous strategy, the higher temperature increases NO_x formation. On the other hand, retarding the injection in GDI engines operating under stratified conditions can lead to improve the efficiency and NO_x emissions but worsen the smoke and incomplete combustion [11].

Nowadays, modern injection systems give room to more complex injection patterns, allowing the use of up to 8 injection events in some cases. On the one hand, CI engines use pilot injections to reduce noise and NO_x emissions with low effect on engine performance [12, 13]. Additionally, coupled post injections are useful to complete the combustion of the PM while splitting the main injection improves the fuel/air mixture, accelerating combustion progress and shortening combustion duration [14]. Finally, late post injections are used to increase the exhaust temperature in order to either warm up the aftertreatment systems during cold start to increase its efficiency or to help the regeneration processes of the particulate filter and the NO_x adsorption catalyst [2]. However, this late post injection has negative effects on consumption since it is burned at the end of the expansion process. On the other hand, splitting the injection in GDI engines helps to reduce the cycle to cycle dispersion and to increase the resistance to knocking [15].

Furthermore, the versatility of the current injection systems in CI engines also allows obtaining different and more complicated injection rate shapes than the conventional one, thus achieving more control over the HRR shape. Using boot or ramps shapes during the needle lift event allows improving the combustion performance in terms of efficiency and NO_x emissions, especially in the medium/high load zone [16, 17].

In SI engines, the use of lean or ultra-lean burn ratios is a well-known and proven strategy to increase indicated efficiency and reduce pollutant emissions [18]. This technique benefits from the better combustion quality, the lower heat transfer losses and the possibility to use higher compression ratios. However, operating under high AFR is not always easy since the lower fuel concentration requires greater energy to start the combustion. Thus, several approaches have been assessed to tackle this issue, being the prechamber approach [19, 20] one of the most efficient among them. According to Jamrozik *et al.* [21], this technology uses an additional small prechamber, connected to the cylinder, in which the lean mixture is aspirated and an additional injector enrich the mixture up to nearly stoichiometric conditions (only in stratified charge conditions). This prechamber mixture is ignited, and the pressure rise forces the flame to be pushed out through the connecting channel into

the cylinder, where both flame and emission gases initiate the lean mixture combustion process.

The cylinder deactivation approach consists of deactivating the fuel injection in some cylinders of the engine and increasing it in the remaining ones to maintain the demanded torque [22], being this technique valid for both CI and SI engines. Since load is increased in the active cylinders to maintain the power of the complete engine, low load zones, where both efficiency and exhaust temperature used to be low, are avoided thus obtaining higher efficiency and exhaust temperatures in the active cylinders. Additionally, if this approach is used along with a Variable Valve Timing (VVT) [23, 24], the efficiency increases due to the power save of the non lifted valves and the pumping work avoided in the deactivated cylinders. This conjunction leads to reaching an improvement between 2-4 % $\dot{m}_f H_v$ respect to the non deactivated cases at low load. Moreover, the exhaust temperature is also higher with the VVT since there is no cold flow from the deactivated cylinders, reaching an increase up to 200°C without penalty in consumption [25].

2.2.1.2 Air management

A sophisticated injection system including technologies explained in the previous section needs a proper air management to provide the required trapped air mass and composition in every operating condition. The principal air management strategies used nowadays to optimize the indicated cycle and/or emissions are described in this section.

Firstly, a correct design of the intake/exhaust manifolds is mandatory to take advantage of pulsating waves in order to enhance the cylinder filling process for the most relevant operating conditions [26, 27]. Furthermore, technologies such as Variable Valve Timing (VVT) are becoming more usual nowadays to increase the volumetric efficiency and/or reducing the pumping losses [28] by optimizing the intake/exhaust processes through different valves timings and lifts depending on the operating conditions.

Nowadays, the boosting pressure strategy is used in almost all applications of ICE, thus leading to gas densities above ambient pressure [29] intended to increase the combustion efficiency [30, 31] and to cut down CO [32] and PM [26] emissions. Additionally, the highest O_2 availability allows increasing the fuel injected leading to engines with higher rated power. However, the higher pressure evolution means higher in-cylinder temperature that, in conventional Diesel combustion (CDC) is translated into an increase of NO_x formation [30] and in conventional gasoline combustion increases the knocking risk [33–

36]. This effect can be reduced in both ICE concepts using an intercooler between the compressor and the cylinder. This system is intended to mitigate the temperature increase suffered by the gas in the compression process and increase the density of the gas.

Normally, the boosting strategy is applied by means of a turbocharger that uses the exhaust gases to speed up a turbine sharing the shaft with the compressor. This system brings an additional benefit in consumption due to the utilisation of exhaust energy that would be lost in other cases. The geometry of this turbocharger can be fixed with a waste-gate valve or variable to regulate the demanded boost pressure. The problem of this approach is the time or *'lag'* between the power demand and delivery. To solve this problem, some OEM's equip their engines with either smaller turbochargers with lower inertia and/or electric compressors independent of the exhaust process, leading to complex multi-stage chargers.

Exhaust gas recirculation (EGR) is a practical and economical strategy to reduce the combustion temperature, and hence the NO_x formation, that consists on the recirculation of exhaust gases to the intake line. However, this lower temperature extends the combustion duration with a negative impact on the thermal efficiency [26] and also increases the PM emissions [37]. There are two types of EGR depending on the places where the gases are taken from the exhaust line and introduced to the intake one. On the one hand, the short-route or high pressure EGR takes the gases before the turbocharger and redirects them to the intake manifold. On the other hand, the long-route or low pressure EGR collects the exhaust gases downstream the turbine and takes them upstream the compressor. Nowadays, it is a common practice to install both types in ICE along with coolers in one or both lines to cool down the gases before its introduction in the intake line [38].

Internal Gas Recirculation (IGR) is an strategy intended to keep in the cylinder a fraction of burned mass by means of appropriate valve timing [39]. The effect of IGR on emissions is similar to those of EGR, thus reducing NO_x formation. However, unlike EGR, IGR cannot be cooled down, thus it helps to increase the temperature at IVC and during the compression stroke. This higher temperature affects the combustion phasing and duration and increases the susceptibility to knocking in SI engines [40]. Therefore, although unavoidable, IGR is reduced as much as possible in CDC while it is combined with EGR in premixed combustion [41], specially with low reactivity fuels [42]. In this combustion mode, the combination of these two techniques leads to achieve low emissions and high efficiency since the higher temperature of IGR

increases the charge reactivity [42], thus helping to cut down the HC and CO emissions [41] as a result of a better combustion completion.

Air motion in the chamber is a key issue to improve the air-fuel mixing process and achieve faster burning rates [29], therefore ICE are designed to generate vorticity in the chamber that leads to enhanced turbulence during the combustion development, thus improving PM emissions and consumption [43, 44]. The main air rotation macro structures that can be found in ICE are swirl and tumble, being differentiated by their rotary axis. The swirl movement is prompted by chamber configurations consisting of a shallow bowl in the piston crown [29] and it is applied in CI engines, whilst the tumble movement is enhanced by pentroof combustion chambers [45–47] of SI engines. However, these techniques have also some drawbacks such as the increase of NO_x emissions due to the enhanced combustion process and the higher heat transfer (HT) in the chamber due to the greater gas velocity that increases the heat transfer coefficient [43]. These competing effects lead to different scenarios depending on the engine speed and load. Thus, some OEMs have implemented in their engines a method to variate the swirl ratio (SR) and, starting from low swirl conditions (quiescent), they are able to adjust it depending on the operating point.

Alternative cycles such as Miller or Atkinson [48] in which the intake valves are still open during part of the compression stroke lead to lower pumping work, that finally leads to higher efficiency but also to a penalty in torque/power due to the lower in-cylinder trapped mass. This strategy could be performed using a fixed intake valve lift profile in the whole range of the engine map [48], with a certain penalty in rated power, or along with a VVT system [49] to perform it in the partial load zone, maintaining the conventional cycle in the full load curve.

2.2.2 Heat transfer

Taking into account that HT to chamber walls accounts for 15-40% $\dot{m}_f H_v$ [50] depending on the operating condition, it is normal that researchers have focused on reducing this important loss in order to optimize the indicated cycle. There are two main approaches dealing with heat transfer used nowadays to increase the engine performance. On the one hand, the low heat rejection strategy looks for the reduction of the heat transfer to the engine in order to improve the efficiency. On the other hand, the thermal management approach is focused on the smart design of the engine architecture to use the

heat transfer as an advantage rather than a drawback or at least mitigate its impact when it is unavoidable.

2.2.2.1 Low heat rejection engines

This strategy is intended to reduce the HT to the combustion chamber walls with the objective of achieving better indicated efficiency [29]. However, a decrease in HT is not directly transferred into the equivalent gain on efficiency, but also part of this energy is rejected to the exhaust gases. It is worth to note that the main HT mechanism in the combustion chamber of an ICE is convection, which governing equation is the following:

$$Q_{convection} = hA\left(T_{gas} - T_{wall}\right) \tag{2.1}$$

where h is the film coefficient, A is the wall surface in contact with the gas and T_{gas} and T_{wall} are the temperatures of the in-cylinder gas and combustions chamber walls respectively.

When analysing this equation, three different approaches aimed at reducing heat transfer can be easily identified if the engine geometry (A) is maintained:

- On the one hand, the reduction of the film coefficient can be achieved by decreasing the gas velocity (swirl or tumble) inside the combustion chamber. As commented in Section 2.2.1.2, these motions normally have a positive effect on the mixing process, thus enhancing the combustion velocity and affecting positively GIE. However, the drawback of increasing these motions is the increment of heat transfer due to the higher film coefficient. Thus, the balance between these competing effects when gas motion is enhanced is an interesting analysis and it will be a key topic in this work (see Section 5.2.1).

- On the other hand, the reduction of the term within the parenthesis can be addressed following two different approaches:

  - By reducing the gas temperature. There are several approaches intended to reduce the charge temperature such as the EGR or IGR addition, novel low temperature combustion modes or injecting water inside the combustion chamber.
  - By increasing the wall temperature. Thermal barrier coatings applied to the combustion chamber are used to increase the wall temperature, thus reducing the heat transfer in the cycle.

2.2.2.1.1 Decreasing in-cylinder temperature

Regarding the first approach, as commented, there are several strategies to reduce the temperature of the chamber along the cycle evolution. Besides the heat transfer reduction achieved by lowering the gas temperature, other benefits derived from this temperature decrease are reduced NO_x formation during the combustion and the higher heat capacity ratio of the cooler charge. Since the EGR and IGR techniques were already explained in Section 2.2.1.2, only some low temperature combustion modes and the water injection strategy are described here.

The evolution of the engine subsystems presented in Section 2.2.1 along with researchers' efforts to find cleaner and more efficient combustions have made different improvements possible. Among them, the development of alternative combustion modes are a promising alternative to increase the indicated efficiency, reduce heat transfer and cut-down pollutant emissions [2, 5] respect to conventional Diesel combustion (CDC) [51, 52] and conventional gasoline combustion (CGC) [53]. Most of these new developed alternative combustion modes can be categorized as low temperature combustions (LTC), which makes reference to all combustions which temperature evolution is below the conventional one, thus decreasing the HT and NO_x emissions while increasing or at least maintaining the indicated efficiency.

One of the first developed LTC concepts was the Homogeneous Charge Compression Ignition (HCCI), in which an homogeneous premixed charge of air, fuel and residual gases is burned by autoignition, allowing a combustion with lower temperature and lower fuel/air ratios than CDC. This combustion mode allows to cut down NO_x and PM emissions and also presents some potential to reduce BSFC thanks to the faster HRR and lower HT [54]. However, since it requires a precise control of pressure and temperature and a complex homogeneous charge preparation for an optimum autoignition, it can only be applied in a narrow operating range. Thus, its application results in some problems such as long warm-up periods and high HC and CO emissions levels [55, 56] that, over the years, have been tried to be solved through several variations of the HCCI concept. Among them, premixed charge compression ignition [57, 58], active radical combustion [59], modulate kinetics [60] and partially premixed combustion [42, 61] have been developed. These new concepts use new air management, fuel injection and mixture formation strategies to extend their operating range [62] and to reduce their limiting factors, such as pre-ignition, knocking [63] and HC emissions [60], while achieving high indicated efficiency [64].

There is another LTC strategy that, unlike HCCI methods that reduce the charge reactivity through the decrease of the mixture temperature, controls the charge reactivity through the injection of both low and high reactivity fuels that lead to a reactivity stratification along the chamber. This approach is called Reactivity Controlled Compression Ignition (RCCI) [65, 66] and, theoretically, solves most of the problems presented by the previous modes. RCCI concept improvements regarding NO_x and PM emissions have been reported [67–69] but, unfortunately, its main drawback is that its combustion efficiency is lower than the one obtained with CDC and CGC (high HC and CO emissions) due to the unburned fuel trapped in the crevice volumes and the flame quenching near the walls [69, 70]. Nonetheless, the optimization of the piston shape along with a reduction of the crevice volumes reduce this issue [71], reaching indicated efficiencies higher than 50 % $\dot{m}_f H_v$ in light-duty engines [72] and 55 % $\dot{m}_f H_v$ in high-duty engines [73].

Finally, the last strategy to decrease the charge temperature consists of injecting water, in the same order of magnitude as the injected fuel, in the cylinder. Under high temperatures, a thermal dissociation process occurs to the water forming hydroxide and hydrogen, which absorbs heat during combustion [74], and also provides extra oxygen to the combustion. Besides the gas mean temperature reduction, the injected water also reduces the local temperature of the flame, thus decreasing NO_x emissions [75]. Additionally, in SI engines this lower temperature also increases the knocking resistance, permitting the use of higher boosting pressures or fuel with lower octane number than the conventional [75]. There are different approaches to inject the water into the engine: some studies inject it directly into the combustion chamber by using either a dedicated water injector [75] or in an emulsion with the fuel through the main injector [76], while other studies have opted to supply the water at some point of the intake lines [77].

2.2.2.1.2 Thermal barrier coatings

The last approach to reduce heat transfer consists of thermal isolation of the combustion chamber by means of Thermal Barrier Coatings (TBC). The use of coatings has an impact on different processes that finally affect positively the engine efficiency [78–80]: a lower HT results in higher temperature and pressure, with the consequent increase on indicated efficiency, torque and power [78, 80]. Additionally, the energy availability at exhaust [81] is also augmented, which can be used in recovery cycles [82] or turbocharging and turbocompounding systems [83], leading to benefits up to 15% in fuel consumption with these configurations [84, 85].

In the past, the application of coatings made of ceramic materials with low thermal conductivity and high temperature durability resulted in an effective way to reduce the heat rejection [86, 87]. However, these materials have some important drawbacks such as the lower volumetric efficiency as a consequence of the higher heat transfer to the intake gas. The greater wall temperature of these materials increased the gas temperature with the consequent increase of NO_x production.

Nowadays, novel alloys with low thermal conductivity and volumetric heat capacity, such as Silica-reinforced porous anodized aluminium (SiRPA) [88], are able to partially reproduce the transient gas temperature, reducing in this way the difference of temperature between the gas and walls and hence, the heat rejection to the combustion chamber walls. These properties lead to lower wall temperature during the intake process in comparison with conventional coating materials, improving in this way the volumetric efficiency [88]. Unlike a conventional block engine without coating in which the wall temperature remains almost constant along the cycle, this approach claims for a temperature swing of 140°C. However, since its maximum benefit on GIE is not clearly stated in the literature, it will be briefly evaluated in Section 4.4.2.3.

Finally, one of the main drawbacks of engines equipped with TBC is the increase of NO_x emissions due to the higher combustion temperatures. Nonetheless, HC, CO and PM emissions are reduced for this high temperature that helps the oxidation reactions [89].

2.2.2.2 Engine thermal management

A good definition of Engine Thermal Management (ETM) could be the adequate control of all thermal fluxes of the engine in order to reduce emissions and/or consumption [90]. In ICE, the most important thermal fluxes are those associated with the cooling of both hot metallic parts, aimed at reducing thermal stresses, and the lubrication system to avoid oil degradation and to work in the designed temperature range. ETM is focused on the smart design and operation of all these sub-systems and their interactions to increase the engine performance [91–93].

ETM strategies are aimed at reaching the optimum temperature of metal parts, liquids (coolant and oil) and aftertreatment equipment as soon as possible after the engine start and maintaining it during its operation in order to enhance the engine performance. When the coolant temperature increases, the HT is slightly reduced, due to the temperature gradient reduction, and

the gas temperature increases as can be seen in Figure 2.1. This higher gas temperature results in shorter ignition delay, short pre-mixed combustion and fast combustion completion [26], thus it can be stated that high coolant temperatures are beneficial for improving the engine efficiency [94], but, on the contrary, they enhance the NO_x formation process. Additionally, the efficiency of aftertreatment systems such as SCR is very low when its temperature is below 250°C, thus a fast warming up of these systems through an exhaust temperature increase also leads to a reduction in NO_x emissions.

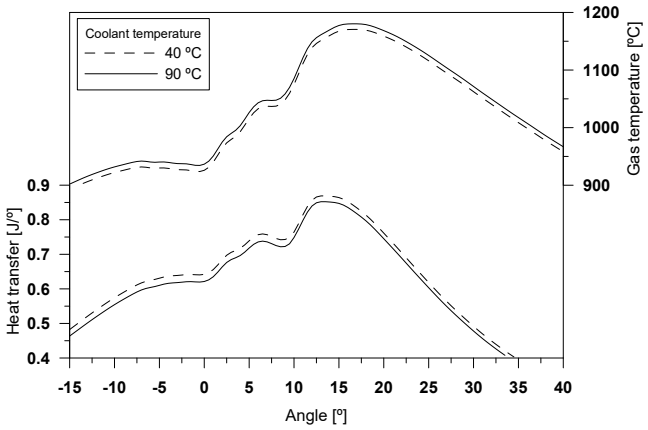

Figure 2.1. *Coolant temperature influence on the gas temperature and HT. Source: [95].*

The most inefficient scenario for a conventional cooling system is the one taking place in the cold-start, where all materials and components are cold. Hence, high thermal loads would be desirables [96] to reach the optimal engine operation temperature, reducing in this way the heat losses and friction [97]. According to Torregrosa *et al.* [90], reductions of about 20% in the warm-up time reduce HC and CO emissions about 16% and 12%, and BSFC about 1.6% with a minimum effect on NO_x and PM.

Even though the highest benefits observed using these strategies are found in Brake Thermal Efficiency (BTE) due to the reduction of friction and auxiliary losses, a no negligible part of this benefit comes from the heat transfer reduction inside the cylinder. Additionally, since these strategies have impact on emissions, it is considered that it is worth to describe them briefly. Thus, some of the ETM aimed to increase the engine performance are the following:

- A simple way to control the coolant flow without changing so much the engine architecture is the use of electric valves at the coolant pump outlet [91]. This approach allows reducing the coolant flow at cold-start conditions and low power operating conditions to speed-up the warm-up process with the above explained benefits.

- Traditionally, the cooling systems are designed to ensure the engine integrity at maximum engine power [90], leading to overcooling the engine and, hence, increasing the fuel consumption and energy wasting [98] in a broad range of the engine map. These systems consist on a mechanical pump driven by the engine, where the volumetric flow is proportional to the engine speed. A further step is the use of an electric pump instead of the mechanical one to adjust the coolant flow, or even switch it off, according to the instantaneous engine thermal requirements independently of the engine speed [99].

- Additionally, the traditional thermostat could be substituted by a *smart thermostatic valve* [100] that, thanks to its lower response time and higher temperature resistance, could be operated much more efficiently.

- A variable displacement and/or variable speed oil pump [101] could be operated to deliver only the required oil flow depending on the operating conditions would benefit the fuel consumption.

- An important issue nowadays is the low efficiency of the aftertreatment systems under low temperature conditions, leading to important pollutant emissions during the warm-up period. Hence, several strategies are being developed and used by OEMs to increase the exhaust temperature during the cold start, thus shortening the warm-up time of the aftertreatment systems. Some of these strategies are late post injections [102], cylinder deactivation [24], Variable Valve Actuation (VVA) to perform and early exhaust valve opening and/or IGR [103], non cooled EGR, ... Unfortunately, most of these approaches have a negative impact on indicated efficiency, hence big efforts have to be done to calibrate them correctly trying to minimize their penalty on fuel consumption.

2.3 Methodologies to assess the indicated cycle

There are several tools aimed to study or improve the indicated cycle. These tools can be grouped according to the type of simulation tool in which they are based, as following:

- Computational Fluid Dynamics (CFD) models are a three-dimensional (3D) approach that uses numerical analysis to solve and analyse problems that involve fluid flows. Drawbacks of this simulation tool are, on the one hand, the requirement of an extensive calibration campaign and, on the other hand, those simulations are time-consuming. Therefore, it is normally used to simulate isolated parts of the engine.
- One-dimensional tools (1D) are able to predict accurately the gas dynamics, representing flow and heat transfer in pipes and related components, through the entire engine. However, the analysis of the processes inside the combustion chamber, main topic of this work, is carried out using a zero-dimensional model.
- Finally, zero-dimensional models (0D) does not consider space resolution, but they are still time dependent. They do not require high computational effort and they are able to give accurate results in a short time [29] given a suitable preliminary calibration.

Taking into account that the objective of this work is to assess and optimize the indicated cycle, it is considered that the 0D model approach is a suitable tool thanks to its simplicity and low computational effort while being accurate enough to take into account for main in-cylinder phenomena. Thus, a predictive 0D model [104] (see Section 3.3.1) is used to solve the mass and energy conservation equations during closed cycle so that the instantaneous state of the gas within the combustion chamber (pressure and temperature) is obtained. In this section, some methodologies based on a 0D approach to assess and optimize either benefit of the previous strategies on the engine performance or the potential of a certain ICE architecture are presented.

2.3.1 Global Energy Balance

The Global Energy Balance (GEB) analysis of an ICE [50, 105–116] consists on tracking the paths followed by the fuel energy provided to the engine until leaving the engine. Analysing the evolution of the energy considering the engine as a black box where a known amount of energy is

converted into brake power, heat rejection and exhaust gases energy, it is an interesting approach to evaluate new engine strategies and technologies. Therefore, the thermal analysis of the engine allows identifying the repartition of the chemical fuel energy into the final energy destination, thus improving the understanding of the mechanisms affecting the engine consumption.

Among the mentioned works, Payri *et al.* [50] completed the analysis by modelling the internal energy flows that convert the fuel energy into the mentioned engine outputs. In this way, the measurable changes in the experimental variables can be explained through the analysis of internal processes that are modelled, especially heat transfer.

Following, a brief definition of each term of the external thermal balance along with the ranges found in the literature [95] for conventional CI and SI engines are given below and plotted in Figure 2.2:

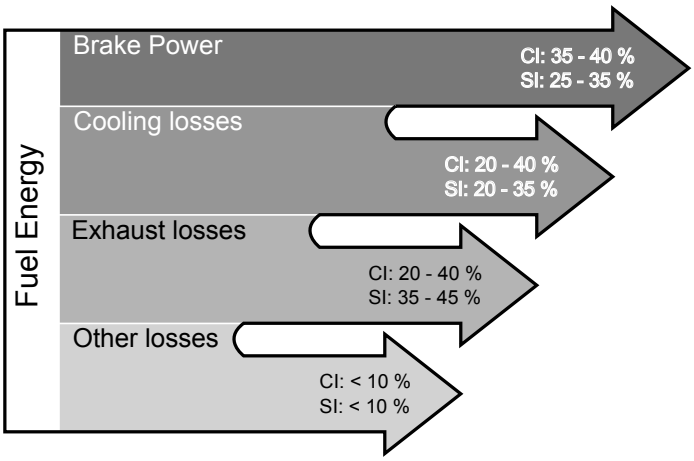

Figure 2.2. *Main terms and percentages of the Global Energy Balance in CI and SI engines. Source: [95].*

- Brake efficiency is higher in CI than in SI and, additionally, being also greater at high load and low engine speed [105, 109] (close to 40% $\dot{m}_f H_v$in CI and 35% $\dot{m}_f H_v$ in SI) compared to low load and engine speed conditions(around 35% $\dot{m}_f H_v$ in CI and 25% $\dot{m}_f H_v$ in SI), despite the indicated efficiency is slightly higher at low load. This is easily explained taking into account that at low load an important part of the indicated power is used to beat the friction and activate the auxiliary elements and at high engine speed the friction losses increase.

- The heat rejection takes into account the heat transfer to the coolant and oil coming from HT from chamber and ports, friction and auxiliary activation energy. This term is maximum at low load and engine speed, where indicated efficiency is minimum, reaching values up to 40% $\dot{m}_f H_v$ in CI and 35% $\dot{m}_f H_v$ in SI.

- Exhaust losses account for the net enthalpy variation between intake and exhaust ports. This term ranges from 20% $\dot{m}_f H_v$ at low load and engine speed up to above 40% $\dot{m}_f H_v$ at high load and engine speed in CI engines and between 35% $\dot{m}_f H_v$ and 45% $\dot{m}_f H_v$ in SI engines.

- Lastly, there are other minor terms such as blow-by losses or the unburned fuel that, taken together, mean less than 10% $\dot{m}_f H_v$ in the whole engine map of a conventional either CI or SI engine.

Using this approach allows to evaluate the effect of various parameters or strategies such as the engine load and climatic conditions [105, 108], injection settings and intake strategies [117], boosting strategy [110], EGR level [118], swirl ratio [43] or coolant and intake temperatures [119] on the engine performance.

2.3.2 Split of losses

This method [120] compares the experimental cycles that take place in a real ICE with the Otto cycle (maximum efficiency ideal cycle under non realistic conditions) and assesses all efficiency losses that separate them. A real cycle is a result of the ideal Otto cycle and the addition of several losses. Each efficiency loss, at the same time, represents a decrease in efficiency that the methodology is able to quantify. This methodology allows to identify the main sources of losses in the combustion process, thus being really useful when comparing different technologies. There is a limitation in this approach related with the order in which all these losses are computed, but, in any case, the global analysis is trustworthy [121].

Thirouard *et al.* [121] applied this approach to two engines with different displacement but same compression ratio to compare the downsizing strategy. There, the highest difference found among efficiency losses was in the HT effect, lower in the bigger engine, that led to efficiencies 2% and 4% higher at medium load and low load respectively in the bigger engine respect to the smaller one. Same authors also used this analysis to evaluate a new combustion mode based on Lifted Flame Diffusive Combustion (LFDC) [122], a combination of

an increased number of small nozzle holes, high injection pressure, low swirl motion and an open large bowl design. The conclusion of this analysis was that gains in terms of consumption with the new combustion concept were due specially to the lower heat transfer to the walls.

Later on, this methodology will be applied to a swirl parametric study, setting the base for the detailed analysis presented in Section 5.2.1.3.

2.3.3 Combustion law shaping

Over the last years, various authors have studied the best theoretical combustion law in ICE operating under different operating conditions and combustion modes [123–128]. Additionally, these studies are able to take into account various restrictions from the thermo-mechanical (maximum peak pressure or maximum pressure rise rate [125–128]) or from the pollutant (NO_x emissions [125, 127]) points of view.

Even though most optimum combustion laws resultant from this analysis are not achievable in real engines, efficiencies obtained with this methodology establish the boundary of the considered engine operating under a certain combustion mode. Furthermore, when used together with a trustworthy NO_x predictive model, this analysis is able to provide the penalty in efficiency derived from reducing NO_x production.

This analysis was carried out by Eriksson *et al.* [124, 125] in a SI engine. In [124] authors optimized the combustion law of an operating point by coupling a simple thermodynamic model of a SI engine with an optimizer without taking into account any restriction. This analysis was improved in [125], where authors included a NO model and performed the previous analysis but including the impact of some constraints such as peak pressure, pressure rise rate, knocking occurrence and NO production in the combustion shape. The two stage combustion found as optimum when considering pressure and knocking limits rose to a four phase combustion when NO constraints were taking into account.

Similarly, Okamoto *et al.* [126] performed a study to obtain the optimum combustion law, concluding that Sabathé cycle provided the highest efficiency. Afterwards, they tried to reproduce this heat release shape, both numerically and experimentally, by using three injectors and a newly designed combustion chamber. Results from this analysis showed that the tradeoff between NO_x and soot was improved, while brake thermal efficiency (BTE) was also enhanced.

Later on, Guardiola *et al.* [127, 128] applied the same analysis to a CDC and to a Reactivity Controlled Compression Ignited (RCCI) engines

respectively. Both works found that the optimum heat release law (HRL) when pressure restrictions were imposed (maximum peak pressure and maximum pressure rise rate) is the one that results in an in-cylinder pressure that follows exactly the imposed limits. NO_x emissions were also restricted in [127] resulting in delayed and slower combustions when this limit was tightened. Additionally, in [127] authors tried to replicate experimentally the optimum theoretical HRL finding differences in ISFC up to 25 g/kWh between the theoretical solution and the experiment.

Bibliography

[1] European Parliament. "Commision regulation (EU) No 333/2014 OF the European Parliament and of the Council of 11 March 2014 amending Regulation (EC) No 443/2009 to define the modalities for reaching the 2020 target to reduce CO2 emissions from new passenger cars". *Official Journal of the European Union*, Vol. 103 n^o 333, pp. 15–21, 2014.

[2] Mohan B., Yang W. and Chou S.K. "Fuel injection strategies for performance improvement and emissions reduction in compression ignition engines - A Review". *Renewable and Sustainable Energy Reviews*, Vol. 28, pp. 664–676, 2013.

[3] Wloka J.A., Pflaum S. and Wachtmeister G. "Potential and Challenges of a 3000 Bar Common-Rail Injection System Considering Engine Behavior and Emission Level". *SAE Int. J. Engines*, Vol. 3 n^o 1, pp. 801–813, 2010.

[4] Wang X., Huang Z., Zhang W., Kuti O.A. and Nishida K. "Effects of ultra-high injection pressure and micro-hole nozzle on flame structure and soot formation of impinging diesel spray". *Applied Energy*, Vol. 88 n^o 5, pp. 1620–1628, Mayo 2011.

[5] Pickett L.M. and Siebers D.L. "Soot in diesel fuel jets: effects of ambient temperature, ambient density, and injection pressure". *Combustion and Flame*, Vol. 138 n^o 1-2, pp. 114–135, Julio 2004.

[6] Su T., Chang C., Reitz R., Farrell P., Pierpont A. and Tow T. "Effects of Injection Pressure and Nozzle Geometry on Spray SMD and D.I. Emissions". *SAE Technical Paper 952360*, 1995.

[7] Dogde L.G., Simescu S., Neely G.D., Maymar M.J., Dickey D.W. and Savonen C.L. "Effect of Small Holes and High Injection Pressures on Diesel Engine Combustion". *SAE Technical Paper 2002-01-0494*, 2002.

[8] Robert Bosch GmbH. Gasoline Systems. *Gasoline Direct Injection. Key technology for greater efficiency and dynamics.* Robert Bosch GmbH, Stuttgart, Germany, 2015.

[9] Payri F., Olmeda P., Martín J. and Carreño R. "Experimental analysis of the global energy balance in a DI diesel engine". *Applied Thermal Engineering*, Vol. 89, pp. 545–557, Octubre 2015.

[10] Agarwal A.K., Srivastava D.K., Dhar A., Maurya R.K., Shukla P.C. and Singh A.P. "Effect of fuel injection timing and pressure on combustion, emissions and performance characteristics of a single cylinder diesel engine". *Fuel*, Vol. 111, pp. 374–383, Septiembre 2013.

[11] Oh H. and Bae C. "Effects of the injection timing on spray and combustion characteristics in a spray-guided DISI engine under lean-stratified operation". *Fuel*, Vol. 107, pp. 225 – 235, 2013.

[12] Badami M., Mallamo F., Millo F. and Rossi E.E. "Influence of Multiple Injection Strategies on Emissions , Combustion Noise and BSFC of a DI Common Rail Diesel Engine". *SAE Technical Paper 2002-01-0503*, 2002.

[13] Hiwase S.D., Moorthy S., Prasad H., Dumpa M. and Metkar R.M. "Multidimensional Modeling of Direct Injection Diesel Engine with Split Multiple Stage Fuel Injections". *Procedia Engineering*, Vol. 51, pp. 670–675, Enero 2013.

[14] Li X., Zhou H., Zhao L., Su L., Xu H. and Liu F. "Effect of split injections coupled with swirl on combustion performance in DI diesel engines". *Energy Conversion and Management*, Vol. 129, pp. 180–188, 2016.

[15] Costa M., Sementa P., Sorge U., Catapano F., Marseglia G. and Vaglieco B. "Split Injection in a GDI Engine Under Knock Conditions: An Experimental and Numerical Investigation". *SAE Technical Paper*, 2015.

[16] Desantes J.M., Benajes J., Molina S. and González C.A. "The modification of the fuel injection rate in heavy-duty diesel engines. Part 1: Effects on engine performance and emissions". *Applied Thermal Engineering*, Vol. 24 n^o 17-18, pp. 2701–2714, Diciembre 2004.

[17] Desantes J.M., Benajes J., Molina S. and González C.A. "The modification of the fuel injection rate in heavy-duty diesel engines. Part 2: Effects on combustion". *Applied Thermal Engineering*, Vol. 24 n^o 17-18, pp. 2715–2726, Diciembre 2004.

[18] Germane G., Wood C. and Hess C. "Lean Combustion in Spark-Ignited Internal Combustion Engines - A Review". *SAE Technical paper 831694*, 1983.

[19] Toulson E., Schock H. and Attard W. "A Review of Pre-Chamber Initiated Jet Ignition Combustion Systems". *SAE International Journal of Engines*, 2010.

[20] Castilla C., Elias G., Rückert V., Braga A. and Molina R. "A review of prechamber ignition systems as lean combustion technology for SI engines". *Applied Thermal Engineering*, Vol. 128, pp. 107–120, 2018.

[21] Jamrozik A. and Tutak W. "A study of performance and emissions of SI engine with a two-stage combustion system". *Chemical and Process Engineering - Inzynieria Chemiczna i Procesowa*, Vol. 32 n^o 4, pp. 453–471, 2011.

[22] Ramesh A., Shaver G., Allen C., Nayyar S., Gosala D., Parra D. and Koeberlein E. "Utilizing low airflow strategies , including cylinder deactivation , to improve fuel efficiency and aftertreatment thermal management". *International Journal of Engine Research*, Vol. 18 n^o 10, pp. 1005–1016, 2017.

[23] Flierl R., Lauer F., Breuer M. and Hannibal W. "Cylinder Deactivation with Mechanically Fully Variable Valve Train". *SAE Int. J. Engines*, Vol. 5 n^o 2, pp. 207–215, 2012.

[24] Ramesh A., Gosala D., Allen C., Joshi M., McCarthy J., Farrell L., Koeberlein E. and Shaver G. "Cylinder Deactivation for Increased Engine Efficiency and Aftertreatment Thermal Management in Diesel Engines". *SAE Technical Paper 2018-01-0384*, Vol. 1 n^o 1, pp. 1–10, 2018.

[25] Ding C., Roberts L., Fain D., Ramesh A., Shaver G., McCarthy Jr J., Ruth M., Koeberlein E., Holloway E. and Nielsen D. "Fuel efficient exhaust thermal management for compression ignition engines during idle via cylinder deactivation and flexible valve actuation". *International Journal of Engine Research*, Vol. 17 n^o 6, pp. 619–630, 2016.

[26] Payri F. and Desantes J.M. *Motores de combustión interna alternativos*. Reverté, ISBN 978-84-291-4802-2, Barcelona, 2011.

[27] Malkhede D.N. and Khalane H. "Maximizing Volumetric Efficiency of IC Engine through Intake Manifold Tuning". *SAE Techinical Paper 2015-01-1738*, 2015.

[28] Parvate-Patil G.B., Hong H. and Gordon B. "An assessment of intake and exhaust philosophies for variable valve timing". *SAE Technical Paper 2003-32-0078*, 2003.

[29] Heywood J.B. *Internal Combustion Engines Fundamentals*. McGraw-Hill, ISBN 978-0-07-028637-5, New York, 1988.

[30] Rakopoulos C.D., Dimaratos A.M., Giakoumis E.G. and Rakopoulos D.C. "Evaluation of the effect of engine, load and turbocharger parameters on transient emissions of

diesel engine". *Energy Conversion and Management*, Vol. 50 n^o 9, pp. 2381–2393, Septiembre 2009.

[31] Canakci M. "Combustion characteristics of a DI-HCCI gasoline engine running at different boost pressures". *Fuel*, Vol. 96, pp. 546–555, Junio 2012.

[32] Karabektas M. "The effects of turbocharger on the performance and exhaust emissions of a diesel engine fuelled with biodiesel". *Renewable Energy*, Vol. 34 n^o 4, pp. 989–993, apr 2009.

[33] Zhen X., Wang Y., Xu S., Zhu Y., Tao C., Xu T. and Song M. "The engine knock analysis - An overview". *Applied Energy*, Vol. 92, pp. 628–636, apr 2012.

[34] Galloni E., Fontana G. and Staccone S. "Numerical and experimental characterization of knock occurrence in a turbo-charged spark-ignition engine". *Energy Conversion and Management*, Vol. 85, pp. 417–424, sep 2014.

[35] De Bellis V. "Performance optimization of a spark-ignition turbocharged VVA engine under knock limited operation". *Applied Energy*, Vol. 164, pp. 162–174, feb 2016.

[36] Yang Y., Dec J.E., Sjöberg M. and Ji C. "Understanding fuel anti-knock performances in modern SI engines using fundamental HCCI experiments". *Combustion and Flame*, Vol. 162 n^o 10, pp. 4008–4015, oct 2015.

[37] Abd-Alla G.H. and Abdalla G. "Using exhaust gas recirculation in internal combustion engines: a review". *Energy Conversion and Management*, Vol. 43 n^o 8, pp. 1027–1042, 2002.

[38] Park Y. and Bae C. "Experimental study on the effects of high/low pressure EGR proportion in a passenger car diesel engine". *Applied Energy*, Vol. 133, pp. 308–316, Noviembre 2014.

[39] Benajes J., Novella R., De Lima D., Tribotté P., Quechon N., Obernesser P. and Dugue V. "Analysis of the combustion process, pollutant emissions and efficiency of an innovative 2-stroke HSDI engine designed for automotive applications". *Applied Thermal Engineering*, Vol. 58 n^o 1-2, pp. 181–193, Septiembre 2013.

[40] Bourhis G., Chauvin J., Gautrot X. and de Francqueville L. "LP EGR and IGR Compromise on a GDI Engine at Middle Load". *SAE Int. J. Engines*, Vol. 6 n^o 1, pp. 67–77, 2013.

[41] Bression G., Soleri D., Savy S., Dehoux S., Azoulay D., Hamouda H., Doradoux L., Guerrassi N. and Lawrence N. "A Study of Methods to Lower HC and CO Emissions in Diesel HCCI". *SAE Int. J. Fuels Lubr.*, Vol. 1 n^o 1, pp. 37–49, 2009.

[42] Benajes J., Martín J., Novella R. and Thein K. "Understanding the performance of the multiple injection gasoline partially premixed combustion concept implemented in a 2-Stroke high speed direct injection compression ignition engine". *Applied Energy*, Vol. 161, pp. 465–475, jan 2016.

[43] Benajes J., Olmeda P., Martín J., Blanco-Cavero D. and Warey A. "Evaluation of swirl effect on the Global Energy Balance of a HSDI Diesel engine". *Energy*, Vol. 122, pp. 168–181, 2017.

[44] Wei S., Wang F., Leng X., Liu X. and Ji K. "Numerical analysis on the effect of swirl ratios on swirl chamber combustion system of DI diesel engines". *Energy Conversion and Management*, Vol. 75, pp. 184–190, Noviembre 2013.

[45] Achuth M. and Mehta P.S. "Predictions of tumble and turbulence in four-valve pentroof spark ignition engines". *International Journal of Engine Research*, Vol. 2 n^o 3, pp. 209–227, Enero 2001.

[46] Huang R.F., Huang C.W., Chang S.B., Yang H.S., Lin T.W. and Hsu W.Y. "Topological flow evolutions in cylinder of a motored engine during intake and compression strokes". *Journal of Fluids and Structures*, Vol. 20 n^o 1, pp. 105–127, Enero 2005.

[47] Maharudrppa-Mallikarjuna J. "Effect of Manifold Orientation on Non-Reacting In-Cylinder Tumble Flows in an IC Engine with Pentroof Piston - An Investigation Using PIV". *SAE Technical Paper 2010-01-0956*, 2010.

[48] Al-Sarkhi A., Jaber J. and Probert S. "Efficiency of a Miller engine". *Applied Energy*, Vol. 83, pp. 343–351, 2006.

[49] Murata Y., Kusaka J., Daisho Y., Kawano D., Suzuki H., Ishii H. and Goto Y. "Miller-PCCI Combustion in an HSDI Diesel Engine with VVT". *SAE International Journal of Engines*, Vol. 1 n^o 1, pp. 444–456, 2009.

[50] Payri F., Olmeda P., Martín J. and Carreño R. "A New Tool to Perform Global Energy Balances in DI Diesel Engines". *SAE Int. J. Engines*, Vol. 7 n^o 1, pp. 43–59, 2014.

[51] Uyehara O.A. "Factors that Affect BSFC and Emissions for Diesel Engines : Part 1 - Presentation of Concepts". *SAE Techinical Paper 870343*, 1987.

[52] Beck N.J. and Uyehara O.A. "Factors That Affect BSFC and Emissions for Diesel Engines : Part II Experimental Confirmation of Concepts Presented in Part I". *SAE Techinical Paper 870344*, 1987.

[53] Wang C., Xu H., Herreros J.M., Wang J. and Cracknell R. "Impact of fuel and injection system on particle emissions from a GDI engine". *Applied Energy*, Vol. 132, pp. 178–191, Noviembre 2014.

[54] Stanglmaier R.H. and Roberts C.E. "(HCCI): Benefits , Compromises , and Future Engine Applications". *SAE Techinical Paper 1999-01-3682*, 1999.

[55] Bendu H. and Murugan S. "Homogeneous charge compression ignition (HCCI) combustion: Mixture preparation and control strategies in diesel engines". *Renewable and Sustainable Energy Reviews*, Vol. 38, pp. 732–746, Octubre 2014.

[56] Alkidas A.C. "Combustion advancements in gasoline engines". *Energy Conversion and Management*, Vol. 48 n^o 11, pp. 2751–2761, Noviembre 2007.

[57] Neely G.D., Sasaki S. and Leet J.A. "Experimental Investigation of PCCI-DI Combustion on Emissions in a Light-Duty Diesel Engine". *SAE Techinical Paper 2004-01-0121*, 2004.

[58] Aoyama T., Hattori Y., Mizuta J. and Sato Y. "An Experimental Study on Premixed-Charge Compression Ignition Gasoline Engine". *SAE Techinical Paper 960081*, 1996.

[59] Ishibashi Y. and Asai M. "Improving the Exhaust Emissions of Two-Stroke Engines by Applying the Activated Radical Combustion". *SAE Techinical Paper 960742*, 1996.

[60] Kimura S., Aoki O., Kitahara Y. and Aiyoshizawa E. "Ultra-Clean Combustion Technology Combining a Low-Temperature and Premixed Combustion Concept for Meeting Future Emission Standards". *SAE Technical Paper 2001-01-0200*, 2001.

[61] Benajes J., Molina S., Novella R. and De Lima D. "Implementation of the Partially Premixed Combustion concept in a 2-stroke HSDI diesel engine fueled with gasoline". *Applied Energy*, Vol. 122, pp. 94–111, jun 2014.

[62] Bedoya I.D., Saxena S., Cadavid F.J., Dibble R.W. and Wissink M. "Experimental evaluation of strategies to increase the operating range of a biogas-fueled HCCI engine for power generation". *Applied Energy*, Vol. 97, pp. 618–629, Septiembre 2012.

[63] Palma A., Del Core D. and Esposito C. "The HCCI Concept and Control , Performed with MultiAir Technology on Gasoline Engines". *SAE Technical Paper 2011-24-0026*, 2011.

[64] Dec J.E. and Yang Y. "Boosted HCCI for High Power without Engine Knock and with Ultra-Low NOx Emissions - using Conventional Gasoline". *SAE Int. J. Engines*, Vol. 3 n^o 1, pp. 750–767, 2010.

[65] Benajes J., Molina S., García A. and Monsalve-Serrano J. "Effects of direct injection timing and blending ratio on RCCI combustion with different low reactivity fuels". *Energy Conversion and Management*, Vol. 99, pp. 193–209, jul 2015.

[66] Kokjohn S.L., Hanson R.M., Splitter D.A. and Reitz R.D. "Fuel reactivity controlled compression ignition (RCCI): a pathway to controlled high-efficiency clean combustion". *International Journal of Engine Research*, Vol. 12 n^o 3, pp. 209–226, 2011.

[67] Benajes J., Pastor J.V., García A. and Monsalve-Serrano J. "The potential of RCCI concept to meet EURO VI NOx limitation and ultra-low soot emissions in a heavy-duty engine over the whole engine map". *Fuel*, Vol. 159, pp. 952–961, nov 2015.

[68] Benajes J., Molina S., García A. and Monsalve-Serrano J. "Effects of low reactivity fuel characteristics and blending ratio on low load RCCI (reactivity controlled compression ignition) performance and emissions in a heavy-duty diesel engine". *Energy*, Vol. 90, pp. 1261–1271, oct 2015.

[69] Heuser B., Kremer F., Pischinger S., Rohs H., Holderbaum B. and Körfer T. "An experimental investigation of dual-fuel combustion in a light duty Diesel engine by in-cylinder blending of ethanol and Diesel". *SAE Int. J. Engines*, Vol. 9 n^o 1, pp. 11–25, 2015.

[70] Belarte E. *Estudio del proceso de combustión premezclada controlada por la reactividad del combustible en un motor de encendido por compresión*. Doctoral Thesis, Universitat Politècnica de València, 2015.

[71] Benajes J., Pastor J.V., García A. and Monsalve-Serrano J. "An experimental investigation on the influence of piston bowl geometry on RCCI performance and emissions in a heavy-duty engine". *Energy Conversion and Management*, Vol. 103, pp. 1019–1030, oct 2015.

[72] Dempsey A.B., Walker N.R. and Reitz R.D. "Effect of Piston Bowl Geometry on Dual Fuel Reactivity Controlled Compression Ignition (RCCI) in a Light-Duty Engine Operated with Gasoline/Diesel and Methanol/Diesel". *SAE Int. J. Engines*, Vol. 6 n^o 1, pp. 78–100, 2013.

[73] Kokjohn S.L. and Reitz R.D. "Reactivity Controlled Compression Ignition and Conventional Diesel Combustion: A Comparison of Methods to Meet Light-Duty NOx and Fuel Economy Targets". *International Journal of Engine Research*, Vol. 0 n^o 0, pp. 1–17, 2013.

[74] Özcan H. and Söylemez M.S. "Thermal balance of a LPG fuelled, four stroke SI engine with water addition". *Energy Conversion and Management*, Vol. 47 n^o 5, pp. 570–581, Marzo 2006.

[75] Mingrui W., Thanh-Sa N., Turkson R., Jinping L. and Guanlun G. "Water injection for higher engine performance and lower emissions". *Journal of the Energy Institute*, Vol. 90 n^o 2, pp. 285–299, 2017.

[76] Lif A. and Holmberg K. "Water-in-diesel emulsions and related systems". *Advances in Colloid and Interface Science*, Vol. 123-126 n^o SPEC. ISS., pp. 231–239, 2006.

[77] Sahin Z., Tuti M. and Durgun O. "Experimental investigation of the effects of water adding to the intake air on the engine performance and exhaust emissions in a di automotive diesel engine". *Fuel*, Vol. 115 n^o x, pp. 884–895, 2014.

[78] Hazar H. "Effects of biodiesel on a low heat loss diesel engine". *Renewable Energy*, Vol. 34 n^o 6, pp. 1533–1537, Junio 2009.

[79] Mohamed-Musthafa M., Sivapirakasam S.P. and Udayakumar M. "Comparative studies on fly ash coated low heat rejection diesel engine on performance and emission characteristics fueled by rice bran and pongamia methyl ester and their blend with diesel". *Energy*, Vol. 36 n^o 5, pp. 2343–2351, 2011.

[80] Chan S.H. "Performance and emissions characteristics of a partially insulated gasoline engine". *International Journal of Thermal Sciences*, Vol. 40 n^o 3, pp. 255–261, Marzo 2001.

[81] Parlak A. "The effect of heat transfer on performance of the Diesel cycle and exergy of the exhaust gas stream in a LHR Diesel engine at the optimum injection timing". *Energy Conversion and Management*, Vol. 46 n^o 2, pp. 167–179, Enero 2005.

[82] Macián V., Serrano J.R., Dolz V. and Sánchez J.P. "Methodology to design a bottoming Rankine cycle, as a waste energy recovering system in vehicles. Study in a HDD engine". *Applied Energy*, Vol. 104, pp. 758–771, apr 2013.

[83] Taymaz I. "An experimental study of energy balance in low heat rejection diesel engine". *Energy*, Vol. 31 n^o 2-3, pp. 364–371, Febrero 2006.

[84] Jaichandar S. and Tamilporai P. "Low Heat Rejection Engines - An Overview". *SAE Technical Paper 2003-01-0405*, 2003.

[85] Abedin M.J., Masjuki H.H., Kalam M.A., Sanjid A. and Ashraful A.M. "Combustion, performance, and emission characteristics of low heat rejection engine operating on various biodiesels and vegetable oils". *Energy Conversion and Management*, Vol. 85, pp. 173–189, Septiembre 2014.

[86] Bryzik W. and Kamo R. "TACOM/Cummins Adiabatic Engine Program". *SAE Transactions*, Vol. 92, pp. 1063–1087, 1983.

[87] Osawa K. "Performance of Thin Thermal Barrier Coating on Small Aluminum Block Diesel Engine". *SAE Technical Paper 910461*, 1991.

[88] Wakisaka Y., Inayoshi M., Fukui K., Kosaka H. and Hotta Y. "Reduction of Heat Loss and Improvement of Thermal Efficiency by Application of Temperature Swing Insulation to Direct-Injection Diesel Engines". *SAE Int. J. Engines*, 2016.

[89] Ciniviz M., Hasimoglu C., Sahin F. and Salman M.S. "Impact of thermal barrier coating application on the performance and emissions of a turbocharged diesel engine". *Proceedings of the Institution of Mechanical Engineers, Part D: Journal of Automobile Engineering*, Vol. 222 n^o 12, pp. 2447–2455, 2008.

[90] Torregrosa A.J., Broatch A., Olmeda P. and Romero C. "Assessment of the influence of different cooling system configurations on engine warm-up, emissions and fuel consumption". *International Journal of Automotive Technology*, Vol. 9 n^o 4, pp. 447–458, 2008.

[91] Allen D.J. and Lasecki M.P. "Thermal Management Evolution and Controlled Coolant Flow". *SAE Techinical Paper 2001-01-1732*, 2001.

[92] Chastain J.H. and Wagner J.R. "Advanced Thermal Management for Internal Combustion Engines - Valve Design , Component Testing and Block Redesign". *SAE Techinical Paper 2006-01-1232*, Vol. 1 n^o 1, pp. –, 2006.

[93] Zhou B., Lan X., Xu X. and Liang X. "Numerical model and control strategies for the advanced thermal management system of diesel engine". *Applied Thermal Engineering*, Vol. 82, pp. 368–379, Mayo 2015.

[94] Torregrosa A.J., Olmeda P., Martín J. and Degraeuwe B. "Experiments on the influence of inlet charge and coolant temperature on performance and emissions of a DI Diesel engine". *Experimental Thermal and Fluid Science*, Vol. 30 n^o 7, pp. 633–641, 2006.

[95] Carreño R. *A comprehensive methodology to analyse the Global Energy Balance in Reciprocating Internal Combustion Engines*. Doctoral Thesis, 2016.

[96] Andrews G., Ounzain A., Li H., Bell M., Tate J. and Ropkins K. "The Use of a Water/Lube Oil Heat Exchanger and Enhanced Cooling Water Heating to Increase Water and Lube Oil Heating Rates in Passenger Cars for Reduced Fuel Consumption and CO2 Emissions During Cold Start". *SAE Techinical Paper 2007-01-2067*, 2007.

[97] Roberts A., Brooks R. and Shipway P. "Internal combustion engine cold-start efficiency: A review of the problem, causes and potential solutions". *Energy Conversion and Management*, Vol. 82, pp. 327–350, Junio 2014.

[98] Kang H., Ahn H. and Min K. "Smart cooling system of the double loop coolant structure with engine thermal management modeling". *Applied Thermal Engineering*, Vol. 79, pp. 124–131, 2015.

[99] Pang H.H. and Brace C.J. "Review of engine cooling technologies for modern engines". *Proc. Inst. Mech. Engrs.*, Vol. 218 n^o 11, pp. 1209–1215, 2004.

[100] Wagner J., Srinivasan V., Dawson D. and Marotta E. "Smart Thermostat and Coolant Pump Control for Engine Thermal Management Systems". *SAE International*, Vol. - n^o 724, 2003.

[101] Murray L., Staley D., Sorch K., Yager C. and Bruno M. "Control and diagnostic systems for a variable capacity engine oil pum and an engine oil pressure sensor". *US Patent*, Vol. 2 n^o 12, pp. 1–9, 2014.

[102] Honardar S., Busch H., Schnorbus T., Severin C., Kolbeck A. and Korfer T. "Exhaust Temperature Management for Diesel Engines Assessment of Engine Concepts and Calibration Strategies with Regard to Fuel Penalty". *SAE Technical Paper*, 2011.

[103] Piano A., Millo F., Di Nunno D. and Gallone A. "Numerical Assessment of the CO2 Reduction Potential of Variable Valve Actuation on a Light Duty Diesel Engine". *CO2 Reduction for Transportation Systems Conference*, n^o Ivc, 2018.

[104] Payri F., Olmeda P., Martín J. and García A. "A complete 0D thermodynamic predictive model for direct injection diesel engines". *Applied Energy*, Vol. 88 n^o 12, pp. 4632–4641, Diciembre 2011.

[105] Caton J.A. "Operating Characteristics of a Spark-Ignition Engine Using the Second Law of Thermodynamics : Effects of Speed and Load". *SAE Techinical Paper 2000-01-0952*, 2000.

[106] Teng H., Regner G. and Cowland C. "Waste Heat Recovery of Heavy-Duty Diesel Engines by Organic Rankine Cycle Part I: Hybrid System of Diesel and Rankine Engines". *SAE Technical Paper 2007-01-0537*, 2007.

[107] Edwards K.D., Wagner R. and Graves R.L. "Identification of Potential Efficiency Opportunities in Internal Combustion Engines Using a Detailed Thermodynamic Analysis of Engine Simulation Results". *SAE Technical Paper 2008-01-0293*, 2008.

[108] Boulahlib M.S., Boukebbab S., Gaci F. and Kholai O. "Experimental Study of Energy Balance for Air-Cooled DI Diesel Engines Operating in Hot Climates". *SAE Techinical Paper 2009-01-1974*, 2009.

[109] Smith L.A., Preston W.H., Dowd G., Taylor O. and Wilkinson K.M. "Application of a First Law Heat Balance Method to a Turbocharged Automotive Diesel Engine". *SAE Technical Paper 2009-01-2744*, 2009.

[110] Durgun O. and Şahin Z. "Theoretical investigation of heat balance in direct injection (DI) diesel engines for neat diesel fuel and gasoline fumigation". *Energy Conversion and Management*, Vol. 50 n^o 1, pp. 43–51, Enero 2009.

[111] Edwards K.D., Wagner R. and Briggs T. "Investigating Potential Light-duty Efficiency Improvements through Simulation of Turbo-compounding and Waste-heat Recovery Systems". *SAE Techinical Paper 2010-01-2209*, 2010.

[112] Teng H. "Waste Heat Recovery Concept to Reduce Fuel Consumption and Heat Rejection from a Diesel Engine". *SAE Int. J. Commer. Veh.*, Vol. 3 n^o 1, pp. 60–68, 2010.

[113] He M., Zhang X., Zeng K. and Gao K. "A combined thermodynamic cycle used for waste heat recovery of internal combustion engine". *Energy*, Vol. 36 n^o 12, pp. 6821–6829, Diciembre 2011.

[114] Fu J., Liu J., Feng R., Yang Y., Wang L. and Wang Y. "Energy and exergy analysis on gasoline engine based on mapping characteristics experiment". *Applied Energy*, Vol. 102, pp. 622–630, Febrero 2013.

[115] Singh S., Garg A., Gupta A. and Permude A. "Analysis of Thermal Balance of Diesel Engine and Identification of Scope for Waste Heat Recovery". *SAE Techinical Paper 2013-01-2744*, 2013.

[116] Yamaguchi T., Aoyagi Y., Uchida N., Fukunaga A., Kobayashi M., Adachi T. and Hashimoto M. "Fundamental Study of Waste Heat Recovery in the High Boosted 6-cylinder Heavy Duty Diesel Engine". *SAE Int. J. Mater. Manf.*, Vol. 8 n^o 2, 2015.

[117] Tauzia X. and Maiboom A. "Experimental study of an automotive Diesel engine efficiency when running under stoichiometric conditions". *Applied Energy*, Vol. 105, pp. 116–124, Mayo 2013.

[118] Olmeda P., Martin J., Garcia A. and Blanco D. "Evaluation of EGR Effect on the Global Energy Balance of a High Speed DI Diesel Engine". *SAE Papers*, Vol. 2016-01-06, 2016.

[119] Payri F., Martín J., Garcia A. and Carreño R. "Experimental and Theoretical Analysis of the Energy Balance in a DI Diesel Engine". *SAE Technical Paper 2015-01-1651*, 2015.

[120] Weberbauer F., Rauscher M., Kulzer A., Knopf M. and Bargende M. "Generally applicate split of losses for new combustion concepts". *MTZ worldwide*, Vol. 66 n^o 2, pp. 17–19, 2005.

[121] Thirouard M., Knop V. and Pacaud P. "Downsizing or cylinder number reduction in Diesel engines : effect of unit displacement on efficiency and emissions". In *THIESEL 2012 Conference on Thermo- and Fluid Dynamic Processes in Diesel Engines*, pp. 1–19, 2012.

[122] Thirouard M, Laget O and Zaccardi J.M. "An Innovative High Efficiency Diesel Combustion Concept with reduced Heat Loss". In *THIESEL 2016 Conference on Thermo- and Fluid Dynamic Processes in Direct Injection Engines*, pp. 1–16, 2016.

[123] Shibata G., Ishi K., Ushijima H., Shibaike Y., Ogawa H. and Foster D. "Optimization of Heat Release Shape and the Connecting Rod Crank Radius Ratio for Low Engine Noise and High Thermal Efficiency of Premixed Diesel Engine Combustion". *SAE Technical Paper*, 2015.

[124] Eriksson L. and Sivertsson M. "Computing Optimal Heat Release Rates in Combustion Engines". *SAE International Journal of Engines*, Vol. 8 n^o 3, pp. 2015–01–0882, 2015.

[125] Eriksson L. and Sivertsson M. "Calculation of Optimal Heat Release Rates under Constrained Conditions". *SAE Int. J. Engines*, 2016.

[126] Okamoto T. and Uchida N. "New Concept for Overcoming the Trade-Off between Thermal Efficiency, Each Loss and Exhaust Emissions in a Heavy Duty Diesel Engine". *SAE International Journal of Engines*, Vol. 9 n^o 2, pp. 2016–01–0729, 2016.

[127] Guardiola C., Climent H., Pla B. and Reig A. "Optimal Control as a method for Diesel engine efficiency assessment including pressure and NOx constraints". *Applied Thermal Engineering*, Vol. 117, pp. 452–461, 2017.

[128] Guardiola C., Pla B., García A. and Boronat V. "Optimal heat release shaping in a reactivity controlled compression ignition (RCCI) engine". *Control Theory and Tenchnology*, Vol. 15 n^o 2, pp. 117–128, 2017.

Chapter 3

Experimental and theoretical tools

Contents

3.1 Introduction

To perform the activities described in Chapters 4 and 5, some dedicated experimental installations along with modelling tools to reproduce the internal engine processes are required. On the one hand, complex installations are needed to perform accurate measurements. On the other hand, models strongly supported by physics are necessary to correctly reproduce the phenomena taking place in ICE under different operating conditions.

The core of the modelling work carried out in this work relies on a thermodynamic model developed in previous works [1–3], intended to calculate the gas conditions in the chamber and to reproduce the intake/exhaust processes and the phenomena involved. Additionally, a model aimed to reproduce the NO_x emissions and a statistical optimization tool coupled with the previously mentioned models were used in the present work.

Taking into account previous considerations, the first part of this chapter is focused on the complete description of the engines features, as well as the instrumentation of the facilities where the experimental work was carried out. Finally, the second part of this chapter deals with the description of the thermodynamic model, the NO_x emissions model and the optimization tool used in the present work.

3.2 Experimental installations

Two different engine configurations, sharing the geometry of the combustion chamber and the cylinder head, have been used in the present work. The first configuration is a 4-stroke, compression ignition, multicylinder, High Speed Direct Injection (HSDI) Diesel engine. This engine was used in the analysis of efficiency losses and in the theoretical optimization presented in Chapter 4 and in the swirl study shown in Chapter 5. The second engine is also a 4-stroke compression ignition engine, but in this case it is a single-cylinder version derived from the multicylinder one. In the next sections, the description of each experimental facility and their specific characteristics are presented.

3.2.1 Multicylinder engine

3.2.1.1 Engine architecture and hardware

Taking into account that the control and the thermal response of a production engine are really different than in a single-cylinder one used for research purposes [4], a multicylinder engine was selected to have an operation closer to the real automotive application in spite of the possible cylinder dispersion. Specifically, a production 4-cylinder engine calibrated for EURO 4 was chosen to perform most of the experimental work. Its main characteristics are summarized in the first column of Table 3.1.

	Multicylinder	**Single-cylinder**
Cylinders	4 in-line	1
Bore	90.4 mm	90.4 mm
Stroke	82 mm	82 mm
Unitary displacement	477 cm^3	477 cm^3
Compression ratio	17.5:1	17.1:1
Air management	Turbocharged	Screw compressor
Maximum power	110 kW at 4000 rpm	27.5 kW at 4000 rpm
Maximum torque	315 Nm at 2000 rpm	80 Nm at 2000 rpm
Combustion mode	CDC	CDC
Injection system	Bosch common rail (solenoid)	Bosch common rail (solenoid)
Valves per cylinder	4	4
Swirl Ratio range	1.4 - 3	0 - 5

Table 3.1. *Engines technical data.*

The DRIVVEN software was used for the engine control and data acquisition. This system control different combustion parameters, such as combustion phasing or duration, and some engine settings, such as the EGR valve position, VGT position, injection quantity and timing, and swirl and throttle valves, by modifying the required parameters. Thus, this tool works as a conventional control unit and, additionally, it is able to acquire, analyse and record different instantaneous signals from the engine (e.g., in-cylinder pressure, intake and exhaust pressures, rail pressure and the current clamp signal corresponding to the injection command).

This engine has 2 different intake ports, a tangential port that generates large scale swirl and a helical port, opposed to the previous one, that is aimed

at breaking this swirl motion. Additionally, the engine is equipped with a swirl valve located upstream of the helical port of each cylinder that allows varying the air distribution through both ports, thus changing the swirl ratio. Closing the valve gets decreases the air mass flow through the helical port, thus increasing the mass flow through the swirl generator port (tangential) with the consequent higher swirl ratio. The highest swirl level (SR=3) is reached when this valve is completely closed. On the contrary, when this valve is open, the air comes into the cylinder through both ports and the swirl motion promoted by the tangential one is reduced by the air flow coming through the opposed helical one, leading to the lowest swirl ratio (SR=1.4).

Additionally, to provide information for the lumped conductance model calibration and validation, 88 thermocouples were installed at different locations in the engine block and cylinder-head [5].

3.2.1.2 Test bench characteristics

Table 3.2 summarizes the complete test bench measuring equipment used in the multicylinder installation.

To have detailed information of the intake and exhaust gases thermodynamic conditions, several pressure and temperature sensors were located along all gases paths, as plotted in Figure 3.1.

The gas mean temperatures were measured using K-type thermocouples whilst the mean pressures were measured with piezo-resistive pressure transmitters. The measurement of the air mass flow was performed with an AVL Flowsonix Air while the injected fuel mass was measured with an AVL 733S Fuel meter and the blow-by leakage with an AVL blow-by meter. The exhaust emissions were analysed by means of an exhaust monitoring equipment (Horiba MEXA 7100 DEGR), which also allowed measuring the CO_2 concentration at intake manifold to determine the EGR rate [6].

The most important source of experimental information for the thermodynamic model is the in-cylinder pressure. To measure the pressure trace, 4 Kistler 6125C piezo-electric transducers were installed in the glow plug hole of each cylinder. The signal provided by each sensor with a resolution of 0.5° was conditioned with a Kistler 5011B amplifier and then collected by DRIVVEN. Considering the importance of the accurate measurement of the in-cylinder pressure, the acquisition chain was calibrated prior to the experimental test campaign according to the manufacturer calibration methodology.

Additionally, the original coolant and oil circuits were adapted and instrumented to measure the mass flows and temperatures necessary to

Variable	Equipment	Range	Accuracy[1]
Speed	Dynamometer	6000 rpm	0.03% fs.
Torque	Dynamometer	±450 Nm	0.05% fs.
Cylinder pressure	Kistler 6125C	0-250 bar	0.3% lin.
Amplifier	Kistler 5011B	± 10 V	-
Air flow	AVL Flowsonix Air	20 to 720 kg/h	2%
Fuel flow	AVL 733S Fuel meter	0-150 kg/h	0.2%
Blow-by flow	AVL blow-by Meter	1.5-75 l/min	1.5%
Temperature	K-type Thermocouples	-200 to 1250 °C	1.5 °C
	PT100 RTD	-200 to 850 °C	0.2°C
Mean pressure	Kistler Piezo-resistive	0-10 bar	0.1-0.2% lin.
	Transmitters		
Gases analysis	Horiba mexa		1-4% fs.
	7100 DEGR		
Coolant flow	Krohne 4010 Optiflux	±12 m/s	0.5%
Fuel cooler	Yoko Admag	0-10 m/s	0.5%
	AE208MG		

Table 3.2. *Multicylinder test bench instrumentation.*

determine the heat rejection to the coolant, oil and intercooler independently, as shown in Figure 3.2. Taking into account that the temperature drop in the coolers was expected to be small, the temperatures along the liquid lines were measured with RTDs due to their higher accuracy (±0.2°C) in comparison with K-type thermocouples (±1.5°C). Furthermore, several Proportional-Integral-Derivative controllers (PID) along with their corresponding valves were installed in the water supply lines of the coolant, oil, air and fuel coolers to ensure the engine thermal stability.

To ensure a stable thermal behaviour of the engine, stabilization periods between 20 and 40 minutes were required before measuring. It was assumed that thermal stabilization was reached when the temperature variation rate of all the liquids (coolant, cooling water and oil) was lower than 1ºC/min. The thermal stabilization was evaluated in the liquids instead of the material because liquids reach their thermal stabilization later than engine material

[1] fs. means full scale. and lin. means linearity.

due to the higher thermal inertia and the high thermal diffusivity of the metal. Thus, when the liquid stabilization was reached, the metal temperature was also stable.

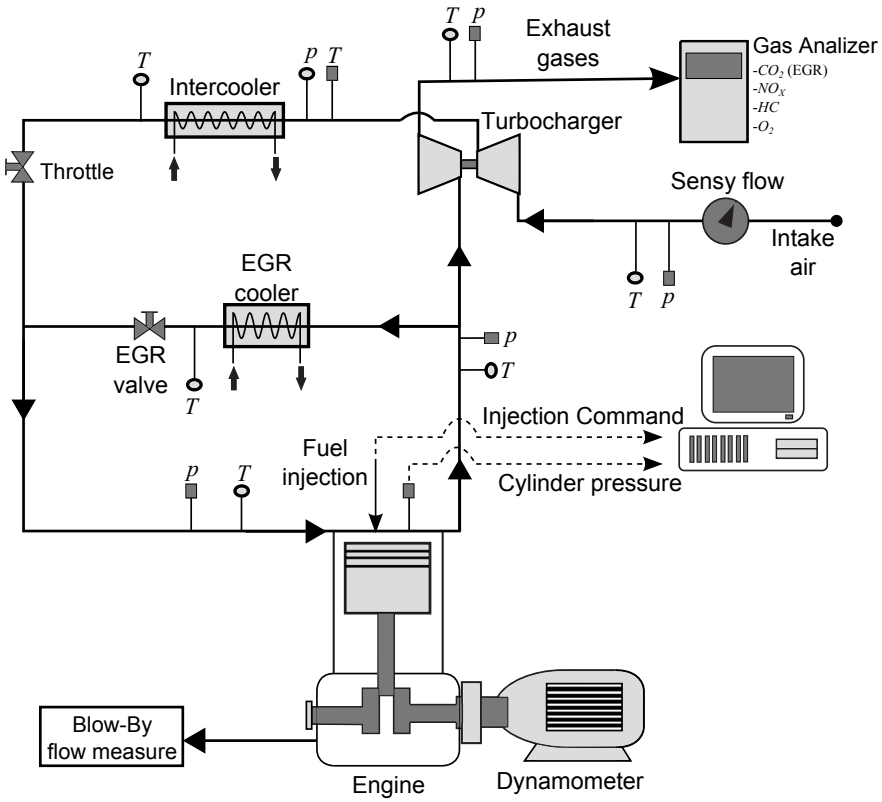

Figure 3.1. *Scheme of the gas lines instrumentation of the multicylinder engine.*

An in-house developed software called SAMARUC was used for the acquisition of the low-frequency signals (mass flows, mean pressures and temperatures) and for visualizing the engine operating parameters and controlling the operating conditions. The sensors signals were collected and processed by a PXI platform excepting the RTD signals, which were registered by means of a Datalogger 34972A LXI data acquisition system.

3.2.2 Single-cylinder engine

To avoid any possible cylinder-to-cylinder dispersion in air and/or fuel throughout the injection settings study presented in Chapter 5, the

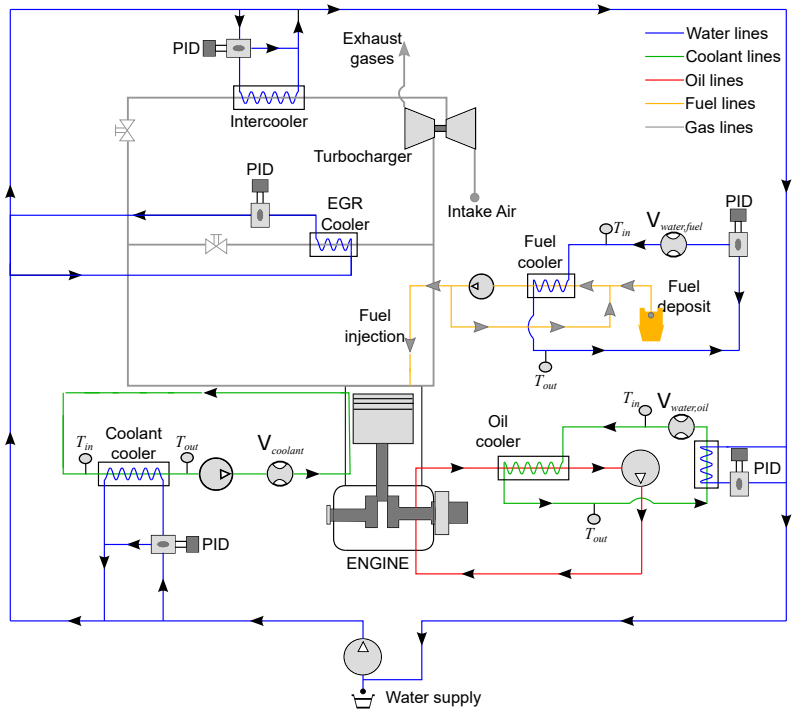

Figure 3.2. *Scheme of the cooling, lubricating and injection lines instrumentation of the multicylinder engine.*

experimental work in that study was performed in a single-cylinder engine version of the multicylinder one. In the next sections, the engine architecture and the test bench facility are described.

3.2.2.1 Engine architecture and hardware

The single-cylinder engine was derived from the multicylinder one and, therefore, they shared the main characteristics as shown in Table 3.1. The geometry of its combustion chamber was exactly the same as the multicylinder engine but the compression ratio was a bit lower (17.5 to 17.1) due to a deviation in its manufacturing process. The cylinder head was also maintained from the multicylinder configuration.

Additionally, this engine was equipped with an additional swirl valve in the tangential port in order to achieve SR conditions below to 1. The combination of the two valves located in both tangential and helical ports, led to achieve

a SR variation (from almost 0 up to 5), wider than the achieved in the multicylinder engine (from 1.4 up to 3), thus giving the single-cylinder engine more swirl versatility.

3.2.2.2 Test bench characteristics

The single-cylinder engine was assembled into a fully instrumented test cell, shown in Figure 3.3. The measuring equipment is summarized in Table 3.3.

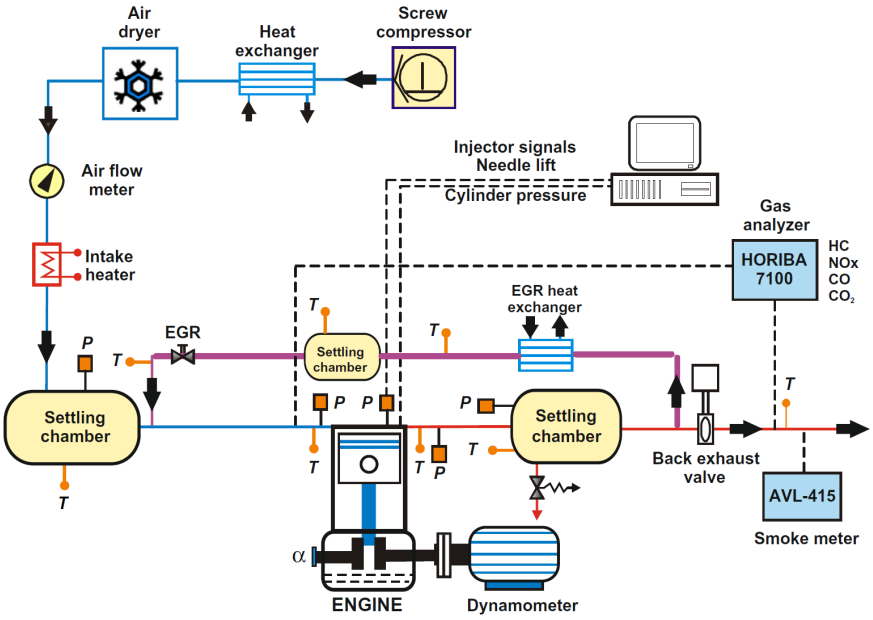

Figure 3.3. *Single-cylinder test cell scheme. Source: [7].*

The engine was fed with the compressed air provided by an external compressor that, after passing through an air dryer system to control the relative humidity of the air, allowed reaching the boost pressure required at each operating point. A throttle valve located at the exhaust line (after the exhaust settling chamber) was used to simulate the back-pressure that the turbine would produce in the multicylinder engine. The experimental cell also included a high pressure EGR system. Water and oil cooling circuits were also independent from the engine, and their temperatures were strictly controlled and monitored during all the tests. The fuel consumption of the engine was measured with a gravimetric dynamic fuel meter.

Variable	Equipment	Range	Accuracy[2]
Speed	Dynamometer	7000 rpm	0.006% fs.
Torque	Dynamometer	±450 Nm	0.1% fs.
Cylinder pressure	Kistler 6125C	0-250 bar	0.5% lin.
Amplifier	Kistler 5011B	± 10 V	-
Air flow	Elster RVG65	0.6-100 m^3/h	1%
Fuel flow	AVL 733S	0-75 kg/h	0.12%
Blow-by flow	AVL blow-by meter	1.5-75 l/min	1.5%
Temperature	K-type Thermocouples	-200-1250 °C	1.5 °C
	PT100 RTD	-200 to 850 °C	0.2°C
Mean pressure	Kistler Piezo-resistive	0-10 bar	0.1-0.2% lin.
	Transmitters		
Gases analysis	Horiba mexa	-	1-4% fs.
	7100 DEGR		
Smoke	AVL 415	0-10 FSN	2%

Table 3.3. *Single-cylinder test bench instrumentation.*

The injection settings control was performed by using the same commercial controller system - DRIVVEN - as in the multicylinder engine. This tool acted as a conventional control unit which allowed the user to change the fuel injection settings such as the rail pressure and the position and energizing times of up to five injection events.

The most relevant mean variables of the test cell and engine, pollutant emissions, and low frequency signals were recorded using the same in-house developed software (SAMARUC) as in the multicylinder engine installation. The high-frequency signals such as the in-cylinder pressure, intake and exhaust pressures, injector signal and rail pressure were acquired using a Yokogawa DL708E Oscillographic recorder synchronized with an optical angular encoder with a resolution of 0.5°. The in-cylinder pressure was measured by means of a Kistler 6125C piezoelectric sensor coupled to an amplifier Kistler 5011B to condition the signal.

[2]fs. means full scale. and lin. means linearity.

3.3 Theoretical tools

3.3.1 Thermodynamic tools

This section is dedicated to the comprehensive explanation of the base model used to estimate the thermodynamic processes within the combustion chamber by solving the 1^{st} law of thermodynamics. This thermodynamic model, which was developed internally in previous works [1–3, 8, 9], is the core of the theoretical tools used in the work. It can be used for two complimentary purposes that share the same sub-models and thermodynamic hypothesis as shown in Figure 3.4.

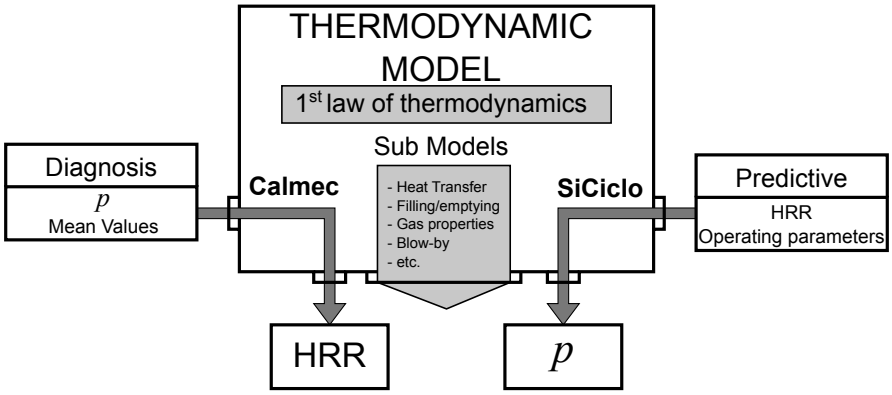

Figure 3.4. *Scheme of the thermodynamic model. Source: [3].*

On the one hand, the combustion diagnosis approach allows to calculate the HRR using the instantaneous in-cylinder pressure as main input along with other variables that characterize the engine operation. The name of the in-house developed tool aimed to perform such analysis is Calmec. On the other hand, the complimentary approach predicts the in-cylinder pressure based on the combustion law and some other representative variables of the operating condition. This tool was also developed internally and its name is SiCiclo.

Even though the main objective of this model is the calculation of the in-cylinder gas conditions, it also includes some sub-models intended to reproduce the intake/exhaust processes and the phenomena involved (HT in the chamber and ports, mass flows, etc.). This model was originally defined by Tinaut [10] and Armas [1], who stated the basic hypothesis and proposed the initial required sub-models. The model was improved by Martín [2], who

introduced several sub-model upgrades to achieve better accuracy on the HRR and heat fluxes determination in Calmec, and included all the sub-models in the predictive tool SiCiclo [11]. Finally, Carreño [3] further improved the uncertainties adjustment used during the engine characterization and the heat transfer and mechanical losses models.

The hypothesis and simplifications assumed to solve the first law of thermodynamics in the combustion chamber are the following [3]:

1. **The combustion chamber is considered an open system**. This assumption is made in both, open cycle[3] (due to the flows through the intake/exhaust valves) and closed cycle[4] (due to injection and blow-by).

2. **Chamber pressure is uniform in the chamber**. This is usually assumed in combustion calculations because both fluid and flame velocities are much smaller than the speed of sound [12].

3. **Three species are considered in the chamber**: air, fuel vapour and stoichiometric combustion products. In a DI Diesel engine operating with CDC, the flame front is located at the stoichiometric fuel-air ratio region during the mixing-controlled burning phase, thus this hypothesis is suitable. In the case of PPC, this hypothesis is not completely accurate; however, to take into account the particular characteristics of the mixture process requires complex mixing-combustion models, which are out of the scope of this work.

4. **Perfect gas behaviour is assumed**. As reported by Lapuerta et al. [13], the error by considering perfect gas inside the chamber is negligible, thus this assumption is suitable for the application presented in this work.

5. **Specific heats depend on temperature and gas composition**. The value of the specific heat is highly dependent on temperature and gas composition. Taking into account that at high load the mean gas temperature can range between 80°C at IVO up to 1800°C at TDC, and that the fuel injection and combustion change the charge composition, this hypothesis is useful to improve accuracy and is consistent with the the hypotheses 3 and 4.

[3] Open cycle is defined as the engine operation when at least one of the valves is open, i.e. between EVO and IVC.

[4] Closed cycle is defined as the engine operation when all valves are closed, i.e. between IVC and EVO.

6. **Internal energy is calculated assuming mean uniform temperature within the chamber**. This is the most uncertain hypothesis assumed, taking into account that the calculation of the gas internal energy depends on the temperature. This can be especially important for the burned products at the beginning of the combustion; however, the error diminishes as the combustion advances because the dilution and the heat transfer tend to make the temperature uniform.

7. **Convective heat transfer to the chamber walls is considered**. As stated in Chapter 2.2.2, the cooling losses in conventional ICEs (mostly due to HT to the chamber walls) can range between 15% $\dot{m}_f H_v$ and 40% $\dot{m}_f H_v$; therefore, HT is a key topic in this work. Radiation is not considered explicitly due to its low relative weight, usually lower than 1% $\dot{m}_f H_v$ [14].

8. **Deformation of the engine mechanism is assumed**. The engine mechanism (i.e. piston, connecting rod and crankshaft) undergoes mechanical deformations due to high pressure and the inertial loads.

The combination of these basic hypotheses with some specific sub-models, briefly described in next paragraphs, allows calculating all terms of the in-cylinder energy balance, in order to obtain the gas state during open and closed cycle and the HRR or in-cylinder pressure. Even though these sub-models are thoroughly explained in [2, 3], a brief explanation of them is given below:

- The engine filling and emptying model [15] is a simple model of the complete engine, which describes the physical processes taking place during the intake-exhaust strokes (between EVO and IVC).

- A combustion chamber mass balance taking into account the fresh air mass, the EGR mass, the residual mass, the short circuit mass and the blow-by mass is performed step by step in order to calculate accurately the instantaneous evolution of the in-cylinder trapped mass.

- The energy balance during closed cycle is calculated by solving the first law of thermodynamics in an open system. The objective is to obtain either the combustion law or the in-cylinder pressure (see Figure 3.4) considering all energy terms involved in the chamber. The final equation solved in the thermodynamic model (once developed as explained in [2, 3]) is the following:

$$\mathrm{dHR} = \mathrm{m_c\ c_{v,c}\ dT + dQ + p\ dV - (h_{f,inj} - u_{f,g})\ dm_{f,ev} + R\ T\ dm_{bb}} \quad (3.1)$$

where dHR is the heat released by combustion in a calculation step[5] and the terms in the right-hand side are, from left to right, the variation of the sensible internal energy of the gas, the heat transfer to the walls, the work done by the gas, the energy required for fuel injection, evaporation and heating (details of its determination can be found in [2]), and finally, the flow work associated with the blow-by leakage.

- The HT from gases to the combustion chamber walls is calculated using two coupled models. The first one is based on the well-known Woschni proposal [16, 17], in which the HT from the gases to the combustion chamber walls is determined from the engine geometry, thermodynamic properties of the gas (p and T) and some operating conditions. The complete modified model is thoroughly described in [3] and the equation of the convective heat transfer coefficient is the following:

$$h = CD^{-0.2}p^{0.8}T^{-0.546}\left[C_{W1}c_m + C_{W2}c_u + C_2\frac{V_d T_{IVC}}{V_{IVC}p_{IVC}}(p - p_0)\right]^{0.8} \quad (3.2)$$

where C and C_2 are constants with values 0.12 and 0.001 respectively, D is the cylinder diameter, p and T are the in-cylinder instantaneous pressure and gas mean temperature respectively, c_m is the mean piston speed, c_u is the instantaneous tangential velocity of the gas in the chamber (see [18] for a detailed description of this term), p_0 is the pressure in motoring conditions assuming a polytropic evolution, C_{W1} and C_{W2} are constants to be adjusted; V_d is the displaced volume and T_{IVC}, V_{IVC} and p_{IVC} are the temperature, volume and pressure respectively at the intake valve closing.

Besides, a proper HT determination by means of the Woschni model requires an accurate wall temperature estimation. Therefore, the second model is a lumped conductance model [9, 19, 20] that estimates the wall temperatures and the detailed HT repartition to the coolant and oil. In this way, HT and lumped models work together to provide an accurate estimation of the HT.

[5] The HRR can be obtained directly by dividing dHR by the angle step, HRR = dHR/dα.

- An injection rate model is implemented to calculate accurately the mass balance, gas composition and energy balance. Depending on the available information, it can be estimated using the injection settings provided by the ECU, the injection command or the needle lift signal.

- The accurate prediction of the instantaneous blow-by mass leakage is needed to accurately estimate the instantaneous in-cylinder mass. This flow is modelled based on the equation of the adiabatic flow nozzle [21] improved by Carreño in [3].

- A mechanical deformations model allows taking into account the deformation of the combustion chamber due to the high in-cylinder pressures and inertia of elements in motion. Therefore, the thermodynamic model includes a sub-model [2] that calculates this phenomenon.

3.3.1.1 Calibration

To perform a precise combustion diagnosis and pressure prediction it is necessary to reduce the uncertainty on the determination of some parameters that affect the in-cylinder calculations. Such parameters are the following:

- Pressure pegging: since the in-cylinder pressure is measured using piezoelectric sensors, they do not provide an absolute pressure value but a pressure variation. Thus, a correct pressure pegging is necessary in the combustion diagnosis analysis, where the in-cylinder pressure is the main source of information.

- Compression ratio. It affects the instantaneous volume calculation and hence the gas temperature. An accurate value is necessary in order to perform a good estimation of the gas properties.

- Engine deformations. It also affects the instantaneous volume calculation but to a lower extent than the compression ratio.

- Heat transfer model fitting. The adjustment of the coefficients of the HT model (C_{W1} and C_{W2}) is important in order to calculate accurately the heat transfer to the combustion chamber walls.

- TDC position. The determination of the TDC has a great impact on the p-V diagram, thus affecting the indicated power calculation.

The determination of the last 4 parameters is carried out by means of a procedure called *"engine characterization"*. Even though the methodology followed to calibrate these uncertainties is thoroughly detailed in [3], a brief explanation is included in this section. This calibration is carried out in motoring conditions and it is split in three main phases as can be seen in Figure 3.5 and summarized below:

1. First, the compression ratio and the deformation and heat transfer models are calibrated.
2. Then, taking into account the models calibrated in the first step, the TDC position is calculated using the Hohenberg's proposal [22].
3. Finally, it is necessary to adjust the pressure pegging at each test.

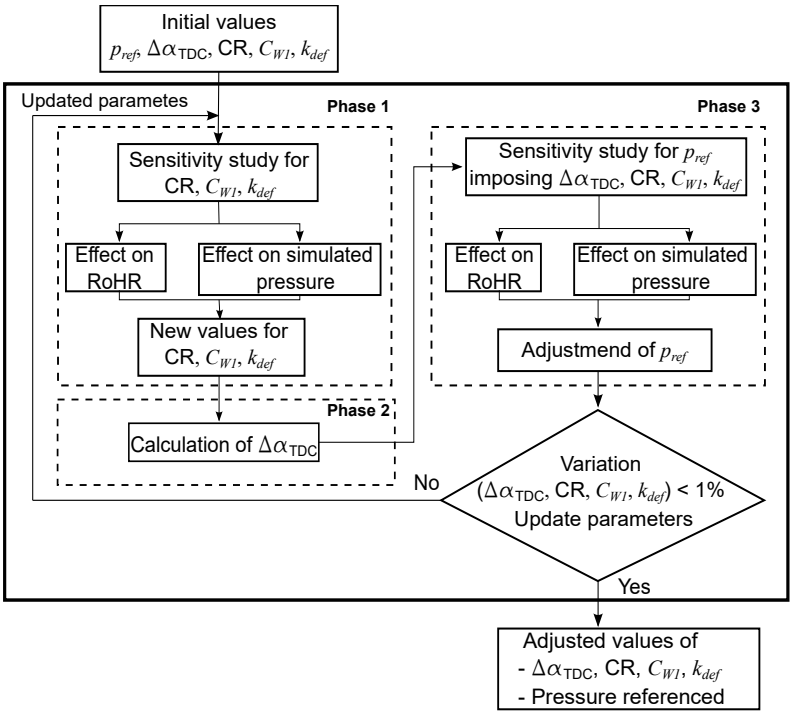

Figure 3.5. *Engine characterization. Source: [3].*

The calibration in the first and last steps can be summarised as follows. Starting from a reference set of values, a sensitivity study to determine the effect of each uncertainty during the closed cycle is carried out. The effect of

each uncertainty is assessed in terms of the uncertainty on HRR in the first step (it should be zero since there is no fuel injection in motoring conditions) and in the comparison between simulated and experimental in-cylinder pressures in the last step.

Then, knowing the contribution of each uncertainty to the error, a minimization of the difference between the real and simulated pressures and the HRR residuals is carried out using a Multiple Linear Regression [23]. The result of this characterization is a set of adjusted values of compression ratio, engine deformation, heat transfer constants, TDC position and pressure pegging that minimize the error.

The results of these parameters in the two studied engines are summarized in Table 3.4. As can be seen, the CR was a bit lower in the single-cylinder case, the deformation constant was similar and the heat transfer constants were slightly similar, with a lower impact of SR (C_{W2}) on heat transfer in the single-cylinder engine case.

Engine	Cylinder	CR	TDC_{pos}	k_{def}	C_{W1}	C_{W2}
Multicylinder	1	17.4	357.3	1.6	0.85	0.29
Multicylinder	2	17.3	177.3	1.6	0.85	0.29
Multicylinder	3	17.5	537.3	1.6	0.85	0.29
Multicylinder	4	17.7	717.3	1.6	0.85	0.29
Single-cylinder	1	17.1	243.75	1.8	1	0.25

Table 3.4. *Engines characterization.*

3.3.1.2 Validation

In this section, the validation of the thermodynamic model is performed comparing the evolution of the in-cylinder pressure and the GIE of some experimental points versus those modelled by the predictive tool. In the first case, the experimental (solid lines) and modelled (dashed lines) in-cylinder pressures are compared in Figure 3.6 at four different operating conditions (engine speed 1500 and 3500 rpm and bmep around 3 and 14 bar). As can be observed, the evolution of the experimental in-cylinder pressure is well followed by the model and only some little discrepancies can be discerned.

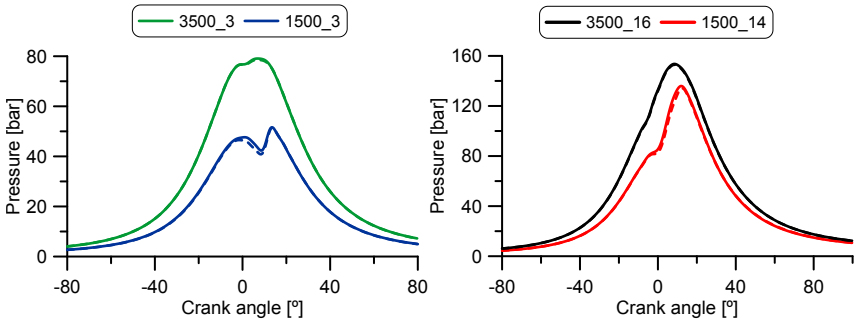

Figure 3.6. *Experimental and modelled in-cylinder pressure of various operating points in the multicylinder engine.*

In any case, the accuracy of the model is high as can be seen in Figure 3.7, where the comparison between experimental and modelled GIE is presented at different operating conditions covering the whole engine map. As can be seen, the error of the model is very low with an average of 0.1% $\dot{m}_f H_v$ and a maximum error of 0.3% $\dot{m}_f H_v$. Therefore, it can be concluded that the model is good enough to reproduce in-cylinder conditions in the present work.

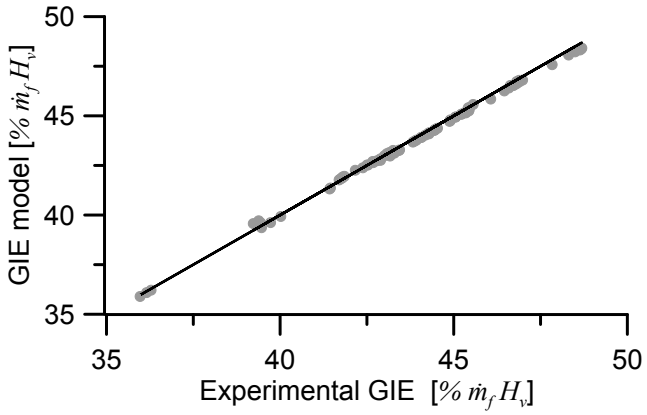

Figure 3.7. *Experimental and modelled GIE.*

3.3.2 NO_x emissions model

Since thermal formation is responsible of most NO_x emissions in Diesel combustion and it takes place at high temperatures and equivalence ratios close to 1, it can be stated that in CDC the majority of NO_x emissions are produced in the flame front area. Thus, the NO_x model used in this study is based on the calculation of the thermal NO_x formation described firstly by Zeldovich [24] and later extended by Bowman [25] in a modified-Zeldovich mechanism. Specifically, the model used in this work was proposed by Arrègle *et al.* [26] and improved some years later in [27, 28].

According to the referred model, the thermal NO_x production during the combustion event can be calculated as follows:

$$NO_x{}^{th} = \int_{SOC}^{EOC} k_f \; HRR \; e^{\frac{-k_{act}}{T_{ad}+\Delta T(n,N)}} \; d\alpha \tag{3.3}$$

where k_f represents the proportionality between the HRR(α) and the amount of reactants passing through the flame and k_{act} is a constant to model the NO_x reaction rate with an Arrhenius-like correlation depending on the temperature of the reactants. This temperature, as can be seen in the equation, is estimated as the adiabatic temperature (T_{ad}) with a correction depending on the engine speed and load ($\Delta T(n, N)$).

The HRR used in this model can be obtained either experimentally, using the combustion diagnosis model calculation, or imposed, as an input of the predictive model. Differently, the adiabatic temperature is always calculated following the methodology presented in [27, 28] with the in-cylinder pressure being the main input.

Additionally, the model takes into account the NO_x reduction produced when NO_x molecules re-entrain into the flame. It is considered that all NO_x re-entrained into the flame coming from either recirculated EGR or the current cycle is completely reduced. Once this phenomenon is considered, the NO_x concentration at the exhaust is given by the following equation:

$$Y_{NO_{x,exh}} = \frac{NO_x{}^{th}(1 - F_r K_{re} \epsilon)}{m_{air} + m_{fuel} + m_{EGR} F_r \epsilon} \tag{3.4}$$

where F_r is the relative fuel to air ratio, K_{re} represents the ratio between the re-entrained NO_x and the total amount produced, and ϵ stands for the efficiency of the re-entrained NO_x reduction (0.5 and 1 respectively as proposed in [27, 28]).

Finally, although the thermal formation mechanism is the most representative one on Diesel combustion, prompt [29] and via N_2O [30] mechanisms are also important at low temperature combustions [31]. Thus, a correction based on the maximum adiabatic flame temperature is applied to the calculation of the thermal NO_x formation. A potential function ranging from 1 at high flame temperature to almost 0 at low oxygen concentration, where thermal NO_x formation is negligible, was fitted for cycles with low adiabatic flame temperatures [28]:

$$K\left(T_{ad,max}\right) = \frac{{NO_X}^{th}}{{NO_X}^{total}} = \left(m\left(T_{ad,max} - T_0\right)\right)^n \tag{3.5}$$

being $T_{ad,max}$ the maximum adiabatic temperature reached in the considered cycle, T_0 the initial temperature from which NO_x thermal formation starts; and m and n constants to adjust the potential function.

3.3.2.1 Calibration

Due to the high dependency of NO_x formation on local phenomena such as the flame front location, the model needs to be calibrated in every engine to achieve good accuracy. The calibration was divided in two steps: first, tests with high adiabatic flame temperature were used to characterize the thermal NO_x formation mechanism and, finally, tests with low adiabatic flame temperature were employed to fit the correction over the thermal NO_x production. The calibration was carried out using 34 operating conditions, represented in dots in Figure 3.8, that cover the whole engine map.

As commented before, the first part of the calibration deals with the calculation of the reaction temperature correction using operating conditions with maximum adiabatic temperatures beyond 2700 K. This temperature correction, aimed to capture the diffusive flame characteristics, is plotted in Figure 3.8, where it can be seen that it ranges from -70 K to -200 K. As can be seen, the reduction increases as load is reduced and engine speed is augmented excepting at very low engine speed.

On the other hand, the second part of the calibration was intended to estimate the NO_x formation through other mechanisms than the thermal one at low adiabatic flame temperatures. This correction as a function of the adiabatic temperature is plotted in Figure 3.9, where it can be seen that at some low load points with EGR rates around 35%, the thermal mechanism represents only about 50% of the total NO_x production. Due to the low number of points below this temperature, it was decided to keep the same shape of

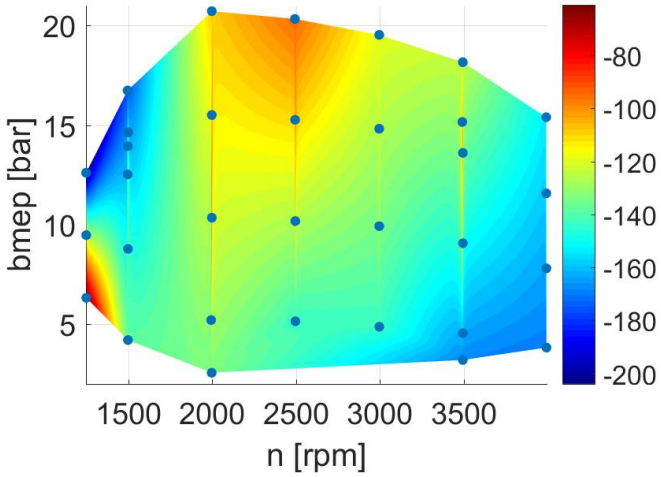

Figure 3.8. *Temperature reaction correction map.*

the calibration curve than in the work where this calibration methodology was developed [28]. As shown, with adiabatic temperatures higher than 2700 K this correction is around 1 due to the previous calibration.

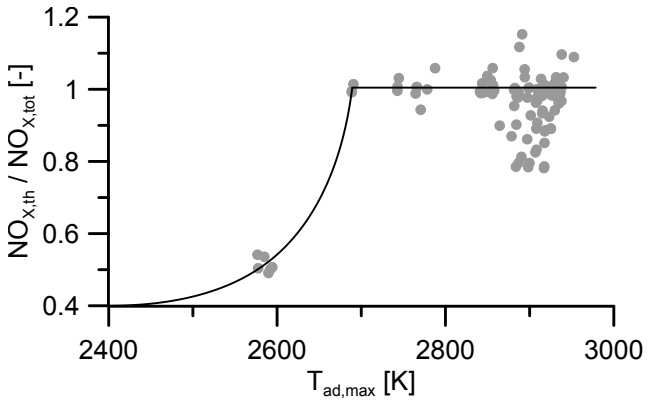

Figure 3.9. *Thermal* NO_x *and NOx measured ratio as a function of the maximum adiabatic flame temperature.*

3.3.2.2 Validation

The NO_x model was validated over 100 points covering the whole range of the engine map. Figure 3.10 shows the comparison between modelled and experimental NO_x emissions in the validation tests, resulting in a mean error of around 11%. Taking into account that errors resulting from other works are in the same range [27, 28], it can be concluded that the accuracy of the model is reasonably good.

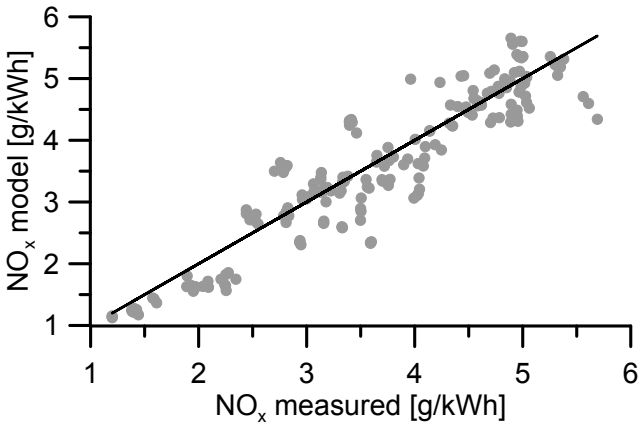

Figure 3.10. *Experimental and modelled* NO_x *emissions.*

3.3.3 Optimization tool

The methodology followed during the theoretical optimization presented in Chapter 4 is based on genetic algorithms (GA). Genetic algorithms, developed by John Holland [32] in the 1960s, are heuristic search methods used for finding optimized solutions based on the theory of natural selection and evolutionary biology. Basically, they search for the best combination of a set of inputs in order to optimize a fitness function defined by either one objective (single objective optimization) or several ones (multiobjective optimization). The general steps followed by a genetic algorithm are summarized in Figure 3.11 and defined here using the definition given by Mitchell [33]:

1. Initialization. A set of designs representative of the design space is chosen as initial population. A correct selection of the number of

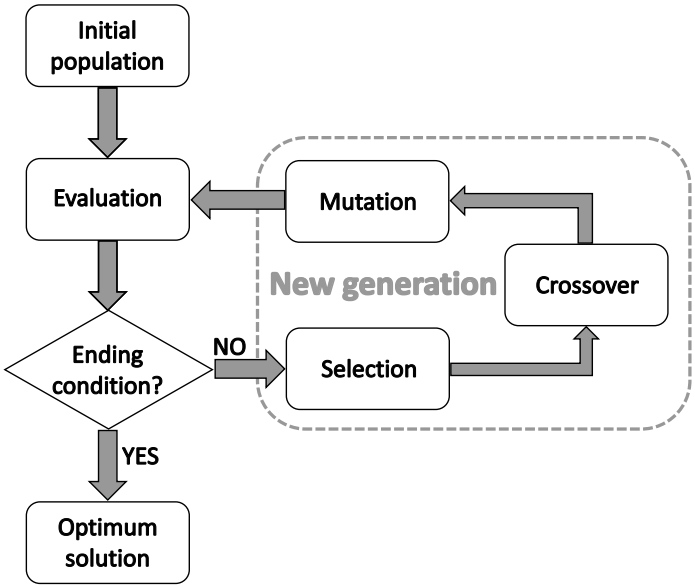

Figure 3.11. *Methodology followed by the genetic algorithm.*

combinations and the methodology followed to generate this initial population is a key issue to avoid that either the algorithm lead to poor solutions [34] or it expend more computation time in finding the optimum solution. The size of this initial population defines also the size of the next generations. There are different approaches to generate it (randomly, incremental space filler (ISF), Sobol algorithm [35] ...).

2. Evaluation. The available combinations are assessed in terms of the fitness function of the problem.

3. It is checked whether or not the end of the optimization has been reached. Normally it is defined by setting a maximum number of generations although other criteria such a maximum calculation time, the convergence between generations or even a manual stop can be used to define the final generation. If the ending criteria is reached the optimization finishes here, if not a new generation with the same size than the initial one is proposed following a certain genetic approach that uses the following operators:

- Selection. This operator selects the best combinations of inputs for reproduction in terms of the fitness function. The fitter the combination, the more times it is likely to be selected to reproduce.
- Crossover. It consists of two designs of the parent generation exchanging their genetic material to form a new design in the next generation.
- Random mutation of new offspring. This operator randomly modifies the genetic material of a design to create a new design in the next generation.

4. Go to step 2.

3.3.3.1 Setting up the problem

Once the general steps of a genetic algorithm have been explained, the definition of the study problem along with the specific characteristics of the GA used to solve it are detailed here. The main objective of the optimization was to find the best combustion that either maximized gross indicated efficiency (first cases) or maximized gross indicated efficiency while minimizing NO_x emissions (final optimization).

The first step was the selection of the factors to optimize. Since the objective was to give total freedom to the HRR shape, the input factors were the result of splitting the non dimensional HRR into 8 sectors (16 inputs). Every time that the optimization algorithm proposed a set of inputs, they were interpolated and converted into a continuous HRR that was evaluated by the predicting tool and the NO_x model and its results were returned back as feedback for the algorithm. When the optimization was finished, the optimum set of inputs were translated into the optimum HRR that optimized the defined problem.

On the other hand, the characteristics of the genetic algorithm were the following. First of all, the initial population was created following a Sobol algorithm [35] (Monte Carlo numerical method) that generates samples to fill the design space in a uniform way. A sensitivity analysis of the size of this initial population was performed to obtain the best compromise between accuracy and calculation time, resulting in 125 designs as the optimum value.

The specific genetic algorithm used to create new generations was the Non-dominated Sorting Genetic Algorithm for Multi-Objective Optimization (NSGA-II) [36] that uses both crossover and mutation to obtain individuals with better characteristics than the parents and to inhibit the premature

convergence in local maximum/minimum. The occurrence probability of these two parameters was set to 1 and 0.9 out of 1 respectively, which means that it was likely that both variations occur. Finally, the termination criterion was established by a maximum number of generations. After some parametric studies, it was concluded that beyond the 50^{th} generation the optimum combustion did not change and thus the convergence was ensured beyond this point, therefore the maximum number of generations was set to 56 to give a little margin.

Bibliography

[1] Armas O. *Diagnóstico experimental del proceso de combustión en motores Diesel de inyección directa.* Servicio de Publicaciones UPV, ISBN 84-7721-772-X, Valencia, 1999.

[2] Martín J. *Diagnóstico de la combustión en motores de Diesel de inyección directa.* Reverté, ISBN 978-84-291-4717-9, Barcelona, 2012.

[3] Carreño R. *A comprehensive methodology to analyse the Global Energy Balance in Reciprocating Internal Combustion Engines.* Doctoral Thesis, 2016.

[4] Torregrosa A.J., Olmeda P., Martín J. and Degraeuwe B. "Experiments on the influence of inlet charge and coolant temperature on performance and emissions of a DI Diesel engine". *Experimental Thermal and Fluid Science*, Vol. 30 n^o 7, pp. 633–641, 2006.

[5] Broatch A., Olmeda P., García A. and Salvador-Iborra J. "Impact of swirl on in-cylinder heat transfer in a light-duty diesel engine". *Energy*, Vol. 119, pp. 1010–1023, 2017.

[6] Bermúdez V., Lujan J.M., Pla B. and Linares W.G. "Effects of low pressure exhaust gas recirculation on regulated and unregulated gaseous emissions during NEDC in a light-duty diesel engine". *Energy*, Vol. 36 n^o 9, pp. 5655–5665, 2011.

[7] Benajes J., Martín J., García A., Villalta D. and Warey A. "Swirl ratio and post injection strategies to improve late cycle diffusion combustion in a light-duty diesel engine". *Applied Thermal Engineering*, Vol. 123, pp. 365–376, 2017.

[8] Benajes J., Olmeda P., Martín J. and Carreño R. "A new methodology for uncertainties characterization in combustion diagnosis and thermodynamic modelling". *Applied Thermal Engineering*, Vol. 71, pp. 389–399, 2014.

[9] Payri F., Olmeda P., Martín J. and Carreño R. "A New Tool to Perform Global Energy Balances in DI Diesel Engines". *SAE Int. J. Engines*, Vol. 7 n^o 1, pp. 43–59, 2014.

[10] Tinaut F. *Contribución al estudio del proceso de combustión en motores de encendido por compresión de inyección directa.* Doctoral Thesis, Universidad Politécnica de Valencia, 1986.

[11] Payri F., Olmeda P., Martín J. and García A. "A complete 0D thermodynamic predictive model for direct injection diesel engines". *Applied Energy*, Vol. 88 n^o 12, pp. 4632–4641, Diciembre 2011.

[12] Williams F. *Combustion Theory.* The Benjamin/Cummings Publishing Co, ISBN 978-0201407778, 1985.

[13] Lapuerta M., Ballesteros R. and Agudelo J. "Effect of the gas state equation on the thermodynamic diagnostic of diesel combustion". *Applied Thermal Engineering*, Vol. 26 n^o 14-15, pp. 1492–1499, Octubre 2006.

[14] Benajes J., Martín J., García A., Villalta D. and Warey A. "In-cylinder soot radiation heat transfer in direct-injection diesel engines". *Energy Conversion and Management*, Vol. 106, pp. 414–427, 2015.

[15] Payri F., Galindo J., Martín J. and Arnau F.J. "A Simple Model for Predicting the Trapped Mass in a DI Diesel Engine". *SAE Techinical Paper 2007-01-0494*, 2007.

[16] Woschni G. "A Universally Applicable Equation for the Instantaneous Heat Transfer Coefficient in the Internal Combustion Engine". *SAE Technical Paper 670931*, 1967.

[17] Woschni G. "Die Berechnung der Wandverluste und der thermischen Belastung der Bauteile von Dieselmotoren.". *MTZ*, Vol. 31 n^o 12, pp. 491–499, 1970.

[18] Payri F., Margot X., Gil A. and Martín J. "Computational Study of Heat Transfer to the Walls of a DI Diesel Engine". *SAE Technical paper 2005-01-0210*, Abril 2005.

[19] Torregrosa A.J., Olmeda P., Degraeuwe B. and Reyes M. "A concise wall temperature model for DI Diesel engines". *Applied Thermal Engineering*, Vol. 26 n^o 11-12, pp. 1320–1327, Agosto 2006.

[20] Torregrosa A.J., Broatch A., Olmeda P. and Martín J. "A contribution to film coefficient estimation in piston cooling galleries". *Experimental Thermal and Fluid Science*, Vol. 34 n^o 2, pp. 142–151, Febrero 2010.

[21] Aghdam E.A. and Kabir M.M. "Validation of a blowby model using experimental results in motoring condition with the change of compression ratio and engine speed". *Experimental Thermal and Fluid Science*, Vol. 34 n^o 2, pp. 197–209, Febrero 2010.

[22] Hohenberg G. "Definition und Eigenschaften des thermodynamischen Verlustwinkels von Kolbenmaschinen". *Automobil-Industrie*, Vol. 4, pp. 15–21, 1976.

[23] Weisberg S. *Applied Linear Regressions.* John Wiley & Sons, ISBN 0-471-66379-4, 3rd edition, 2005.

[24] Zeldovich J. "The Oxidation of Nitrogen on Combustion and Explosions". *European Physical Journal A. Hadrons and Nuclei*, Vol. 21, pp. 577–628, 1946.

[25] Bowman C.T. "Kinetics of pollutant formation and destruction in combustion". *Progress in Energy and Combustion Science*, Vol. 1 n^o 1, pp. 33 – 45, 1975.

[26] Arrègle J., López J.J., Guardiola C. and Monin C. "Sensitivity study of a NOx estimation model for on-board applications". *SAE Technical Paper 2008-01-0640*, 2008.

[27] Guardiola C., López J.J., Martín J. and García-Sarmiento D. "Semiempirical in-cylinder pressure based model for NOX prediction oriented to control applications". *Applied Thermal Engineering*, Vol. 31 n^o 16, pp. 3275–3286, 2011.

[28] Guardiola C., Martín J., Pla B. and Bares P. "Cycle by cycle NOx model for diesel engine control". *Applied Thermal Engineering*, Vol. 110, pp. 1011–1020, 2017.

[29] Fenimore C.P. "Formation of nitric oxide in premixed hydrocarbon flames". *Symposium (International) on Combustion*, Vol. 13 n^o 1, pp. 373 – 380, 1971. Thirteenth symposium (International) on Combustion.

[30] Heywood J.B. *Internal Combustion Engines Fundamentals.* McGraw-Hill, ISBN 978-0-07-028637-5, New York, 1988.

[31] Desantes J.M., López J.J., Redón P. and Arrégle J. "Evaluation of the thermal NO formation mechanism under low temperature diesel combustion conditions". *International Journal of Engine Research*, Vol. 13 n^o 6, pp. 531–539, 2012.

[32] Holland J.H. *Adaptation in natural and artificial systems.* University of Michigan Press, Ann Arbor, MI, 1975.

[33] Mitchell M. *An introduction to genetic algorithms.* MIT Press, Cambridge, Massachusetts.

[34] Pelikan M., Goldberg D. and Cantu-Paz E. "Bayesian Optimization Algorithm, Population Sizing, and Time to Convergence". *Proceedings of the 2Nd Annual Conference on Genetic and Evolutionary Computation*, pp. 275–282, 2000.

[35] Sobol I.M. *Computaional Methods of Monte Carlo.* Nauka, Moscow, 1973.

[36] Deb K., Agrawal S., Pratap A. and Meyarivan T. "A Fast Elitist Non-Dominated Sorting Genetic Algorithm for Multi-Objective Optimization : NSGA-II". *Lecture Notes in Computer Science*, Vol. 1917, 2000.

Chapter 4

Theoretical optimization of HRL

Contents

4.1 Introduction

An ICE is characterized by its efficiency, that represents the ratio between the energy delivered by the machine and the energy provided to it. This energy conversion is carried out by performing a thermodynamic cycle, which is the consecutive evolution of a fluid experimenting processes from an initial thermodynamic state and returning back to the same state. Additionally, if some simplifications of the phenomena taking place in a real system are made (see next section), this cycle is considered as ideal.

However, cycles occurring in real ICE (real cycles) are far from the ideal ones, resulting in lower efficiencies than the provided ones by these ideal cycles. These differences are due to the existence of several efficiency losses derived from the non ideal thermo and fluid dynamic processes occurring in real cycles. The higher these efficiency losses are, the lower the efficiency is, thus the main objective when an efficiency optimization approach is proposed, is to reduce them.

As commented in Chapter 1, apart from the fuel consumption problem, the other important issue that nowadays drives the engine development is the pollutant emissions, concretely NO_x emissions continues being the hardest problem for Diesel engines. However, unlike other pollutant species such as CO, HC and PM, the prediction accuracy of this specie is acceptable when using the well-known model developed by Zeldovich [1] due to its high dependency on the combustion temperature as demonstrated by several authors [2, 3]. Thus, the application of a NO_x model should provide an accurate estimation of the emission of this pollutant by an ICE operating under a certain cycle.

In this chapter, the main ideal cycles are described and the maximum efficiency of the studied multicylinder engine performing such cycles is briefly

assessed. This analysis should give an overview of the maximum achievable ICE efficiency operating under such cycles. Then, the efficiency losses inherent to ICE operation that separate the ideal cycles from the real ones are evaluated separately. The aim of this study is the identification of the main effects susceptible to give higher gains when they are reduced.

After that, the best theoretical combustion in terms of efficiency is studied taking into account the real thermodynamic processes taking place in the combustion chamber. This methodology is applied under different scenarios to explore possible benefits obtained by improving the engine mechanical robustness or reducing the heat rejection to the combustion chamber walls. On the one hand, several peak pressure and pressure rise rate limits are assessed to understand the potential of increase any of them by improving the engine robustness. On the other hand, the optimization is also assessed in a scenario in which some combustion chamber walls are coated with a specific material called SiRPA reported by Wakisaka *et al.* [4], capable to change its surface temperature during the cycle trying to reproduce the gas transient temperature, thus reducing the heat transfer from the combustion chamber to the walls.

Finally, NO_x emissions are also included in the optimization to obtain the optimum combustion law that maximizes efficiency and minimizes this pollutant. Even though, the accuracy of the NO_x model is somehow limited under the very fast combustions resulting from the theoretical optimization stages (see Sections 4.4.2.4 and 5.4.1), it is very useful to understand the effect of reducing this pollutant on efficiency, through the quantification of the potential penalty trends.

It is important to remark that both the analysis of the efficiency losses of the cycle and the HRL theoretical optimization use the gross indicated efficiency as a reference and/or objective. Thus, neither mechanical losses nor pumping losses are considered in any of these sections.

Taking into account previous comments, this chapter is structured as follows. The first section deals with the description of the most important ideal cycles. Secondly, the effect on GIE of all efficiency losses inherent to ICE operation are assessed separately. Then, the following section deals with the combustion theoretical optimization under different restrictions. Finally, a summary of the chapter is performed in the conclusions section.

4.2 Ideal thermodynamic cycles

Ideal thermodynamic cycles working with air are the simplest representation of an ICE operation. These cycles are a cyclic evolution of a certain mass (control mass), exchanging heat and work with the outside, therefore they can be considered as closed cycles. Throughout recent history, several cycles have been defined to represent ideally different heat engines. In this way, Rankine cycle stands for steam turbines, Brayton cycle represents gas turbines, while Diesel and Otto standard cycles traditionally have been used to represent compression ignition and spark ignition engines respectively. All of them use a perfect gas (air) along the whole cycle and that is why they are known as air-standard ideal cycles [5, 6]. The simplifications made in these ideal theoretical cycles are the following:

- No leakages are considered.
- There are no losses due to heat rejection.
- There are no exhaust losses.
- Processes are reversible.
- The working fluid is air and its properties are constant.
- The combustion process is substituted by a heat addition at constant volume and constant pressure.
- Heat addition corresponds to a complete combustion.
- The trapping air process is substituted by a heat transfer process at constant volume.

In addition to these considerations, an ideal cycle must also meet the following bases when it is used to represent a real cycle:

- The processes are similar to those occurring in the real cycle.
- Same compression ratio as the real cycle.
- The supplied specific energy is the same than in the real cycle.
- Same pressure and temperature at the beginning of the compression process.

In this section the most important ideal cycles and their maximum efficiencies are briefly evaluated in the specific engines used in this work.

4.2.1 Carnot cycle

In 1824 Sadi Carnot proposed this cycle, which defines the maximum efficiency for systems undergoing power cycles. It is a reversible power cycle operating between two thermal reservoirs, temperatures of which are T_C and T_H [5]. Figure 4.1 shows the p-v diagram of a Carnot cycle in which the system is a gas in a piston-cylinder assembly.

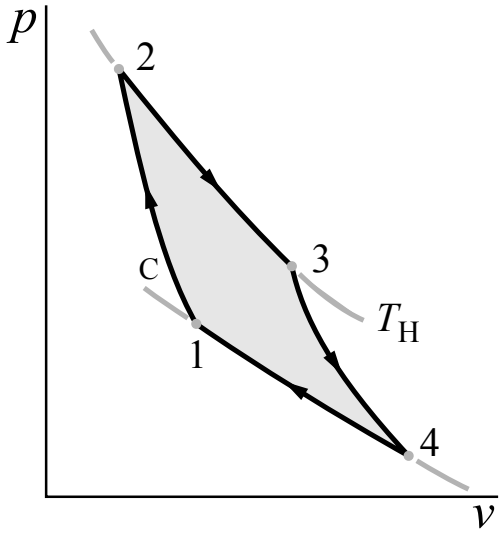

Figure 4.1. *p-v diagram of a Carnot cycle power gas.*

In a Carnot cycle, the system undergoes a series of four internally reversible processes, as can be seen in Figure 4.1:

- ***Process 1-2:*** The gas is compressed adiabatically to state 2 at temperature T_H.
- ***Process 2-3:*** The gas expands isothermally, while receiving energy Q_{23} from the hot reservoir by heat transfer.
- ***Process 3-4:*** The gas expands adiabatically until reaching temperature T_C.
- ***Process 4-1:*** The gas is compressed isothermally to its initial state while it discharges energy Q_{41} to the cold reservoir by heat transfer.

This cycle provides the maximum thermal efficiency of a power cycle, which is given by the following equation:

$$\eta = \left(1 - \frac{T_C}{T_H}\right) 100 \tag{4.1}$$

Taking into account this equation, if the air-standard cycle considerations explained above are assumed, it is enough to know the temperatures of both thermal reservoirs to assess the Carnot efficiency. The cold temperature would be the intake temperature, which could be set at 298 K as a representative value for ambient temperature, while the high temperature could be the adiabatic temperature of a stoichiometric Diesel combustion (close to 2600 K according to Glaude et al. [7] for blends selected as Diesel models). Then, Carnot efficiency for a Diesel ICE should be:

$$\eta = \left(1 - \frac{298}{2600}\right) 100 = 88.5\% \tag{4.2}$$

This value gives the maximum ideal efficiency achievable in a thermodynamic cycle operating between these 2 temperatures. Figure 4.2 shows the evolution of Carnot efficiency versus T_H for $T_C = 298$ K.

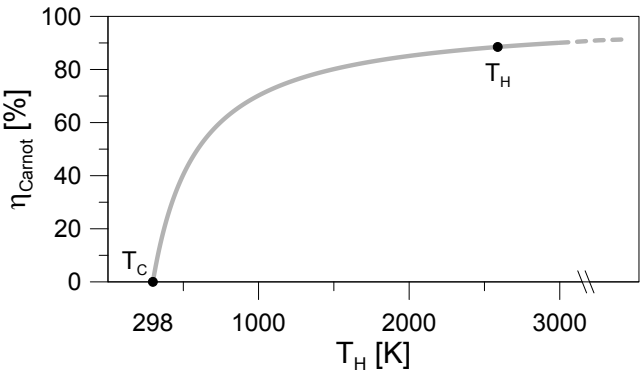

Figure 4.2. *Carnot efficiency versus T_H, for T_C = 298 K.*

However, due to the impossibility of performing its processes by an ICE, this cycle cannot be translated to ICE, but it is more suitable for systems undergoing a Rankine cycle. Nonetheless, many authors have used it either as and efficiency ceiling [8–10] or as a starting point to propose different cycles as shown in next sections.

4.2.2 Constant volume or Otto cycle

The air-standard Otto cycle is an ideal cycle that assumes that the heat addition occurs instantaneously while the piston is at top dead centre. This cycle, which is shown on the *p-v* and *T-s* diagrams of Figure 4.3, is normally associated to spark ignition engines, due to its faster combustion process in comparison with CI engines, and it is the cycle with highest efficiency suitable for ICE operation.

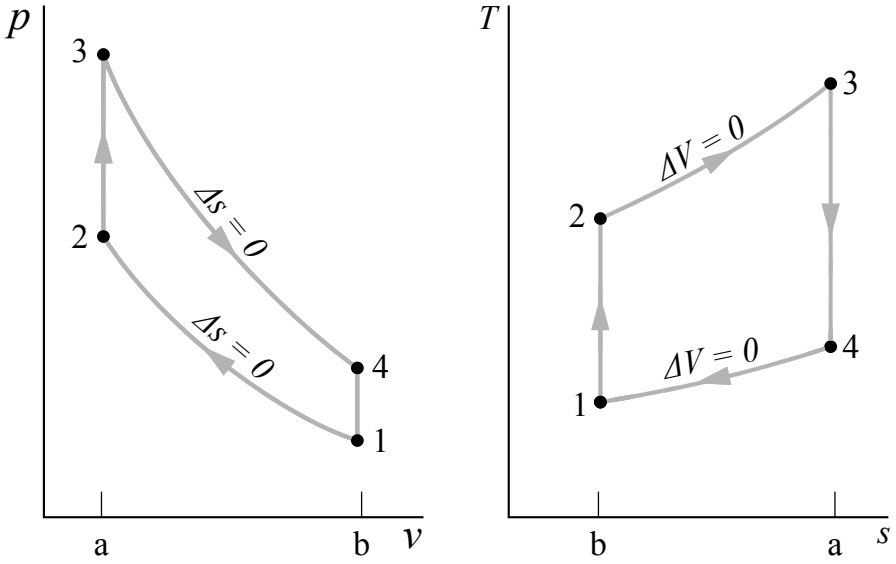

Figure 4.3. *p-v and T-s diagrams of an Otto cycle power gas.*

The cycle consists of four internally reversible processes in series:

- ***Process 1-2:*** Isentropic compression of the air as the piston moves from bottom dead centre to top dead centre.
- ***Process 2-3:*** Constant-volume heat addition (Q_{23}) to the air from an external source while the piston is at top dead centre. This process is intended to represent the ignition of the fuel-air mixture and the subsequent rapid burning and it requires a certain amount of work.
- ***Process 3-4:*** It is an isentropic expansion (power stroke).
- ***Process 4-1:*** It completes the cycle by a constant-volume process in which heat (Q_{41}) is rejected from the air while the piston is at bottom dead centre.

Taking into account the previous considerations, the energetic balance of this cycle can be written as [11]:

$$\eta = \left(1 - \frac{T_1}{T2}\right) 100 = \left(1 - \left(\frac{V_2}{V_1}\right)^{\gamma-1}\right) 100 = \left(1 - \frac{1}{r^{\gamma-1}}\right) 100 \tag{4.3}$$

where r is the compression ratio defined as $r = \frac{V_1}{V_2}$.

Main conclusion extracted from this equation is that Otto efficiency increases when compression ratio is augmented and it is not function of the ratio between pressures during compression and expansion processes and, consequently, nor of heat added to the system. As it was stated at the beginning of Section 4.2, ideal cycles use air with constant specific heat capacity ratio (perfect gas) along the cycle evolution, therefore a constant value of γ could be set as $\gamma = 1.4$. Figure 4.4 represents the Otto efficiency evolution as a function of the compression ratio. Taking into account that the compression ratio of the studied engines are around $r = 17.5$, their Otto efficiency, as can be also shown in Figure 4.4, is:

$$\eta = \left(1 - \frac{1}{17.5^{1.4-1}}\right) 100 = 68.2\% \tag{4.4}$$

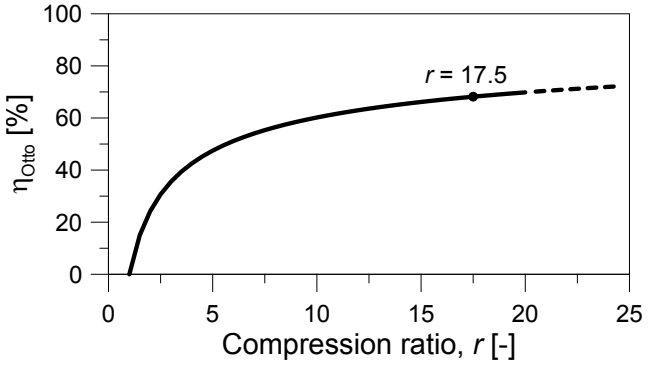

Figure 4.4. *Thermal efficiency of the air-standard Otto cycle for* $\gamma = 1.4$.

As commented, this is the maximum efficiency achievable by an ICE assuming all the previous considerations. Even though this efficiency is far from real ones found in ICE, both CI and SI, this cycle has been largely used by several authors as a reference for their efficiency studies [12–15].

4.2.3 Constant pressure or Diesel cycle

This cycle is normally associated with compression ignition ICE and its main characteristic is that there is a constant-pressure process in which the heat is added to the cycle. This cycle is composed of 4 processes explained below as can be seen in Figure 4.5:

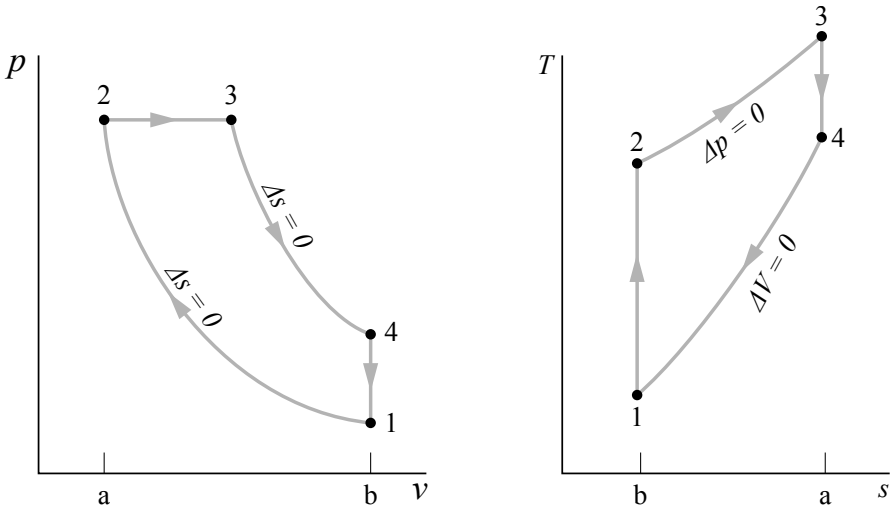

Figure 4.5. *p-v and T-s diagrams of a Diesel cycle power gas.*

- ***Process 1-2:*** Isentropic compression of the air as the piston moves from bottom dead centre to top dead centre.
- ***Process 2-3:*** Constant-pressure heat addition (Q_{23}) to the air from an external source. This process starts when the piston is at top dead centre. This process typically represents a slow Diesel combustion in large engines, where diffusion combustion is controlled by the injection process.
- ***Process 3-4:*** It is an isentropic expansion (power stroke).
- ***Process 4-1:*** It is a constant-volume process in which heat (Q_{41}) is rejected from the air while the piston is at bottom dead centre.

If the efficiency analysis is performed here, as it was done in the Otto cycle, and taking into account that the *cutoff ratio* is defined as $\beta = \frac{V_3}{V_2}$, it can be

obtained:

$$\eta = \left(1 - \frac{1}{r^{\gamma-1}} \frac{\beta^{\gamma} - 1}{\gamma\,(\beta - 1)}\right) 100 \tag{4.5}$$

Here it can be discerned that Diesel efficiency increases with compression ratio as in Otto cycle and it decreases when cutoff ratio gets higher (combustion gets longer). Figure 4.6 represents the Otto efficiency and Diesel efficiency for two different cutoff ratios (1.5 and 4.5) as a function of the compression ratio. These cutoff ratios have been obtained by taking into account the shortest (18°) and longest (52°) combustions that take place within the whole operating map of the studied engine. As can be observed, Otto efficiency is always higher than Diesel efficiencies for the same compression ratio. Additionally, it can be also appreciated that Diesel efficiency is highly dependent on cutoff ratio, leading to an efficiency loss around 12% $\dot{m}_f H_v$ when increasing cutoff ratio from 1.5 to 4.5 at the same compression ratio than the studied engine (r = 17.5).

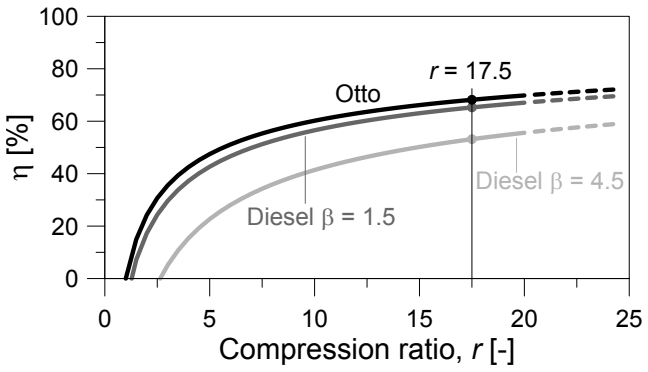

Figure 4.6. *Thermal efficiency of the air-standard Otto and Diesel cycles for* $\gamma = 1.4$ *and cutoff ratios* $\beta = 1.5$ *and* $\beta = 4.5$.

In particular, Diesel efficiency for the compression ratio of the studied engine and the presented cutoff ratios is:

$$\eta_{\beta=1.5} = \left(1 - \frac{1}{17.5^{1.4-1}} \frac{1.5^{1.4} - 1}{1.4\,(1.5 - 1)}\right) 100 = 65.3\% \tag{4.6}$$

$$\eta_{\beta=4.5} = \left(1 - \frac{1}{17.5^{1.4-1}} \frac{4.5^{1.4} - 1}{1.4\,(4.5 - 1)}\right) 100 = 53.2\% \tag{4.7}$$

Again, this cycle is still far from reflecting the real one but, in this case, the efficiency for a long combustion is not so far from real efficiencies. Therefore, this cycle has been used as a base for assessing new approaches intended to increase the cycle performance. Among these studies, Hoffmann *et al.* [16] determined the optimum piston trajectory for a Diesel cycle. Besides, Parlak [17] worked on the effect of heat transfer on several design parameters such as compression ratio and cutoff ratio on Diesel cycle performance. Later on, Ebrahimi [18] performed a thermodynamic analysis assessing the effects of variable stroke length and compression ratio on Diesel cycle efficiency.

4.2.4 Limited pressure or Sabathé cycle

This cycle was patented in 1908 by Louis Gaston Sabathé [19] and it is an intermediate case between the constant pressure and constant volume cycles. It is the one that reflects more closely the pressure variations of the real cycle of SI and CI engines as there is a constant-volume process followed by a constant-pressure process. The processes represented in this cycle area, as can be seen in Figure 4.7, are the following:

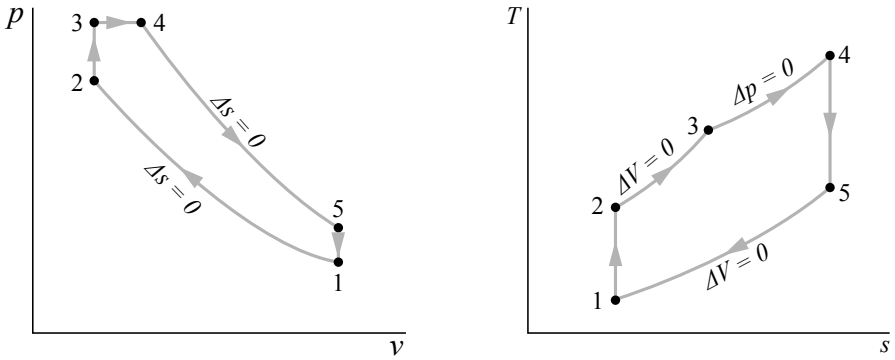

Figure 4.7. *p-v and T-s diagrams of a Sabathé cycle power gas.*

- ***Process 1-2:*** Isentropic compression of the air as the piston moves from bottom dead centre to top dead centre.
- ***Process 2-3:*** Constant-volume heat addition (Q_{23}) to the air from an external source until reaching a certain pressure while the piston is at top dead centre. This process represents a rapid combustion until a pressure limit is reached.

- ***Process 3-4:*** Constant-pressure heat addition (Q_{34}) to the air from an external source. This process starts when the piston is still at top dead centre and just after the constant-volume process.
- ***Process 4-5:*** It is an isentropic expansion (power stroke).
- ***Process 5-1:*** It is a constant-volume process in which heat (Q_{51}) is rejected from the air while the piston is at bottom dead centre.

The efficiency analysis for this cycle, taking into account that pressure ratio and cutoff ratio are defined as $\alpha = \frac{p_3}{p_2}$ and $\beta = \frac{V_4}{V_2}$ respectively, is given by the following equation:

$$\eta = \left(1 - \frac{1}{r^{\gamma-1}} \frac{\alpha\beta^{\gamma} - 1}{\alpha - 1 + \gamma\alpha\,(\beta - 1)}\right) 100 \tag{4.8}$$

Indeed, both Otto and Diesel cycles are specific cases of Sabathé cycle. In the first case, Otto cycle is derived from this cycle when V_4 and V_2 are equal ($\beta = 1$ - constant volume combustion). In the second case, Diesel cycle is obtained by making equal p_2 and p_3 ($\alpha = 1$), thus obtaining a constant pressure evolution between points 2 and 4. The efficiency of this cycle for the studied engine is difficult to assess in the same conditions than previous cycles since it would be necessary to impose a certain peak pressure limit, thus conditioning its maximum efficiency. In any case, as commented, in a conventional ICE β could be between 1.5 and 4.5 while α could move between 1 and 2, thus leading to a cycle efficiency between Otto and Diesel cycles.

As commented, this cycle is more representative of an ICE operation and it has been stated as the maximum efficiency cycle by some authors [20, 21] when only maximum peak pressure constraint is taken into account. Additionally, other authors [22] have used it as a reference when presenting some new concepts of thermodynamic cycles.

4.2.5 Summary

Table 4.1 reflects a summary of the efficiency of the explained ideal cycles operating in the studied engine. As can be observed, there is a huge gap between the Carnot cycle and the others due to the different thermodynamic processes, being more similar to the real ones in Otto, Diesel or Sabathé cycles. Among these 3, different efficiencies are given by the different combustion processes carried out at each cycle, being Otto cycle the most efficient one.

Cycle	Carnot	Otto	Diesel	Sabathé[1]
Efficiency [% $\dot{m}_f H_v$]	88.5	68.2	65.3 / 53.2	68.2 / 53.2

Table 4.1. *Efficiency of ideal cycles operating in the studied engine.*

In any case, these cycles and efficiencies are far from reality because, apart from the efficiency loss derived from the use of a certain combustion, there are other issues affecting real cycles. However, ideal cycles are not valid to asses these additional efficiency losses sources due to the assumption of the hypothesis explained in Section 4.2. Thus, next section is intended to explain these efficiency losses that take place in real cycles affecting negatively their efficiency.

4.3 Analysis of the efficiency losses of a thermodynamic cycle

Starting from Otto cycle, maximum efficiency one, the real cycle of a specific operating condition can be obtained by taking into account all efficiency losses that exist in a real cycle. Then, since the total effect of efficiency losses is different at each operating condition, they result in distinct real cycles and their respective different GIE. Figure 4.8 shows the experimental gross indicated efficiency of the real cycles in the complete map of the multicylinder engine. As can be observed, the zone with the highest GIE is located at high engine speed and medium load reaching efficiencies higher than 48% $\dot{m}_f H_v$. In any case, these efficiencies are far from Otto efficiency calculated for the compression ratio of this engine (68.2% $\dot{m}_f H_v$). The objective of this section is to understand the effect of the efficiency losses that contribute to this efficiency loss and to assess their relative weight.

4.3.1 Methodology

The efficiency losses that affect a real cycle of an ICE decreasing its efficiency and separating it from Otto cycle are extensively described in next sections and can be categorized as follows:

[1] Calculated as an intermediate value between Otto and Diesel efficiencies.

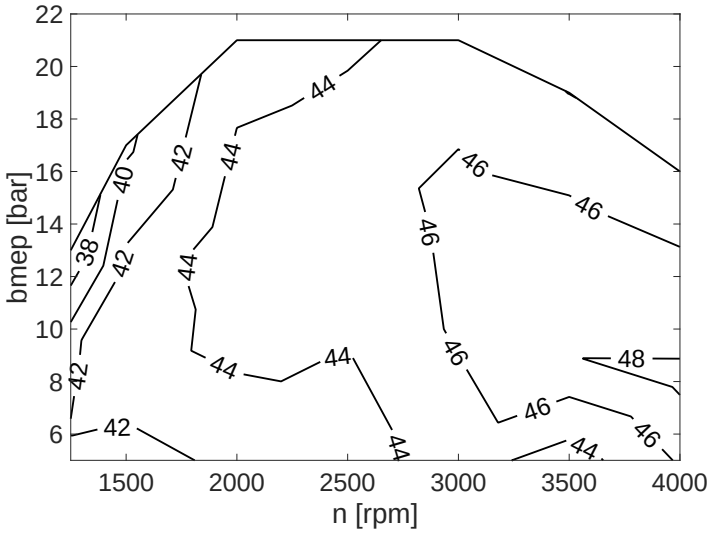

Figure 4.8. *Gross indicated efficiency [% $\dot{m}_f H_v$].*

1. Combustion development efficiency losses: this term includes the combustion centring, velocity and incomplete combustion efficiency losses.
2. Heat transfer to the chamber walls.
3. Gas properties efficiency losses: this term includes the heat capacity ratio change due to temperature and composition variations.
4. Air management efficiency losses: non centred valves timing and blow-by leakage efficiency losses.

Unfortunately, these effects are interconnected and it is not possible to isolate them experimentally. Therefore, simulation tools are necessary in order to quantify independently the impact of these interconnected effects. This assessment has already been documented in previous works [12, 14, 23] and it is known as *"Split of losses"* analysis. In these works, a 0D thermodynamic model is used to assess the impact of each efficiency loss on GIE in a cumulative way, reaching Otto efficiency at the end of the analysis. However, this methodology presents the disadvantage that the order in which the effects are assessed have an important influence on the final result because they are interconnected and cannot be separated [14, 23]. Furthermore, a "correct" order in which the efficiency losses should be assessed does not exist.

Since the objective of this section is not to obtain the exact impact of each efficiency loss on GIE but to provide a rough estimation of their importance, a simple analysis in which they are evaluated separately is good enough. This analysis has been conducted using the predictive 0D model described in Section 3.3.1 (SiCiclo) by, starting from the experimental point, trying to remove completely the considered efficiency loss at a time. Then, this higher efficiency is compared with the experimental measurement, to asses the GIE variation obtained when the specific efficiency loss is not considered.

Even though there are some efficiency losses that are easily removable such as blow-by, centred VT, heat capacity ratio change and heat transfer, this is not the case of the combustion development. So far, the combustion development that maximizes the GIE has been evaluated only in ideal conditions (Otto cycle), but not taking into account the remaining efficiency losses. Therefore, the maximum efficiency combustion that should be used in order to eliminate the combustion development efficiency loss is not still clear (see Section 4.4) and thus, this efficiency loss was assessed following different approaches. On the one hand, the experimental combustion was compared with an instantaneous combustion located at the TDC. On the other hand, a more realistic scenario was considered in which the combustion centring, velocity and incomplete term were varied according to the variations of combustion centring, velocity and completeness observed along the engine map.

As commented, this approach does not pretend to give exact results but to provide an idea about how important each efficiency loss is. Therefore, the main conclusion provided by this section is a ranking of the most important sources of losses that will be useful for addressing future efficiency enhancing strategies.

The methodology has been applied to 28 operating conditions representative for the engine operation map, as can be observed in Figure 4.9, which have been experimentally measured in the multicylinder engine. Then, results from these specific points are interpolated in order to plot *"iso-effect"* lines covering the whole engine map in the same way that GIE shown in Figure 4.8. In next subsections, figures will show the GIE variation due to the modification of the considered efficiency loss with respect to the nominal experimental conditions. Positive values always mean that the considered change would increase GIE and vice versa.

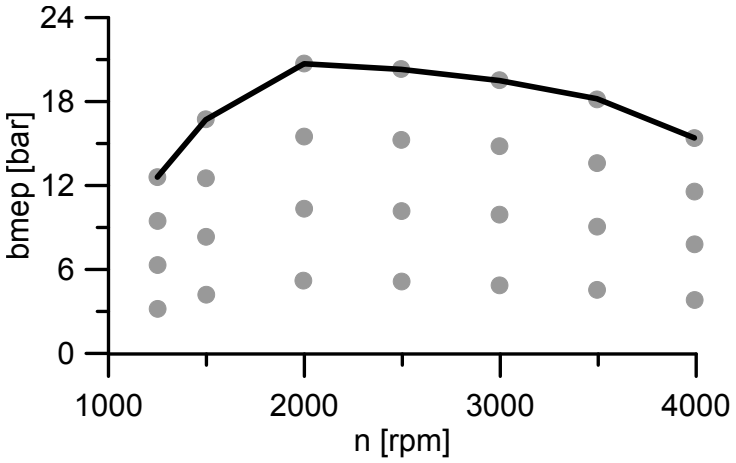

Figure 4.9. *Full load curve and operating conditions included in the analysis of cycle efficiency losses.*

4.3.2 Combustion development

This efficiency loss refers to the efficiency loss due to a non ideal combustion process. A real combustion is not necessarily located in the optimum crank angle(°), its duration differs from the optimal one (instantaneous) and probably not all the injected fuel could be burnt. These efficiency losses lead to an efficiency reduction that is different depending on the operating point.

As commented in the previous section, this efficiency loss was assessed in two different ways. The first evaluation has been done by comparing the experimental combustion with an instantaneous combustion located at the TDC, even though there is not guarantee that this combustion would be the most efficient one under these conditions (see Section 4.4). Figure 4.10 represents the GIE variation with respect to the nominal point when considering an instantaneous combustion at the TDC. As can be observed, the GIE variation when this efficiency loss is removed increases with engine speed and load, reaching more than +7% $\dot{m}_f H_v$ in the top right corner of the map, where the combustion duration is the highest one within the engine map. As observed in the bottom-left part of the plot, the GIE benefit when performing an instantaneous combustion at the low load and engine speed region is minimum (less than +1% $\dot{m}_f H_v$). There, the worsening of other efficiency losses, specially the heat transfer (which effect is maximum at this

area - see next section), counterbalances the GIE gain due to the better combustion velocity.

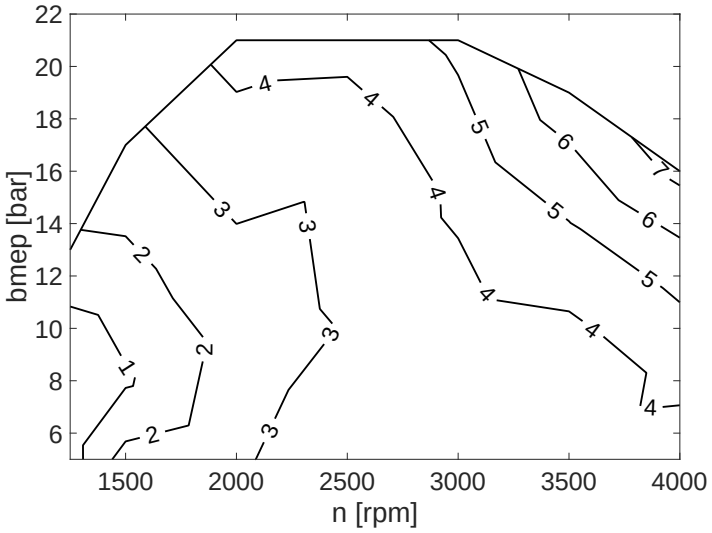

Figure 4.10. *GIE variation with respect to the nominal point when considering an instantaneous combustion at the TDC [% $\dot{m}_f H_v$].*

The second evaluation, described in the next three subsections, proposes a more realistic scenario in which the impact of the combustion centring, velocity and incomplete term is assessed separately by varying each term according to the ranges observed in the engine map.

4.3.2.1 Combustion centring

The non optimal combustion centring has a certain impact on GIE. To evaluate the effect of a shifted combustion, in this subsection the efficiency change when the experimental HRL is moved is shown.

On the one hand, Figure 4.11 shows the effect of advancing 5° the combustion process while keeping the same heat release law when comparing to the nominal point. As can be seen, there is a slight improvement below $+1\%$ $\dot{m}_f H_v$, being this increase more important at low load and engine speed and at medium-high engine speed and high load.

On the other hand, Figure 4.12 shows the effect of delaying 5° the experimental combustion from the reference position. It can be seen that

efficiency decays between -0.6% $\dot{m}_f H_v$ and -1.6% $\dot{m}_f H_v$ in the whole engine map.

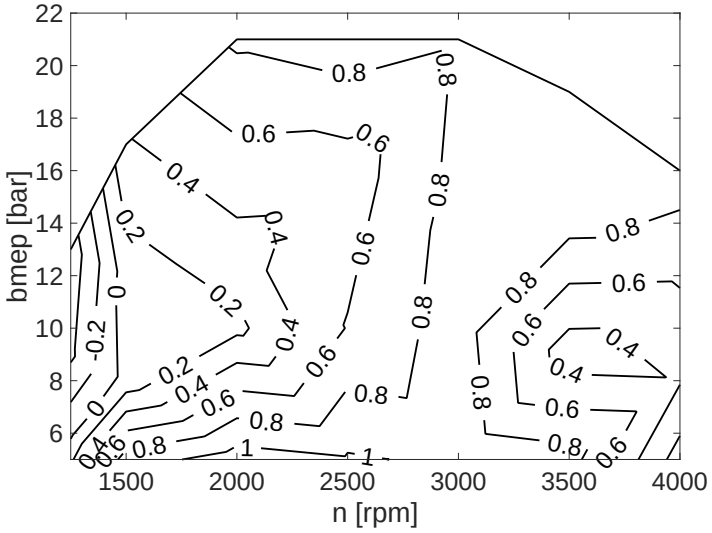

Figure 4.11. *GIE variation with respect to the nominal point when advancing the experimental HRL 5° [% $\dot{m}_f H_v$].*

As can be observed, the trends shown in Figures 4.11 and 4.12 are not monotonous with load and/or engine speed because the OEM has set this position along with other parameters to get the best engine performance not only regarding GIE, but also in terms of pollutant emissions ... For this reason, the behaviour when moving the combustion can change differently depending on the load or engine speed. However, what is consistent is that advancing combustion (until a certain position) increases efficiency while moving it backwards has a negative effect on GIE.

Even though combustion was shifted considerably (10° from advanced to delayed scenarios), the cumulative effect on GIE is moderate being lower than 3% $\dot{m}_f H_v$ in all cases (taking into account both variations). This fact, even though it cannot be directly extrapolated to larger shifts, implies that the optimum combustion centring (CA50) is placed between 7°ATDC and 14°ATDC in all cases and it is not possible to obtain important changes on GIE when moving it.

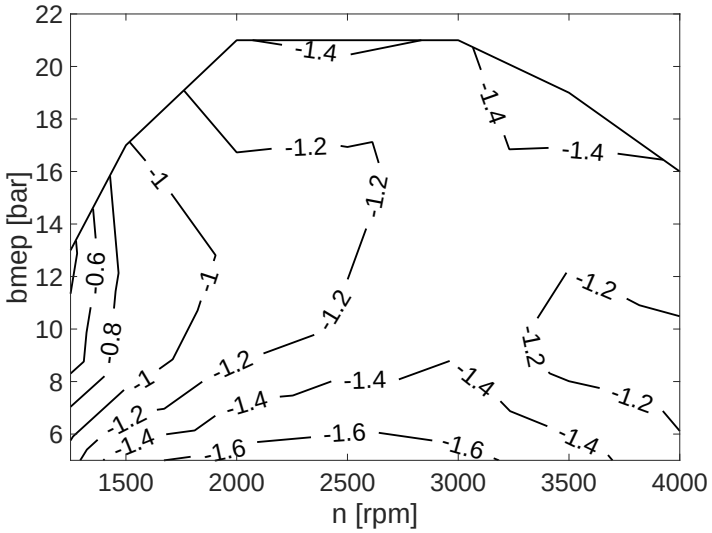

Figure 4.12. *GIE variation with respect to the nominal point when delaying the experimental HRL 5° [% $\dot{m}_f H_v$].*

4.3.2.2 Combustion velocity

As can be derived from Otto cycle, the ideal combustion is an instantaneous event at TDC, therefore longer combustion durations lead to lower GIE. To assess the impact of changing the combustion duration on efficiency, a dedicated study where the duration of the experimental HRL is shortened or enlarged 25% with respect to the nominal point is performed here. Note that since combustion duration is different at each operating condition, these relative changes are not translated into a fixed duration in crank angle degrees (4° at low and 13° high load).

On the one hand, Figure 4.13 shows the effect of shortening 25% the combustion duration in the complete engine map while maintaining the combustion centring. As can be seen, there is always an efficiency improvement which increases with load and engine speed, reaching more than +2% $\dot{m}_f H_v$ at high engine speed and load. At this zone of high load and engine speed, combustions are longer in crank angle degrees and shortening them 25% leads to higher reduction in crank angle degrees than at low load and engine speed.

Furthermore, combustion duration has a bigger influence on the cycle development at high load than at low load due to the higher quantity of injected fuel and, additionally, combustion duration (in°) increases with engine

speed. Both factors are consistent with results presented here where the combustion shortening it is more important in the high speed and high load region.

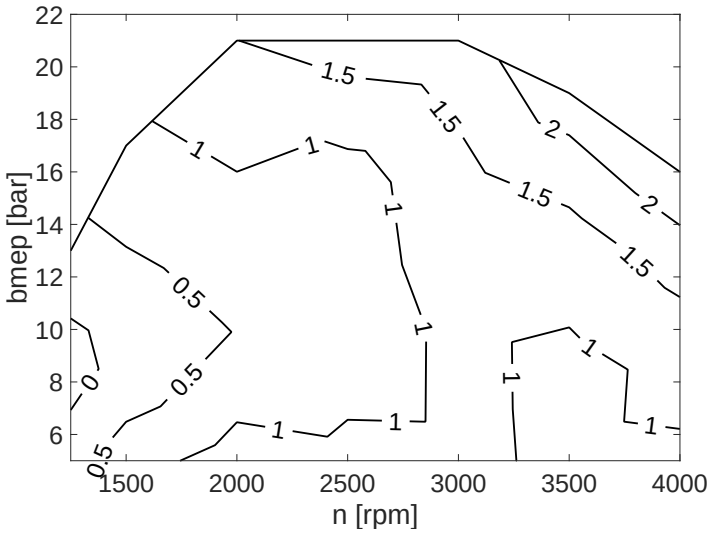

Figure 4.13. *GIE variation with respect to the nominal point when shortening 25% the experimental HRL duration [% $\dot{m}_f H_v$].*

On the other hand, Figure 4.14 shows the GIE variation when extending 25% the combustion duration in the whole engine map also while maintaining the combustion centring. It can be seen that this change affects negatively GIE and it becomes worst when load and engine speed increase, reaching values higher than -2.5% $\dot{m}_f H_v$ at high load and engine speed. The reason of this worsening with load and engine speed is the same than explained in the previous paragraph.

As can be observed, both variations presented in Figures 4.13 and 4.14 are approximately symmetrical and their minimums and maximums are located exactly in the same regions.

4.3.2.3 Incomplete combustion

From the energy point of view, in CDC normally it is assumed that the total amount of injected fuel is burned in the closed cycle. However, that is not totally true and there is always some amount of fuel that is not burned and goes

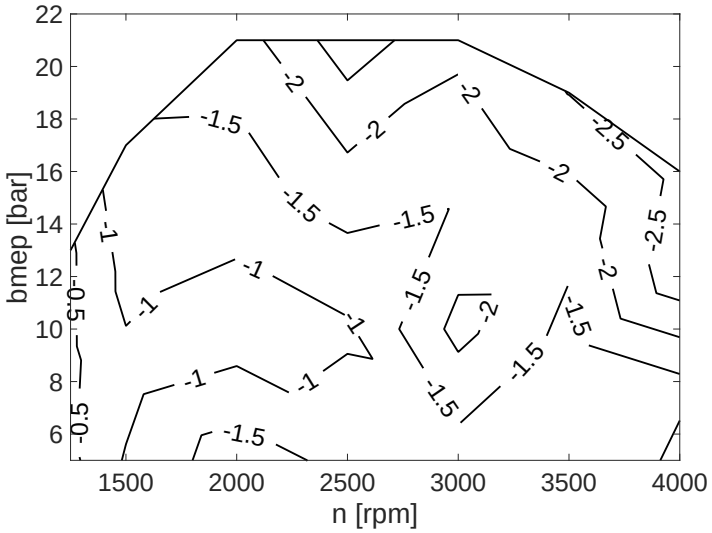

Figure 4.14. *GIE variation with respect to the nominal point when extending 25% the experimental HRL duration [% $\dot{m}_f H_v$].*

out the chamber during the exhaust process. This energy can be determined by considering the HC, CO and soot emissions measured at tailpipe as:

$$\dot{H}_{ic} = \left(Y_{HC} H_{v,HC} + Y_{CO} H_{v,CO} + Y_C H_{v,C}\right) \dot{m}_{exh} \tag{4.9}$$

where Y_{HC}, Y_{CO} and Y_C are the mass fractions of HC, CO and soot, and $H_{v,HC}$, $H_{v,CO}$ and $H_{v,C}$ are their heating values respectively[2].

On the one hand, Figure 4.15 shows the energy term relative to the unburned species in the exhaust gases measured in the complete operating map of the engine. As can be seen, this term barely exceeds 0.4% $\dot{m}_f H_v$ at high load and low engine speed and at low load and high engine speed. The rest of the map is below this value and between 0.1% $\dot{m}_f H_v$ and 0.2% $\dot{m}_f H_v$ in most cases, being below 0.1% $\dot{m}_f H_v$ at the high load and engine speed area.

On the other hand, Figure 4.16 shows the effect on GIE of burning the HC, CO and soot existent in the exhaust gases. As can be observed, this increment is around 45% of the fuel energy (representative value of the GIE in

[2] $H_{v,HC}$ has been assumed to have a value of 42.9 MJ/kg the same as Diesel fuel, $H_{v,CO}$ of 10.1 MJ/kg and $H_{v,C}$ of 32.8 MJ/kg

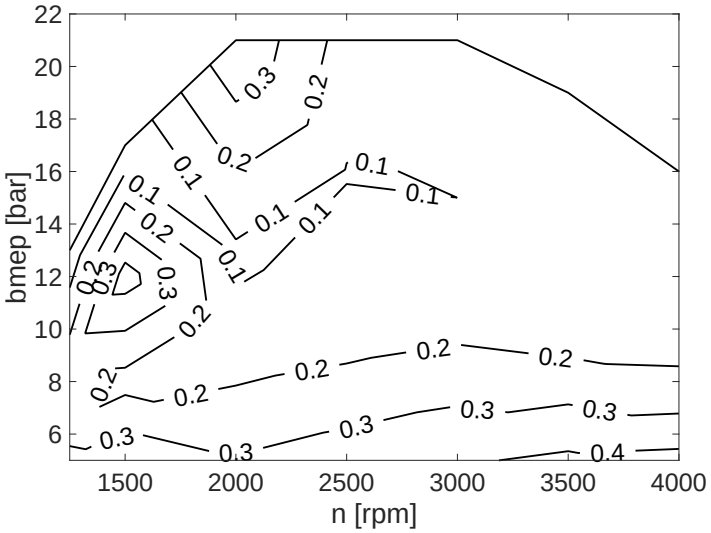

Figure 4.15. *Incomplete combustion term [% $\dot{m}_f H_v$].*

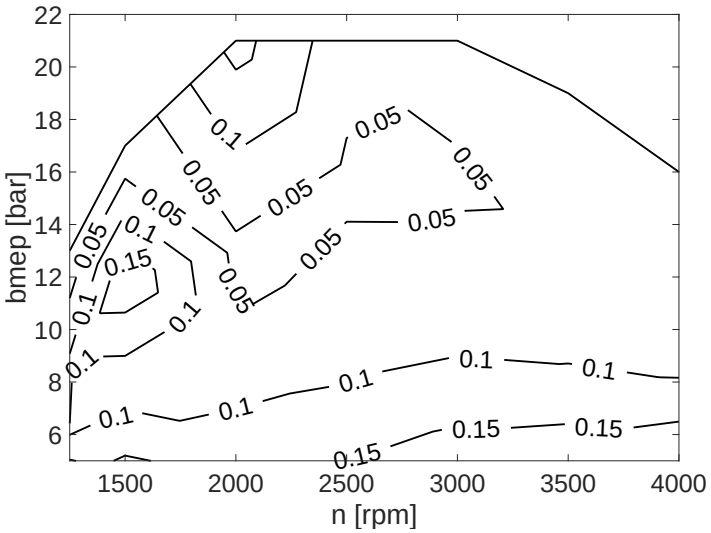

Figure 4.16. *GIE variation with respect to the nominal point when burning the remaining fuel existent in the exhaust gases [% $\dot{m}_f H_v$].*

the engine map) presented in Figure 4.15 and it does not exceed +0.2% $\dot{m}_f H_v$ in any case.

4.3.3 Heat transfer

This term takes into account the energy lost due to heat rejection to the combustion chamber walls. Figure 4.17 shows the percentage of fuel energy lost through heat transfer.

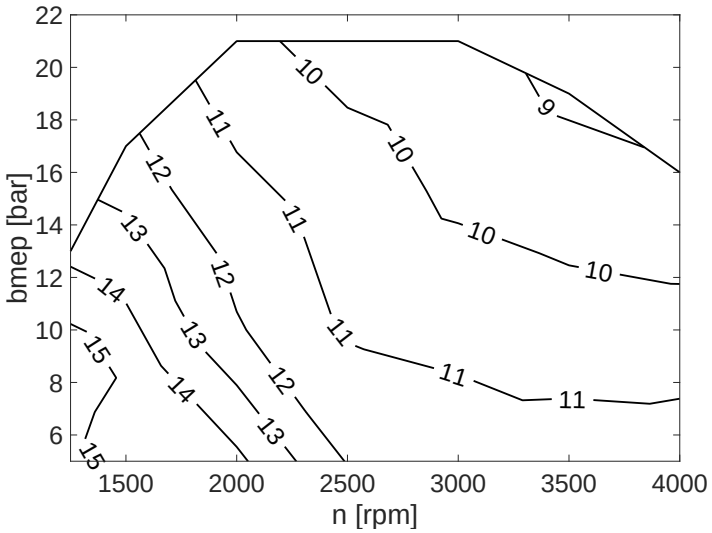

Figure 4.17. *Heat transfer to the chamber walls [% $\dot{m}_f H_v$].*

It can be seen that, as expected, this term is higher at low load and engine speed (15% $\dot{m}_f H_v$) and it decreases with both of them reaching values below 9% $\dot{m}_f H_v$ in the high load and engine speed area. The reason why this term is higher at low engine speed is the higher residence time of the hot gas along the cycle in comparison with higher engine speeds. It can be appreciated that this process is one of the most important terms in the chamber since it represents 9-15% $\dot{m}_f H_v$. However, if this efficiency loss is completely avoided the energy loss is not directly transferred to an efficiency increase, but some part is also used to increment the charge temperature, thus increasing the energy lost during the exhaust process.

In this subsection, the effect on GIE of two different HT scenarios is assessed: on the one hand, the total HT is removed resulting in an adiabatic

engine, on the other hand, a more realistic scenario assesses the GIE variation when just half of the HT is considered. Such study was performed by means of the heat transfer submodel, previously adjusted following the methodology explained in Section 3.3.1, embedded in the thermodynamic tool SiCiclo.

Figure 4.18 shows the effect of considering an adiabatic engine, while Figure 4.19 shows the variation of gross indicated efficiency when 50% of the total HT is computed. As can be observed, the trend is similar in both cases and the effect on GIE is linear with HT. Thus, the maximum gains are +5% $\dot{m}_f H_v$ and +2.6% $\dot{m}_f H_v$ at 0% and 50% HT scenarios respectively, while the minimum effects are +2.5% $\dot{m}_f H_v$ and +1.2% $\dot{m}_f H_v$ respectively. As it was commented, even though HT means 15% $\dot{m}_f H_v$ in the low load area, in an hypothetical adiabatic engine only 5% $\dot{m}_f H_v$ could be recovered in the best case if the combustion was maintained.

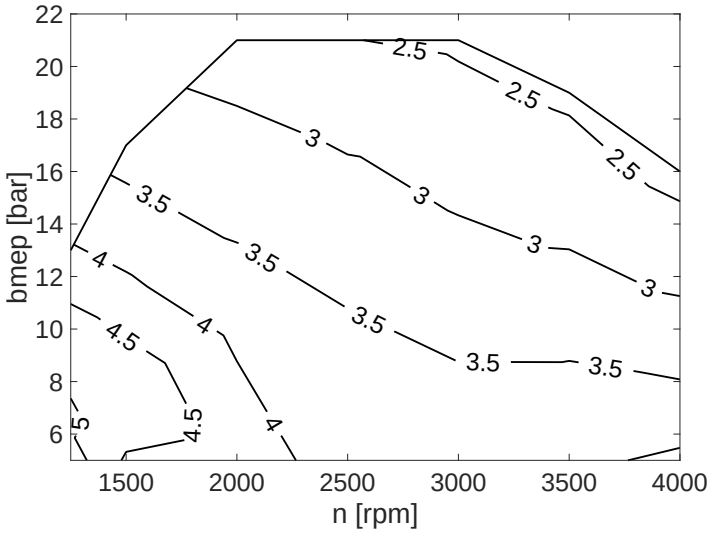

Figure 4.18. *GIE variation with respect to the nominal point when removing completely HT [% $\dot{m}_f H_v$].*

4.3.4 Gas properties

This efficiency loss accounts for the effect on indicated efficiency of the fluid properties variation due to changes in composition and/or temperature. As stated in equation 4.3, the maximum efficiency of a cycle increases with the

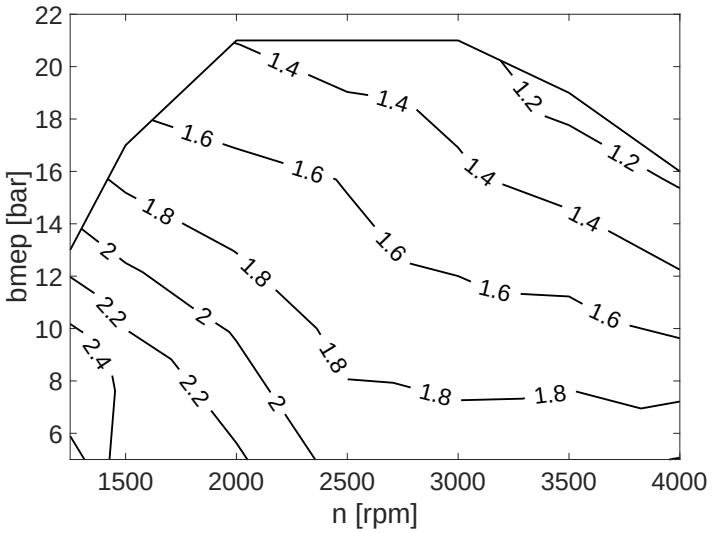

Figure 4.19. *GIE variation with respect to the nominal point when removing half of the HT [% $\dot{m}_f H_v$].*

compression ratio (see Figure 4.4) and with the heat capacity ratio ($\gamma = \frac{c_p}{c_v}$), as shown in Figure 4.20. Since both of them vary along the cycle, considering or not this change in the heat capacity ratio calculation has a certain impact. Regarding the composition variations, the heat capacity ratios of dry air and CO_2 at 293 K have been remarked in Figure 4.20. As can be observed, the heat capacity ratio of CO_2 is slightly lower than the dry air one and, since CO_2 mass fraction is higher in burnt gases, a γ decrease can be expected as combustion advances, and the fraction of burned gases increases, along the cycle.

On the other hand, γ also diminishes as the temperature of the charge increases. Figure 4.21 shows the evolution of the heat capacity ratio of the air at different temperatures, where a big decrease of γ when the air temperature increases can be observed.

Thus, it is clear that the efficiency of a cycle depends on variations of both temperature and composition of the charge along the cycle. In this subsection, the effect of considering or not the variation of both parameters in the γ determination are evaluated separately and finally combined. In this way, the GIE variation when considering a real gas with variable heat capacity ratio (real cycle) versus and ideal one with constant γ (ideal cycle) is determined.

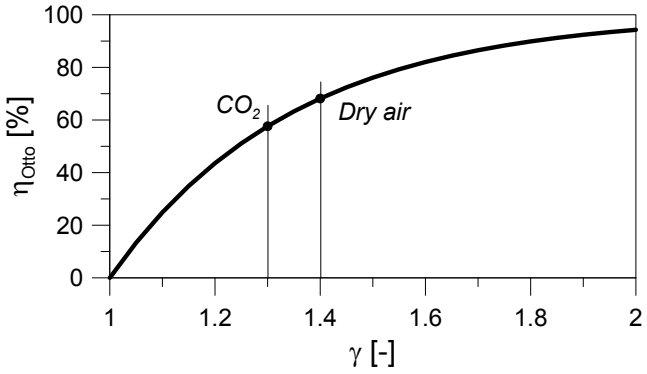

Figure 4.20. *Thermal efficiency of Otto cycle as a function of γ for a compression ratio of 17.5.*

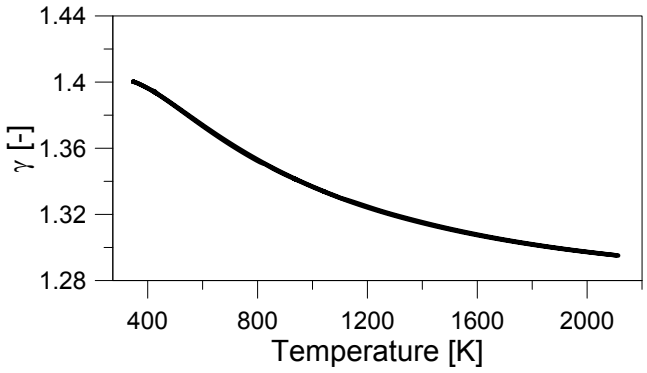

Figure 4.21. *γ evolution as a function of temperature for air.*

On the one hand, Figure 4.22 shows the variation of indicated efficiency when specific heat ratio does not change with temperature. In this study, the heat capacity ratio has been computed using the temperature at IVC of each test. As shown, there is an almost uniform value between +3% $\dot{m}_f H_v$ and +4% $\dot{m}_f H_v$ in the complete engine map, being this effect higher where higher temperatures are reached.

On the other hand, the variation of indicated efficiency due to considering just air along the complete cycle is plotted in Figure 4.23. As can be seen,

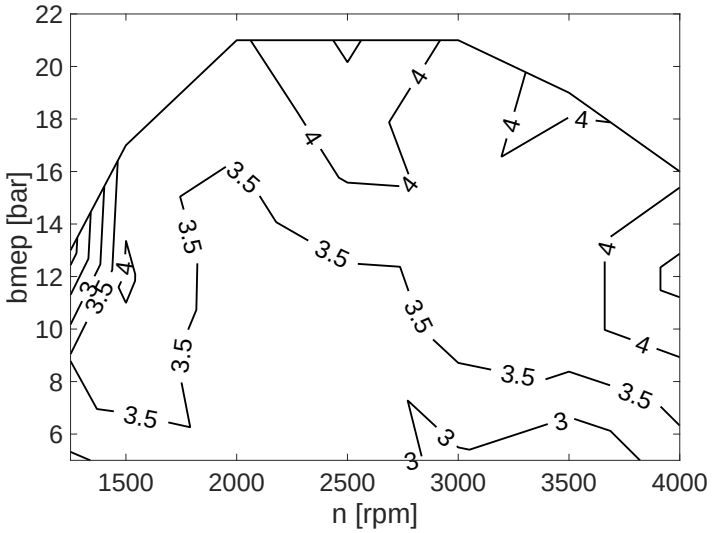

Figure 4.22. *GIE variation with respect to the nominal point if omitting the change of γ with temperature [% $\dot{m}_f H_v$].*

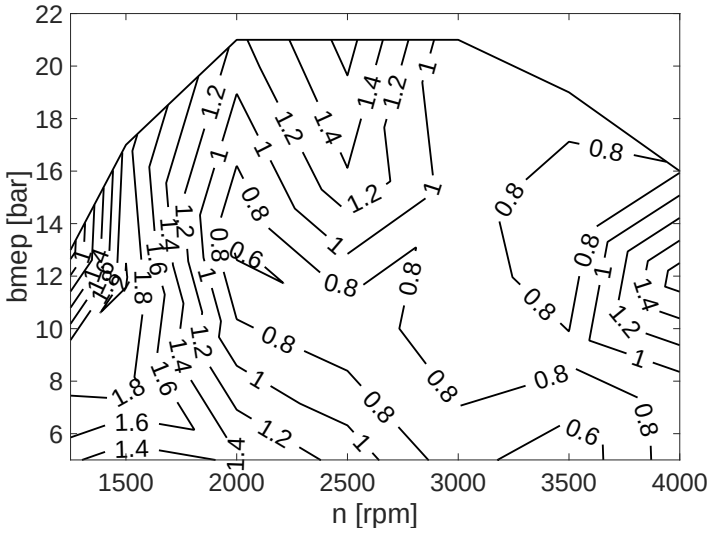

Figure 4.23. *GIE variation with respect to the nominal point if omitting the change of γ with composition [% $\dot{m}_f H_v$].*

this effect is lower than the previous one, ranging from +0.8% $\dot{m}_f H_v$ up to +1.8% $\dot{m}_f H_v$ in the engine map.

Finally, the combined effect is plotted in Figure 4.24 and it can be appreciated that it has similar distribution as the temperature effect but its value is approximately +0.5% $\dot{m}_f H_v$ higher. As a conclusion, not considering the heat capacity ratio changes with temperature and composition leads to an efficiency increase ranging from +3.5% $\dot{m}_f H_v$ to +5% $\dot{m}_f H_v$.

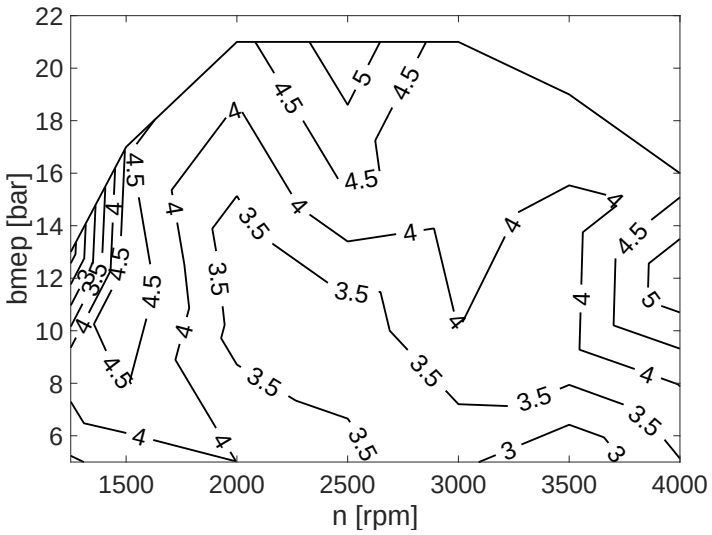

Figure 4.24. *GIE variation with respect to the nominal point when changes of γ with neither composition nor temperature are considered [% $\dot{m}_f H_v$].*

4.3.5 Air management

In this subsection, two phenomena related to the air management process in a real engine are assessed separately. On the one hand, when opening and closing events of intake and exhaust valves do not coincide with dead centres, there is an efficiency variation that is assessed in this section. On the other hand, GIE decrease experimented when gas is leaked through the gap between piston rings and liner to the crankcase is also evaluated in this section.

4.3.5.1 Valves timing

Normally, intake and exhaust valves are operated mechanically by camshafts in conventional ICE. This operation mode makes that acceleration during the opening and closing events must be limited by different parameters such as noise or rebounds. Additionally, delaying IVC up to a certain value has positive effects on the volumetric efficiency due to a better cylinder filling.

Advancing EVO, even though decreases GIE (considered only during the high pressure indicated loop), decreases importantly pumping work due to a better emptying process of the cylinder. Taking into account these considerations, OEMs normally delay IVC and advance EVO with the consequent loss in GIE due to the closed cycle shortening, even though the net indicated efficiency is not necessarily lower.

In this subsection, the GIE variation due to this shortening of the closed cycle is assessed. Nonetheless, varying the IVC timing has a direct impact on the cycle evolution due to the different in-cylinder conditions at the beginning of the closed cycle. However, if the conditions in the shifted IVC were modified to obtain the same compression than in the original IVC, the resultant GIE would not be affected. Thus, it was decided to maintain the IVC in the original position and to modify only the EVO position. Thus, Figure 4.25 shows the effect of delaying the EVO from its original position (53° before BDC) up to the BDC. As can be seen, GIE increased in the whole engine map due to the enlargement of the closed cycle, being this increment higher at low engine speed (+0.6% $\dot{m}_f H_v$).

4.3.5.2 Blow-by

This subsection deals with the effect of gas leakage from the combustion chamber through the gap between piston rings and liner to the crankcase on indicated efficiency. To asses the impact of this term, a hypothetical scenario without blow-by is considered. First of all, the experimental percentage of blow-by with respect to the total trapped mass is plotted in Figure 4.26. As can be seen, blow-by is more important at low engine speed mainly due to the higher residence time of the gas inside the combustion chamber. No clear effect of load is observed due to the fact that increasing load in a turbocharged engine implies increasing intake pressure and thus in-cylinder pressure increases both blow-by leakage and trapped mass.

Figure 4.27 represents GIE variation with respect to the nominal point when no blow-by leakages are considered. It can be seen that the gain when

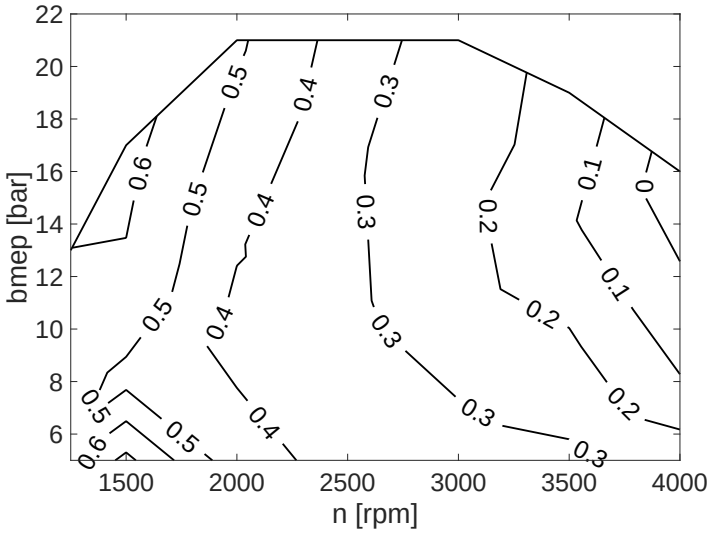

Figure 4.25. *GIE variation with respect to the nominal point when moving the EVO from its original position up to the BDC [% $\dot{m}_f H_v$].*

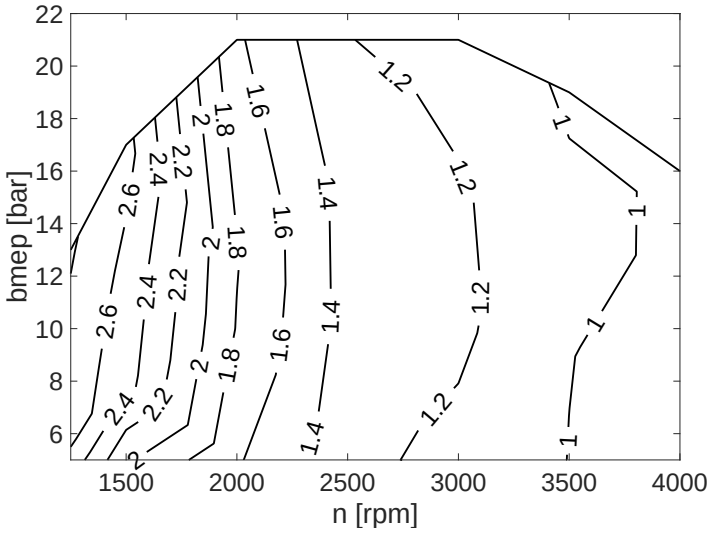

Figure 4.26. *Experimental blow-by mass respect to total trapped mass at IVC [%].*

there is not blow-by ranges from +0.4% $\dot{m}_f H_v$ at high load and engine speed to +1% $\dot{m}_f H_v$ at low load and engine speed. As expected, this term decreases when engine speed increase due to the lower experimental blow-by quantity in this area as shown in Figure 4.26. Additionally, a slight decreasing trend when load is incremented can be appreciated. Even though the blow-by percentage does not decrease with load, the distribution of the blow-by leakage along the cycle is displaced towards the expansion stroke as load increases due to the higher in-cylinder pressure. There, the mass leakage has lower influence on GIE than in the compression stroke, where this loss implies lower peak pressure.

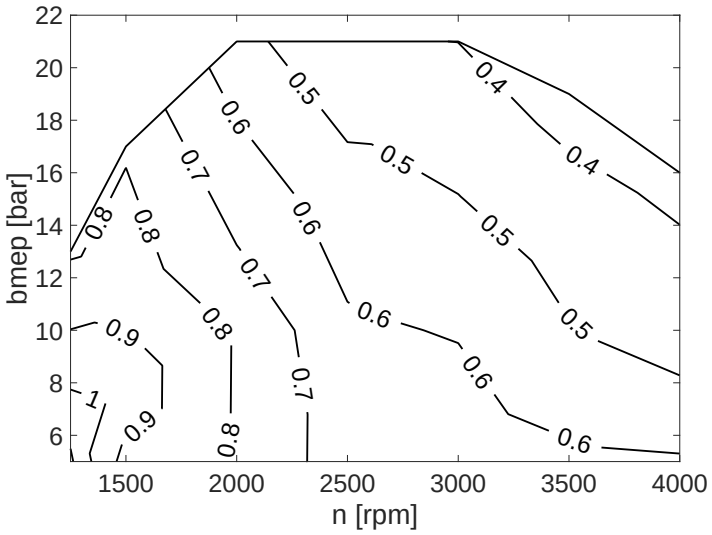

Figure 4.27. *GIE variation with respect to the nominal point when no considering blow-by leakages [% $\dot{m}_f H_v$].*

4.3.6 Summary

In order to summarize the findings of the analysis of the efficiency losses of a thermodynamic cycle presented above, Table 4.2 collects results of the maximum GIE variation found in each cycle efficiency loss assessed previously by order of importance. Regarding the combustion development, results from the two assessed scenarios have been included here, where the second scenario includes the three efficiency losses referring to the combustion development

(centring, velocity and incomplete term). In any case, considering any of them does not change the resultant efficiency losses ranking.

Efficiency loss	Maximum GIE variation [% $\dot{m}_f H_v$]	Engine map region [-]
Combustion development (Instantaneous combustion)	7.3	High speed - High load
Combustion development (Centring+Velocity+Incomplete term)	6.8	High speed - High load
Heat transfer	5	Low speed - Low load
Heat capacity ratio. Temperature	4	Medium speed - High load
Heat capacity ratio. Composition	2	Low speed - Medium load
Blow-by	1	Low speed - Low load
VT in dead centres	0.6	Low speed - High load

Table 4.2. *Summary of GIE variations in the analysis of the efficiency losses of a thermodynamic cycle.*

As shown, the ranking of the most important efficiency loss is occupied by combustion development in the first position, heat transfer appears in second place, while the third most important efficiency loss is the heat capacity ratio change due to temperature variations. Unfortunately, neither heat transfer nor heat capacity ratio change due to temperature variation efficiency losses are directly modifiable in an existent engine and both of them depend in part on the combustion development. However, the combustion development efficiency loss of a cycle is easily "removable" by computing the optimum combustion development that results in the highest GIE. Furthermore, the experimental modification of this efficiency loss is also simple to achieve in a CI engine by modifying the fuel injection pattern or the air management.

Thus, the next section is aimed to find theoretically the optimum combustion development, in terms of both velocity and centring, that provides the maximum GIE under different scenarios. Such scenarios will be useful to assess the impact on GIE due to several limitations derived from engine mechanical limits, NO_x emission regulation and/or engine hardware performance.

4.4 Theoretical optimization of HRL

As commented in Section 4.2, the maximum efficiency of an ICE is given by Otto cycle (68.2% in the studied engine). However, ideal cycle hypothesis are far away from real conditions leading to efficiencies much higher than the highest achievable one in real conditions. This efficiency gap is explained by the effect of the efficiency losses affecting real cycles as described in the previous section.

As stated in the summary of the previous analysis, the most important efficiency losses are combustion development, heat transfer and the heat capacity ratio change due to temperature variations. Among them, the combustion development efficiency loss could be eliminated if the optimum combustion evolution that provides the highest efficiency was computed. Thus, in this section, a study in which the HRL is theoretically optimized has been performed in different operating conditions of the engine map. This study has been carried out in several stages to assess the effect on optimum combustion and GIE of realistic conditions such as heat transfer, pressure limits or NO_x emissions. Thus, the objectives of this section are the following:

- To asses the best combustion evolution by computing the optimum HRL in terms of GIE and the penalties derived from the compliance to some mechanical limits.
- To evaluate the potential benefit of reducing the thermal limitation in realistic conditions by means of the application of a specific coating to cylinder-head and piston.
- To evaluate the effect of NO_x emissions limitations on the optimum HRL and to analyse the trade-off between the best achievable GIE and NO_x emissions.

4.4.1 Methodology

As commented, the main objective of this section is the optimization of the HRL to maximize GIE and minimize NO_x emissions under different constrained conditions. To do that, a 0D model has been coupled to an optimization tool that, using genetic algorithms, is able to obtain the best HRL that optimizes GIE, in the first two cases, and GIE along with NO_x emissions in the last study. Figure 4.28 shows the information flow between the optimization tool and the models when performing the optimization.

As can be seen, the optimization tool proposes a set of inputs that allows shaping the HRL, which is used by both 0D and NO_x models to perform the cycle calculation obtaining GIE and NO_x emissions as main outputs. The optimization tool receives these results as feedback and proposes a new set of inputs as a function of the fitness of the previous ones.

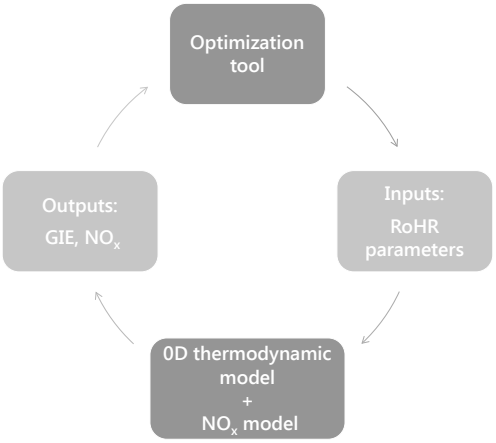

Figure 4.28. *Methodology of optimization.*

The combustion parametrization has been done by splitting the HRR in 8 sectors in which the optimization tool is able to modify the duration (in crank angle degrees) and the HRR value (non dimensional), resulting in 16 inputs. Each iteration, the tool proposes a set of inputs, the HRR is constructed interpolating these values and, prior to the 0D model execution, this shaped HRR is scaled in order to have a cumulated heat release that coincides with the fuel energy. Then, the thermodynamic cycle and NO_x emissions are computed using the resultant HRL and these outputs along with additional ones such as the peak pressure and the maximum pressure rise rate in the cycle are provided to the optimization tool, that evaluates the fitness of the iteration. More details of the optimization tool can be found in Section 3.3.3.

As commented in Chapter 1, the RDE cycle will be used as a certification cycle from September 2019 onwards. This cycle will be the first one tested on the road and it extends the engine operating range under examination with respect to the previous legislation. Figure 4.29 shows the full load curve of the multicylinder engine (black line) along with the engine map areas covered by different legislation (blue, grey and red lines) and the experimental operating conditions optimized in this section (green dots). As can be seen, both NEDC

and WLTP cover a little portion of the low engine speed map, unlike the new RDE that forces OEM's to optimize the whole engine map.

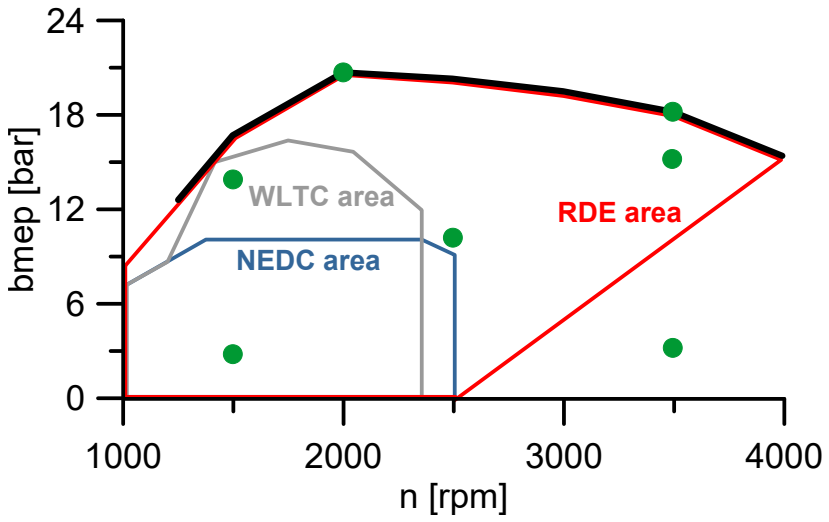

Figure 4.29. *Full load curve, certification cycles areas and operating conditions included in the optimization.*

As can be seen in Figure 4.29, the optimization methodology presented here has been applied to 7 operating conditions that represent the whole engine map in order to cover the total RDE area. This experimental matrix (main characteristics of which are presented in Table 4.3) includes 5 points at partial load and 2 additional characteristic points: maximum torque and maximum power points. These points will be named by using a composition of 2 numbers, the first one means the engine speed in revolutions per minute while the second one refers to the experimental bmep in bar (engine speed_bmep).

Once the optimization methodology has been explained, the results section is structured as follows:

- The optimum HRR is calculated in all studied points with and without heat transfer and without considering pressure limits. This step assesses the change of optimum HRL shape and GIE due to the effect of heat transfer.
- Then, the effect of different pressure limits (peak pressure and pressure rise rate) is assessed on the optimum HRL and GIE. This step provides

Engine speed [rpm]	bmep [bar]	Boost pressure [bar]	Intake temperature [°C]	EGR [%]	Rail pressure [bar]	Fuel mass [mg/cc]	GIE [%]	sNO_x [g/kWh]
1500	2.8	1.08	45	35	390	10.4	42.25	0.53
1500	13.9	1.75	45	3	1040	45.7	42.20	3.61
2000	20.7	2.18	47	0	1240	59.7	43.29	5.01
2500	10.2	1.85	46	0	1240	29.1	44.29	5.18
3500	3.2	1.58	45	0	910	13.5	44.20	2.8
3500	15.2	2.33	45	0	1590	43.9	46.04	5.13
3500	18.2	2.37	45	0	1600	54.2	44.08	4.13

Table 4.3. *Experimental data set.*

a more realistic combustion since experimental operating conditions are also limited by these constraints.

- A temperature swing coating is applied to the piston top and cylinder head surfaces in the 0D model under nominal constraints, thus providing the best achievable cycles under this insulated scenario, more realistic than adiabatic conditions explored in the first step.
- Finally, NO_x emissions are also considered in the optimization study obtaining a trade-off between efficiency and NO_x. Thus, the HRL shapes obtained in this section could be compared to the experimental ones.

4.4.2 Results and discussion

4.4.2.1 Optimum HRL without constraints

This subsection studies the optimum HRL of the selected points when no constraints are considered. Additionally, this study has also been performed considering an adiabatic engine to assess the change in the optimum combustion due to heat transfer. Figure 4.30 shows the results of this initial optimization performed at 1500_3 and at 3500_19. These points have been chosen to compare two extreme operating conditions, since the behaviour of the HRL at intermediate points was similar. As can be seen, adiabatic combustions developed instantaneously (0.5 is the minimum allowed by the calculation step) and the Start of Combustion (SOC) obtained at 1500_3 and

3500_19 was 1.5 °ATDC and 1 °ATDC respectively, while the GIE reached was 53.2% and 54.5% respectively. These slightly delayed combustions with respect to Otto cycle are due to the consideration of real processes such as blow-by, combustion chamber deformation and the heat capacity ratio change due to composition and temperature variations (unlike the ideal cycle that does not take them into account).

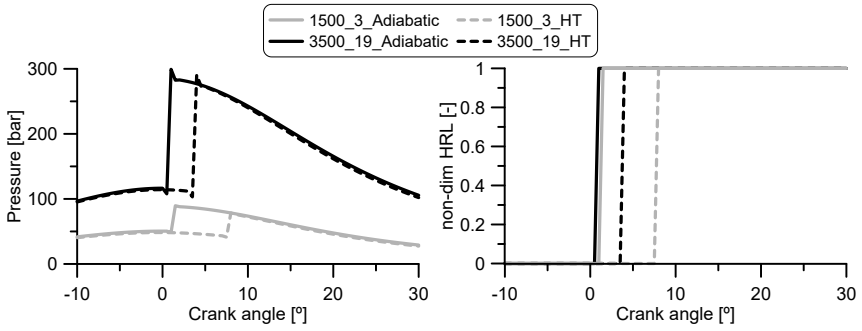

Figure 4.30. *Evolution of optimum pressure and HRL in adiabatic and non constrained conditions at 1500_3 and 3500_19.*

When heat transfer was considered, combustion was delayed but its duration was maintained instantaneous. SOCs of 1500_3 and 3500_19 were delayed 6.5° and 3° respectively resulting in an efficiency loss of -8.2% $\dot{m}_f H_v$ and -3.7% $\dot{m}_f H_v$ respect to the adiabatic case. As can be seen, heat transfer is more important at low engine speed and load leading to a more delayed optimum combustion and a higher efficiency loss.

Figure 4.31 shows the GIE variation respect to adiabatic unconstrained conditions when considering HT in the engine map. The two cases presented in Figure 4.30 corresponded to the extreme conditions of load and engine speed, thus a monotonous behaviour can be appreciated in intermediate points.

As a conclusion of this subsection, it can be confirmed that the optimum combustion develops as fast as it is allowed to. If no constraints are considered its duration is instantaneous, as Otto cycle, but its SOC is delayed respect to TDC and its efficiency is not as high due to the consideration of different real phenomena such as blow-by leakage, deformation, real gas properties and fuel vaporization. Additionally, HT consideration produces a delay in the optimum HRL and it has an important effect on GIE ranging from -8% $\dot{m}_f H_v$ at low load and engine speed to -4% $\dot{m}_f H_v$ at high load and engine speed.

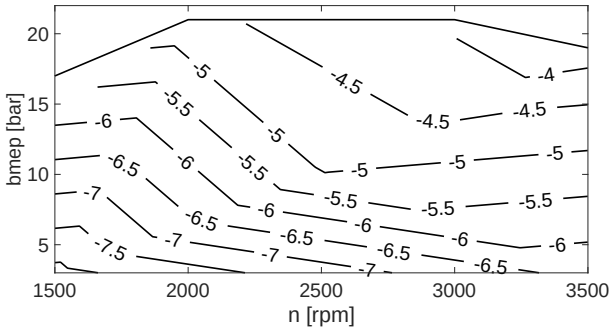

Figure 4.31. *GIE variation respect to adiabatic unconstrained conditions when considering HT in engine map [% $\dot{m}_f H_v$].*

4.4.2.2 Optimum HRL with pressure constraints

In this subsection, the optimum HRL has been studied when two different pressure constraints are considered. The first limit is the pressure rise rate (PRR), which is related to combustion noise, while the second one is the peak pressure (PP), value of which is limited by OEMs to avoid mechanical problems. In the studied engine, its constructor set a PRR limit of 10 bar/° and a maximum pressure of 160 bar to keep the engine integrity. However, current innovative engine design and materials allow overcoming these limits leading to engine blocks able to cope with maximum pressures up to 210 bar [24]. For this reason, the study does not only focus on the nominal limits of this engine but also in other plausible boundaries.

First of all, different PRR limits were applied to the optimization study at 3500_19, obtaining the results plotted in Figure 4.32 where also the unconstrained solution is shown. For the sake of brevity, this point will be the only one plotted here since the optimum combustions in the rest of the points followed the same behaviour. As can be seen, the optimum HRL is shaped in a way to exactly reproduce the pressure evolution marked by the PRR limit considered. Combustion duration increased and SOC advanced as limit became more restrictive, thus keeping the combustion centre not so far from TDC.

Plots of Figure 4.33 show the GIE variation when considering different PRR limits (2.5 bar/° at left and 10 bar/° at right) in the engine map. As can be seen, at low load the effect of both limits is similar leading to an efficiency

loss of about -1.4% $\dot{m}_f H_v$ while at high load the most tightened PRR scenario decreases efficiency -2.8% $\dot{m}_f H_v$ and the most relaxed one -1.8% $\dot{m}_f H_v$.

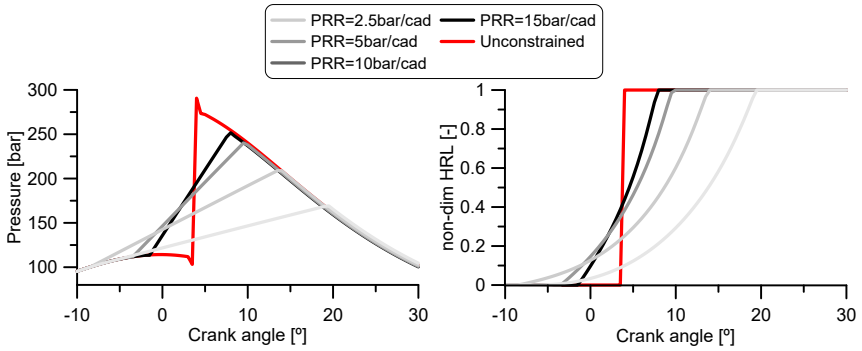

Figure 4.32. *Evolution of optimum pressure and HRL at 3500_19 when different PRR limits are imposed.*

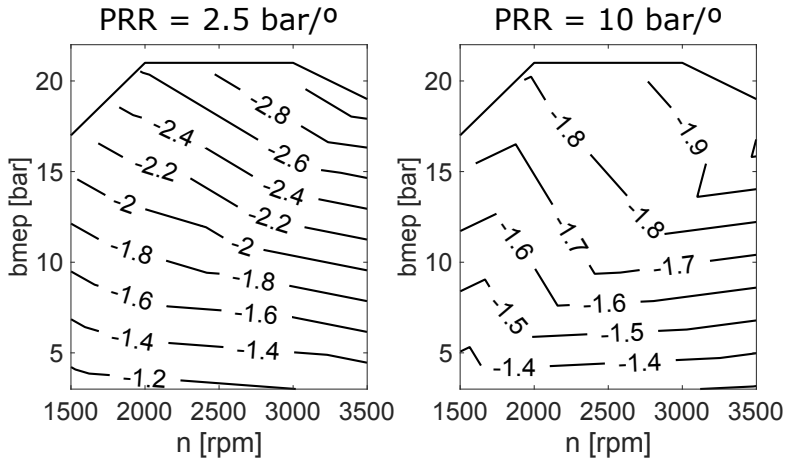

Figure 4.33. *GIE variation respect to unconstrained optimum with HT when considering different PRR limits in engine map [% $\dot{m}_f H_v$].*

On the other hand, when different peak pressure limits were applied to the unconstrained solution, Figure 4.34 was obtained. As shown, the optimum HRL with PP constraints is divided into two stages: the first one is an instantaneous combustion up to the limited pressure is reached and the second one consists on the heat release necessary to maintain this pressure constant

until the total amount of fuel is burned. When limit is tightened, SOC of the optimum HRR advances while the duration of the combustion at constant pressure increases.

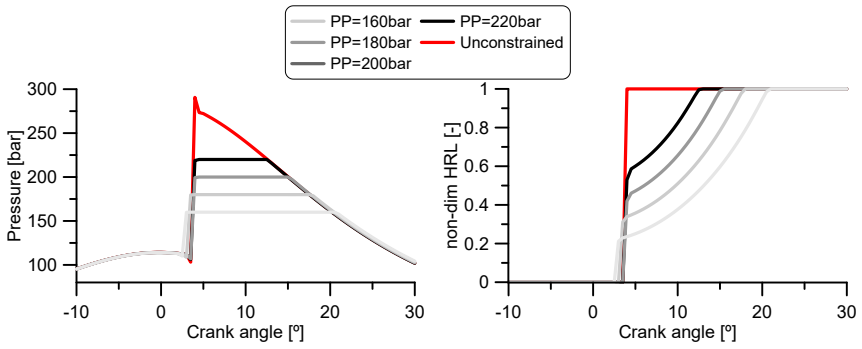

Figure 4.34. *Evolution of optimum pressure and HRL at 3500_19 when different PP limits are imposed.*

Figure 4.35 shows GIE variation when considering different PP limits (160 bar at left and 220 bar at right) in the engine map. First of all, GIE at low load is not affected since peak pressure in the optimum unconstrained solution in this region did not reach the imposed peak pressure limits. The efficiency loss due to the consideration of this PP limits increases monotonously with load, reaching -2.5% $\dot{m}_f H_v$ in the most constrained scenario and around -1% $\dot{m}_f H_v$ in the most relaxed one.

Finally, Figure 4.36 shows the evolution of the pressure and HRL at 3500_19 when both PRR and PP limits were considered in three scenarios: the first one represents the most constrained situation (PRR=2.5 bar/° and PP=160 bar), the second one corresponds with the most relaxed one (PRR=15 bar/° and PP=220 bar) while the third one stands for the nominal limits of the engine (PRR=10 bar/° and PP=160 bar). Additionally, the experimental evolution and the optimum unconstrained solution have also been included in this graph to compare them with the optimum limited solutions. It can be seen that the optimum constrained combustion follows exactly the limits imposed leading again to a two-stage combustion, where the first stage is defined by the imposed PRR until the limited peak pressure is achieved and then, the HRL is shaped to maintain constant this maximum pressure until the total available energy is released. If the experimental combustion is compared with the constrained solution under nominal limits, it can be seen that the experimental one is

much longer and its maximum pressure gradient and peak pressure are lower than the theoretical one.

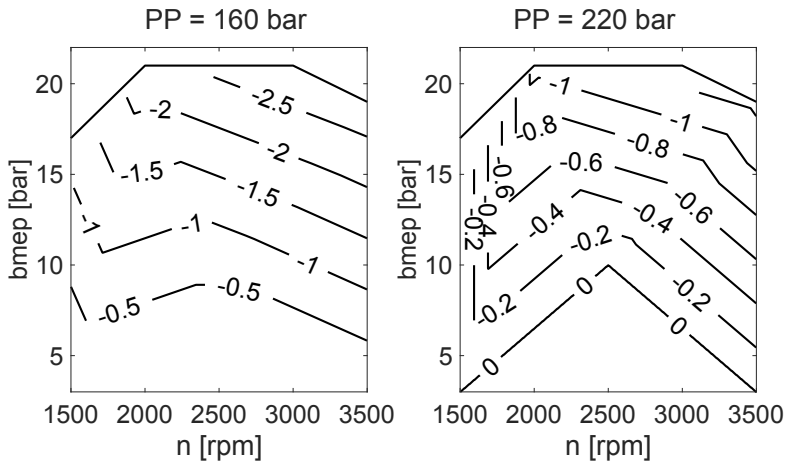

Figure 4.35. *GIE variation respect to unconstrained optimum with HT when considering different PP limits in engine map [% $\dot{m}_f H_v$].*

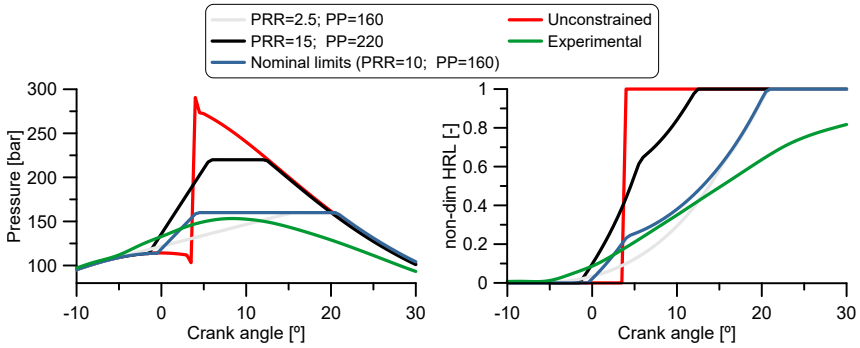

Figure 4.36. *Evolution of optimum pressure and HRL at 3500_19 when different PP and PRR limits are imposed.*

Figure 4.37 shows the GIE variation when considering nominal pressure limits (PRR=10 bar/° and PP=160 bar) in the engine map if it is compared with the non constrained scenario. It can be seen that this efficiency loss is mainly dependant on load, except at low engine speed and high load where it can also be discerned a dependency on engine speed because the peak pressure

limit was not reached at this region. In any case, the reduction of GIE due to the consideration of nominal limits ranges from -1.4% $\dot{m}_f H_v$ at low load to -2.8% $\dot{m}_f H_v$ at high load and engine speed.

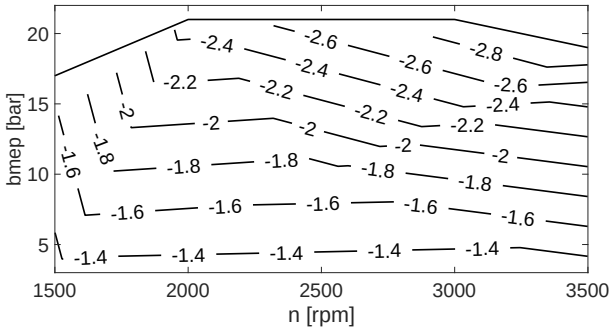

Figure 4.37. *GIE variation respect to unconstrained optimum with HT when considering nominal pressure limits (PRR = 10 bar/° and PP = 160 bar) in engine map [% $\dot{m}_f H_v$].*

The conclusion stated in the previous subsection is also valid in this one, the optimum combustion develops as fast as it is allowed to. In this case, when pressure limits were taken into account, the optimum HRL was shaped in a way to reproduce exactly the considered constraints. GIE evolution under nominal pressure limits was plotted in Figure 4.38, where it can be seen an almost linear increase with load and engine speed starting from 44% and reaching GIE above 48% at the high load and engine speed region. This efficiency map establishes the maximum GIE achievable in the studied engine taking into account heat transfer and real pressure limits and it sets up the basis for the following studies.

4.4.2.3 Temperature swing insulation scenario

In order to asses the efficiency limits under a realistic thermal insulation scenario, unlike the ideal one presented in Section 4.4.2.1, the GIE variation experimented when applying a TBC on combustion chamber walls was assessed. Thus, the HRL was optimized here assuming that some combustion chamber walls were coated with 100 μm of a previously reported material named as *"silica-reinforced porous anodized aluminium"* (SiRPA) [4] under nominal pressure limits. This material is capable to quickly change its surface temperature during the entire cycle following the gas transient temperature

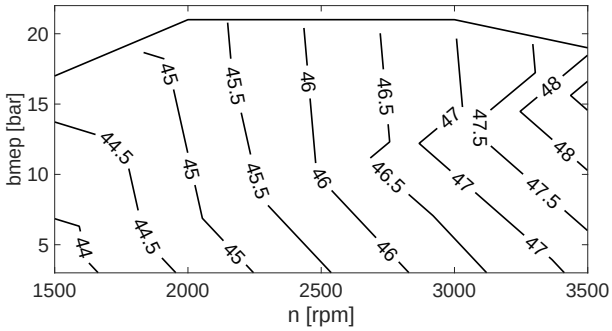

Figure 4.38. *GIE in engine map when considering nominal pressure limits (PRR = 10 bar/° and PP = 160 bar) [% $\dot{m}_f H_v$].*

due to its low volumetric specific heat capacity (1300 kJ/m^{3}K), half the one of solid aluminium, and thanks to its low thermal conductivity (0.67 W/mK).

These properties permit that its temperature swings along the combustion cycle, reducing the temperature drop between gas and walls with the consequent lower heat rejection, higher efficiency and enhancement of exhaust gas temperatures. Additionally, lower temperatures during the intake stroke contribute to higher volumetric efficiencies. However, since this study is focused on thermal efficiency in closed cycle, only the effects of this coating on GIE are assessed. It is considered that only cylinder head and piston top surface are suitable for this coating, being not possible to apply it on the cylinder liner because of the friction with piston rings.

Figure 4.39 shows the temperature of the different combustion chamber walls and the gas mean temperature along the cycle with and without coating at 1500_3, which was the most benefited point when conducting this approach due to its higher heat rejection. As can be seen, the coating allows a temperature swing of around 60 K in the surfaces where coating was applied. Since this variation is much lower than the change of gas mean temperature along the cycle (20 times lower in this case), the effect produced in the optimum combustion is limited, and thus only a 0.5° earlier combustion when coating is applied can be appreciated in the gas temperature rise in Figure 4.39. The variation of surface temperature along the cycle depends on the operating conditions, reaching 200 K at low engine speed and high load, but in no case, this variation supposes more than 10% of the gas mean temperature change and its influence on the optimum combustion is reduced to a slightly earlier combustion as explained.

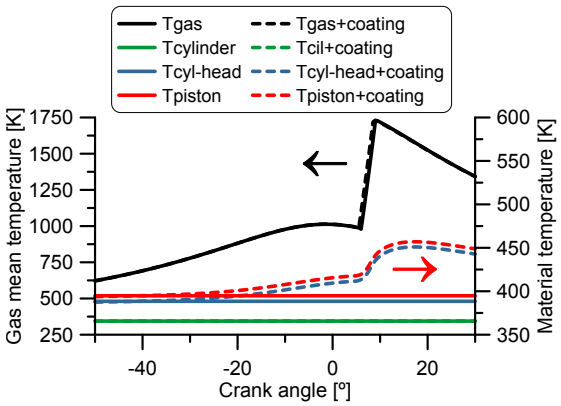

Figure 4.39. *Evolution of gas mean temperature and combustion chamber walls temperature with and without coating at 1500_3.*

Figure 4.40 shows the GIE variation in the engine map due to the consideration of this coating. As can be observed, points at low load and low engine speed are the most benefited ones when this approach is followed due to its higher heat transfer. However, the maximum benefit obtained due to the use of this coating does not reach +0.5% $\dot{m}_f H_v$ in this zone and it is around +0.25% $\dot{m}_f H_v$ at the high load and engine speed zone. These results show a clear lower potential benefit in comparison with the optimistic +2% $\dot{m}_f H_v$ reported by Kawaguchia *et al.* [25].

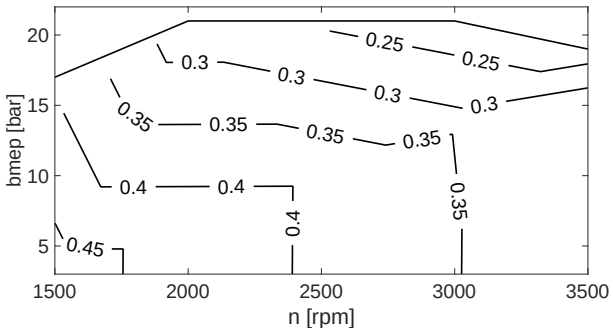

Figure 4.40. *GIE variation respect to nominal constrained optimum due to the application of a temperature swing coating on cylinder-head and piston top surface [% $\dot{m}_f H_v$].*

Once the effect of coating on GIE has been quantified, the analysis continues in next section with additional limitations due to pollutants and coming back to conventional walls properties. As explained, the maximum potential benefit of coating on GIE is lower than +0.5% $\dot{m}_f H_v$. Since the consideration of NO_x limits in next section will lead to combustion at lower temperatures, the coating effect would be even lower, thus this strategy is not considered in the next section.

4.4.2.4 Optimum HRL with nominal constraints and NO_x model

In this subsection NO_x emissions were also included in the optimization methodology under nominal constraints (PP=160 bar and PRR=10 bar/°). Unlike previous analysis in which there was just one objective (GIE), including NO_x emissions in the assessment leads to a multiobjective optimization problem with infinite solutions depending on the weight of each objective, thus resulting in a trade-off between efficiency and NO_x emissions. It is necessary to take into account that the NO_x model used in this work, as explained in Section 3.3.2, is a semiempyrical model that has been calibrated in the operation range of the engine. Thus, even though it is useful to understand trends, the accuracy of the prediction of NO_x emissions under such very rapid combustions is not completely guaranteed, as later discussed.

As extracted from previous sections, the optimum combustion in terms of GIE was the fastest achievable one taking into account the imposed limits. Additionally, it is well-known that high temperature combustions enhance NO_x formation. Thus, optimum solutions when GIE and NO_x emissions are considered should be rapid combustions at low temperature. Evolution of mean gas temperature and HRL at some specific NO_x emissions levels along with the optimum constrained solution under nominal limits and the experimental results are plotted in Figure 4.41 at 3500_19.

For the sake of brevity, evolution of optimum HRL and pressures in all points are not shown but their behaviour are pretty similar to the ones plotted at this point. Main changes when NO_x was forced to be reduced were that SOC was delayed and the first part of the combustion developed slower, however, the total combustion duration did not vary significantly (it was always around 20° in this point) because the second combustion stage was accelerated in order to increase GIE. As explained, optimum combustions developed quickly but delayed from TDC as NO_x constraint became tighter to avoid high gas temperatures. This 2-stage combustion became even more differentiated as NO_x was reduced, the first one became slower while the second one increased progressively its velocity.

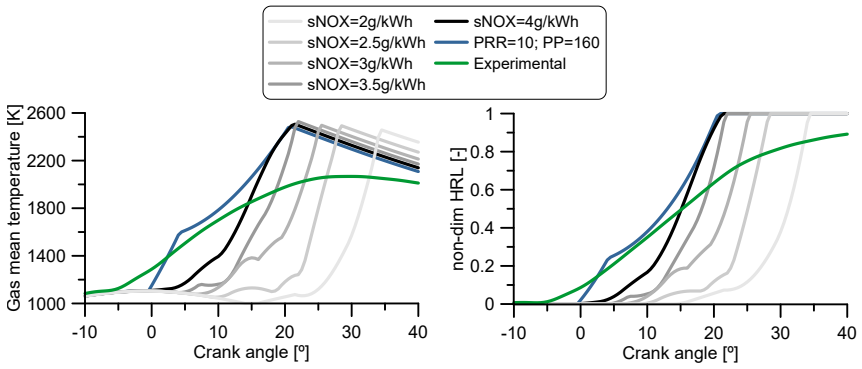

Figure 4.41. *Evolution of gas mean temperature and HRL at 3500_19 under different* NO_x *emissions levels.*

In the left plot of Figure 4.42, the red line represents the best solutions in terms of maximum GIE and minimum NO_x emissions obtained after the heat release optimization (red dots) at 3500_19. Additionally, other points of interest are also plotted there: the green point stands for the experimental measurement, the blue point represents the constrained optimum solution without NO_x limits and greyscale points correspond to greyscale lines represented in Figure 4.41. As can be seen, the optimization methodology has improved the experimental GIE and specific NO_x emissions, achieving an improvement of +3% $\dot{m}_f H_v$ in GIE if the experimental NO_x emissions (4.13 g/kWh) are maintained and a reduction of 1.5 g/kWh in NO_x if the experimental GIE (44.1% $\dot{m}_f H_v$) is kept constant.

If the optimum trade off between GIE and NO_x is analysed, it can be observed that a maximum GIE of 47.9% $\dot{m}_f H_v$ is achieved when no NO_x emissions are taken into account (resultant from previous optimization) while the minimum NO_x emissions are 1.64 g/kWh with a penalty in GIE, which is reduced to 36.6% $\dot{m}_f H_v$. In any case, since the medium zone of the tradeoff with efficiencies higher than 44% $\dot{m}_f H_v$ and NO_x emissions below 4 g/kWh should be the target zone, three of the greyscale points located in this area will be later analysed. It is important to remark that this operating condition is the maximum power point in the engine map, so emissions ranging from 2 g/kWh to 5 g/kWh can be considered as normal.

The right plot of Figure 4.42 shows the GIE and NO_x emissions optimization in all the studied points along with their experimental values. As can be seen, all tradeoffs improved clearly the experimental measurement,

ranging from 1 g/kWh to 5 g/kWh of NO_x emissions and GIE from 34% to 48% covering a wide range of optimum solutions. The only one tradeoff out of these ranges is 1500_3, NO_x emissions of which are much lower and GIE -4% $\dot{m}_f H_v$ lower than the other points, due to the use of 35% of EGR. These results are coherent with the experimental measurement, which is also in the same range, validating in this way the obtained tradeoff.

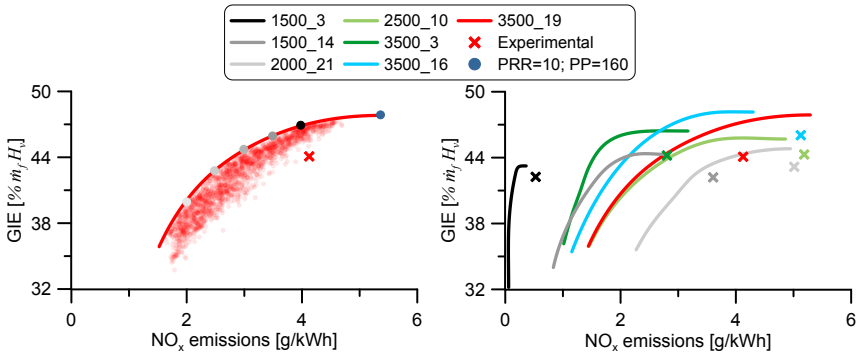

Figure 4.42. *Optimum tradeoff between GIE and* NO_x *emissions at 3500_19 (left plot) and at all studied points (right plot).*

If these optimized tradeoffs were compared with the optimum cycle without NO_x constraints or with the experimental points, several conclusions could be extracted. On the one hand, the first study is aimed to compare the NO_x emissions levels of both theoretical optimization and experimental cases. However, since in some cases experimental emissions were higher than the worst case of the optimization, it was decided to compare them at 50% of the experimental NO_x value. Thus, Figure 4.43 represents GIE variation of emitting 50% of experimental NO_x in the engine map when comparing to the optimum combustion under nominal limits of PP and PRR. As can be seen, meeting these emissions targets supposes a GIE decrease that ranges from -1% $\dot{m}_f H_v$ at low load and engine speed to -8% $\dot{m}_f H_v$ at high load.

On the other hand, Figure 4.44 shows the variation of NO_x emissions in relative value respect to the experimental case if experimental GIE of each studied point is assumed in the theoretical optimization. As can be observed, at low load and engine speed the optimization allows a reduction of 65% in NO_x emissions if the experimental GIE is maintained, while at high load a decrease of 30% is achieved at the same GIE.

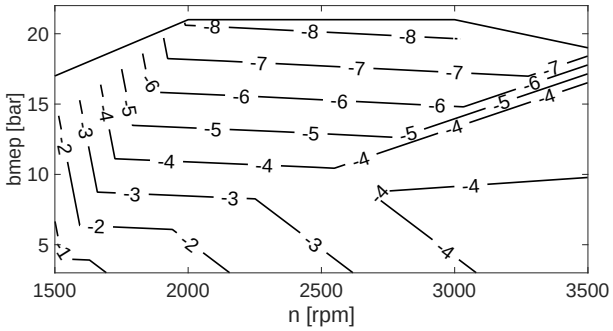

Figure 4.43. *GIE variation respect to nominal constrained optimum when decreasing* NO_x *emissions up to 50% the experimental value in [%* $\dot{m}_f H_v$*].*

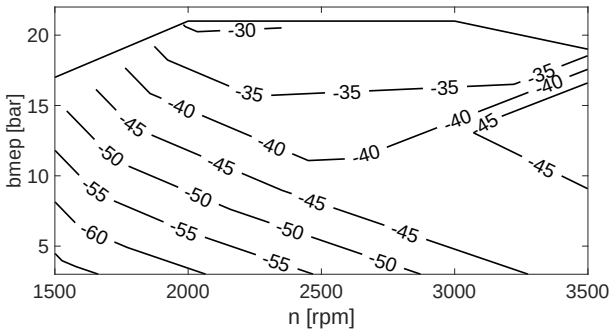

Figure 4.44. *Relative reduction respect to experimental* NO_x *emissions value if experimental GIE is assumed in the theoretical optimization [%].*

4.5 Conclusions

In this chapter, the main ideal cycles and its maximum efficiency in the studied engine have been dealt with. Additionally, an assessment of all efficiency losses that separate these ideal cycles from the real ones has been performed. Finally, it has been analysed the optimum HRL in terms of GIE under different scenarios using a detailed 0D predictive model that includes all relevant phenomena such as fuel vaporization, blow by leakages, combustion chamber deformation and real gas properties. The optimization has been performed under different scenarios defined by the consideration of some constraints such as maximum peak pressure or maximum pressure rise rate and the assessment of heat transfer, considering an adiabatic engine or a

temperature swing coating applied to piston top and cylinder head. Finally, NO_x emissions have also been included in the optimization process obtaining tradeoffs between GIE and NO_x in all studied points. Main conclusions of the chapter are the following:

- The maximum GIE obtained with an ideal cycle in the studied engine was given by the Otto cycle and it reached 68.2%. However, the assumption of the hypothesis related to ideal cycles led to efficiencies much higher than the obtained ones under real conditions.
- The efficiency losses with higher effect on GIE by importance order were the combustion development (around 7% $\dot{m}_f H_v$), then heat transfer appeared in second place with about 5% $\dot{m}_f H_v$, while the third most important efficiency loss was the heat capacity ratio change due to temperature variations (4% $\dot{m}_f H_v$).
- Unconstrained optimum HRL with adiabatic chamber assumption was an instantaneous combustion starting around 1°ATDC with GIE ranging from 52% $\dot{m}_f H_v$ to 55.5% $\dot{m}_f H_v$ depending on the operating point. These instantaneous combustions were not placed in the TDC due to the consideration of real processes such as blow-by, combustion chamber deformation and heat capacity ratio change due to composition and temperature variations (unlike ideal cycles that do not take them into account).
- Heat transfer assessment under no constraints delayed the optimum HRL but it continued being an instantaneous combustion. GIE decreased from -4% $\dot{m}_f H_v$ at high load and engine speed to -8% $\dot{m}_f H_v$ at low load and engine speed when nominal HT was considered.
- Optimum HRL when peak pressure and/or pressure rise rate limits were considered was divided into two stages: the first one burnt as quick as it was allowed (instantaneously if no PRR limit was applied or following the imposed pressure gradient if a PRR limit was considered) until the maximum pressure was reached, then the HRL was shaped to exactly obtain the maximum pressure marked by the limit until the total amount of fuel was burnt. The scenario where nominal limits (PRR=10 bar/° and PP=160 bar) were applied to the studied points led to an efficiency reduction ranging from -1.4% $\dot{m}_f H_v$ at low load to -2.8% $\dot{m}_f H_v$ at high load when comparing to the previous non restricted optimum solutions.
- The application of a temperature swing coating to the piston top surface and cylinder head walls did not have a big impact on optimum HRL, and

made that optimum combustions started slightly earlier. These changes were translated to a marginal GIE increase ranging from less than +0.5% $\dot{m}_f H_v$ at low load and engine speed to +0.25% $\dot{m}_f H_v$ at high load and engine speed.

- The consideration of NO_x emissions in the optimization problem led to a non unique optimum solution, but a set of optimum HRL that maximized GIE while minimizing NO_x emitted. This group of solutions formed the expected tradeoff between these 2 variables, conditioning the final choice to the requirements of the specific operating condition. In any case, decreasing NO_x emissions until 50% of the experimental value implied a penalization on GIE up to -8% $\dot{m}_f H_v$ at high load when comparing to the optimum combustion under nominal limits of PP and PRR. Additionally, if the experimental GIE of each point is maintained in the optimum theoretical tradeoff, a decrease ranging from 30% at high load to 65% at low load in NO_x emissions was achieved when comparing with the experimental emissions.

Bibliography

[1] Zeldovich J. "The Oxidation of Nitrogen on Combustion and Explosions". *European Physical Journal A. Hadrons and Nuclei*, Vol. 21, pp. 577–628, 1946.

[2] Patterson M., Kong S., Hampson G. and Reitz R. "Modeling the Effects of Fuel Injection Characteristics on Diesel Engine Soot and NOx Emissions". *SAE Transactions*, Vol. 103, pp. 836–852, 1994.

[3] Guardiola C., López J.J., Martín J. and García-Sarmiento D. "Semiempirical in-cylinder pressure based model for NOX prediction oriented to control applications". *Applied Thermal Engineering*, Vol. 31 n^o 16, pp. 3275–3286, 2011.

[4] Wakisaka Y., Inayoshi M., Fukui K., Kosaka H. and Hotta Y. "Reduction of Heat Loss and Improvement of Thermal Efficiency by Application of Temperature Swing Insulation to Direct-Injection Diesel Engines". *SAE Int. J. Engines*, 2016.

[5] Moran M.J., Shapiro H.N., Boettner D.D. and Bailey M.B. *Fundamentals of Engineering Thermodynamics, 8th Edition:*. Wiley, 2014.

[6] Çengel Y.A. and Boles M.A. *Thermodynamics: An Engineering Approach*. Cengel series in engineering thermal-fluid sciences. McGraw-Hill, 2011.

[7] Glaude P., Fournet R., Bounaceur R. and Molière M. "Adiabatic flame temperature from biofuels and fossil fuels and derived effect on NOx emissions". *Fuel Processing Technology*, Vol. 91 n^o 2, pp. 229–235, 2010.

[8] Curzon F. L. and Ahlborn B. "Efficiency of a Carnot engine at maximum power output". *American Journal of Physics*, Vol. 43 n^o 1, pp. 22–24, 1975.

[9] Chen L., Sun F. and Wu C. "Influence of heat transfer law on the performance of a Carnot engine". *Applied Thermal Engineering*, Vol. 17 n^o 3, 1997.

[10] Fu J., Liu J., Feng R., Yang Y., Wang L. and Wang Y. "Energy and exergy analysis on gasoline engine based on mapping characteristics experiment". *Applied Energy*, Vol. 102, pp. 622–630, Febrero 2013.

[11] Payri F. and Desantes J.M. *Motores de combustión interna alternativos*. Reverté, ISBN 978-84-291-4802-2, Barcelona, 2011.

[12] Weberbauer F., Rauscher M., Kulzer A., Knopf M. and Bargende M. "Generally applicate split of losses for new combustion concepts". *MTZ worldwide*, Vol. 66 n^o 2, pp. 17–19, 2005.

[13] Rakopoulos C.D. and Giakoumis E.G. "Second-law analyses applied to internal combustion engines operation". *Progress in Energy and Combustion Science*, Vol. 32 n^o 1, pp. 2–47, 2006.

[14] Thirouard M., Knop V. and Pacaud P. "Downsizing or cylinder number reduction in Diesel engines : effect of unit displacement on efficiency and emissions". In *THIESEL 2012 Conference on Thermo- and Fluid Dynamic Processes in Diesel Engines*, pp. 1–19, 2012.

[15] Wissink M., Splitter D., Dempsey A., Curran S., Kaul B. and Szybist J. "An assessment of thermodynamic merits for current and potential future engine operating strategies". *International Journal of Engine Research*, Vol. 18 n^o 1-2, pp. 155–169, 2017.

[16] Hoffmann K., Watowich S. and Berry R. "Optimal paths for thermodynamic systems: The ideal diesel cycle". *Journal of Applied Physics*, Vol. 58 n^o 6, pp. 2125–2134, sep 1985.

[17] Parlak A. "The effect of heat transfer on performance of the Diesel cycle and exergy of the exhaust gas stream in a LHR Diesel engine at the optimum injection timing". *Energy Conversion and Management*, Vol. 46 n^o 2, pp. 167–179, Enero 2005.

[18] Ebrahimi R. "Performance of an irreversible Diesel cycle under variable stroke length and compression ratio". *Journal of American Science*, Vol. 6 n^o 1, pp. 58–64, 2010.

[19] Sabathé, L. "Internal Combustion Engine". *United States Patent Office*, 1908.

[20] Okamoto T. and Uchida N. "New Concept for Overcoming the Trade-Off between Thermal Efficiency, Each Loss and Exhaust Emissions in a Heavy Duty Diesel Engine". *SAE International Journal of Engines*, Vol. 9 n^o 2, pp. 2016–01–0729, 2016.

[21] Guardiola C., Climent H., Pla B. and Reig A. "Optimal Control as a method for Diesel engine efficiency assessment including pressure and NOx constraints". *Applied Thermal Engineering*, Vol. 117, pp. 452–461, 2017.

[22] Postrzednik S. and Zmudka Z. "Achievement of the charge exchange work diminishing of an internal combustion engine in part load". *Transport Problems*, Vol. 7 n^o 1, pp. 63–76, 2012.

[23] Broatch A., Martín J., García A., Blanco-Cavero D., Warey A. and Domenech V. "Application of a zero-dimensional model to assess the effect of swirl on indicated efficiency". *International Journal of Engine Research*, pp. 1–12, 2018.

[24] Steinparzer F., Nefischer P., Hiemesch D. and Rechberger E. "The New BMW Six-cylinder Top Engine with Innovative Turbocharging Concept". *MTZ worldwide*, Vol. 77 n^o 10, pp. 38–45, 2016.

[25] Kawaguchi A., Iguma H., Yamashita H., Takada N., Nishikawa N., Yamashita C., Wakisaka Y. and Fukui K. "2016-01-2333 Thermo-Swing Wall Insulation Technology; - A Novel Heat Loss Reduction Approach on Engine Combustion Chamber". *SAE Technical Paper*, n^o 2016-01-2333, 2016.

Chapter 5

Experimental optimization of HRL and assessment of real combustion effect on indicated cycle

Contents

5.1 Introduction

As concluded in the previous chapter, the most important efficiency losses in the in-cylinder processes are heat transfer, combustion development (mainly velocity) and heat capacity ratio change due to temperature variations, so that efforts when optimizing a certain cycle should be addressed to reduce them.

The combustion development efficiency loss could be reduced following different approaches aimed to enhance the air-fuel mixing and combustion processes such as the swirl ratio increment [1] or the injection pattern optimization, among others already mentioned in Chapter 2.

Regarding heat transfer effect, some strategies are aimed to decrease the gas temperature or to apply a thermal insulation to the combustion chamber walls. Approaches such as the addition of high EGR quantities [2] or low temperature combustion concepts based on dual fuel [3] have been used to reduce gas temperature and thus, diminish heat transfer to combustion chamber. Additionally, thermal insulations such as conventional thermal barrier coatings [4] or temperature swing coatings [5], as the one studied in Section 4.4.2.3, are being developed to reduce heat transfer to combustion chamber.

Finally, the efficiency losses related to the heat capacity ratio change due to temperature variations could be reduced using the same strategies mentioned in the previous paragraph for decreasing the gas temperature.

On the one hand, all the strategies dealing with the thermal insulation require specific hardware, out of the scope of this work. It is also the case of the strategies based on new low temperature combustion modes. On the other hand, the main phenomenon affecting the gas temperature (and thus HT and specific heat) is the combustion development. Furthermore, the combustion velocity is something controllable, up to a certain point, thanks to the sophisticated injection systems and advanced air management strategies used nowadays in CI engines. As indicated, injection settings and swirl can be used to enhance the combustion velocity thus, these two techniques are assessed thoroughly in this chapter in order to go deeper in the effects of their changes on the combustion development and thus, on the engine performance.

It must also be considered that, although the efficiency losses have been presented separately, they are interconnected and each change affecting one of them has a certain impact in the remaining two. For instance, using swirl motion to enhance the combustion velocity leads to an increase of the heat transfer. Thus, the assessment of a certain strategy cannot be done just looking at GIE but performing a dedicated analysis to isolate the effect of every efficiency loss on the final GIE. Thus, the split of losses analysis presented in Chapter 2 is applied here to assess the impact of both efficiency losses on GIE variations when performing the analysis of the swirl.

Then, some operating conditions are experimentally optimized. This optimization assesses the best combination of both parameters in terms of gross indicated efficiency and NO_x emissions. The optimum HRL derived from this experimental optimization is compared then with the best combustion laws obtained in the theoretical analysis carried out in Chapter 4. Unlike the theoretical optimum HRL, the experimental one depends on the combustion development resulting from the air and fuel mixing process. If the existent hardware allowed these processes to be perfect and the combustion velocity was not limited, the experimental optimization should reach the theoretical one. Therefore, differences in these 2 approaches should be attributed to the combustion velocity limit derived from the use of a certain hardware. This comparison could be useful as a tool to perform a benchmarking between different hardware architectures.

Taking into account the previous considerations, this chapter is structured in three parts. The first one is focused on the evaluation of two techniques (swirl and injection settings) used to improve combustion development. Then, using the conclusions extracted in this first analysis, the second one deals with the experimental HRL optimization in terms of GIE and NO_x emissions of different experimental conditions. Finally, the third section of this chapter is

a comparison between this experimental optimization and the theoretical one developed in the previous chapter taking into account GIE and NO_x emissions to obtain the impact on GIE and NO_x of the combustion development limitation due to the existent hardware.

5.2 Assessment of different techniques to enhance combustion velocity

In this section, two of the most common strategies followed nowadays in Diesel engines to increase combustion velocity are evaluated. On the one hand, air motion in the chamber is a key issue to improve the air-fuel mixing process and achieve faster burning rates [6]. Therefore, modern Diesel engines are designed to generate high Swirl Ratios (SR) in the chamber that lead to enhanced turbulence during the combustion process, specially in the late combustion part, thus reducing soot emissions and consumption [7]. On the other hand, different injection strategies combining the use of high injection pressures and multiple injection events are used nowadays by OEMs to limit pollutant emissions while keeping thermal efficiency as high as possible.

5.2.1 Swirl approach

The main air rotation macro structures that can be found in ICE are swirl and tumble, being differentiated by their rotary axis (swirl rotates around the cylinder axis while tumble around the diametrical axis) and by the combustion mode in which they are applied: swirl is used in CDC while tumble is common in CGC. Both are generated during the intake process thanks to the ports geometry and evolve during compression thanks to the combustion chamber configuration.

Since the engines assessed in the work operate under CDC mode, this section is focused only in swirl motion. There are two different kinds of intake ports in CI engines aimed to apply this technique; a tangential port, used to generate swirl motion, and a opposed helical port that brakes it and has a higher flow capacity. During the compression stroke, the swirl movement is promoted by the chamber geometry consisting of a shallow bowl in the piston crown [6] that allows accelerating the air rotation thanks to the angular momentum conservation.

A common technique used to get variable swirl consists in placing a throttle valve upstream of the helical port [8]. When high flow is required, this valve is

fully open achieving the lowest swirl ratio, while it is completely closed when a high swirl level is required. High swirl conditions normally are used at low load and engine speed, when less fresh air is necessary, while low swirl is set at high speed and load to reach a suitable air feeding through the helical port. In return, this technique has a big impact on the air management process since it produces a higher pressure drop in the helical port due to the control valve. This makes necessary a higher boost pressure to get the same trapped mass in the cylinder, therefore the turbine section must be reduced to reach the required intake pressure. These changes and derived consequences will be evaluated in this study.

Apart from the benefits on combustion enhancement, there are some disadvantages derived from the use of swirl. The main problem is the enhancement of HT in the chamber due to the higher gas velocity that increases the heat transfer coefficient. The swirl characteristics have been widely studied, and most HT correlations include a term accounting for its contribution to the characteristic gas velocity used to calculate the HT coefficient [9, 10]. Therefore, swirl leads to a contradictory scenario where it benefits efficiency through the improved combustion development and worsens it due to the increased HT. Thus, an adequate swirl level could be used to optimize the GIE, soot and NO_x trade-off [11].

5.2.1.1 Methodology

The objective of this study is the assessment of the swirl effect on the engine performance. With this aim, two combined methodologies, namely global energy balance and split of losses, are applied to an experimental swirl parametric study performed at different operating conditions. In this section the experimental activity performed in the test bench is described followed by an explanation of both analysis used to asses the swirl effect.

5.2.1.1.1 Experimental work

To assess the swirl effect, a study was carried out at six different operating conditions, chosen for being the most representative ones for the WLTP performance of the multicylinder engine described in Chapter 3. Again, these points are named in this chapter by using a composition of 2 numbers, the first one refers to the engine speed in revolutions per minute while the second one refers to the bmep in bar (engine speed_bmep). Their most significant variables can be seen in Table 5.1. For the sake of brevity, and taking into

account that points can be grouped according to their behaviour, only three of them (1500_8, 1500_14 and 3000_14 - marked in bold in Table 5.1) will be analysed in detail. Since 1500_8, 2000_2 and 2000_5 points have a similar behaviour, it was decided to show 1500_8 (intermediate load). Another group with similar trends was found, which consists of 2000_15 and 3000_14, from which the last point was chosen. The last studied point was 1500_14 that shows an intermediate behaviour between the 2 previous groups. In this way, the study shows a load sweep at constant speed (1500 rpm) and an engine speed sweep at constant load (14 bar).

Speed [rpm]	bmep [bar]	SR [-]	Boost pressure [bar]	Air mass flow [g/s]	EGR [%]	Rail pressure [bar]	SOE Main [°ATDC]	Fuel quantity Main [mg/cc]
1500	**8**	**1.4 / 3**	**1.33 / 1.4**	**29.8**	**0**	**750**	**0.8 / 1.4**	**23.5**
1500	**14**	**1.4 / 3**	**1.73 / 1.78**	**38.5**	**0**	**1050**	**0.15 / 0.1**	**42.8**
2000	2	1.4 / 3	1.17 / 1.23	38.8	0	450	0.2 / 0.7	6.8
2000	5	1.4 / 3	1.36 / 1.44	44.0	0	650	-1.2 / -0.4	14.7
2000	15	1.4 / 3	2.29 / 2.46	72.3	0	1250	-3.5 / -3.7	47.4
3000	**14**	**1.4 / 3**	**1.93 / 2.16**	**88.5**	**0**	**1400**	**-11.1 / -11**	**40.4**

Table 5.1. *Measured operating points.*

Swirl ratio was varied from 1.4 to 3 in 4 levels (1.4 / 2 / 2.5 / 3). These ratios were provided by the engine manufacturer as a function of the swirl valve position. Hence, the complete test matrix is composed of 6 (points) x 4 (swirl levels) x 3 repetitions of each point, although, as commented, only 3 of the points will be analysed in detail in this section.

To isolate the effects of swirl variation, all engine parameters except this one were kept constant. Therefore, swirl sweeps were performed with the same intake temperature (45°C) and trapped mass at the IVC, as well as the same combustion phasing (CA50=13°ATDC) and injected fuel mass, which was fixed for each point. Regarding the intake pressure, it was adjusted at each swirl level to get the same inlet mass flow. Furthermore, coolant (87°C) and oil (95°C) temperatures were kept constant in all tests, thus avoiding interferences in the heat fluxes and friction losses when the swirl sweeps were performed.

The injection strategy consisted of two pilot injections to reduce the combustion noise and a main injection. Pilot quantities (1.5 mg/cc) and dwell times (0.8 ms) were kept constant for all the points. Then, the main injection quantity was set to meet the required bmep at the reference conditions of each point (SR = 1.4), but in the swirl sweep the injected fuel was maintained, as commented above, thus leading to different bmep at different SR levels.

Additionally, the timing of the main injection, and thus of the whole injection train, was set to obtain a CA50 of 13°ATDC in each test. Hence, the complete injection train was moved with swirl changes as can be seen in Table 5.1.

5.2.1.1.2 Global Energy Balance analysis

The Global Energy Balance or GEB (see scheme in Figure 5.1), developed by Carreño [12], was used to evaluate the effect of changing the swirl ratio on engine performance. This methodology considers all energy transformations and thermal processes taking place in a DI Diesel engine. In the next paragraphs, a brief description of the analysed terms is provided. An extensive explanation of the methodology can be found in [12].

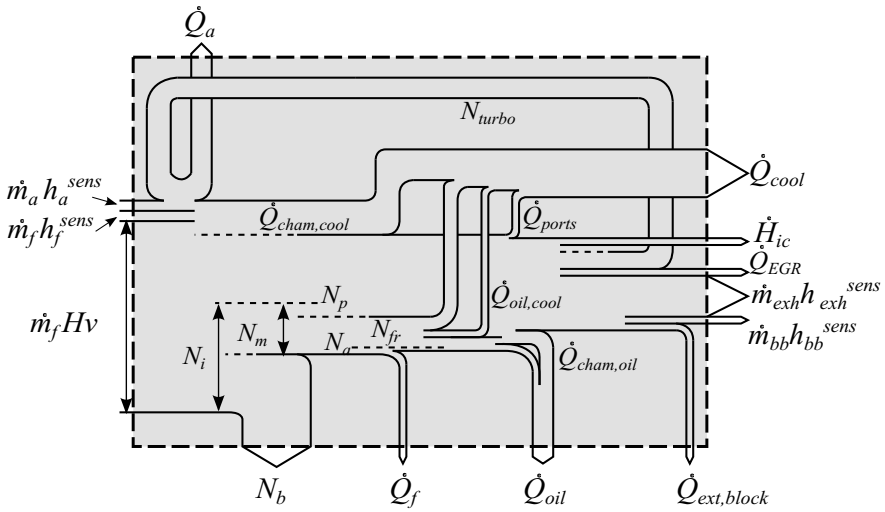

Figure 5.1. *Global Energy Balance scheme.*

From the external point of view (outside the dashed line in Figure 5.1), the engine was considered as a black box with some energy flows entering and some others leaving it. Since these flows are external they can be directly measured and used for the validation and completion of the internal analysis, which is mainly based on theoretical models.

The terms included in the external GEB are thoroughly explained in [12]. In brief, the main input is the fuel chemical energy $\dot{m}_f H_v$. The main outlet energy flows are the brake power N_b, the heat flow to the coolant $\dot{Q}_{cool}$, the net sensible energy of the exhaust gases $\dot{H}_g \approx (\dot{m}_{exh} h_{exh}^{sens} - \dot{m}_a h_a^{sens} - \dot{m}_f h_f^{sens})$, the

heat flow rejected to the oil exchanger $\dot{Q}_{oil}$, the heat flow in the intercooler $\dot{Q}_a$ and the heat flow rejected to the EGR cooler $\dot{Q}_{EGR}$. Other outlet terms with lower importance are the convective and radiative HT to the ambient from the engine external surface $\dot{Q}_{ext,block}$, the enthalpy flow due to blow-by losses (externally collected) $\dot{H}_{bb}$, the energy losses due to incomplete combustion $\dot{H}_{ic}$ and the heating of the fuel returning to the tank $\dot{Q}_f$. Since the importance of these last terms are low, they were included, along with the experimental uncertainties, in a miscellanea term called $\dot{Q}_{misc}$.

Unlike the terms involved in the external GEB, those related to the internal GEB (inside the dashed line in Figure 5.1) cannot be easily measured, except the indicated power that can be obtained from in-cylinder pressure. Thus, to obtain an accurate estimation of the rest of terms, several submodels [12] (dealing with engine heat transfer and mechanical losses) were necessary in combination with the available experimental in-cylinder pressure. As detailed in Section 3.3.1, these submodels are included in the in-house developed 0D combustion diagnosis tool (Calmec) used during this study.

The internal GEB includes the following main terms: the indicated power N_i, which is split into brake power N_b and mechanical losses N_m (due to the pumping power N_p, friction losses N_{fr} and the auxiliary losses N_a -power to drive fuel, oil and cooling pumps-). Regarding the heat rejection in the chamber, main issue in the work, the heat flow to the chamber is calculated through the lumped model (explained in Section 3.3.1), thus obtaining the heat transfer to coolant $\dot{Q}_{cham,cool}$, oil $\dot{Q}_{cham,oil}$ and ports $\dot{Q}_{ports}$.

The combination of internal and external balances allows to complete the characterization of the engine performance.

5.2.1.1.3 Split of losses analysis

As assessed in Section 4.2, the maximum theoretical efficiency reachable by an internal combustion engine is the Otto cycle, which maximum GIE only depends on the compression ratio. Starting from the Otto cycle, the real cycle of a specific operating point can be obtained by means of the subtraction of all the efficiency losses of the cycle to this maximum efficiency or ideal "ceiling". The total effect of the efficiency losses is different at each point, resulting on distinct real GIE.

The evaluation of the 8 efficiency losses, described in Section 4.3, separately, is an interesting way to assess what are the most important causes of the efficiency change in a parametric study. However, if some variables

are kept constant during the experimental measurement, the analysis can be simplified while keeping its potential outcomes.

Thus, if IVC conditions (pressure, mass, temperature and composition) are maintained, computing the effect of the real working gas is not important because it is more or less the same within the parametric study. Another possible experimental way to simplify this analysis is to keep the same combustion centring (CA50), thus eliminating this effect. Finally, taking into account that the incomplete combustion and blow-by terms are small (the change in any of them in the parametric study is lower than 0.1% $\dot{m}_f H_v$ in all cases) and the non centred valve timing effect is roughly the same at a given operating point, it can be assumed that evaluating their possible change in a parametric study is not necessary.

If the methodology explained is followed when performing the experimental measurement and the minor terms are neglected, it is possible to simplify the analysis from 8 to 2 steps. Hence, heat transfer and HRR velocity are the only responsible of the indicated efficiency variation, thus simplifying the comparison among parametric levels.

Taking into account the previous comments, the split of losses analysis [13] is applied to the swirl parametric studies following the next steps:

1. Original cycle: simulation of k-points in SiCiclo was carried out using experimental conditions (p, T, composition at IVC) and imposing the experimental HRR. GIE deviation with respect to experimental values was lower than 0.3% $\dot{m}_f H_v$ in all cases.

2. Then, the adiabatic cycle at each parametric level was calculated with SiCiclo, thus obtaining the efficiency achievable without HT.

3. The difference between the original and adiabatic efficiencies (steps 1 and 2) is the impact of HT on GIE. Then, ΔHT effect at each SR level was computed as the difference of the modeled GIE between a certain parametric level and the reference one. This term computes the impact of HT change on GIE promoted by the variation of the studied parameter.

4. The adiabatic cycles calculated in step 2 should reach the same GIE in all parametric levels if the combustion velocity was the same. Therefore, if this adiabatic efficiency is not the same it is due to changes in the combustion velocity promoted by the variation of the studied parameter. The difference between a level and the reference one will be called ΔHRR velocity effect.

The proposed methodology is a conceptual approach that assesses the controlling phenomena affecting GIE when a certain variable is changed. This is useful to understand the physics of the in-cylinder processes and to develop solutions to enhance the benefits and/or mitigate the counterparts when performing a certain parametric study. Finally, it should be taken into account that even though this methodology is a completely general approach that can be applied to any ICE, results derived from this analysis cannot be generalized to every engine due to the specific characteristics (combustion chamber geometry, injector performance, ...) of the studied engine.

5.2.1.2 Assessment of swirl effect using GEB

In this subsection, the experimental and modelled results, along with the discussion regarding the swirl effect on engine performance are presented. Graphs show mostly experimental results, provided that they are available. Modelled results will be discussed when experimental results are not available. Figure 5.2 shows the GEB of the three points with the lowest swirl ratio, which will be the reference points for the analysis. In the left-hand graph, the power of the different energy terms is represented, while in the right part their relative value in percentage of the total fuel energy is plotted. As shown at the left plot, the three points are clearly different, being the fuel power 56 kW, 97 kW and 184 kW respectively.

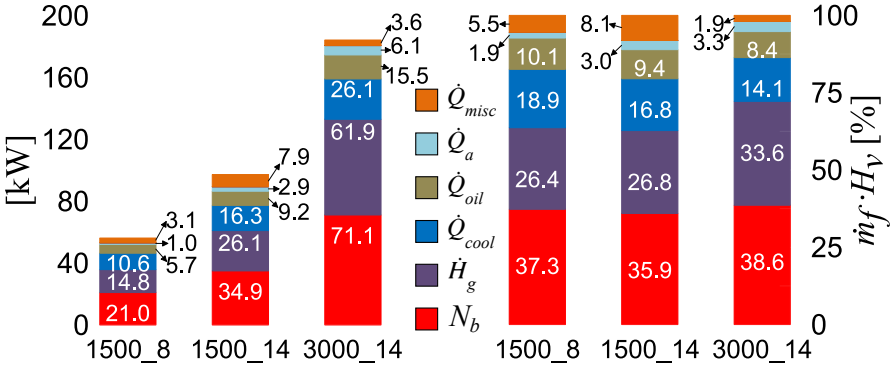

Figure 5.2. *External GEB for the reference points (SR=1.4).*

In relative terms, a higher brake efficiency in the 3000_14 case can be highlighted(38.6% $\dot{m}_f H_v$ in this last case vs 37.3% $\dot{m}_f H_v$ and 35.9% $\dot{m}_f H_v$ at 1500_8 and 1500_14 respectively). Regarding the heat transfer to coolant and oil, a decrease with load and engine speed can be observed. While this term

represents 29% $\dot{m}_f H_v$ in the 1500_8 case (18.9% $\dot{m}_f H_v$ to coolant and 10.1% $\dot{m}_f H_v$ to oil), it is about 26.2% $\dot{m}_f H_v$ in the 1500_14 test (16.8% $\dot{m}_f H_v$ to coolant and 9.4% $\dot{m}_f H_v$ to oil).

These trends are in agreement with the expected behaviour; on the one hand, increasing the load (from bmep=8 to 14) leads to higher gas temperature, thus the difference between mean gas and wall temperatures (proportional to the heat flow) increases about +20%. Besides, the heat transfer coefficient augments by 30% mainly due to the higher pressure. As a consequence, the heat transfer to chamber walls is about 1.5 times higher. However, the fuel power is 1.7 times higher at 1500_14 with respect to 1500_8, thus the higher the load, the lower the relative weight of the heat transfer. On the other hand, an increase on engine speed leads to higher heat transfer coefficient in the chamber, which is proportional to c_m powered to 0.8 (see Section 3.3). However, the available time for heat transfer is inversely proportional to c_m and therefore it becomes the controlling factor.

With respect to heat transfer in the intercooler, the load seems to dominate the trends, thus it was about 3% $\dot{m}_f H_v$ in the two 14 bar bmep points while its weight was lower at the lowest load (1.9% $\dot{m}_f H_v$). This was consequence of the higher boost pressure reached in those high load points (1.73 bar and 1.93 bar in 1500_14 and 3000_14 respectively, whilst it was 1.33 bar at low load). If exhaust gases sensible enthalpy is analysed, it seems to be dependent on speed, thus 3000_14 had the highest value (33.6% $\dot{m}_f H_v$), unlike the other two where this term was about 26.5% $\dot{m}_f H_v$. This big difference can be explained by the hotter exhaust temperature produced by the longer combustion (in°) because of the higher load and engine speed and the lower relative chamber heat rejection.

Finally, the miscellanea term $\dot{Q}_{misc}$ shows a global trend to diminish when the engine speed increases. This is mainly due to the reduction of the heat rejection to the ambient and the lower experimental uncertainties when measuring and computing (using fluid flow rates and temperatures) the thermal flows.

Once the external GEB of the reference points have been analysed, the variation of energy terms due to swirl ratio changes is assessed. Firstly, the brake efficiency term and the sub-terms affecting this parameter are thoroughly assessed. Then, the HT to the different parts and fluids is evaluated. After that, the exhaust gases sensible enthalpy variation with swirl increment is presented. Finally, changes in other minor terms of the GEB when SR increases are analysed.

5.2.1.2.1 Brake efficiency

Figure 5.3 shows the variation of brake efficiency along with the parameters affecting it, in a swirl ratio sweep in the 3 analysed points. These variations are referred to the reference points shown in Figure 5.2 (SR=1.4), while error bars, calculated as the maximum difference between the 3 repetitions and their average value, are plotted above and below the average value in the figure. In the three cases, increasing swirl ratio led to a worse brake efficiency at the highest swirl level (-1.2% $\dot{m}_f H_v$, -1.4% $\dot{m}_f H_v$ and -2.3% $\dot{m}_f H_v$ respectively). However, the trend with the SR is not monotonous, thus in the 1500_14 case there is a maximum BTE at the intermediate level (SR=2), while in the other two points, intermediate swirl ratios do not lead to a clear efficiency reduction. As equation 5.1 shows, brake power (N_b) is the difference between gross indicated power (N_i) and mechanical losses, i.e. pumping (N_p), auxiliary (N_a) and friction losses (N_{fr}) and thus, its behaviour can be analysed taking into account these terms:

$$N_b = N_i + N_p - N_a - N_{fr} \tag{5.1}$$

where N_p is negative (it is obtained by integrating pdV from exhaust to intake BDCs) while the rest of terms in equation 5.1 are positive.

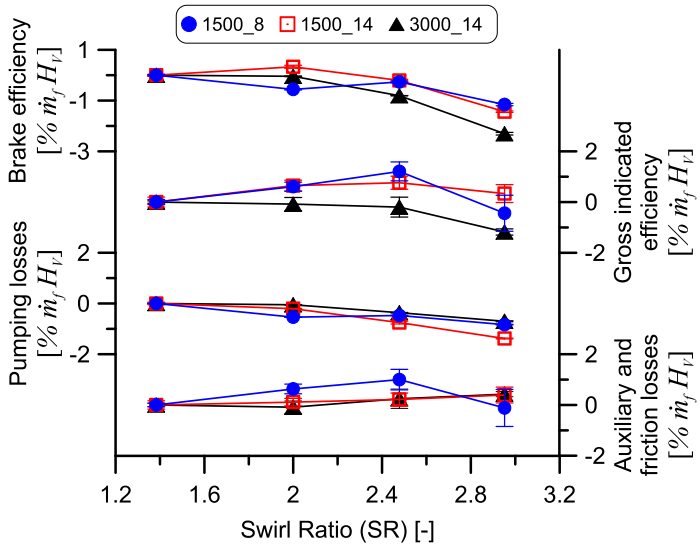

Figure 5.3. *Variation of parameters affecting experimental brake efficiency with SR.*

Regarding the gross indicated efficiency, key topic in the analysis, increasing swirl ratio enhances air-fuel mixing during the first stages of injection-combustion due to the higher air velocity which implies higher turbulent behaviour. This mixture process improvement leads to an enhancement of the pilot and premixed combustion that can be seen in the sharper slope of the main HRR up to its peak at the three points shown in Figures 5.4, 5.5 and 5.6 and also in the shorter delay time shown in Figure 5.7. As a consequence of this combustion enhancement, the pressure rate gets slightly higher as can be seen in the bottom part of Figures 5.4, 5.5 and 5.6. This faster combustion has a positive effect on gross indicated efficiency, at least during the first combustion stage.

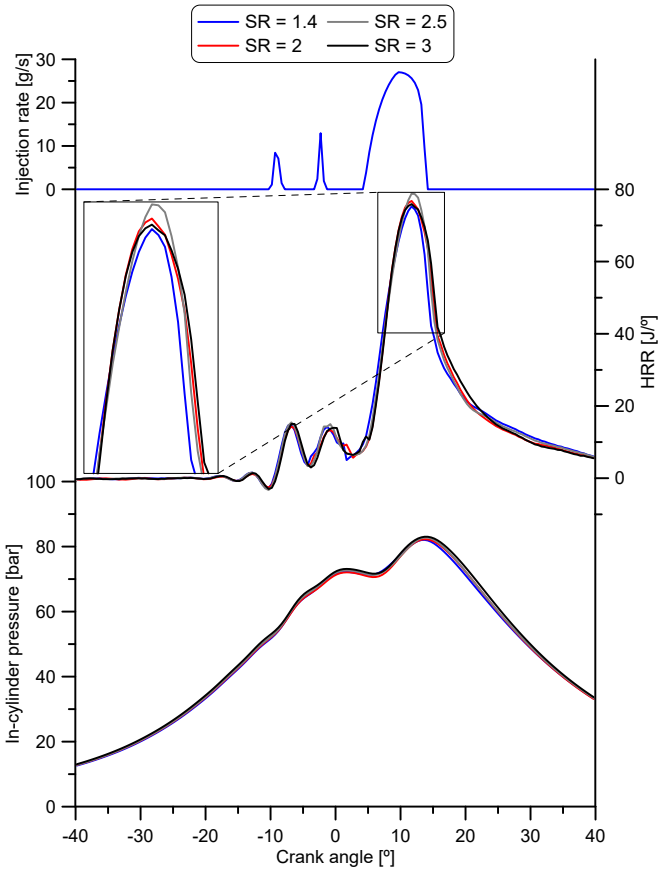

Figure 5.4. *Experimental in-cylinder pressure and HRR at 1500_8.*

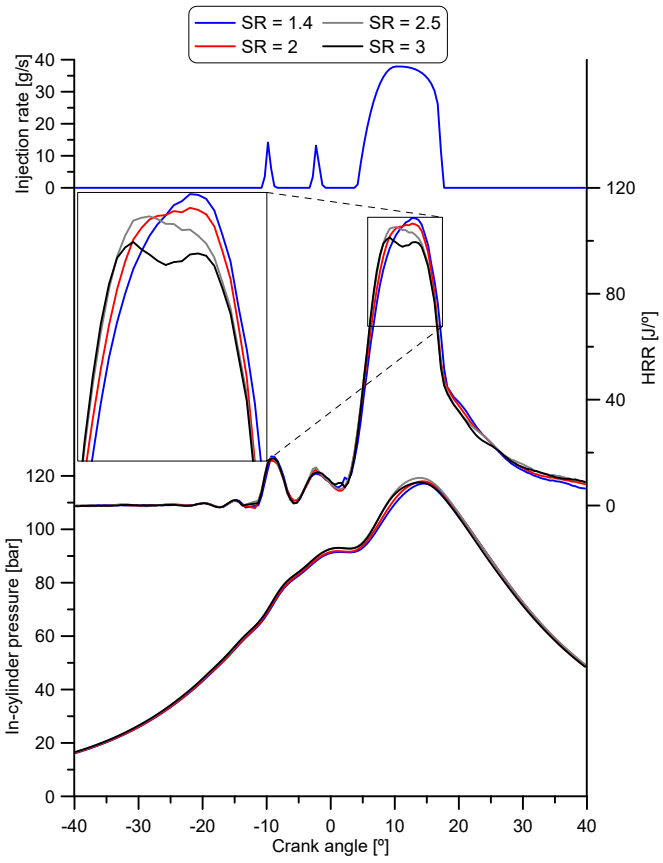

Figure 5.5. *Experimental in-cylinder pressure and HRR at 1500_14.*

With respect to the next stages of HRR, their behaviour is different depending on the load and engine speed. An enhancement of its peak with swirl can be seen at the lowest load point (1500_8) in Figure 5.4 where the higher air velocity helped to get a sharper slope and also a higher HRR peak. However, this trend is not followed at the highest swirl ratio (SR=3), where the HRR peak goes down. It has been checked that this behaviour does not take place in all the repetitions and cycles but it is quite usual at this low load point. This phenomenon can be explained by the combustion worsening also observed at high load and later described. At this point (1500_8), the HRR just after the main peak was also higher when swirl increased thus leading to a faster fuel burn rate (up to 22°ATDC). As a result of the described combustion behaviour, the combustion duration tends to shorten, as can be observed in

Figure 5.7 and, since CA50 is set at the same°, CA90 is reached earlier. This leads to a lower temperature at the end of the expansion (see Figure 5.8) and, consequently, to a lower exhaust temperature.

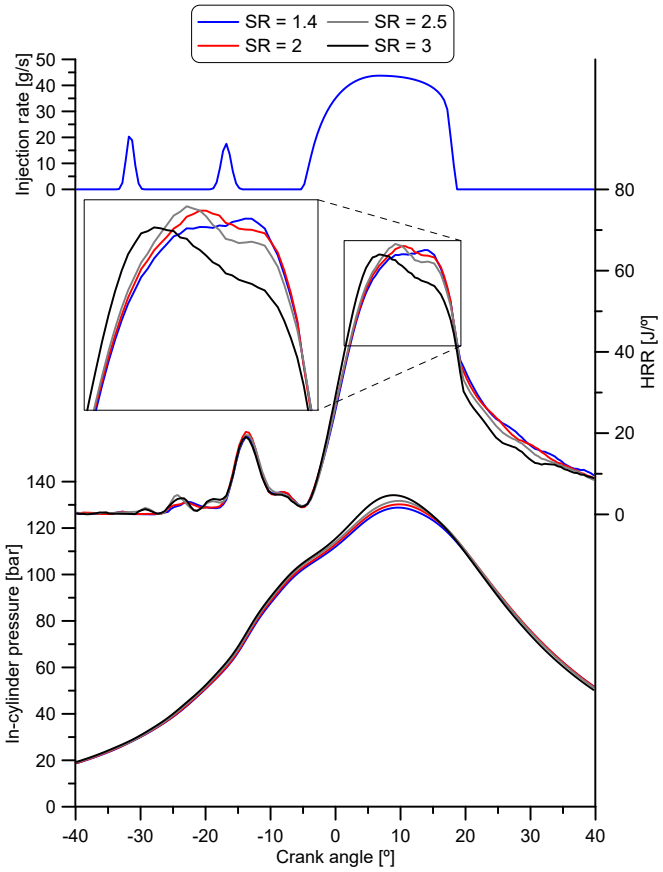

Figure 5.6. *Experimental in-cylinder pressure and HRR at 3000_14.*

Regarding the other 2 points (high load), as can be seen in Figures 5.5 and 5.6, a lower HRR peak was achieved when swirl increased, especially at SR=3. This combustion velocity limitation contributes to worsen the HRR evolution just after the peak, thus extending the CA90 and the combustion duration (Figure 5.7). As a consequence of the longer combustion duration, the exhaust gas temperature went up at these points when swirl increased, as can be seen in the late part of the instantaneous gas temperature in Figure 5.8 and in Section 5.2.1.2.3.

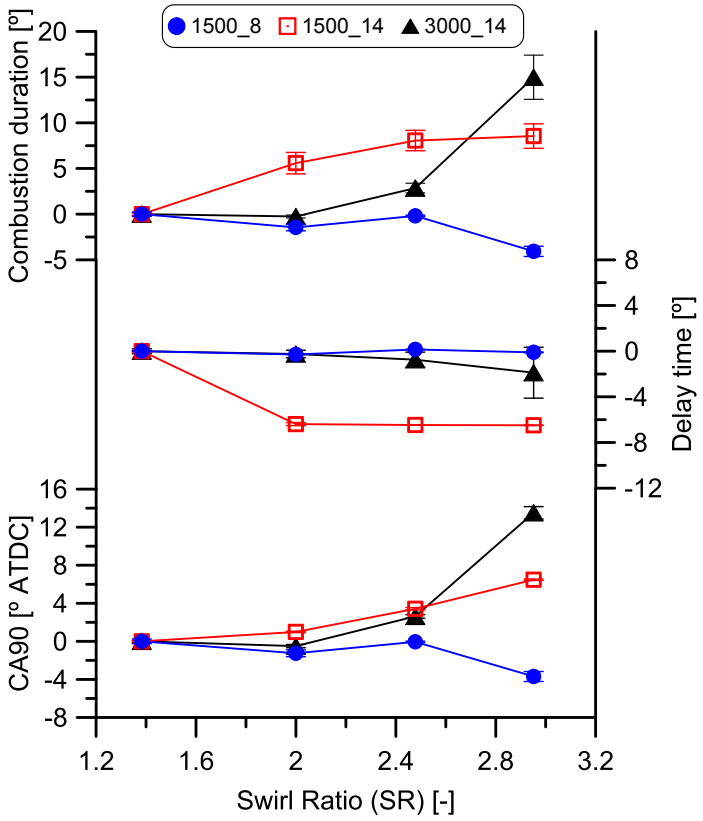

Figure 5.7. *Variation of combustion duration, delay time and CA90 with SR.*

Although the accurate explanation of the combustion worsening at high load (also seen at low load and high SR) would require a more specific analysis such as CFD calculations or optical techniques (out of the work scope) to clarify the involved phenomena, some hints will be given to focus the problem. On one hand, the high rotation motion promoted by high swirl ratios forces adjacent sprays to interact between them, thus worsening the air-fuel mixture process [14]. On the other hand, de la Morena *et al.* [15] found that high swirl ratios displace the combustion towards the squish region at high load, acting as a barrier and limiting the spray tip velocity and penetration. Thus, the spray is deflected towards the fire deck, preventing it from efficiently entraining fresh air in the piston bowl. Both phenomena are probably causing the observed HRR trends, with an almost monotonous behaviour at high load while it only affects at very high SR at low load.

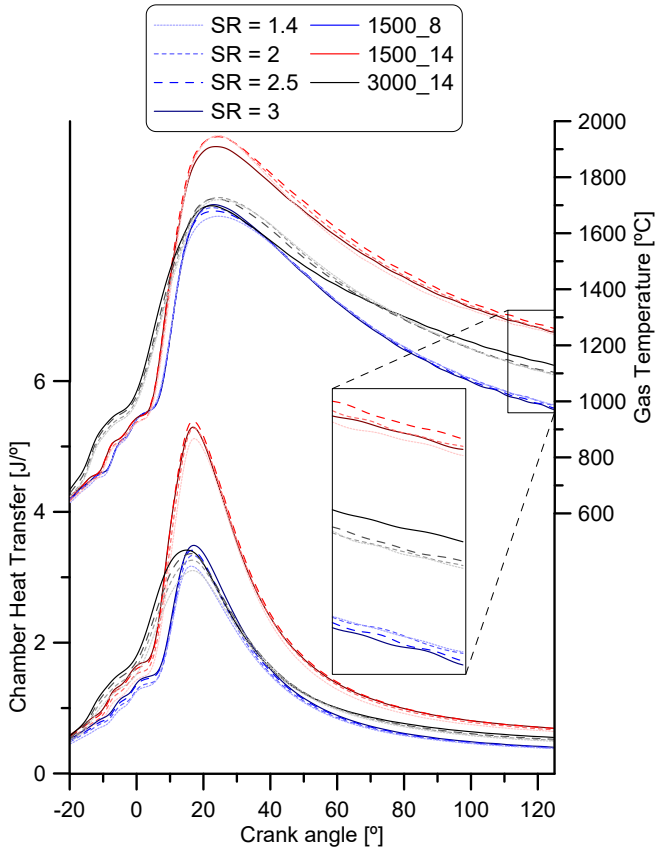

Figure 5.8. *Modelled HT in the chamber and gas mean temperature.*

Due to the air velocity increment achieved when swirl is increased, the heat transfer coefficient also increases leading to higher HT in the chamber, as shown in Figure 5.8. This effect can be clearly seen up to the heat rejection peak (about 15°ATDC), where the effect of higher pressure and temperature due to the faster combustion at the initial stage is more evident. Heat transfer enhancement has a negative impact on gross indicated efficiency in all the three studied points. However, the combination of enhanced HT and different combustion velocity leads to a non monotonous GIE behaviour as it will be discussed in Section 5.2.1.3.

Benefits observed in some points at intermediate SR in terms of gross indicated efficiency do not lead to brake efficiency improvements (see Figure 5.3), mainly due to the increase of pumping losses. This term increased almost

linearly when swirl ratio went up. As explained in the engine characteristics subsection, the way to increase swirl consists in closing the valve located upstream of the helical port. This increases the restriction to the intake air flow, which produces a pressure drop, making necessary a more closed VGT position to reach the required higher boost pressure and hence to get the same trapped mass in the cylinder as when it is open (SR=1.4). As a consequence, pumping losses increased +0.9% $\dot{m}_f H_v$ at 1500_8, +1.4% $\dot{m}_f H_v$ at 1500_14 and +0.7% $\dot{m}_f H_v$ at 3000_14. Although this effect could be reduced by keeping the turbine position constant, this would diminish the intake pressure and the air flow, increasing the fuel to air ratio and thus changing completely the in-cylinder conditions and combustion process.

For the sake of brevity, auxiliary and friction losses have not been plotted separately but the sum of both terms did not show significant variations in the swirl sweep. Auxiliary losses, which depend on fuel, cooling and oil pumps power [16], did not change since the engine speed, injection pressure, coolant mass flow and oil pressure were constant. On the other hand, oil temperature was kept constant, thus no important effect on engine friction took place when swirl increased.

According to the performed analysis, brake efficiency variations were governed by gross indicated efficiency and pumping losses. Since pumping losses and gross indicated efficiency affected brake efficiency negatively in most cases, the global trend in all the points was to decrease. It was found that only in one operating condition, 1500_14 and SR=2, increasing the SR led to higher brake efficiency. At this point, gross indicated efficiency was +0.7% $\dot{m}_f H_v$ better than the reference point due to the better mixing process, while pumping losses were not as important as for highest swirl level (-0.2% $\dot{m}_f H_v$). The combination of these factors led to a brake efficiency +0.4% $\dot{m}_f H_v$ higher than the one at lowest swirl level.

Although these variations might seem hardly measurable, the high repeatability of the measurements (see Figure 5.3) ensure that they are not just noise but real changes.

5.2.1.2.2 Heat transfer

The analysis performed in the previous section regarding the instantaneous evolution of heat transfer in the chamber is extended here through a deeper analysis. Since changes in auxiliary and friction losses, responsible for a portion of the heat transfer to coolant and oil, were almost negligible, the

study will be focused on the heat transfer to the combustion chamber and port walls.

Experimental heat transfer to coolant and oil is presented in Figure 5.9, where it can be seen that both terms increased when SR increased (specially the coolant). Moreover, no clear difference in the behaviour of the three points can be observed neither in heat rejection to coolant nor to oil.

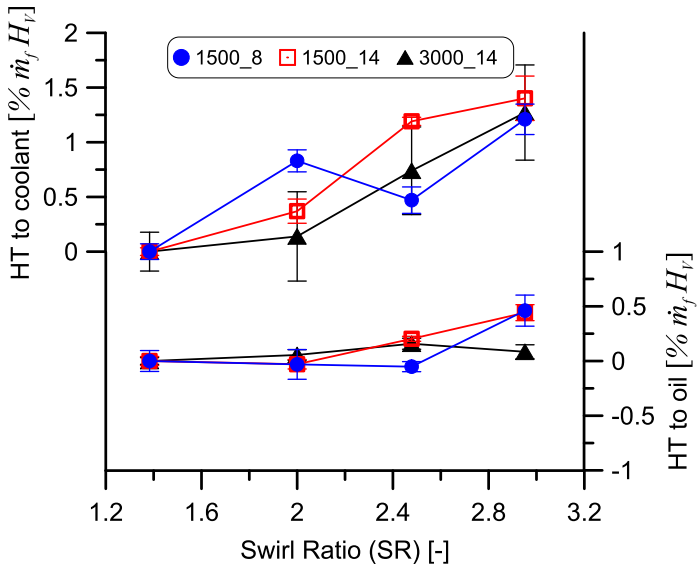

Figure 5.9. *Variation of experimental HT to coolant and oil with SR.*

In the case of the coolant heat transfer, it is shown that the mean value increases between +1.2% $\dot{m}_f H_v$ and +1.5% $\dot{m}_f H_v$ of the fuel energy (depending on the point) when SR went from the minimum to the maximum value. If a detailed analysis of the coolant heat rejection sources is performed, main sub-terms involved are heat rejection to cylinder-head, cylinder liner and ports. The modelled variation of these terms is plotted in Figure 5.10. As shown, both heat transfer to cylinder-head and cylinder liner increased with swirl about +0.6% $\dot{m}_f H_v$ of the fuel energy (each one) in all the points, as a consequence of the changes in air velocity and in-cylinder conditions already described. On the other hand, heat transfer to ports rose about +0.7% $\dot{m}_f H_v$ at high load cases due to the longer combustion and it decreased -0.3% $\dot{m}_f H_v$ (only at the highest SR) at 1500_8 because of the shorter combustion duration.

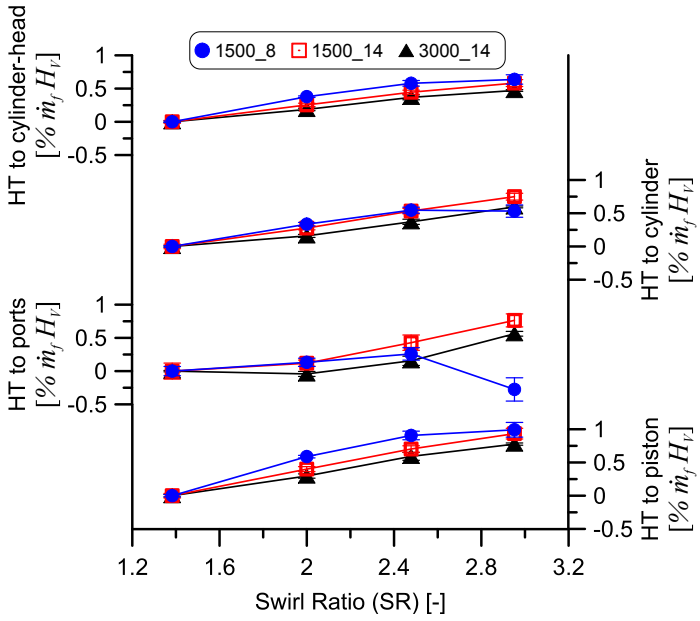

Figure 5.10. *Variation of modeled HT in chamber and ports with SR.*

Regarding HT to oil in Figure 5.9, no significant variation can be seen up to SR=2.5, moreover, only a small rise of about +0.5% $\dot{m}_f H_v$ of the fuel energy was obtained at the highest SR at 1500_8 and 1500_14. Although the tests repeatability is high, the experimental determination of this term is probably on the limit of what can be measured, as discussed in the sensitivity analysis of the same HT model performed by Carreño [12]. Main components of this term, which were modelled, are friction, which hardly changed, and heat transfer to piston, which is plotted at the bottom of Figure 5.10. Modelled piston HT increased almost linearly with swirl, reaching a maximum variation at the highest SR level ranging between 0.8% $\dot{m}_f H_v$ and 1% $\dot{m}_f H_v$ of the fuel energy at different points. If this change is compared with the experimental measurements of the HT to oil (variation lower to 0.5% $\dot{m}_f H_v$), it is possible to say that the model slightly overestimates the effect of swirl on the heat transfer to piston.

5.2.1.2.3 Exhaust gases sensible enthalpy

Another important term in the external balance is the exhaust gases net sensible enthalpy, shown in the top part of Figure 5.11. This enthalpy was

calculated downstream of the turbine and, therefore, in the swirl study it was only affected by the change of exhaust temperature (downstream of the turbine) because the intake flow and temperature were kept constant. Thus, at 1500_8, where the combustion got shorter and the exhaust gases got cooler in the SR sweep (bottom plot of Figure 5.11), this term decreased -0.8% $\dot{m}_f H_v$. Since the combustion duration increased with swirl in the other 2 high load points, exhaust temperatures were higher and sensible enthalpy rose about +0.2% $\dot{m}_f H_v$.

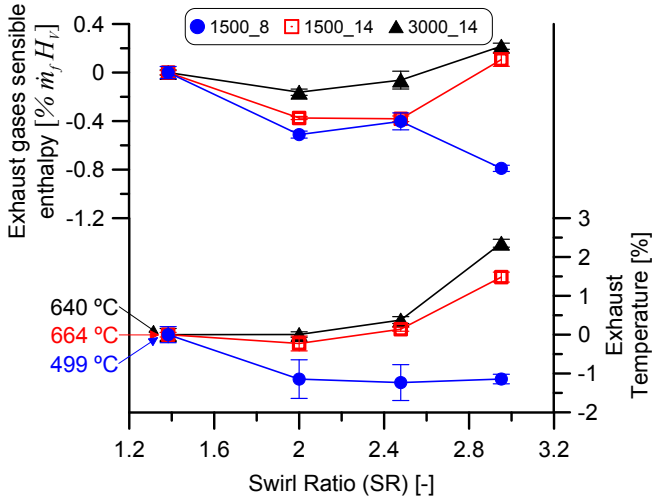

Figure 5.11. *Variation of experimental exhaust gases sensible enthalpy and exhaust temperature with SR.*

5.2.1.2.4 Other terms

To conclude the thermal analysis there are some remaining terms involved in the experimental external balance: heat transfer in the intercooler and the miscellanea term $\dot{Q}_{misc}$. Their variation with swirl ratio change is shown in Figure 5.12.

Regarding heat transfer in the intercooler, a slightly increment was observed during the swirl sweep due to the higher boost pressure required to get the same trapped mass when the swirl valve gets closed to increase swirl ratio. To reach the higher pressure, the compressor work increases and, consequently, the temperature at the compressor outlet increases as well, being

necessary a higher cooling power in the intercooler to maintain the same temperature in the intake manifold (always constant at 45°C). Thus, this cooling power was +0.6% $\dot{m}_f H_v$ higher in the last swirl value at 3000_14, where the pressure increment was also higher (0.2 bar), while it was about +0.3% $\dot{m}_f H_v$ greater in the 1500 rpm cases (with a pressure increase of 50 mbar).

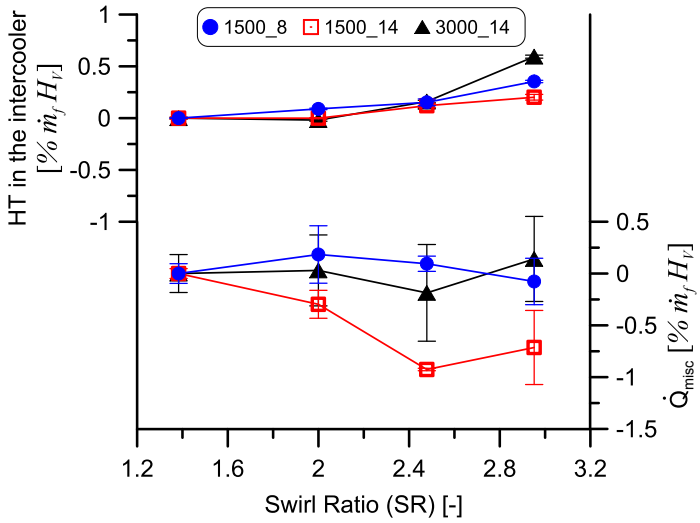

Figure 5.12. *Variation of experimental HT to intercooler and miscellanea term with SR.*

The last term to complete the GEB analysis is $\dot{Q}_{misc}$. As explained in the methodology section, this term includes some minor energy flows ($\dot{Q}_{ext}$, $\dot{H}_{bb}$, $\dot{H}_{ic}$ and $\dot{Q}_f$), as well as the energy unbalance due to experimental uncertainties, and it is not measured but calculated as the total fuel energy minus the brake power, heat transfer and the exhaust gases enthalpy. Due to the small variation of these terms during the swirl sweeps, variation of $\dot{Q}_{misc}$ should be mainly due to uncertainties. As shown in the bottom part of Figure 5.12, changes in this term have a mean value about +0.2% $\dot{m}_f H_v$ in all the cases (a maximum value lower to +1% $\dot{m}_f H_v$) although its repeatability shows a wide variation range of about 1% $\dot{m}_f H_v$. Taking into account that the unbalance includes all the experimental uncertainties during the measurement of the fuel mass, fluids flow rates and temperature drops, it can be considered a suitable result to validate the experimental measurements.

5.2.1.3 GIE assessment based on split of losses analysis

With results of the previous section in mind, it is evident that SR, until reaching a determined value, has a positive effect on the GIE at low engine speed, while it does not seem interesting at high engine speed. However, it is not still clear the balance between combustion and heat transfer changes when SR increments, finally leading to the explained GIE behaviour. Thus, the split of losses approach is applied to the 3 operating conditions in order to find an explanation for the non monotonous behaviour of GIE. Since the experimental matrix was performed maintaining constant IVC conditions (pressure, mass, temperature and composition) and combustion centring, changes in incomplete combustion, blow-by and valves timing are negligible and only 2 of the 8 possible efficiency losses change along the swirl study, as explained in Section 5.2.1.1.3.

The evolution through the methodology steps will be extensively graphed at 1500_14 and the final result will be presented separately. After that, the final results of the other two points are also analysed. Starting from the original efficiency at this k-point (purple bars in Figure 5.13), the first step is to compute the adiabatic cycle at each parametric level. The gain achieved at each level is plotted in red bars in Figure 5.14. Longer bars mean more HT, which is directly transferred into an efficiency loss, thus their difference respect to the lowest level are computed with negative sign in Figure 5.14 as well. These variations are the effect of the HT change on indicated efficiency due to the swirl variation (ΔHT effect). As observed, the increased HT due to the higher gas velocity is responsible for a reduction of -0.4% $\dot{m}_f H_v$ in GIE at the highest SR.

Once the HT effect has been analysed, it is possible to assess the combustion velocity change impact on indicated efficiency. Since there are no additional effects, the absolute adiabatic efficiency achieved at each SR (purple bars + red bars in Figure 5.13) should be the same if combustion was the same at every level. Since it is not the case, this difference is only attributable to the combustion velocity change. When comparing each absolute level with the lowest SR one, the effect of combustion change on indicated efficiency due to the swirl variation (ΔHRR velocity effect) is obtained and also plotted in Figure 5.13. As can be seen, this effect increases GIE at intermediate swirl levels (+0.8% $\dot{m}_f H_v$ at SR=2.5) but this increment is reduced at the highest SR (+0.3% $\dot{m}_f H_v$). This non monotonous behaviour is due to the HRR changes (Figure 5.5) promoted by SR explained in previous paragraphs. As commented, SR affected positively in the first stages of the combustion, but negatively afterwards. The balance between these opposite variations,

positive and with a rising trend up to SR=2.5, starts to decay beyond this swirl level.

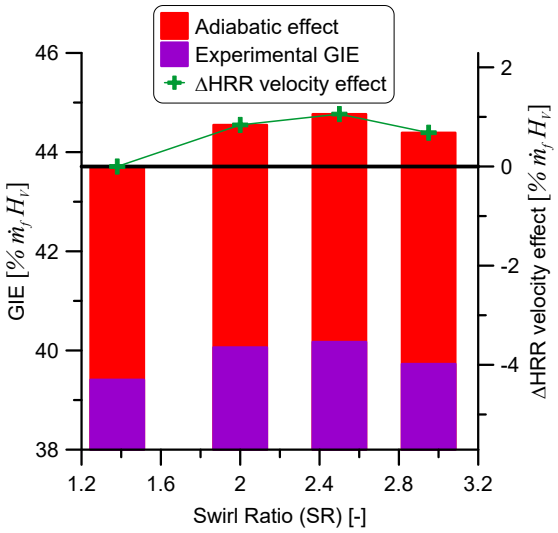

Figure 5.13. *Experimental GIE, adiabatic effect and ΔHRR effect at 1500_14.*

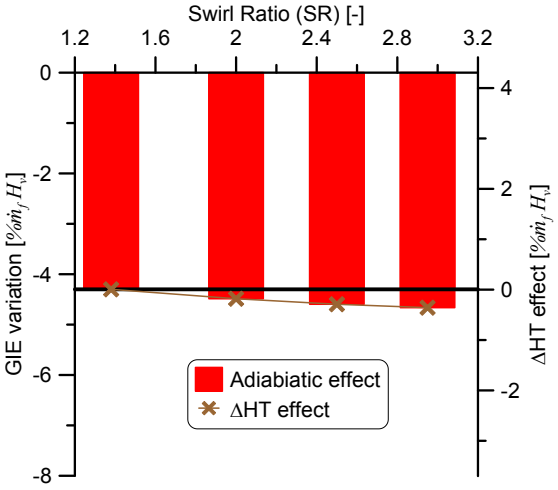

Figure 5.14. *Adiabatic effect and ΔHT effect at 1500_14.*

Both ΔHT and ΔHRR effects are replotted together in Figure 5.15 along with the experimental measured GIE variation at 1500_14. It can be seen that the experimental change is explained by the addition of both effects. As shown, the experimental GIE variation follows the same trend than the ΔHRR velocity effect but its level is slightly lower because the ΔHT effect decreases monotonously. Therefore, it can be concluded that at this point the dominant effect when SR is swept is the variation of the combustion velocity rather than the HT increment.

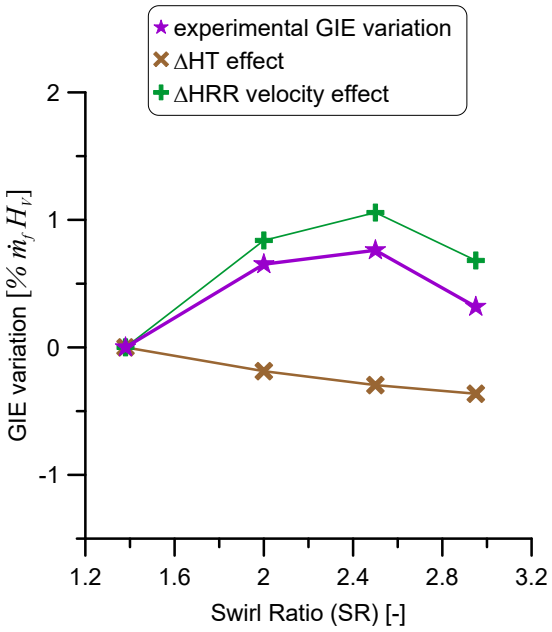

Figure 5.15. *Split of losses at 1500_14.*

Then, the methodology is applied to 1500_8 obtaining Figure 5.16. The analysis at 1500_8 is similar to that performed at 1500_14 but, in this case, both the increase due to the ΔHRR velocity effect up to SR=2.5 (+1.7% $\dot{m}_f H_v$) and the decrease beyond this level (+0.1% $\dot{m}_f H_v$) are steeper. The ΔHT effect is a bit bigger than at higher load (-0.5% $\dot{m}_f H_v$ at SR=3), resulting in a slightly lower variation of the experimental GIE variation but with the same trend than the ΔHRR velocity effect.

Finally, the methodology is applied to 3000_14 in Figure 5.17. There, it can be seen that the ΔHRR velocity effect is almost zero in the first two SR

levels for a later decay beyond SR=2. Differently, the ΔHT effect decreases monotonously and thus, the combined effect of both terms lead to a dramatic GIE variation (-1.2% $\dot{m}_f H_v$) at the highest SR.

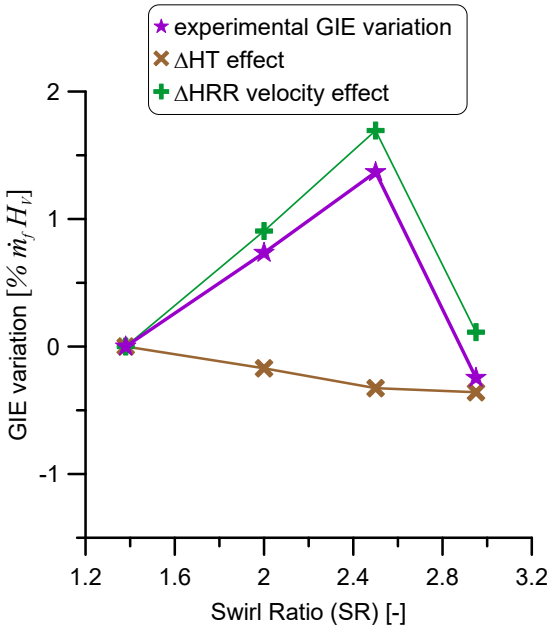

Figure 5.16. *Split of losses at 1500_8.*

Taking into account the previous analysis, it is clear that swirl effect on GIE depends heavily on the operating conditions. However, some global statements can be made if load and engine speed sweeps are considered. On the one hand, when SR increases, the efficiency reduction due to the higher heat transfer diminished with load. This has also been observed at 2000 rpm points, although for the sake of brevity they have not been presented. On the other hand, increasing swirl enhances the initial combustion stages but later tends to worsen the combustion process limiting the HRR peak. The resulting effect of these HRR changes on GIE is positive at intermediate SR, but tends to diminish with both load and speed. As a consequence of the combination of heat transfer and combustion changes, a maximum GIE is found at a certain SR in all points, being located at lower SR when the engine speed increases.

As a conclusion of the previous 2 sections, it can be summarized that the effect of SR on heat transfer is similar in all analysed conditions, with

a monotonous effect on GIE about +0.5% $\dot{m}_f H_v$ at the highest SR level. However, the effect of SR on the combustion process is not the same: in global terms increasing slightly SR enhances the combustion, being the effect on GIE higher at low engine speed and load. In any case, the combustion changes lead to a GIE penalty at very high SR levels at all operating conditions.

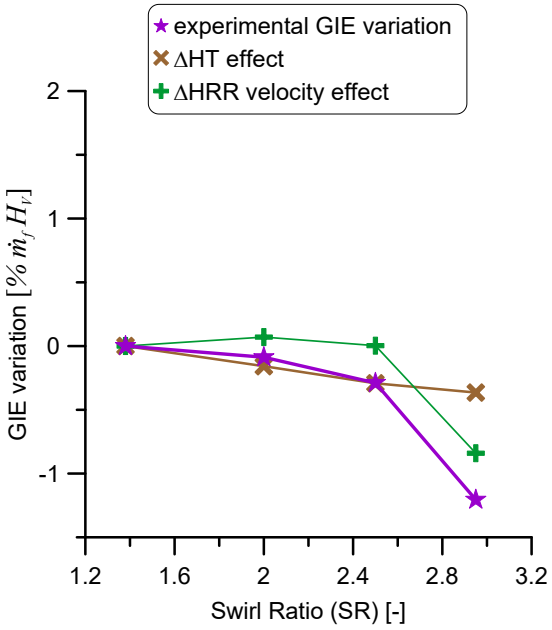

Figure 5.17. *Split of losses at 3000_14.*

5.2.1.4 Emissions

Since swirl has an important effect on both soot and NO_x emissions, some brief results are included here to complete the study. Figure 5.18 shows the experimental NO_x and soot emissions for the three studied points under different SR.

As commented, swirl enhanced the mixing process, thus leading to accelerate the first combustion stages. Consequently, it can be observed a trend to increase NO_x emissions when SR increased in the 3 points. Additionally, there is a decrease beyond SR=2.5 at high load points which matches with the HRR peak deep decay at SR=3.

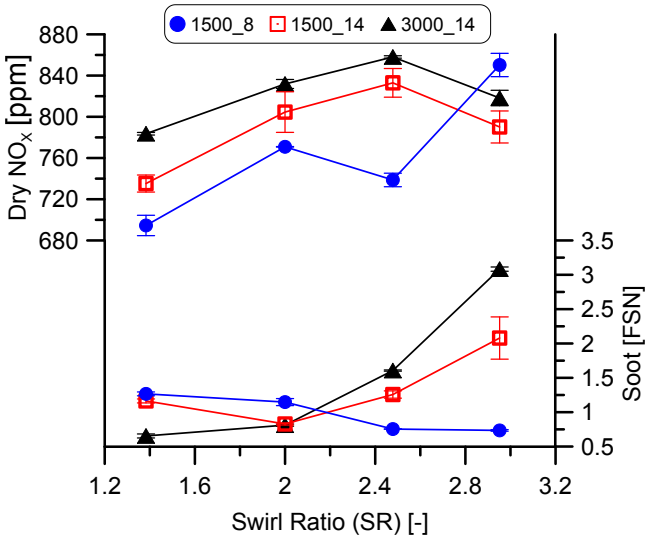

Figure 5.18. *Experimental NO_x and soot emissions.*

Regarding soot emissions, 2 different trends are observed depending on the combustion rate beyond CA50 (13°ATDC). At low load (1500_8), where a continuous improvement of the late combustion with swirl was found (see Figure 5.4), there is a monotonous decrease when increasing SR. On the other hand, soot emissions increased at high load, when at the last part of the combustion, the HRR decreased at high SR (see Figures 5.5 and 5.6), and this increment was steeper at the highest swirl level.

5.2.1.5 Conclusions

A comprehensive analysis based on the GEB and split of losses approaches has allowed determining the effect of swirl increase on engine performance. Main conclusions of this section are:

- Swirl ratio increment did not always affect GIE in the same way, and its global impact depends on the operating conditions and the swirl level. There are two main factors affecting this efficiency: HRR shape and heat transfer.
- HRR has different effect depending on the operating conditions and the combination of the phenomena occurring during the HRR evolution.

During the first combustion stage, HRR was always enhanced when swirl increased due to the better mixture process promoted by the higher air velocity at high swirl levels. However, the maximum combustion rate was affected in different ways depending on load and engine speed. At low load, the HRR peak got higher when swirl increased up to SR=2, unlike the worsening effect seen when increasing SR at high load. This deterioration can be explained because of the interaction between injection sprays due to the high swirl motion and/or the flame displacement towards the squish region produced by this high motion, although further analysis with CFD would be necessary to confirm this point. This combustion degradation was compensated by the enhancement of the HRR during the main combustion rise at 1500_14, but at 3000_14 the negative impact of the peak deterioration was higher than the benefit achieved during the first stage.

- Heat transfer was always higher when swirl increased because of the higher tangential velocity and the consequent major heat transfer coefficient at high swirl ratios. However, the heat rejection difference between extreme swirl levels got lower when load was increased.

- Combination of heat transfer and HRR effects (ΔHT and ΔHRR respectively) led to a maximum GIE at 1500_8 at SR=2.5, where the ΔHRR effect (+1.7% $\dot{m}_f H_v$) is higher than the ΔHT effect (-0.5% $\dot{m}_f H_v$). Similar results are observed at 1500_14 with a maximum GIE also located at SR=2.5, where the ΔHRR and the ΔHT are +1.1% $\dot{m}_f H_v$ and -0.3% $\dot{m}_f H_v$ respectively. Finally, no better GIE was achieved at 3000_14 in the swirl sweep, where both ΔHRR and ΔHT tended to decrease -0.8% $\dot{m}_f H_v$ and -0.4% $\dot{m}_f H_v$ respectively. As a global trend, the SR value where the maximum GIE is found is lower when the engine speed increases.

- Brake efficiency variations were controlled by GIE and pumping losses. Having in mind the previous conclusions and taking into account that pumping losses always increase when swirl gets higher, the global trend of brake efficiency in almost all the points was to decrease (between -0.9% $\dot{m}_f H_v$ and -1.4% $\dot{m}_f H_v$). Only at 1500_14 a higher BTE was found at SR=2 because gross indicated efficiency was better than the reference point due to the enhanced mixing process, while pumping losses only showed a slight worsening with respect to lower SR.

- Heat rejection to coolant increases about +1.3% $\dot{m}_f H_v$ in all the cases when SR augmented. This heat transfer increase is due to the higher

heat transfer to cylinder, cylinder-head and ports that increase about +0.6% $\dot{m}_f H_v$.

- Exhaust gases sensible enthalpy, which depends on the exhaust gases temperature, decreased -0.8% $\dot{m}_f H_v$ at low load (1500_8) with swirl, where the exhaust temperature was lower due to the shorter combustion duration. In the high load points (1500_14 and 3000_14), exhaust temperatures were higher (longer combustion duration) and thus, sensible enthalpy rose about +0.2% $\dot{m}_f H_v$ when swirl increased.

- Regarding NO_x emissions, an increment could be seen when SR increased in all the points. Additionally, there was a decrease beyond SR=2.5 at high load points which matches with the HRR peak deep decay at SR=3 and the low GIE values at this swirl level.

5.2.2 Injection approach

As known, the injection pattern is the controlling factor in the combustion process of Diesel engines. Nowadays, due to the versatility of the state of the art injection systems, injection pressures above 2500 bar and complex injections trains with more than 5 events are achieved in Diesel engines. Such increasing versatility makes that calibration of injection system is becoming a more and more complex task.

Additionally, as seen in the swirl study, even though some improvements were seen in GIE at intermediate SR, swirl impact on BTE was always negative (excepting in one point) while NO_x emissions were also affected negatively. Thus, it was decided to assess the injection strategy under low swirl conditions. Unlike the swirl study, that was carried out in the multicylinder engine (SR between 1.4 and 3), the injection study was performed in the single-cylinder engine (see characteristics in Section 3.2.2) that was equipped with an additional valve in the tangential port that allowed achieving a wider SR variation (from almost 0 up to 5). By closing this additional valve, it was possible to achieve SR levels below to the nominal one (around 1.4), however, SR close to 0 was achieved when this valve was almost completely closed. Keeping in mind that closing an intake port would increase dramatically the pumping losses, as seen in Section 5.2.1, at low load and it would not be feasible at high load, it was decided to choose a low SR value between 0 and 1.4. Thus, a SR of 0.9 was chosen in which the tangential valve was at an intermediate position and the helical valve was completely open.

Therefore, the injection optimization strategy of a 4 events injection pattern is assessed, in this section, under low SR conditions (SR=0.9) in order to increase the engine performance.

5.2.2.1 Methodology

The objective of this study is the assessment of the injection pattern on the engine performance. As there are several variables to be varied, a sweep approach as the one used for the swirl is not approachable here thus, a design of experiments (DoE) has been used to evaluate the effect of each injection setting on GIE and pollutant emissions. In this section, the experimental activity performed in the test bench is described followed by a description of the different DoEs that were applied to the presented operating conditions.

Design of experiments is the name given to the techniques used for guiding the choice of the experiments to be performed in an efficient way [17]. To perform a DoE it is necessary to define the problem by choosing the variables or factors intervening in the problem, along with the range of variability of each factor (design space) and the responses or outputs. Based on the number of experiments chosen by the user, the experiments to be performed are selected following one of the DoE techniques: Randomized Complete Block Design, Latin Square, Full Factorial, ... Once this approach is conducted and the selected tests are measured, it is necessary to analyse the results. To do so, some analysis such as the assessment of the influence of every factor on the responses, modelling the outputs' behaviour as a function of the inputs or optimizing the input values for a given criteria could be performed.

Unlike the swirl study, in which the 6 available points were assessed, this study was only applied to 2 different operating points, representative for the low load and engine speed region of the WLTP, due to its higher number of variables and thus, the experimental work. The characteristics of these two operating points in nominal conditions are displayed in Table 5.2, while their injection settings are plotted in Table 5.3. It is worth to note that the units of the variable used to represent the position of the main injection (SOE main) are °BTDC, which implies that positive values of this variable indicates a start of energizing time earlier than TDC and vice versa.

For the sake of brevity, only the detailed analysis at 2000_5 and the final results at 1500_8 are presented here, while the detailed analysis of this last point can be found in Appendix 5.6.

This study takes into account up to 4 possible injections, resulting in 8 inputs: injection pressure, Start of Energizing time (SOE) of the main

injection, up to 3 dwell times between the 3 injections and the fuel mass of the two pilot and the post injections. The injected mass in the main event is obtained as the difference between the total fuel mass and the sum of the pilots and post injections. Figure 5.19 shows the command signal of a 4-injections train where all inputs, excepting rail pressure, have been marked.

Speed [rpm]	bmep [bar]	load [%]	SR [-]	Boost pressure [bar]	Air mass flow [g/s]	GIE [%]	sNO_x [g/kWh]	Soot [FSN]
1500	8	50	0.9	1.18	7.4	41.8	6.1	1.2
2000	5	25	0.9	1.33	11	43.2	5.4	1.8

Table 5.2. *Main characteristics of operating points assessed in injection parametric study.*

Speed [rpm]	bmep [bar]	load [%]	Rail pressure [bar]	SOE main [°BTDC]	m_{f1} [mg]	$dwell_1$ [ms]	m_{f2} [mg]	$dwell_2$ [ms]	$m_{f,total}$ [mg/cc]
1500	8	50	750	1	1.5	0.5	1.5	0.5	26.2
2000	5	25	650	2	1.5	0.5	1.5	0.5	17.8

Table 5.3. *Injection settings of operating points assessed in injection parametric study.*

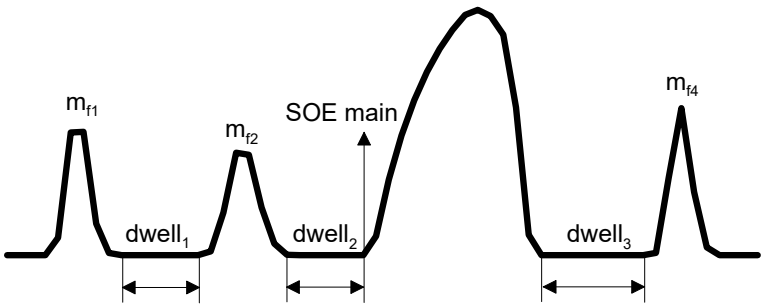

Figure 5.19. *DoE inputs in a 4 injections pattern.*

To assess the impact of each variable in the studied outputs, a study based on DoE was carried out. It is worth to mention that the 8 variables were not

studied in a single DoE, but in two consecutive steps. At the beginning, the possibility of performing a post injection was not considered and, only after performing some exploratory tests once DoE 1 had been already carried out, it was decided to include it in the study. Then, a second DoE, in which the post-injection settings were assessed, based on the optimum point obtained in the first DoE was carried out.

The design used in the DoEs was the 2^k full factorial [18], where 2 means the number of levels considered at each input and k refers to the number of variables. There are other designs that reduce the number of tests to perform such as the Box-Behnken design, experiments of which are defined by $n = 2 \cdot k \cdot (k-1)$. However, according to Lalanne [19], 2^k full factorial designs are very useful for the first steps of a research because they allow obtaining a complete representative swept of the studied parameters taking into account all the extreme positions of the design space. Additionally, the number of tests required in DoE 1 for a Box Behnken design with 6 variables would be 54, only 10 experiments less than the simple full factorial design, and with the drawback of no testing the extreme positions of the design space.

Taking into account that the final number of variables was 8 instead of 6, a Box Behnken design had been more suitable for the analysis. With this design, the experiments would be reduced up to 112 instead of 256 as a result of a 2-level full factorial design applied to 8 variables, and not so far from the 80 combinations finally tested. However, as commented previously, the additional two variables included in DoE 2 were not in the original plan and thus, this approach could not be taken into account.

Then, the first DoE only takes into account the first three injections along with the SOE of the main injection and the injection pressure, resulting in 6 variables (DoE 1). Once this first study was performed, the settings of the two pilot injections were extracted from the best point of this study and imposed in the second study (DoE 2). Therefore, inputs of DoE 2 are rail pressure, SOE of the main injection and dwell time and injected fuel of the post injection, giving a total of 4 variables.

5.2.2.2 Assessment of pilot injection strategy

Table 5.4 shows the inputs of the first DoE (they are named from x_1 to x_6) as well as their respective minimum and maximum levels. It is worthy to mention that the nominal settings represent the medium point of the considered ranges with the exception of the injection pressure, that in the DoE is only incremented. Additionally, the position of the main injection

event (SOE main) is used as reference for the rest of injections thus, the whole injection train is moved when this variable is changed.

Speed [rpm]	bmep [bar]	Rail pressure (A) [bar]	SOE main (B) [°BTDC]	m_{f1} (C) [mg]	$dwell_1$ (D) [ms]	m_{f2} (E) [mg]	$dwell_2$ (F) [ms]
1500	≃8	750 / 1250	-5 / 5	1 / 2	0.25 / 0.75	1 / 2	0.25 / 0.75
2000	≃5	650 / 1150	-5 / 5	1 / 2	0.25 / 0.75	1 / 2	0.25 / 0.75

Table 5.4. *Ranges of variation of inputs in DoE 1.*

Prior to the manual measurement of all operating conditions, since pilot masses could not directly be imposed in the engine control system, an exhaustive campaign to obtain the energizing time necessary for injecting the desired fuel quantity under all possible rail pressure, the start of energizing time and dwell scenarios was carried out. After that, a test campaign consisting of 64 tests resulting from the 2^6 DoE study plus 3 measurements of the centre point (at the beginning, in the medium part and at the end) was carried out in the single-cylinder engine at both nominal points. To control the test to test dispersion, three repetitions of each operating conditions were performed, resulting in 402 tests (2 points x 67 combinations x 3 repetitions).

All tests were performed using the same conditions at the IVC as well as the same total injected fuel mass. Figure 5.20 shows the experimental air and fuel mass flows throughout the first DoE at 2000_5 along with the dispersion between repetitions represented as vertical lines. It can be observed that all values are within a variation of 1% and only some repetitions are out of this range. Therefore, taking into account that sensitivity of most measurement equipments are in this range, it can be assumed that the air trapped mass and injected fuel are constant in the whole study.

Once the whole experimental matrix has been measured, the combustion diagnosis was performed in all tests to obtain typical combustion results such as indicated efficiency, combustion duration, heat transfer... Then, changes in the most relevant ones for the study (gross indicated efficiency, soot and NO_x emissions) were analysed as function of changes in the DoE inputs and the interactions among them.

Figure 5.21 shows the complete Pareto chart of GIE at 2000_5, where the length of each bar is proportional to the value of a t-statistic calculated for the corresponding effect. Any bars beyond the vertical line are statistically significant at a significance level of 5%. This means that effects crossing this line are significant on changes of GIE, while the others can be removed from

the study obtaining Figure 5.22. In these plots, grey colour indicates that the increase of the represented input has a positive effect on the output, while black colour means that increasing the input leads to a diminution of the output. In the case of interactions, grey colour indicates that the increase of both variables leads to an increase of the considered output, while black colour means the contrary.

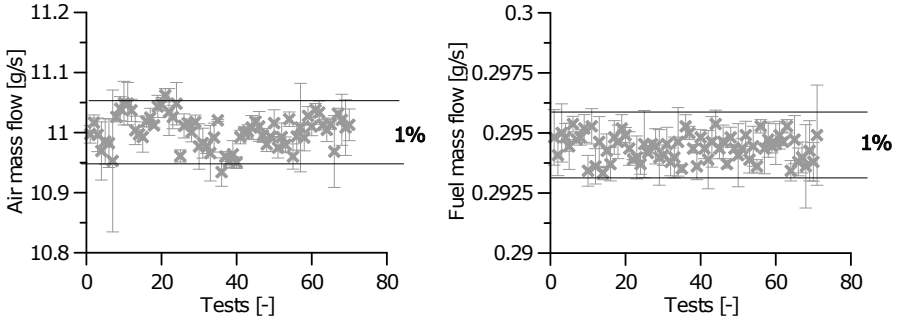

Figure 5.20. *Experimental air and fuel mass flows at 2000_5 in DoE 1.*

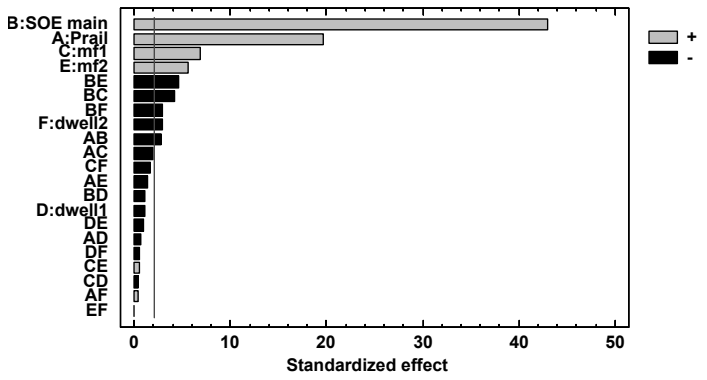

Figure 5.21. *Complete standardized Pareto chart of GIE at 2000_5 in DoE 1.*

In Figure 5.22, it can be observed that the controlling factors for GIE are SOE and injection pressure and both are positive, which implies that increasing injection pressure or advancing SOE has a positive effect on GIE. Indeed, these two factors act directly on centring and velocity combustion efficiency losses explained in Section 4.3, reducing them when increasing their value. In a second level of significance, large pilot masses and a short dwell time between pilot 2 and the main injection event are positive for efficiency.

Additionally, some interactions between the rail pressure and the start of the energizing time with the pilot settings have a certain effect on GIE.

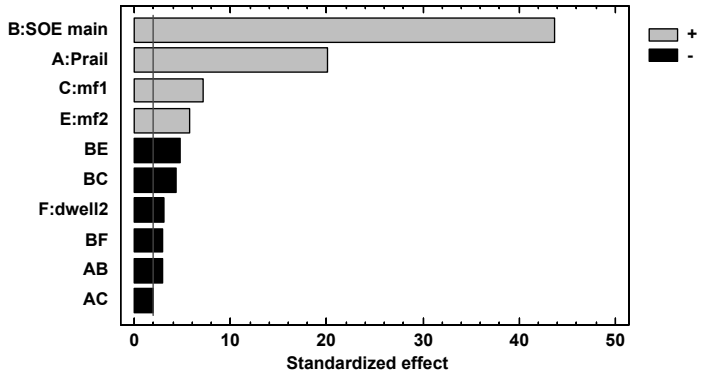

Figure 5.22. *Standardized Pareto chart with significant effects of GIE at 2000_5 in DoE 1.*

Based on this analysis, a statistical model using a linear combination of the significant effects represented in Figure 5.22 as entries, was developed to reproduce GIE. In any case, it is important to remark that this simple model is able to explain 98% of GIE variations as can be seen in the R^2 column, which implies a high level of accuracy.

Then, the statistical study was repeated for the NO_x and soot emissions obtaining the standardized Pareto charts plotted in Figures 5.23 and 5.24, in which the non significant effects have already been removed. On the one hand, Figure 5.23 shows that increasing rail pressure and/or advancing the injection have a big impact on increasing NO_x emissions due to the higher in-cylinder temperatures. Furthermore, large pilot injections lead to also increase NO_x due to the enhancement of the first combustion part while the dwell time between the second pilot and the main event is not significant. Additionally, there are some interactions between the injection pressure and the start of injection with settings of pilot injections that have a little impact on NO_x emissions.

Test	Output	R^2	Intercept	A	B	C	D	E	F	AB	AC
	GIE [%]	0.98	38.7867	$3.8{\cdot}10^{-3}$	0.6255	1.0256	0	0.4117	-0.4251	$-8.4{\cdot}10^{-5}$	$5.8{\cdot}10^{-4}$
2000_5	NO_x [mg/s]	0.99	2.6782	$4{\cdot}10^{-3}$	0.3375	0.8981	1.167	0.1315	0.8911	$3.2{\cdot}10^{-4}$	0
	Soot [FSN]	0.98	5.1226	$-3.5{\cdot}10^{-3}$	-0.1106	-0.1183	0	-0.2210	0.9769	0	0

Test	Output	R^2	AD	AE	AF	BC	BD	BE	BF	CF	DF
	GIE [%]	0.98	0	0	0	$-6.2{\cdot}10^{-2}$	0	$-6.8{\cdot}10^{-2}$	$-8.3{\cdot}10^{-2}$	0	0
2000_5	NO_x [mg/s]	0.99	0	$6.6{\cdot}10^{-4}$	0	$2.9{\cdot}10^{-2}$	$-9{\cdot}10^{-2}$	$5.8{\cdot}10^{-2}$	-0.169	0	-1.7821
	Soot [FSN]	0.98	0	0	$-8{\cdot}10^{-4}$	$1.7{\cdot}10^{-2}$	0	0	0	0	0

Test	Output	R^2	Intercept	A	B	C	D	E	F	AB	AC
	GIE [%]	0.99	35.9994	$5{\cdot}10^{-3}$	0.5780	0.5581	0.89	0.2342	0	$-1.6{\cdot}10^{-4}$	$-4.5{\cdot}10^{-4}$
1500_8	NO_x [mg/s]	0.99	2.1042	$6.7{\cdot}10^{-3}$	0.1101	$1.5{\cdot}10^{-2}$	0.785	0.2028	-0.4094	$5{\cdot}10^{-4}$	0
	Soot [FSN]	0.98	5.6168	$-3.8{\cdot}10^{-3}$	-0.3494	0	0	0.4259	0	$1.8{\cdot}10^{-4}$	0

Test	Output	R^2	AD	AE	AF	BC	BD	BE	BF	CF	DF
	GIE [%]	0.99	$-8.9{\cdot}10^{-4}$	0	0	$-3.3{\cdot}10^{-2}$	0	$-2.4{\cdot}10^{-2}$	0	0	0
1500_8	NO_x [mg/s]	0.99	0	0	0	$2.2{\cdot}10^{-2}$	0	$3.6{\cdot}10^{-2}$	$-8{\cdot}10^{-2}$	0.4219	-0.8325
	Soot [FSN]	0.98	0	$-4.3{\cdot}10^{-4}$	0	0	0	0	0	0	0

Table 5.5. *Coefficients of statistical models at 2000_5 (top) and 1500_8 (bottom) in DoE 1.*

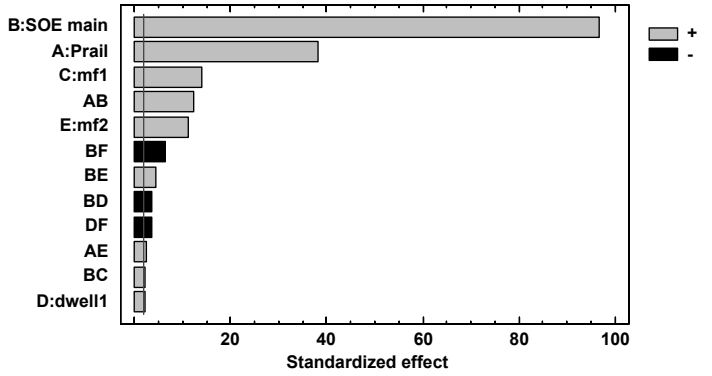

Figure 5.23. *Standardized Pareto chart of NO_x emissions at 2000_5 in DoE 1.*

On the other hand, the standardized Pareto chart of soot emissions displayed in Figure 5.24 shows the contrary behaviour than NO_x emissions but in this case the importance of the two main factors are shifted. Here, increasing injection pressure helps more to cut-down soot emissions than advancing the combustion due to the better mixing process. Additionally, increasing pilot fuel masses also contributes to reduce slightly soot emissions, while dwell time between the second pilot and the main injections seems to have a small impact and it should be reduced in order to decrease soot. Additionally, there are two interactions, between the injection pressure and the dwell 2; and between the start of injection and the mass of the first pilot, that have a little impact on soot emissions.

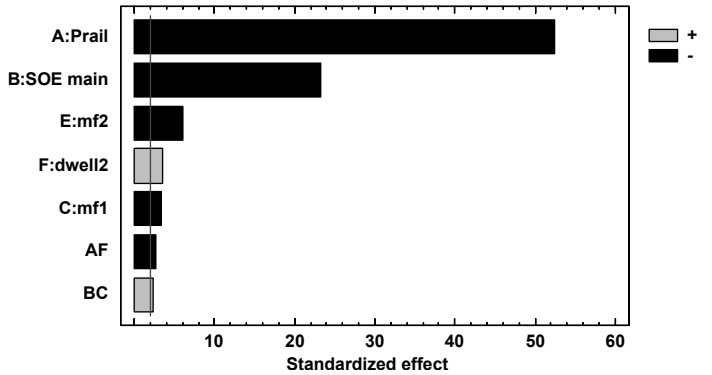

Figure 5.24. *Standardized Pareto chart of soot emissions at 2000_5 in DoE 1.*

As in the case of GIE, two statistical models using only the significant inputs in each case were developed. The coefficients of these models are displayed in Table 5.5 along with the GIE ones and their R^2 were 95% for NO_x emissions and 98% for soot emissions which implies a high level of agreement.

By modelling the responses of intermediate levels (7 levels) of the model entries with a higher resolution than the experiments (2 levels), a three-dimensional smooth response surface is obtained with NO_x and soot emissions in the x and y axis, and GIE in the z axis. However, since for each combination of NO_x and soot emissions the only important GIE is the highest one, Figure 5.25 only presents the top view of this response surface. In this plot it can be seen clearly the existent tradeoff among GIE, soot and NO_x emissions. NO_x emissions are presented in [g/kWh] in order to standardize the format with graphs presented in *Chapter 4*. Additionally, the red point stands for the nominal operating condition, which, as can be seen, can be improved in terms of GIE, NO_x and soot emissions using results from this analysis.

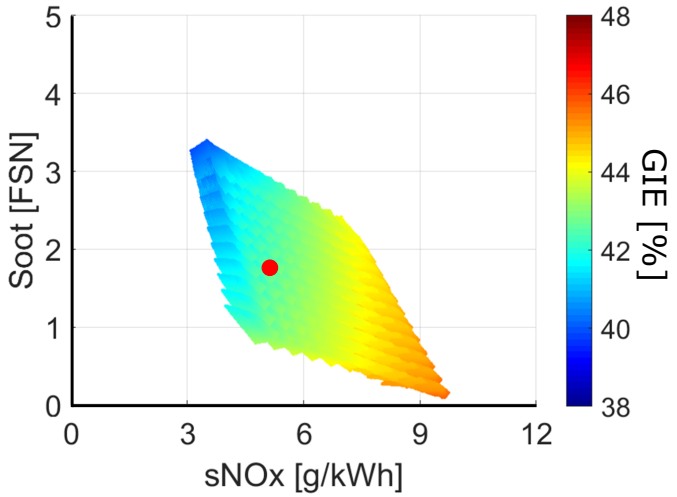

Figure 5.25. *Top view of the response surface of GIE, NO_x and soot emissions models at 2000_5 in DoE 1.*

For the sake of brevity, the standardized Pareto charts of 1500_8 are not described here but they are included in Appendix 5.6.1.1. Main differences at that point are that the significance of the pilot injection settings turns negligible due to their lower weight respect to the higher total injected fuel (higher load).

Figure 5.26 represents the top view of the response surface of the design space, with a higher resolution than experiments, for GIE, soot and NO_x at 1500_8 by using the statistical models, coefficients of which are shown in Table 5.5. Again, the tradeoff among GIE, soot and NO_x emissions is very clear but, compared to the previous point, GIE is lower, soot emissions are higher and NO_x emissions are maintained. As in the previous point, the red point represents the nominal injection settings therefore, the DoE performed here allows to reduce both pollutant emissions while improving GIE at the same time respect to this starting point.

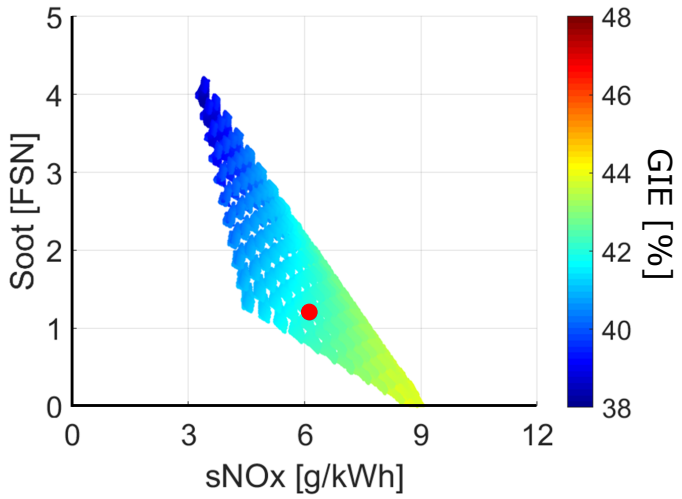

Figure 5.26. *Top view of the response surface of GIE, NO_x and soot emissions models at 1500_8 in DoE 1.*

Once results of DoE 1 have been analysed, it is necessary to choose a set of injection settings to use in DoE 2 in which only the post injection strategy is going to be assessed. Since the theoretical optimization presented in *Chapter 4* only takes into account GIE and NO_x emissions, these 2 parameters were the objectives of this optimization and their relative weights were assumed to be the same. Thus, the objective function was defined as following:

$$OF = \frac{\alpha_{GIE} + \alpha_{NOx}}{\alpha_{GIE} \cdot e^{\frac{GIE - GIE_{obj}}{GIE_{obj}}} + \alpha_{NOx} \cdot e^{\frac{-NOx + NOx_{obj}}{NOx_{obj}}}} \tag{5.2}$$

where α_{GIE} and α_{NOx} make reference to the weight of each factor and both of them were set to 0.5, while GIE_{obj} and NOx_{obj} are the objective of each factor and were set to 100 and 0.1 respectively.

Table 5.6 shows the injection settings along with their respective GIE and pollutant emissions as a result of the optimization of the objective function at both operating conditions. As can be observed, an injection strategy consisting of large (2 mg) pilot injections and close (0.25 ms) events along with the maximum injection pressure and the most delayed combustion provides the best balance in terms of GIE and NO_x emissions within the DoE study at both operating conditions.

Test	Rail pressure [bar]	SOE Main [°BTDC]	m_{f1} [mg]	$dwell_1$ [ms]	m_{f2} [mg]	$dwell_2$ [ms]	GIE [%]	sNO_x [g/kWh]	Soot [FSN]
1500_8	1250	-5	2	0.25	2	0.25	41	4.4	1.6
2000_5	1150	-5	2	0.25	2	0.25	43.1	4.9	0.7

Table 5.6. *Optimum inputs in terms of GIE and* NO_x *emissions in DoE 1.*

Additionally, these optimum solutions have also been included as black dots in the previously presented GIE-NO_x-soot maps in Figure 5.27.

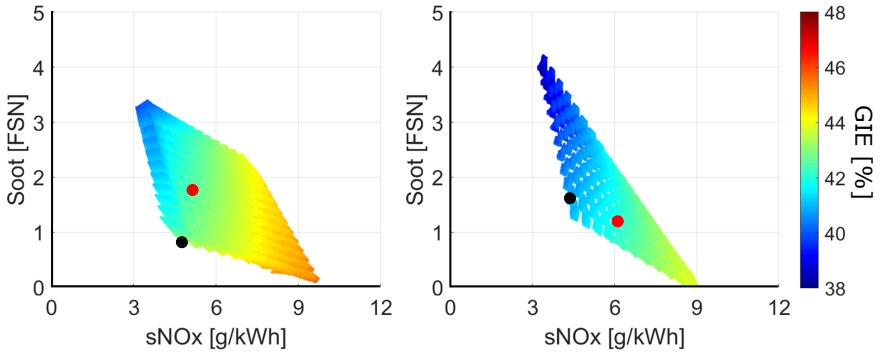

Figure 5.27. *Optimum solutions of DoE 1.*

There, it can be seen that optimum points are located in a zone of medium GIE and NO_x as a result of the same weight given to both parameters in the cost function. In any case, the optimized points show a similar GIE as the nominal settings with a reduction of 0.5 g/kWh and 1.5 g/kWh of NO_x in 2000_5 and 1500_8 respectively. In terms of soot, even though this variable

has not been taken into account in the optimization, optimum point represents a reduction of 1 FSN at 2000_5 and an increase of 0.5 FSN at 1500_8 respect to the nominal point.

The evolution of the HRL and pressure of the optimum cycles along with a comparison with nominal points will be analysed in detail in Section 5.3.

5.2.2.3 Assessment of post-injection strategy

Taking into account conclusions extracted in DoE 1, the effect of the addition of a post-injection to the injection pattern is assessed here. As commented, in this study the fuel masses and dwell times of the pilot injections were taken from the optimum point of the previous DoE presented in Table 5.6 and they remained constant through the whole study. Table 5.7 shows these pilot settings along with the variation ranges of rail pressure, SOE of the main injection, dwell time between the main event and the post-injection and its fuel mass.

Speed [rpm]	bmep [bar]	Rail pressure (A) [bar]	SOE Main (B) [°BTDC]	$m_{f,1}$ [mg]	$dwell_1$ [ms]	$m_{f,2}$ [mg]	$dwell_2$ [ms]	$m_{f,4}$ (C) [mg]	$dwell_3$ (D) [ms]
1500	8	750 / 1250	-5 / 5	2	0.25	2	0.25	2 / 3	0.5 / 0.8
2000	5	650 / 1150	-5 / 5	2	0.25	2	0.25	2 / 3	0.45 / 0.7

Table 5.7. *Ranges of variation of inputs in DoE 2.*

Prior to the experimental measurement, a dedicated campaign to obtain the minimum dwell time between the main and post injections was carried out to ensure that there was time enough for the injector needle to come back to its rest position between the main and post injections. This study resulted in different minimum dwell times depending on the operating condition as can be observed in Table 5.7. Additionally, another dedicated campaign was also performed to obtain the energizing times of the post-injection corresponding to the fuel mass requirements under all possible injection pressures, timing and dwell times defined in the DoE 2 study.

Then, the 2^4 test matrix derived from the DoE definition plus the centre point repeated at the beginning, in the medium part and at the end of the campaign was measured and 3 repetitions of every operating condition were measured to avoid the test to test dispersion. This study resulted in a total of 114 tests (2 points x 19 combinations x 3 repetitions) which were performed using the same conditions at the IVC as well as the same total injected fuel

mass (main injection fuel mass was modified to compensate the post-injection mass variation). Figure 5.28 shows the experimental air and fuel mass flows throughout DoE 2 at 2000_5 along with the dispersion between repetitions represented as vertical lines. Again the dispersion was very low and the repeatability among repetitions was very good.

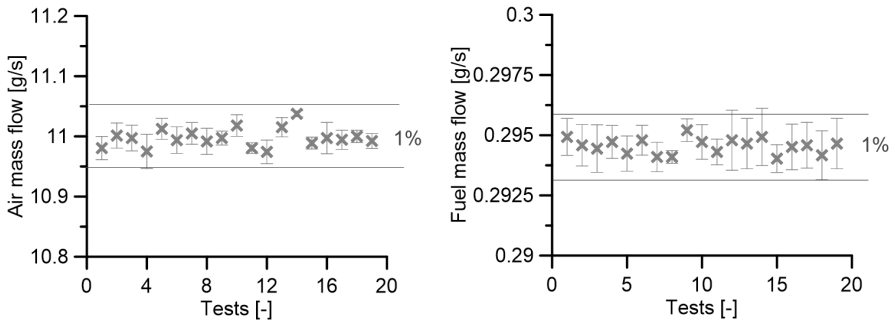

Figure 5.28. *Experimental air and fuel mass flows at 2000_5 in DoE 2.*

Again, the combustion diagnosis analysis was performed in all operating conditions to obtain typical combustion results such as indicated efficiency, combustion duration, heat transfer... Then, gross indicated efficiency, soot and NO_x emissions were analysed as function of changes in the DoE inputs and in their interactions by using standardized Pareto charts.

The standardized Pareto chart of GIE at 2000_5 in this DoE 2 is plotted in Figure 5.29, where it can be seen that the start of energizing time is the most important factor as in the previous DoE for this output. Advancing this point has an important increase effect on GIE. Then, another significant effect is the injection pressure, even though its importance is lower than half the GIE one, efficiency is also increased when this variable is incremented. Finally, the increment of the post-injection fuel mass affects negatively GIE due to large injections in the very late combustion part tend to extend the combustion process, although its significance is quite low. Additionally, the interaction between the rail pressure and SOE and between the SOE and the mass of the post injection have some effect on the output. Based on these results, a statistical model was developed to reproduce the GIE behaviour with an R^2 of 96% using the inputs of DoE 2 as entries of the model. The coefficients of this model at 2000_5 and 1500_8 along with the ones of the other outputs are displayed in Table 5.8.

Regarding the pollutant emissions at 2000_5, Figures 5.30 and 5.31 show the standardized Pareto charts of NO_x and soot in this DoE 2. It is worth to

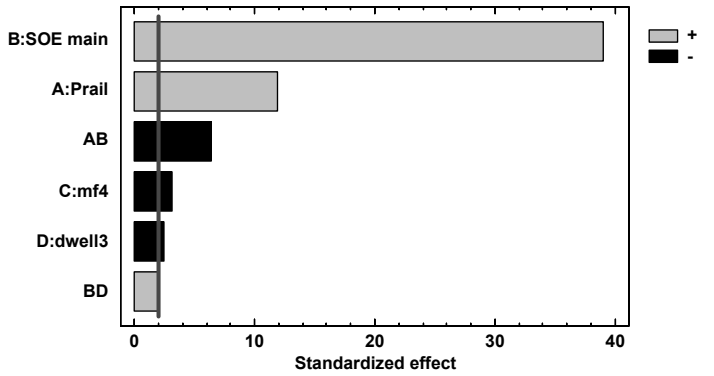

Figure 5.29. *Standardized Pareto chart of GIE at 2000_5 in DoE 2.*

Test	Output	R^2	Intercept	A	B	C	D
	GIE [%]	0.96	43.7563	$2.1{\cdot}10^{-3}$	0.4591	-0.2728	-0.8569
2000_5	NO_x [mg/s]	0.99	4.2526	$7.2{\cdot}10^{-3}$	0.5078	-0.3142	0.3993
	Soot [FSN]	0.96	2.4636	$-2.2{\cdot}10^{-3}$	-0.1133	0	0.3538

Test	Output	R^2	AB	AC	AD	BC	BD
	GIE [%]	0.96	$-2.2{\cdot}10^{-4}$	0	0	0	0.1405
2000_5	NO_x [mg/s]	0.99	$3.2{\cdot}10^{-4}$	0	$-2.3{\cdot}10^{-3}$	0	-0.1366
	Soot [FSN]	0.96	$4.4{\cdot}10^{-5}$	0	0	$1.9{\cdot}10^{-2}$	0

Test	Output	R^2	Intercept	A	B	C	D
	GIE [%]	0.98	39.2182	$3.1{\cdot}10^{-3}$	0.5713	0.1747	-1.303
1500_8	NO_x [mg/s]	0.99	4.5221	$6.7{\cdot}10^{-3}$	0.429	-0.6908	1.8766
	Soot [FSN]	0.98	3.3313	$-2.3{\cdot}10^{-3}$	-0.4646	0.2493	1.6771

Test	Output	R^2	AB	AC	AD	BC	BD
	GIE [%]	0.98	$-1.7{\cdot}10^{-4}$	0	0	$-2.5{\cdot}10^{-2}$	-0.1202
1500_8	NO_x [mg/s]	0.99	$3.4{\cdot}10^{-4}$	$9.3{\cdot}10^{-4}$	$-4.4{\cdot}10^{-3}$	0	-0.1464
	Soot [FSN]	0.98	$1.2{\cdot}10^{-4}$	$-4.1{\cdot}10^{-4}$	0	$4.3{\cdot}10^{-2}$	0.27

Table 5.8. *Coefficients of statistical models at 2000_5 (top) and 1500_8 (bottom) in DoE 2.*

mention that the significance of common factors with DoE 1 (injection pressure and SOE) is maintained in this DoE. In the case of NO_x, the increment of both SOE (advancing) and rail pressure leads to increase NO_x emissions due to the higher combustion temperature reached. Other significant effects are that either the increment of the dwell time between the main and the 4^{th} injection or a reduced post-injection fuel mass help to decrease NO_x emissions slightly. Furthermore, there are some interactions between inputs that have a small effect on the final soot emissions.

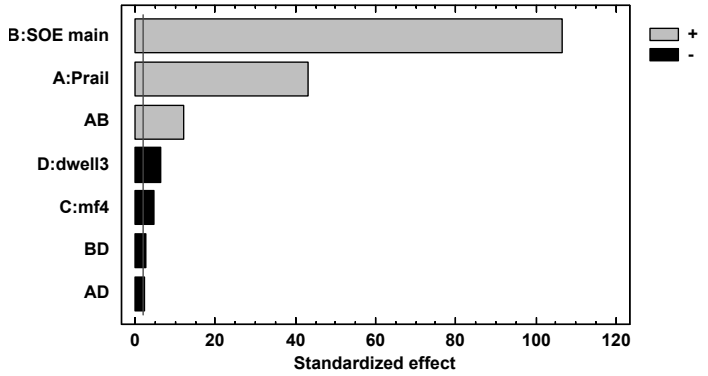

Figure 5.30. *Standardized Pareto chart of NO_x emissions at 2000_5 in DoE 2.*

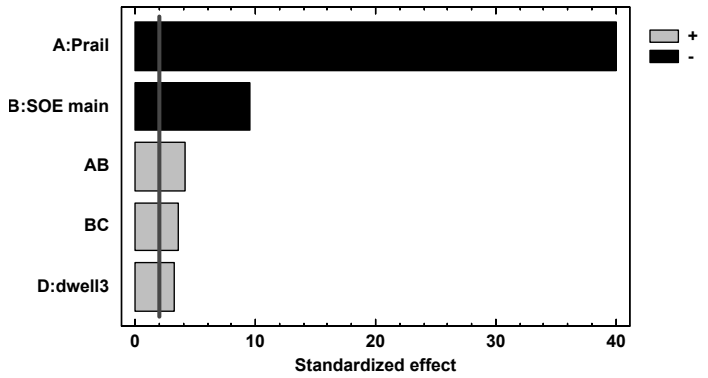

Figure 5.31. *Standardized Pareto chart of soot emissions at 2000_5 in DoE 2.*

In the case of soot, when injection pressure is incremented or SOE is advanced, soot emissions decrease but, in this case, the most important parameter is the rail pressure instead of SOE as in NO_x emissions.

Additionally, soot emissions are not affected by post-injection quantity but they are reduced when dwell time is shortened. Additionally, the interactions between the injection pressure and SOE and between SOE and the mass of the post injection seem to have a little impact on the final soot emissions. Thus, it can be stated that a post injection close to the main injection is interesting to reduce soot.

Finally, two different statistical models were developed using the coefficients displayed in Table 5.8. These two models along with the one extracted from the analysis of changes on GIE were used to obtain the response surface of the design space, top view of which is plotted in Figure 5.32. It can be seen there that NO_x incremented at high GIE values while soot emissions reduction went in the same direction than the GIE enhancement.

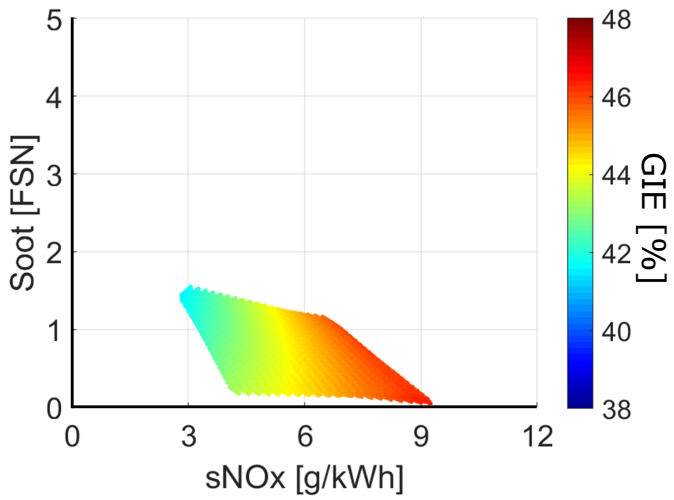

Figure 5.32. *Top view of the response surface of GIE, NO_x and soot emissions models at 2000_5 in DoE 2.*

This plot has been overlapped to the one obtained in DoE 1 at 2000_5 and limits of the first one have been highlighted with a black line in Figure 5.33. It can be discerned that the map in DoE 2 has moved to a lower NO_x and soot emissions zone and, at the same time, the maximum GIE achieved with the post-injection strategy is higher. Additionally, it can be seen that there is an intermediate zone were both 3 and 4-injection strategies provided the same results of NO_x and soot but with higher GIE in the case of DoE 2. Taking into account these changes, different optimization strategies could be approached. On the one hand, a low pollutant emissions strategy with

ultra low soot emissions while maintaining the efficiency could be achieved at the bottom left part of the lines delimiting DoE 1 map. On the other hand, another approach would lead to increase the efficiency while maintaining the experimental NO_x and soot emissions in the coincident zone of both maps.

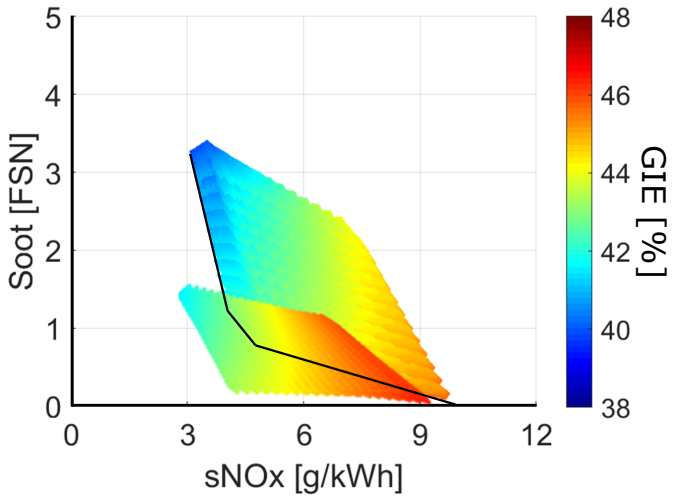

Figure 5.33. *Top view of the response surfaces of GIE, NO_x and soot emissions models at 2000_5 in DoE 1 and DoE 2 .*

Once the post injection strategy has been assessed at 2000_5 the same approach was performed at 1500_8 but, for the sake of brevity and since no significant differences have been found between both points, results can be found in Appendix 5.6.1.2. Based on these results, three statistical models obtained with the linear combination of the significant injection settings, coefficients of which are presented in Table 5.8, were developed to predict GIE, NO_x and soot. Using these three models allowed obtaining the response surface of the design space, top view of which is presented in Figure 5.34. As can be observed, at a same level of soot emissions (horizontal lines) efficiency can be increased with a penalty of NO_x. On the other hand, if NO_x emissions are maintained (vertical lines) it is possible to increase GIE and reduce soot at the same time. Finally, at a given medium efficiency (light blue diagonal), there are different injection settings combinations that lead to different pollutant emissions, NO_x = 5 g/kWh and soot = 0.8 FSN or NO_x = 7 g/kWh and soot = 2.6 FSN.

The plot resulting from DoE 2 has been overlapped to the one obtained in DoE 1 in Figure 5.35 where limits of DoE 1 have been remarked with black

lines. Unlike at 2000_5 these maps coincide almost completely and only a little zone of DoE 2 at the left of the lowest DoE 1 boundary attains better performance than the 3-injections strategy. In this zone, both NO_x and soot emissions are reduced below 6 g/kWh and 1 FSN respectively and the GIE is maintained around 42%.

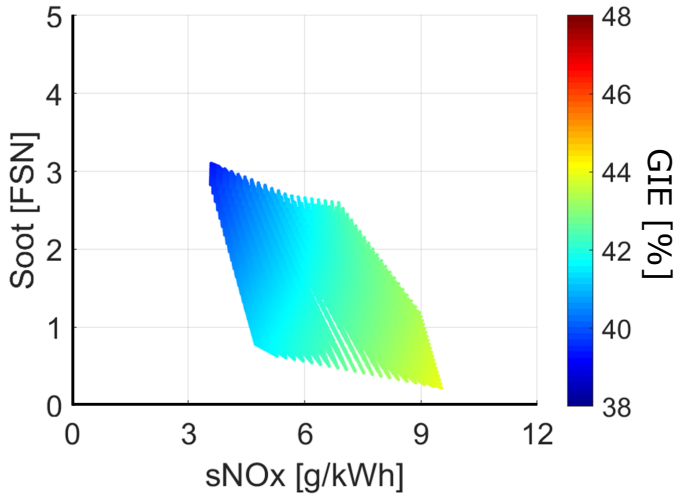

Figure 5.34. *Top view of the response surface of GIE, NO_x and soot emissions models at 1500_8 in DoE 2.*

5.2.2.4 Conclusions

In this section, the effects of the different injection settings on the engine performance have been assessed using two consecutive DoEs at two different operating conditions. Both studies were performed using a low swirl ratio (0.9), to limit the heat transfer penalty at high SR, and maintaining the conditions at the intake valve closing and the total fuel mass delivered along the cycle to ensure a fair comparison between the different injection settings combinations.

On the one hand, DoE 1 was used to assess the effect of the pilot injection settings (dwell and energizing times) along with the injection pressure and the position of the main event on GIE, NO_x and soot emissions. Main conclusions of this first study are that injection pressure and SOE of the main injection are the most significant variables in all cases and the pilot settings combination that provides the best balance (same weight in the objective function) between

GIE and NO_x consists on large pilot quantities (2mg) and close injection events (0.25ms).

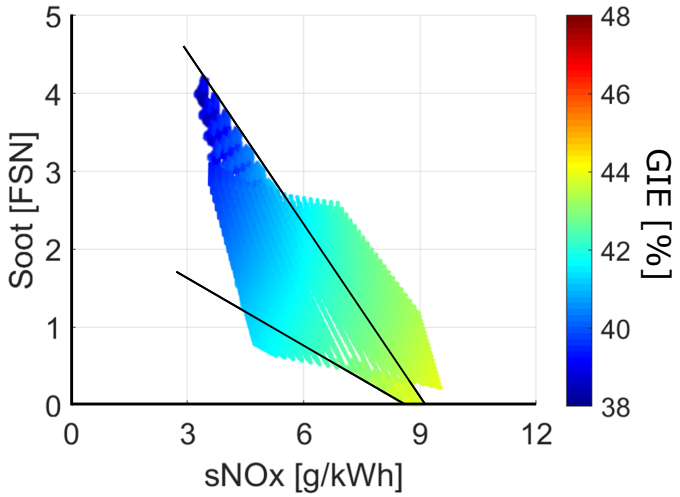

Figure 5.35. *Top view of the response surfaces of GIE, NO_x and soot emissions models at 1500_8 in DoE 1 and DoE 2.*

On the other hand, DoE 2 studied the post-injection settings effects (dwell and fuel mass quantity), using the optimized pilot settings extracted from DoE 1 in terms of GIE and NO_x, along with injection pressure and SOE of the main event. Again, the two most important factors are these last two and, specially at 2000_5, it can be obtained a region out of the DoE 1 where the 4-injections strategy reaches a better performance in terms of GIE, NO_x and soot than the 3-injections one.

The combination of both DoEs allowed achieving improvements in terms of GIE and NO_x emissions respect to the nominal point. In particular, at 2000_5 a big region was found where GIE could be increased up to +1% $\dot{m}_f H_v$, NO_x emissions could be cut down more than -2 g/kWh and soot could be ten times lower than in the nominal point. Similarly, although to a lesser extent, at 1500_8 some benefits were also discovered with a small region in which GIE was maintained but NO_x emissions were -2g/kWh lower and soot could be reduced to the half.

5.2.3 Conclusions

Two experimental approaches commonly followed to improve the combustion velocity have been assessed in this section. The first one deals with the change of the air velocity inside the combustion chamber while the second one modifies the injection pattern in order to improve the engine performance. This section provides a summary of the findings after performing both analysis.

On the one hand, GIE increased at intermediate SR at some operating conditions, despite the heat transfer increment implied by swirl motion, thanks to the combustion enhancement at least during the initial combustion process. However, this gain was not transferred to brake thermal efficiency due to the extra pumping work derived from the valve used to enhance the swirl motion. At the end, BTE was reduced when swirl increased in all operating conditions and at almost all SR levels. Additionally, the swirl enhancement led to an increase of NO_x emissions in all points.

On the other hand, the injection pattern approach seems to be a more flexible technique that allows exploring different combinations of number of injections, energizing times, timings and injection pressures. Such flexibility leads to different options in terms of GIE and NO_x emissions and, unlike with SR, it is possible to improve both of them at the same time with the correct combination of injection settings. Additionally, the gain observed in GIE here should be almost directly transferred to BTE since the pumping work does not increase, in fact, it should decrease in the post injection cases due to the higher exhaust temperature. The only term that would decrease BTE is the increment in mechanical losses due to the higher power delivered to the fuel pump when increasing the injection pressure. Unfortunately, since the injection assessment was performed in a single cylinder engine, BTE results are not trustworthy.

Therefore, it seems clear that the injection strategy could provide better benefits in terms of both GIE and NO_x that the swirl approach.

5.3 Experimental optimization of HRL

In this section, the experimental optimization of the combustion law in terms of GIE and NO_x emissions is carried out using the conclusions extracted from the analysis of swirl and injection pattern in the previous section. Taking into account these conclusions, it was decided to use a low swirl ratio (SR=0.9), to avoid any additional penalty in NO_x and BTE, and to optimize the injection

pattern due to the high flexibility of this approach. Under these conditions, two operating conditions used in the previous analysis were optimized in terms of GIE and NO_x emissions.

Since the injection analysis in section 5.2.2 was performed also at SR=0.9, the models developed in that section are used here to obtain the optimum point in terms of gross indicated efficiency and NO_x emissions. Because soot emissions were not modelled in the theoretical optimization, they are out of this experimental optimization to get a fair comparison between both theoretical and experimental studies. Thus, Figure 5.36 shows the GIE and NO_x results of the same points plotted in Figures 5.33 and 5.35 (corresponding to the design space of DoE 1 and DoE 2) at 2000_5 (left) and 1500_8 (right) along with the nominal point. Actually, these graphs represent a side view of the previous ones with the NO_x emissions in the x-axis.

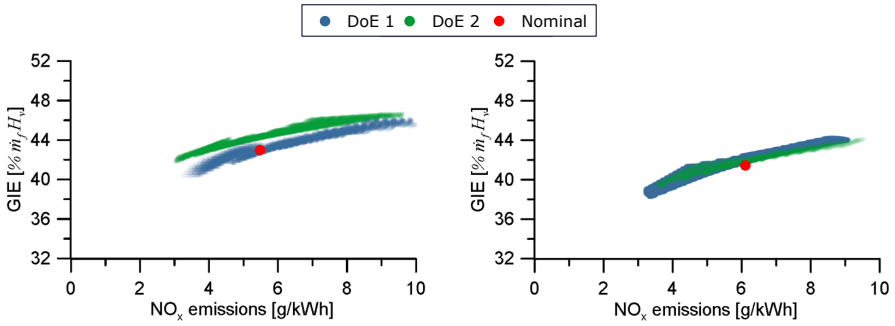

Figure 5.36. *Response surfaces of GIE and NO_x emissions at 2000_5 (left) and 1500_8 (right) in DoE 1 and DoE 2.*

As can be seen, there is a wide band of emissions ranging from 3 g/kWh to 10 g/kWh that can be swept with efficiencies ranging from 38% $\dot{m}_f H_v$ up to 46% $\dot{m}_f H_v$. As explained in the previous section, the use of a post-injection in DoE 2 led to a GIE increase of 1% $\dot{m}_f H_v$ under the same NO_x emissions level at 2000_5. However, at 1500_8 the addition of a post-injection did not improve the best tradeoff between efficiency and NO_x emissions set by DoE 1. In any case, some points of the DoE allowed increasing both GIE and NO_x emissions respect to the nominal point at both operating conditions.

The upper bound of plots presented in Figure 5.36 are plotted in Figure 5.37. These lines represent the best GIE and NO_x tradeoffs achievable at both operating conditions. Additionally, some specific experimental points belonging to these tradeoffs are marked with greyscale dots. These points,

main characteristics and results of which can be found in Table 5.9, establish the maximum GIE achievable under specific NO_x emissions levels and are analysed in detail in the next paragraphs.

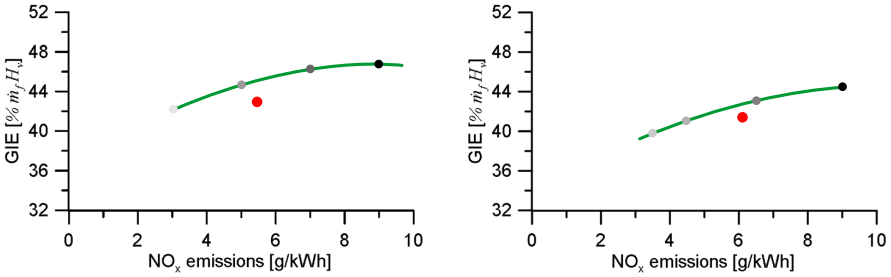

Figure 5.37. *Best tradeoff between GIE and NO_x emissions at 2000_5 (left) and 1500_8 (right) in DoE 1 and DoE 2.*

POINT [-]	Rail pressure (x_1) [bar]	SOE main (x_2) [°BTDC]	$m_{f,1}$ [mg]	$dwell_1$ [ms]	$m_{f,2}$ [mg]	$dwell_2$ [ms]	$m_{f,4}$ (x_3) [mg]	$dwell_3$ (x_4) [ms]	GIE [%]	sNO_x [g/kWh]
Nominal	650	2	1.5	0.5	1.5	0.5	-	-	43.2	5.4
sNO_x=9	1150	5	2	0.25	2	0.25	2	0.45	46.5	9
sNO_x=7	650	5	2	0.25	2	0.25	2	0.45	46.1	7
sNO_x=5	1150	-5	2	0.25	2	0.25	2	0.45	44.2	4.9
sNO_x=3	650	-5	2	0.25	2	0.25	3	0.45	42.2	3

Table 5.9. *Injection settings and GIE and NO_x results of optimum experimental points under different NO_x emissions levels at 2000_5.*

The HRL and in-cylinder pressure evolutions of the greyscale points marked in the left plot of Figure 5.37 at 2000_5 are plotted in Figure 5.38 along with the related to the nominal point. It can be seen that, even though the start of combustion in the nominal point was the most advanced, the CA90 was reached earlier in all cases except in the lowest emissions one. The first reason for this longer combustion is that dwell times between pilot injections are higher in the nominal point that in the other cases (0.5 ms vs 0.25 ms). This is translated into the longer flat zone of the red line between the combustion of the first pilot and the main combustion (from -8°ATDC to 7°ATDC). The second reason is that, as can be observed in Table 5.9, rail pressure of the experimental point (650 bar) is lower than at 5 and 9 g/kWh (1150 bar) and that also leads to a slower combustion development. Another interesting effect

shown in the plot is that CA50 was reached earlier and peak pressure increases as NO_x emissions and GIE were higher, which is coherent with the expected behaviour.

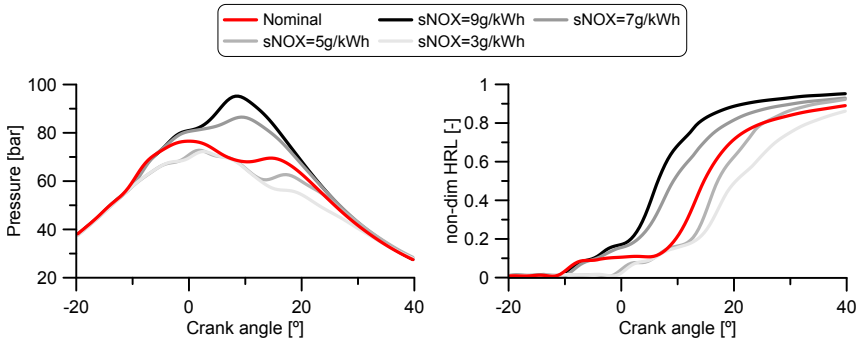

Figure 5.38. *HRL and in-cylinder pressure evolution of experimental optimum points under different NO_x emissions levels at 2000_5.*

It is worth to analyse the behaviour of the most relevant parameters (rail pressure and SOE of main injection) when NO_x was reduced. As observed in Table 5.9, the point with highest NO_x emissions level uses the highest injection pressure and the most advanced SOE that, at the same time, also lead it to the highest GIE. In order to decrease these emissions, the next two NO_x levels took either injection pressure or SOE to its extreme value alternatively while maintaining a little post-injection close to the main event. Finally, the most constrained NO_x level, used the lowest rail pressure and the most delayed SOE along with a large post injection event.

Since no difference on the results at the other operating point (1500_8) were found respect to the observed ones at 2000_5, they were included in Appendix 5.6.2.

5.4 Assessment of real combustion effect on indicated efficiency

In this section, the theoretical optimization strategy performed in Section 4.4 and the more conventional experimental approach followed in Section 5.3 are compared. It is worth to mention that the first one does not take into account any injection or mixing limitation but it gives the best HRL profile

to optimize GIE and predicted NO_x emissions. In fact, the injection settings that would provide the studied HRL are irrelevant since no combustion model is used (the use of a combustion model has been proposed as a future work in Section 6.2).

On the contrary, the experimental optimization is limited by the combustion velocity resulting from the air and fuel mixing process, which at the same time depends on the air motion and fuel injection pattern used at a certain point. If the existent hardware allowed this process to be perfect and the combustion velocity was not limited, the experimental optimization should reach the theoretical one. However, such an ideal injection system does not exist and every hardware has certain limits that set a frontier for the air-fuel mixing process, although there are some works in the literature aimed at reproducing these theoretical combustion laws by means of novel techniques [20], as already discussed in Chapter 2.

Therefore, differences in these two approaches should be attributed to the combustion velocity limit derived from the use of a certain hardware. In such a way, this comparison could be useful as a tool to perform a benchmarking between different hardware architectures.

It is worth to note that, as explained in Section 4.4.2.4, the NO_x emissions model is a semi-empirical model that was successfully calibrated and validated using real combustions along the engine map. Thus, even though trends given by the model are trustworthy, there is no guarantee that the absolute NO_x levels predicted by the model under the fast combustions (lower than 20° in all cases) provided by the theoretical optimization are accurate.

To assess such differences, the experimental optimization obtained in the previous section at 1500_8 and 2000_5 is compared to the theoretical one in terms of GIE and NO_x emissions at the same operating conditions. However, since these two points were not included in theoretical optimization of the engine map carried out in Section 4.4, the same methodology was applied to these two points in the next subsection. Again, this section only shows results of 2000_5 while the ones extracted at 1500_8 can be found in Appendix 5.6.3.2.

5.4.1 Theoretical optimization of HRL

The same methodology presented in Section 4.4 to obtain the optimum theoretical combustion in terms of GIE and NO_x is applied here at 2000_5. This optimization has been performed under the nominal pressure limits of the engine (peak pressure of 160 bar and maximum pressure rise rate of 10 bar/°). GIE and NO_x results of all the iterations of the optimization process

performed in the theoretical study at 2000_5 are plotted in Figure 5.39, where the tradeoff between both variables can be seen clearly.

The upper bound of Figure 5.39, corresponding to the best tradeoff between gross indicated efficiency and NO_x emissions at 2000_5, is plotted in Figure 5.40. Additionally, the greyscale points in the graph represent the highest efficiency combustions under different NO_x levels. This tradeoff presents two differentiated zones: the right part is an almost flat GIE zone where cutting down NO_x does not imply big losses on efficiency, while this situation reverses as NO_x emissions are reduced to the point that the tradeoff becomes vertical. At this second zone, a little reduction in NO_x implies a large penalty on GIE.

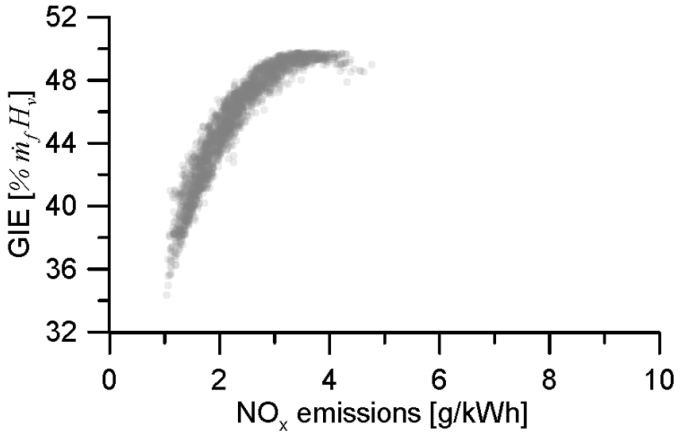

Figure 5.39. *Results of theoretical optimization of GIE and* NO_x *emissions at 2000_5.*

The combustion development and the calculated adiabatic temperature of the greyscale points at 2000_5 are plotted in Figure 5.41 since they are two of the most critical variables in the NO_x formation process [21], as shown in Section 3.3.2. As can be observed in the left plot, the maximum adiabatic temperature had to be reduced in order to cut down NO_x emissions, therefore, the start of the combustion was delayed as these emissions were reduced and the combustion is split in two stages. The first one develops slower while the second one speeds up when NO_x emissions are reduced. This 2-stage combustion scenario was enhanced as NO_x level was tightened.

Results derived from this analysis at 1500_8 are similar to the observed ones at 2000_5, as can be seen in Appendix 5.6.3.1, but with slightly lower GIE values.

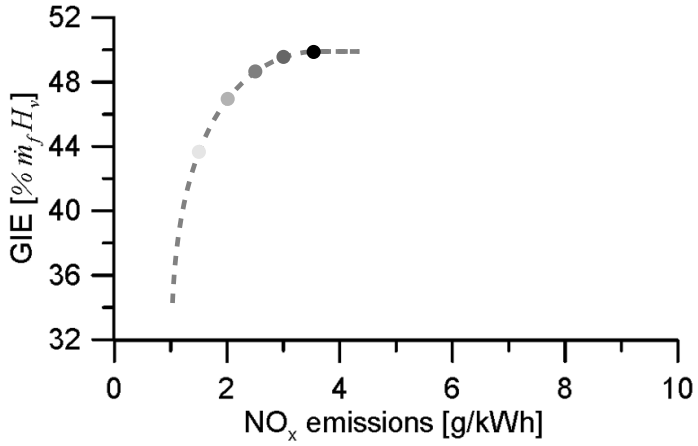

Figure 5.40. *Best theoretical tradeoff between GIE and* NO_x *emissions at 2000_5.*

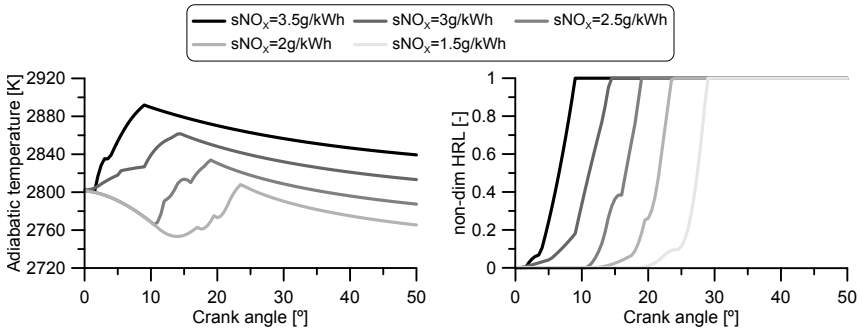

Figure 5.41. *Adiabatic temperature and HRL evolution of optimum theoretical points under different* NO_x *emissions levels at 2000_5.*

5.4.2 Assessment of real combustion effect

As commented in the introduction of this Chapter, differences between experimental and theoretical optimum combustions obtained in previous sections are the result of the combustion development limitations derived from the use of a specific hardware. To quantify this effect, both optimizations are compared in this section.

First of all, the best theoretical and experimental tradeoffs between GIE and NO_x emissions at 2000_5 are plotted together in Figure 5.42 along with the experimental nominal point represented as a blue dot. There, it can be seen that there is a large difference between both optimizations in terms of GIE and NO_x emissions since the theoretical tradeoff reached higher efficiencies (between +6% $\dot{m}_f H_v$ and +8% $\dot{m}_f H_v$ in the region around 4 g/kWh) and lower NO_x emissions (from -1.7 g/kWh at GIE=42% up to -7 g/kWh at GIE=46%) than the experimental ones. In any case, it can be seen that there is room to improve the experimental nominal point by performing either the theoretical or the experimental optimization.

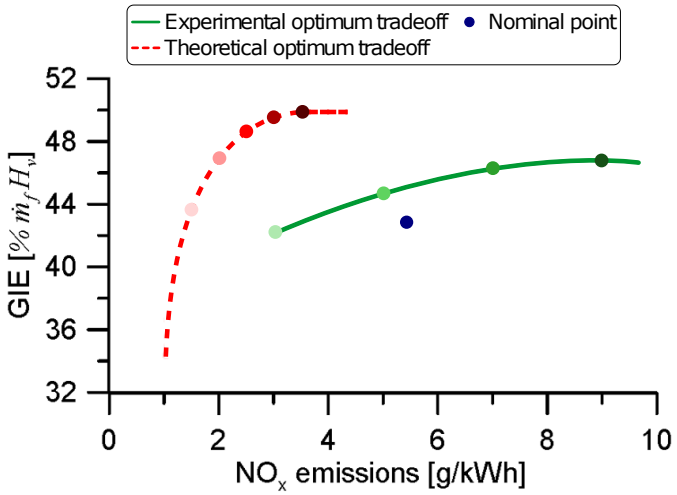

Figure 5.42. *Best theoretical (red) and experimental (green) tradeoffs between GIE and NO_x emissions at 2000_5 .*

Next step is the comparison of theoretical and experimental cycles that, under similar NO_x emissions, led to different gross indicated efficiencies. However, specific NO_x results given by Figure 5.42 do not provide iso-NO_x cycles since they also take into account the efficiency of the cycle. Thus, the tradeoffs have been plotted in Figure 5.43 but presenting the NO_x emissions in milligrams per gram of fuel, thus having comparable cycles in terms of absolute NO_x emissions.

In this figure the NO_x emissions range where both tradeoffs coincide is wider than in Figure 5.43. In order to perform a fair comparison between both optimizations, only the operating conditions belonging to these coincident tradeoff sections (the ones inside the rectangle; 11-24 mg/g_{fuel}) are evaluated

in the next analysis. Thus, Figure 5.44 presents the HRL evolution as a function of the crank angle (left-hand plot) and the adiabatic temperature evolution as a function of the HRL (right-hand plot) of these specific points. As commented in Section 5.4.1, these two parameters are the most critical ones in the NO_x formation process as stated by Arrègle *et al.* [21].

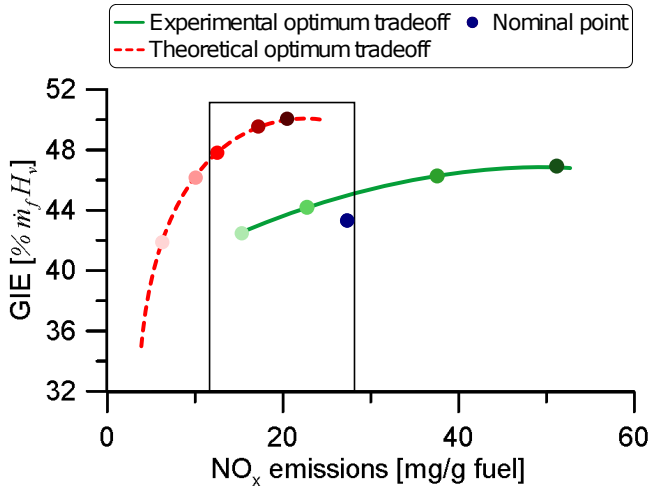

Figure 5.43. *Best theoretical (red) and experimental (green) tradeoffs between GIE and NO_x emissions at 2000_5 .*

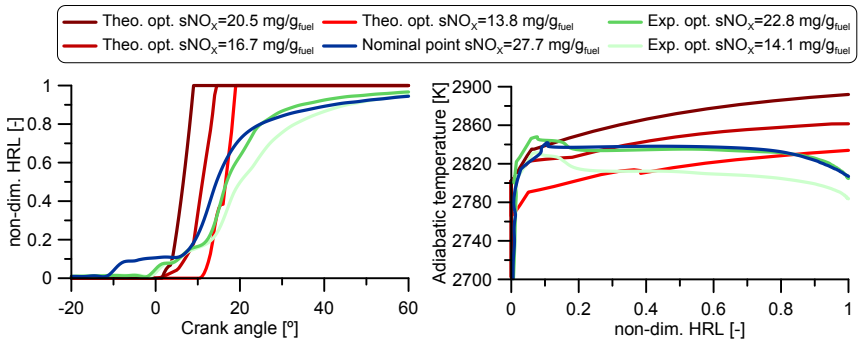

Figure 5.44. *HRL as a function of the crank angle (left) and adiabatic temperature as a function of the HRL (right) of optimum theoretical and experimental points under NO_x emissions between 11-24 mg/g_{fuel} along with the nominal point at 2000_5.*

The HRL plot (left-hand one) shows that theoretical combustions were much faster than the experimental ones and, even though they started later, they were able to finish earlier. These faster combustions led to higher adiabatic temperatures, at least when the theoretical HRL was advanced, as can be seen in the right-hand plot of Figure 5.44. As shown, the two theoretical combustions with the highest efficiency (the darkest red ones) reached the highest adiabatic temperatures of all the cycles (around 40K more than the experimental ones).

Regarding this adiabatic temperature, a clear tendency to raise its maximum can be observed, in both experimental and theoretical cases, when GIE and NO_x emissions were increased. Additionally, it can be observed that the represented experimental and theoretical HRL with NO_x emissions around 14 mg/g_{fuel} reached similar adiabatic temperatures, as it could be expected. However, this behaviour is not observed at higher NO_x levels where, even though adiabatic temperatures of the two theoretical combustions were higher, emissions of those theoretical optimums (20.5 and 16.7 mg/g_{fuel}) were below the optimum experimental ones (22.8 and 20.1 mg/g_{fuel}) and much lower than the experimental nominal point (27.7 mg/g_{fuel}).

This behaviour should be considered as a symptom of the NO_x model limits that, as a physics-based 0D model, is able to predict the trends in both theoretical and real combustions. Moreover, the model performance during the calibration and validation campaigns with real conditions, see Section 3.3.2, was really good. However, when comparing real versus theoretical optimum HRL, it is clear that in some cases (advanced combustions) the direct comparison cannot be done because the extrapolation capability of the model is limited.

In any case, both theoretical and experimental tradeoffs can be still compared in terms of GIE because, although theoretical NO_x emissions are not accurate in absolute terms, they provide the maximum efficiency achieved by both optimizations. Therefore, the difference between the maximum GIE maximums should provide an estimation of the impact on efficiency due to the use of a real injection-combustion system.

When comparing maximum efficiency areas of tradeoffs plotted in Figure 5.42, First remarkable thing is that maximum theoretical efficiency (GIE=49.7%) was +3% $\dot{m}_f H_v$ higher than the maximum experimental one (GIE=46.5%) and this, in turn, also +3% $\dot{m}_f H_v$ higher than the nominal experimental point (43.2%). To assess this difference, cycles of operating points corresponding to the upper-right part of each tradeoff along with the experimental nominal point are compared in Figure 5.45, where their in-

cylinder pressure and HRL evolution are plotted. Colours of the lines in both plots correspond to colours of the dots in Figures 5.42 and 5.43 thus, the darker the line is, the higher its efficiency.

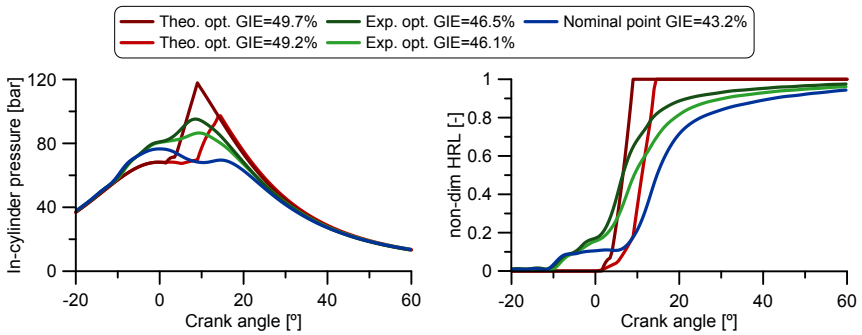

Figure 5.45. *In-cylinder pressure and HRL evolution of theoretical and experimental optimums along with the nominal point at 2000_5.*

As shown in the right-hand plot of Figure 5.45, most significant differences between the theoretical and experimental optimums in terms of combustion development are that theoretical combustions started close to the TDC, around 10° later than the experimental ones, and they were much faster (combustion duration of theoretical cases was between 8° and 15° unlike the experimental cases[1] 34° and 42°) as observed in Table 5.10. Such rapid combustions are also discerned in the high pressure rise rates, limited by the considered restriction in the highest efficiency theoretical case (PRR=10 bar/°) and a bit lower in the other (PRR=9.5 bar/°), observed in the theoretical cases in the left-hand plot of Figure 5.45. In this graph, it can also be seen that the theoretical cycle with maximum efficiency reached a peak pressure (117 bar) more than 20 bar higher than the experimental cases, as a result of its 8° combustion. However, it is remarkable that even though combustions were quite different, the crank angle in which 50% of the total injected fuel was burnt (CA50) is in the same range in all cases (between 7° and 12°ATDC) as observed in Table 5.10.

Therefore, it can be stated that differences observed in GIE between theoretical and experimental cases are mainly due to the different combustion velocity, since theoretical combustions were about 3-5 times faster than the experimental ones. In any case, such high theoretical velocity combustions

[1]Combustion duration of experimental points was calculated as the difference between CA90 and CA10.

Test [-]	SOC [°ATDC]	CA50 [°ATDC]	Combustion duration [°]
Theo. GIE = 49.7%	1.5	7	8
Theo. GIE = 49.2%	0	11.5	15
Exp. GIE = 46.5%	-11.5	7	33.5
Exp. GIE = 46.1%	-10.7	9.5	41.7
Nom. GIE = 43.2%	-13.2	13	55.2

Table 5.10. *Combustion characteristics of maximum experimental and theoretical GIE at 2000_5.*

provide only a gain of +3% $\dot{m}_f H_v$ on GIE, which means that experimental combustions, even though they are totally different than the optimum ones, are not so far from the maximum Diesel combustion at this operating point. This is an interesting conclusion because it sets a ceiling efficiency fro this engine and operating point that, even in the best conditions, can not be overcome.

As can be seen in Appendix 5.6.3, results obtained at 1500_8 were very similar to the presented ones here at 2000_5. In that case, the fast combustions obtained in the theoretical optimization reached GIE=46.7%, only +2.5% $\dot{m}_f H_v$ higher than the slower experimental combustions. It would be interesting to extend this analysis to the complete engine map in order to asses the global behaviour, however, due to time limitations, the analysis was only carried out in these two operating conditions.

As seen in both cases, the most decisive difference when comparing both experimental and theoretical optimums is the combustion velocity. Thus, taking into account that the air-fuel mixing and combustion processes impose the limits on the experimental combustion velocity and that this process is derived from the use of a specific hardware, it is fair to say that differences observed in this section are mainly due to the use of this hardware. Then, this methodology could be applied to assess the performance of different hardware in terms of GIE in such a way that it could become a benchmarking tool when comparing different hardware architectures with the optimum theoretical GIE.

5.5 Conclusions

In this chapter, two of the most common strategies to improve the combustion development in Diesel engines, such as swirl and injection pattern,

were assessed thoroughly. Conclusions of swirl study indicates that even though GIE increased at intermediate SR at some operating conditions, brake thermal efficiency was not improved at all due to the extra pumping work necessary to overcome the closing of the swirl valve used to promote in-cylinder swirl motion and, additionally, NO_x emissions also augmented when swirl was incremented. On the contrary, the injection pattern change has demonstrated to be a more flexible approach that permits improving both GIE and NO_x emissions at the same time when a proper optimization is followed.

Based on this analysis, the combustion of two operating conditions has been optimized experimentally in terms of GIE and NO_x emissions by modifying the injection pattern under low SR conditions (SR=0.9). This optimization has led to tradeoffs with GIE ranging from 42% to 46% and NO_x varying between 3g/kWh to 9g/kWh at 2000_5 and GIE from 38% to 44% and NO_x emissions in the range from 3g/kWh to 9g/kWh at 1500_8. Since this experimental optimization was limited by the combustion velocity imposed by the air-fuel mixing and combustion process (unlike the theoretical one developed in the previous chapter), the comparison between them indicates the impact on GIE of the specific engine hardware.

To obtain this difference, the methodology proposed in Chapter 4 to optimize theoretically the HRL was applied to the same operating conditions in which the experimental optimization had been carried out. As a result, at 2000_5 was obtained a tradeoff with GIE ranging from 36% to almost 50% and NO_x emissions from 1g/kWh to 3.5g/kWh while at 1500_8 the best tradeoff reached GIE from 35% to 47% and NO_x from 1g/kWh to 3g/kWh at 1500_8.

When trying to compare the best theoretical and experimental HRL under the same NO_x levels, it was observed that, even though the prediction of the trends in both theoretical and real combustions was good because the NO_x model is physics-based, in some cases the direct comparison was not possible due to the limited extrapolation capability of the model under combustions very different than the ones used in the calibration and validation campaigns. Instead, differences on the maximum efficiency achieved by both theoretical and experimental optimizations were assessed, concluding that the optimized experimental combustions at both operating conditions were around -3% $\dot{m}_f H_v$ lower in terms of GIE compared to theoretical Diesel combustions restricted by nominal pressure rise rate and peak pressure limits. This difference is explained due to the limited combustion velocity (5 times slower) imposed by the air-fuel mixing and combustion processes derived from the existent engine hardware. In case that a new hypothetical injection system

was able to perform the best possible combustion (maintaining the combustion chamber geometry), the maximum gain would be this margin of 3 % $\dot{m}_f H_v$.

This methodology could be applied to assess the performance of different hardware in terms of GIE in such a way that it could become a benchmarking tool when comparing different hardware architectures with the optimum theoretical GIE.

5.6 Appendix: Detailed analysis at 1500_8

5.6.1 Injection approach

5.6.1.1 Assessment of pilot injection strategy

The assessment of pilot injection strategy was performed in 1500_8, obtaining the Pareto chart for GIE plotted in Figure 5.46. There it can be seen that the only significant effects are the injection pressure, the start of energizing time of the main combustion and, to a lower extent, the fuel mass of the second pilot injection. As can be observed, increasing any of these 3 variables leads to a positive effect on GIE. Additionally, some interactions between the rail pressure and the start of the energizing time with the pilot settings have a certain effect on GIE. The coefficients of the model that reproduces GIE as function of the injection settings with an accuracy of 99% can be found in Table 5.5.

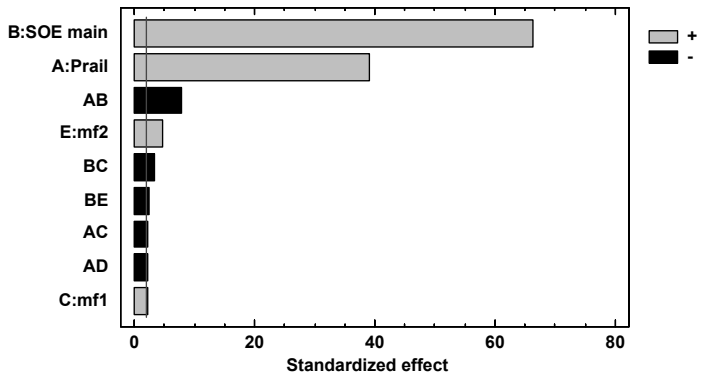

Figure 5.46. *Standardized Pareto chart of GIE at 1500_8 in DoE 1.*

When the Pareto charts for pollutant emissions are observed in Figures 5.47 and 5.48 at 1500_8, it can be seen that rail pressure and SOE of the main injection are the most important effects affecting them. Similarly to 2000_5, increasing rail pressure or advancing the injection increases NO_x emissions, while decreases soot due to the combustion velocity enhancement. Additionally, the standardized Pareto chart of NO_x emissions presents a little effect with the pilot settings and with some interactions between the injection pressure and the start of injection with settings of pilot injections. In the case of soot emissions, apart from the already mentioned injection pressure and

SOE effects, the interaction between both of them and between the injection pressure and the mass of the second injection have some effect on the output. Again, two statistical models were developed to reproduce these emissions as function of the presented significant effects and their coefficients are also displayed in Table 5.5.

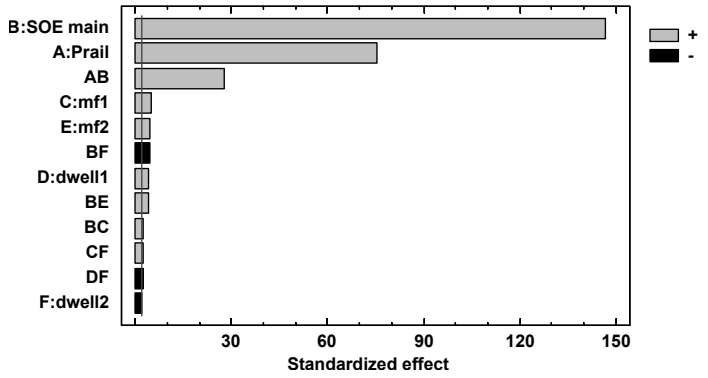

Figure 5.47. *Standardized Pareto chart of NO_x emissions at 1500_8 in DoE 1.*

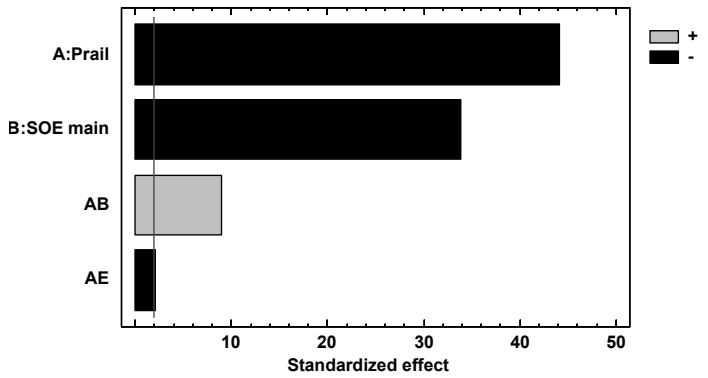

Figure 5.48. *Standardized Pareto chart of soot emissions at 1500_8 in DoE 1.*

5.6.1.2 Assessment of post injection strategy

The standardized Pareto chart of GIE derived from DoE 2 applied to 1500_8 is presented in Figure 5.49 where it can be seen that the two most significant effects are SOE main and the injection pressure as in the previous

point. As in all cases, advancing the injection train or increasing the rail pressure leads to a big improvement in GIE. In a second level of significance, the increment of dwell time results in an efficiency loss, while large post-injections increase GIE. These last results differ from the previous point, where the only significant effect apart from GIE and rail pressure was the fuel mass of the post-injection and its effect was contrary to the presented in this point. Additionally, there are some interactions between inputs that have a small effect on GIE.

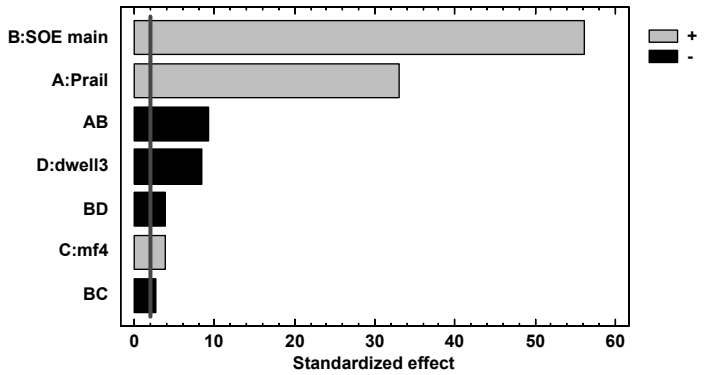

Figure 5.49. *Standardized Pareto chart of GIE at 1500_8 in DoE 2.*

Regarding the effect of post-injection on pollutant emissions at 1500_8, it can be stated that, as in all cases, the two most significant effects are the injection timing and pressure and their increase affects negatively NO_x emissions and leads to cut down soot as can be seen in Figures 5.50 and 5.51. As plotted, the increase of the dwell time between the main and post injections leads to a decrease in NO_x that is coherent with the contrary decrease in GIE due to this change. Additionally, it is worth to note that the increasing this dwell time also increases soot emissions and the significance of this effect is as high as the significance of SOE, which remarks the importance of the oxidation process in the late combustion process in soot. Finally, large post-injections also help to reduce soot although its significance is very low. In both pollutants, there are some interactions between the injection pressure and SOE and the post injection settings that have a small impact on the final outputs.

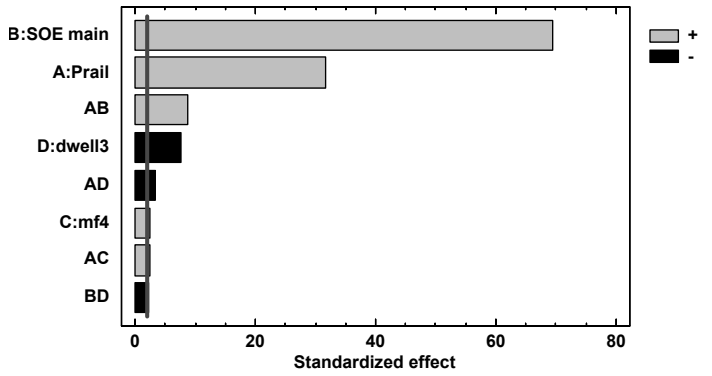

Figure 5.50. *Standardized Pareto chart of NO_x emissions at 1500_8 in DoE 2.*

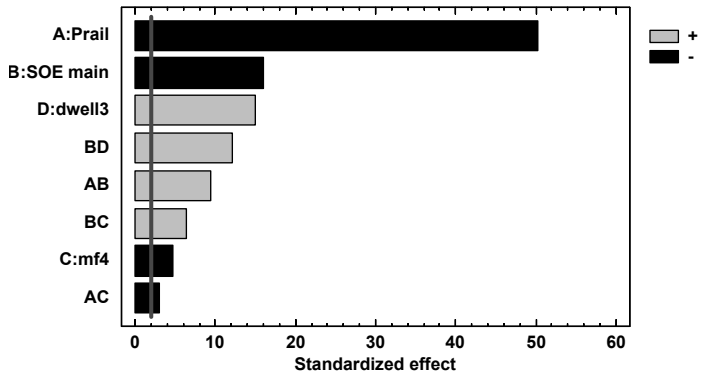

Figure 5.51. *Standardized Pareto chart of soot emissions at 1500_8 in DoE 2.*

5.6.2 Experimental optimization of HRL

Repeating the same analysis performed in Section 5.3 in the point with higher load (1500_8), Figure 5.52 was obtained, where the in-cylinder pressure and HRL of the nominal point and the greyscale points plotted in the right plot of Figure 5.37 under different NO_x levels are plotted. As commented above, the best tradeoff at this point consisted on 3-injections patterns since DoE 2 did not improve the best tradeoff obtained in DoE 1. At this point, conclusions are very similar to those extracted at 2000_5: nominal combustion is slower than the optimum one due to its longer time between the first pilot and the main injections and its lower injection pressure respect to the 4.5 and 9 g/kWh cases.

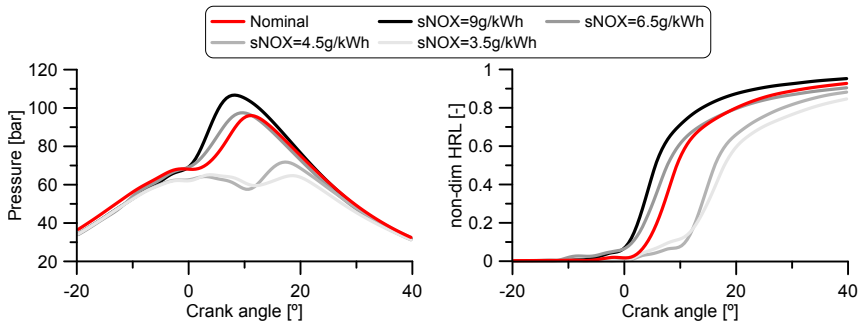

Figure 5.52. *HRL and in-cylinder pressure evolution of optimum experimental points under different NO_x emissions levels at 1500_8.*

It is worth to note that at this point the fuel mass of the pilots have lower relative weight respect to the total fuel mass as can be seen in the plot. Again, at this point, it is also possible to see that the peak pressure increased and the CA50 was reached earlier when GIE and NO_x emissions were enhanced. The injection settings along with the GIE and NO_x emissions in all these optimum solutions and in the nominal point are summarized in Table 5.11.

POINT	Rail pressure (x_1)	SOE main (x_2)	$m_{f,1}$	$dwell_1$	$m_{f,2}$	$dwell_2$	$m_{f,4}$ (x_3)	$dwell_3$ (x_4)	GIE	NO_x
[-]	[bar]	[°BTDC]	[mg]	[ms]	[mg]	[ms]	[mg]	[ms]	[%]	[g/kWh]
Nominal	750	1	1.5	0.5	1.5	0.5	-	-	41.8	6.1
sNO_x=9	1250	5	1	0.25	1	0.25	-	-	44.2	8.6
sNO_x=6.5	750	5	1	0.75	1	0.25	-	-	42.7	6.5
sNO_x=4.5	1250	-5	2	0.25	2	0.25	-	-	41.4	4.5
sNO_x=3.5	750	-5	2	0.25	2	0.25	-	-	39.5	3.5

Table 5.11. *Injection settings and GIE and NO_x results of optimum experimental points under different NO_x emissions levels at 1500_8.*

5.6.3 Assessment of real combustion effect on indicated efficiency

5.6.3.1 Theoretical optimization of HRL

The same methodology presented in Section 4.4 and used in Section 5.4.1 to obtain the optimum theoretical combustion in terms of GIE and NO_x was applied to 1500_8. This optimization has been performed under the nominal pressure limits of the engine (peak pressure of 160 bar and maximum pressure

rise rate of 10 bar/°). GIE and NO_x results derived from this study at 1500_8 are plotted in Figure 5.53, where it can be seen clearly the tradeoff between both variables. As can be observed, results are very similar to those presented at Section 5.4.1 at 2000_5, specially in the bottom part of the tradeoff, with the difference that 2000_5 reached higher GIE and NO_x emissions in the top part of the tradeoff.

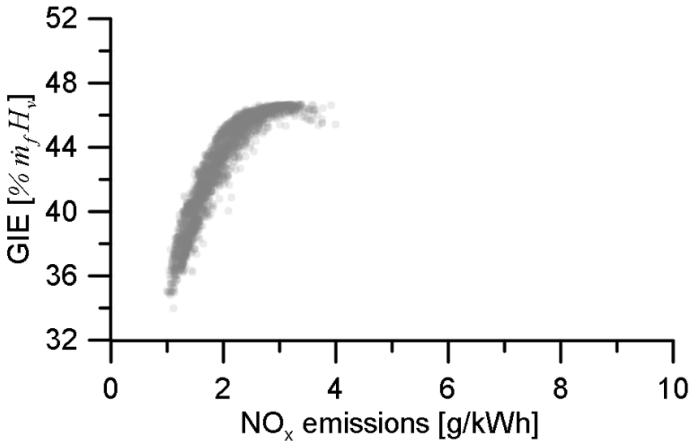

Figure 5.53. *Results of theoretical optimization of GIE and NO_x emissions at 1500_8.*

The best tradeoff between gross indicated efficiency and NO_x emissions obtained in Figure 5.53 at 1500_8 is plotted in Figure 5.54. Additionally, the greyscale points in the graph represent the highest efficiency combustions under different NO_x levels. This tradeoff presents two differentiated zones: the right part is an almost flat GIE zone where cutting down NO_x does not imply big losses on efficiency, while this situation turns inside out as NO_x emissions are reduced to the point that the tradeoff becomes vertical. At this second zone, a little reduction in NO_x implies a big penalty on GIE.

The instantaneous results of the greyscale points at 1500_8 are presented in Figure 5.55, where the adiabatic temperature evolution and the HRL profile are plotted. The behaviour of temperature and combustion when NO_x limits were tightened was exactly the same than at 2000_5. The combustion started later as can be seen in the right plot and its first part was slowed down while the second one was speeded up when NO_x emissions had to be reduced. These effects on combustion resulted in a lower maximum adiabatic temperature, which benefited the reduction of the NO_x formation process.

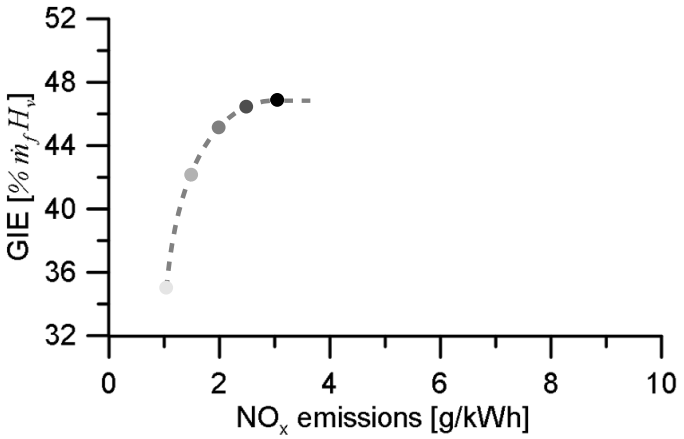

Figure 5.54. *Best theoretical tradeoff between GIE and NO_x emissions at 1500_8.*

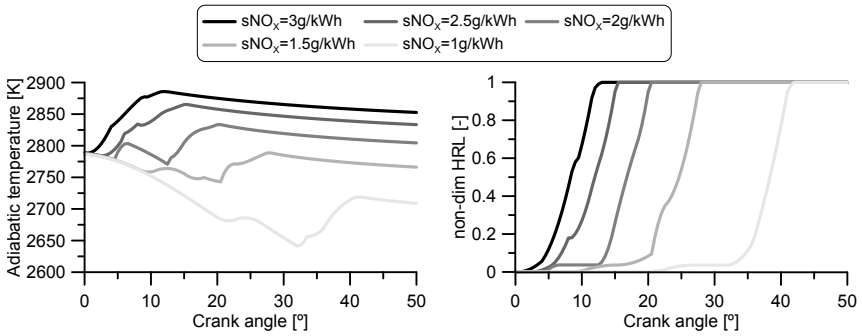

Figure 5.55. *Adiabatic temperature and HRL evolution of optimum theoretical points under different NO_x emissions levels at 1500_8.*

5.6.3.2 Assessment of real combustion effect

The same comparison between the theoretical and experimental optimizations carried out in Section 5.4.2 at 2000_5 was applied to 1500_8. First of all, the best theoretical and experimental tradeoffs between GIE and NO_x emissions at 1500_8 are plotted together in Figure 5.56 along with the experimental nominal point represented as a blue dot. There, it can be seen that there is a large difference between both optimizations regarding GIE and NO_x emissions since the theoretical tradeoff reached higher efficiencies but with lower NO_x emissions. Additionally, it can also be seen that there

is room to improve the nominal point by performing any of the described optimizations.

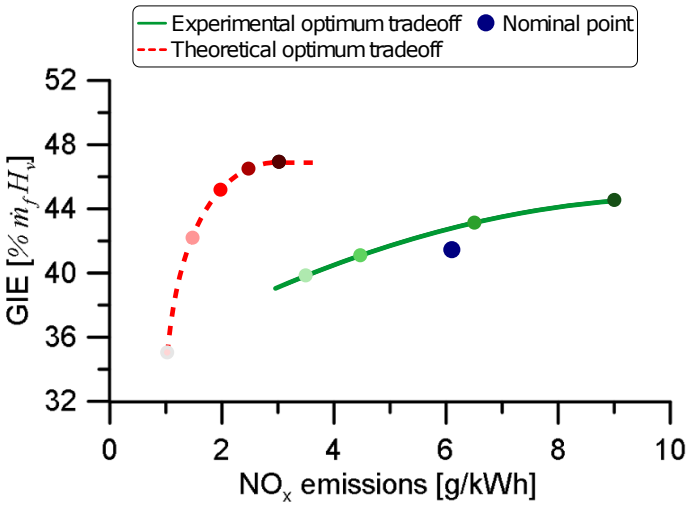

Figure 5.56. *Best theoretical (red) and experimental (green) tradeoffs between GIE and NO_x emissions at 1500_8.*

As stated in Section 5.4.2, the NO_x model presents some limitations although, as a physics-based 0D model, it is able to predict the trends in both theoretical and real combustions. Moreover, the model performance during the calibration and validation campaigns with real conditions, see Section 3.3.2, was really good. However, when comparing real versus theoretical optimum HRL, it is clear that in some cases (advanced combustions) the direct comparison cannot be done because the extrapolation capability of the model is limited.

In any case, both theoretical and experimental tradeoffs can be still compared since they reached different GIE maximum values that, although theoretical NO_x emissions are unknown, provide the maximum performance of both optimizations in terms of GIE. Therefore, the difference between these two GIE maximums should provide the impact on GIE derived from the combustion velocity limit marked by the use of the existent hardware.

Thus, when comparing maximum efficiencies of theoretical and experimental approaches in Figure 5.56, it can be seen that maximum theoretical efficiency (GIE=46.7%) was only +2.5% $\dot{m}_f H_v$ higher than the maximum experimental one (GIE=44.2%) and this, in turn, also +2.4% $\dot{m}_f H_v$ higher than the nominal experimental point (41.8%). To evaluate where this

difference comes from, cycles of operating points corresponding to the upper-right part of each tradeoff along with the experimental nominal point are compared in Figure 5.57, where their in-cylinder pressure and HRL evolution are plotted. Colours of the lines in both plots correspond to colours of the dots in Figures 5.56 thus, the darker the line is, the higher its efficiency.

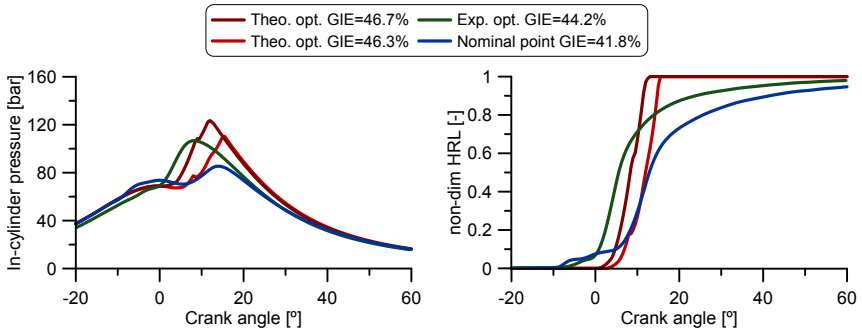

Figure 5.57. *In-cylinder pressure and HRL evolution of optimum theoretical and experimental points under maximum GIE values along with the nominal point at 1500_8.*

As shown in the right-hand plot of Figure 5.57, the most relevant differences among theoretical and experimental HRL are that, unlike the experimental combustions that started around -10°ATDC, the theoretical combustions started close to the TDC and they were around 3 times faster than the experimental ones as observed in the combustion durations stated in Table 5.12. Such rapid combustions were reflected in the high pressure rise rates observed in the theoretical cases, limited by the considered restriction in the highest efficiency theoretical case (PRR=10bar/°) and a bit lower in the other (PRR=9.5bar/°), in the left-hand plot of Figure 5.57. In this graph, it can be also seen that the theoretical cycle with maximum efficiency reached a peak pressure (123 bar) around 15 bar higher than the others, as a result of its 13° combustion. However, it is remarkable that even though combustions were quite different, the crank angle in which 50% of the total injected fuel was burnt (CA50) was in the same range in all cases (between 6 and 12°ATDC) as observed in Table 5.12 and similar to 2000_5.

Therefore, it can be concluded that at this point differences observed in GIE between theoretical and experimental cases are mainly because of theoretical combustions were around 3-4 times faster than the experimental ones. In any case, such high theoretical velocity combustions provided only

Test [-]	SOC [°ATDC]	CA50 [°ATDC]	Combustion duration [°]
Theo. GIE = 46.7%	0.5	8.5	13
Theo. GIE = 46.3%	2.5	12	13.5
Exp. GIE = 44.2%	-8	6	32
Nom. GIE = 41.8%	-10	13	52

Table 5.12. *Combustion characteristics of maximum experimental and theoretical GIE at 1500_8.*

a gain of +2.5% $\dot{m}_f H_v$ on GIE, which means that experimental combustions, even though they are totally different than the optimum ones, are not so far from the maximum efficiency Diesel combustion at this operating point.

Bibliography

[1] Olmeda P, Martín J, Blanco-Cavero D, Warey A and Domenech V. "Effect of in-cylinder swirl on engine efficiency and heat rejection in a light-duty diesel engine". *International Journal of Engine Research*, Vol. 18 n^o 1-2, pp. 81–92, 2017.

[2] Lee Y. and Huh K.Y. "Analysis of different modes of low temperature combustion by ultra-high EGR and modulated kinetics in a heavy duty diesel engine". *Applied Thermal Engineering*, Vol. 70 n^o 1, pp. 776–787, 2014.

[3] Zhang Y., Sagalovich I., De Ojeda W., Ickes A., Wallner T. and Wickman D. "Development of Dual-Fuel Low Temperature Combustion Strategy in a Multi-Cylinder Heavy-Duty Compression Ignition Engine Using Conventional and Alternative Fuels". *SAE International Journal of Engines*, Vol. 6 n^o 3, pp. 2013–01–2422, 2013.

[4] Masera K. and Hossain A. K. "Biofuels and thermal barrier: A review on compression ignition engine performance, combustion and exhaust gas emission". *Journal of the Energy Institute, In Press*, 2018.

[5] Wakisaka Y., Inayoshi M., Fukui K., Kosaka H. and Hotta Y. "Reduction of Heat Loss and Improvement of Thermal Efficiency by Application of Temperature Swing Insulation to Direct-Injection Diesel Engines". *SAE Int. J. Engines*, 2016.

[6] Heywood J.B. *Internal Combustion Engines Fundamentals*. McGraw-Hill, ISBN 978-0-07-028637-5, New York, 1988.

[7] Benajes J., Martín J., García A., Villalta D. and Warey A. "Swirl ratio and post injection strategies to improve late cycle diffusion combustion in a light-duty diesel engine". *Applied Thermal Engineering*, Vol. 123, pp. 365–376, 2017.

[8] Kawashima J. "Research on a variable swirl intake port for high-speed 4-valve DI diesel engine". *JSAE Review*, Vol. 20 n^o 3, pp. 421–424, Julio 1999.

[9] Woschni G. "A Universally Applicable Equation for the Instantaneous Heat Transfer Coefficient in the Internal Combustion Engine". *SAE Technical Paper 670931*, 1967.

[10] Payri F., Margot X., Gil A. and Martín J. "Computational Study of Heat Transfer to the Walls of a DI Diesel Engine". *SAE Technical paper 2005-01-0210*, Abril 2005.

[11] Benajes J., Olmeda P., Martín J., Blanco-Cavero D. and Warey A. "Evaluation of swirl effect on the Global Energy Balance of a HSDI Diesel engine". *Energy*, Vol. 122, pp. 168–181, 2017.

[12] Carreño R. *A comprehensive methodology to analyse the Global Energy Balance in Reciprocating Internal Combustion Engines*. Doctoral Thesis, 2016.

[13] Broatch A., Martín J., García A., Blanco-Cavero D., Warey A. and Domenech V. "Application of a zero-dimensional model to assess the effect of swirl on indicated efficiency". *International Journal of Engine Research*, pp. 1–12, 2018.

[14] Mccracken M E and Abraham J. "Swirl-Spray Interactions in a Diesel Engine". *SAE Technical Paper 2001-01-0996*, Vol. 2001 n^o 724, 2001.

[15] Morena J., Vassallo A., Peterson R. C., Gopalakrishan V. and Gao J. "Influence of Swirl Ratio On Combustion System Performance of a 0.4L Single-Cylinder Diesel Engine". *THIESEL 2014 Conference on Thermo-and Fluid Dynamics Processes in Direct Injection Engines*, 2014.

[16] Payri F., Olmeda P., Martín J. and Carreño R. "A New Tool to Perform Global Energy Balances in DI Diesel Engines". *SAE Int. J. Engines*, Vol. 7 n^o 1, pp. 43–59, 2014.

[17] Cavazzuti M. *Optimization Methods: From Theory to Design.* Springer, Berlin, Heidelberg, 2013.

[18] Montgomery D.C. *Design and Analysis of Experiments.* John Wiley & and Sons Inc., 2012.

[19] Lalanne C. *R Companion to Montgomery's Design and Analysis of Experiments.* John Wiley & and Sons Inc., 2009.

[20] Okamoto T. and Uchida N. "New Concept for Overcoming the Trade-Off between Thermal Efficiency, Each Loss and Exhaust Emissions in a Heavy Duty Diesel Engine". *SAE International Journal of Engines*, Vol. 9 n^o 2, pp. 2016–01–0729, 2016.

[21] Arrègle J., López J.J., Guardiola C. and Monin C. "Sensitivity study of a NOx estimation model for on-board applications". *SAE Technical Paper 2008-01-0640*, 2008.

Chapter 6

Conclusions and future works

Contents

This chapter summarizes the main findings and ideas developed in the document, outlining the main conclusions extracted in the work. Finally, some future paths are suggested for the continuation of the present work.

6.1 Conclusions

This work deals with the assessment and optimization of the indicated cycle of an ICE using a combination of different theoretical approaches, based on 0D modelling, and experimental tools. On the one hand, a theoretical optimization was proposed, assessing the efficiency losses that separate a real cycle from an ideal one and calculating the optimum combustion under realistic conditions and several operational limits such as maximum peak pressure, maximum pressure rise rate and NO_x emissions. On the other hand, two experimental techniques (swirl and injection optimization) were assessed for a later combustion experimental optimization. Finally, the theoretical and experimental optimums were compared to asses the impact of the real combustion velocity, limited by the existent hardware, on engine efficiency. Then, this methodology could become a benchmarking tool when comparing the highest optimum experimental GIE provided by different hardware architectures with the optimum theoretical GIE.

This section is aimed to give answers to the objectives stated in Section 1.3. Following, each particular objective is addressed individually using the conclusions extracted from the works developed in Chapters 4 and 5:

- The first objective stated in the introduction section was to identify and asses the efficiency losses affecting a real cycle unlike an ideal one. The first step to achieve this objective was to assess the efficiency of the studied engine operating under ideal cycles. Results of this part showed that Carnot cycle achieved almost 88%, while Otto and Diesel cycles, more similar to ICE real cycles, scored 68% and around 60% respectively. However, the assumptions considered by such ideal cycles lead to efficiencies much higher than the ones obtained under real conditions.

  Thus, the efficiency losses that separate ideal cycles from a real one were identified and assessed separately. Regarding the efficiency losses related to the non ideal combustion evolution, it was found that advancing the HRL 5° increased GIE no more than +1% $\dot{m}_f H_v$ (non ideal combustion centring), increasing 25% the combustion velocity also increased GIE up to +2% $\dot{m}_f H_v$ (non ideal combustion velocity) and the effect of the incomplete combustion was lower than +0.15% $\dot{m}_f H_v$ in the engine map. Then, it was obtained that considering heat transfer, which is responsible for between 9% $\dot{m}_f H_v$ and 15% $\dot{m}_f H_v$, implies an efficiency loss of -5% $\dot{m}_f H_v$ at most (low load and engine speed). The following efficiency losses were related to the impact of gas properties on heat capacity ratio. On the one hand, not considering the temperature variation along the cycle in the heat capacity ratio calculation leads to an efficiency increase around +3.5% $\dot{m}_f H_v$ in the whole engine map. On the other hand, an efficiency gain from +0.8% $\dot{m}_f H_v$ to +2% $\dot{m}_f H_v$ is achieved if the heat capacity ratio change due to variations in composition is not taken into account. Lastly, there were two minor efficiency losses related to air management namely non centred valves timing (+0.6% $\dot{m}_f H_v$ at most) and blow-by (+1% $\dot{m}_f H_v$ at most). As extracted from this study, the efficiency losses with the highest effect on GIE by order of importance were: firstly the combustion development, then heat transfer appeared in second place, while the third most important efficiency loss was the heat capacity ratio change due to temperature variations.

- The second objective was related to the determination of the efficiency boundaries of an ICE restricted to different operational limits. With this aim, the optimum HRL in terms of GIE under different scenarios

was calculated using a detailed 0D predictive model (SiCiclo) that includes all real relevant phenomena such as fuel vaporization, blow by leakages, combustion chamber deformation and real gas properties. The optimization was performed under different scenarios defined by the consideration of some constraints such as maximum peak pressure or maximum pressure rise rate and the assessment of heat transfer, considering an adiabatic engine or a temperature swing coating applied to piston top and cylinder head. Finally, NO_x emissions were also included in the optimization process obtaining tradeoffs between GIE and NO_x in all studied points.

When no constraints were considered, the optimum HRL was an instantaneous combustion starting around 1°ATDC with efficiencies ranging from 52% to 55.5% depending on the operating point. These instantaneous combustions, unlike ideal cycles, were not placed in the TDC due to the consideration of real phenomena such as blow-by, combustion chamber deformation and the heat capacity ratio change due to temperature and composition variations. Besides, the assessment of heat transfer, still under no constraints, delayed the optimum HRL but its duration continued being instantaneous. Thus, GIE decreased from -4% $\dot{m}_f H_v$ at high load and engine speed to -8% $\dot{m}_f H_v$ at low load and engine speed when nominal HT was considered.

Considering any pressure constraint led to an optimum 2-stage HRL shaped to burn as quick as possible to reach the imposed limits. Thus, the first part of the optimum HRL developed instantaneously when no PRR limit was applied or resulting in the PRR limit until reaching the maximum pressure limit. Then, the second part of the HRL was shaped to maintain this pressure limit until the total amount of fuel was burnt. As an example, imposing the nominal limits (PRR=10 bar/° and PP=160 bar) led to an efficiency loss from -1.4% $\dot{m}_f H_v$ at low load to -2.8% $\dot{m}_f H_v$ at high load when comparing to the restricted optimum solution. Additionally, the impact of temperature swing coating applied on the piston top and cylinder head walls on optimum HRL was assessed, finding a very slight effect of an earlier combustion start. This advancement had a marginal GIE increase ranging from +0.5% $\dot{m}_f H_v$ at low load and engine speed to +0.25% $\dot{m}_f H_v$ at high load and engine speed.

In a last step, NO_x emissions were also included in the optimization problem leading to a non unique optimum solution, but a set of optimum HRLs that maximized GIE while minimized NO_x emitted. This group of solutions formed the expected tradeoff between these 2 variables,

conditioning the final calibration to the selected strategy. Thus, decreasing 50% the experimental NO_x emissions implied a penalization on GIE up to -8% $\dot{m}_f H_v$ at high load when comparing to the optimum combustion under nominal limits. However, if the experimental GIE of each point was maintained, a decrease in NO_x emissions ranging from -30% at high load to -65% at low load was achieved when comparing with the experimental emissions.

- The third objective, aimed at evaluating various techniques to enhance combustion velocity, was achieved by assessing the impact of swirl and injection pattern strategies on both GIE and combustion development. Conclusions of swirl study indicated that even though it implied higher high transfer, it is a suitable technique to enhance the combustion velocity, thus increasing GIE, at intermediate SR and at some operating conditions. However, brake thermal efficiency was not improved at all due to the extra pumping work generated by the valve used to promote in-cylinder swirl motion. Additionally, increasing SR has also negative implications on NO_x emissions. On the contrary, the injection pattern change demonstrated to be a more flexible approach that permitted to improve both GIE and NO_x emissions at the same time if a proper optimization is performed.

- The last objective of the work proposed the assessment of the impact on GIE of the real combustion velocity, which is limited by the available hardware in an ICE. To assess that, the combustion of two operating conditions (2000_5 and 1500_8) was optimized both experimentally and theoretically. On the one hand, the experimental optimization was performed using conclusions of the previous objective: modifying the injection pattern while maintaining low SR conditions was the optimum strategy. This optimization led to tradeoffs with GIE between 42% and 46% and NO_x ranging from 3g/kWh to 9g/kWh at 2000_5 and GIE varying from 38% to 44% and NO_x emissions between 3g/kWh and 9g/kWh at 1500_8. On the other hand, the theoretical optimization resulted in a tradeoff with GIE ranging from 36% to almost 50% and NO_x emissions from 1g/kWh to 3.5g/kWh while at 1500_8 the best tradeoff reached GIE from 35% to 47% and NO_x from 1g/kWh to 3g/kWh at 1500_8.

  When trying to compare the best theoretical and experimental HRL under the same NO_x levels, it was observed that, even though the NO_x model provided a good prediction of the trends in both theoretical and real combustions thanks to the physics supporting the model, in some

cases the direct comparison between experimental and theoretical was not possible due to the limited extrapolation capability of the model under combustions very different than the used ones in the calibration and validation campaigns. Instead, differences on the maximum efficiency achieved by both theoretical and experimental optimizations were assessed, concluding that the optimized experimental combustions were only around -3% $\dot{m}_f H_v$ lower in terms of GIE compared to optimum Diesel combustions restricted by nominal pressure rise rate and peak pressure limits. This difference was explained due to the limited combustion velocity (5 times slower) imposed by the air-fuel mixing and combustion processes derived from the existent engine hardware. This 3% $\dot{m}_f H_v$ value states the maximum gain achievable on GIE if a more efficient engine hardware, installed in the same engine, was able to reproduce the optimum combustion development in these points.

The completion of all these partial objectives, allows assessing and optimizing the indicated cycle of an ICE, which was the main objective of the work.

6.2 Future works

This section is aimed to provide possible paths for continuing and improving the investigation carried out in this work. Following, several approaches to be followed in order to improve the work's quality are presented:

- Firstly, since the methodology presented in Section 5.4 to assess the impact of real combustion on GIE was only applied to two operating points (due to time limitations), it would be interesting to extend this analysis to operating conditions at higher load and/or higher engine speed. These additional results will show if the 3% $\dot{m}_f H_v$ gap observed at 2000_5 and 1500_8 depends on load or engine speed or, on the contrary, if it remains approximately constant along the engine map as observed so far at both operating conditions.

- In a further step, if an accurate injection model along with a reliable combustion model could be included in the thermodynamic tool, an additional step between the theoretical and experimental optimums could be considered. If so, the inputs of the optimization tool would be reduced to rail pressure and the timing and energizing times of

each injection, and the HRL would be a result of the combination of these parameters with the in-cylinder conditions. Unlike the theoretical optimums presented here, these ones could be easily reproduced in the experimental installation in order to check the accuracy of the model.

- If the previous improvement was achieved, results of the optimization will provide combustions closer to the real ones than the theoretical ones obtained in Section 4.4. Then, it would be possible to apply empirical models to contaminants such as soot, HC and CO, physics under their formation processes are not still well known, based on test conditions (intake pressure and temperature, injection settings, ...). The inclusion of these models in the optimization would provide a more complete analysis with results more comparable to calibrations carried out by OEMs, improving the methodology's quality.

- Furthermore, if a 1D model was coupled to the 0D thermodynamic model used in this work, it could be possible to consider additional operating parameters in the optimization problem such as the intake pressure and temperature, total fuel quantity or EGR rate. Results from this new approach will optimize not only the heat release law or the injection settings but the complete operating point. Thus, this optimization could be used in the first steps of the pre-calibration process of an ICE.

- In a final step, if all the previous works were fully accomplished, the methodology could also be applied to transient cycles, such as the WLTP or RDE compliant cycles, to obtain preliminary optimum calibration strategies. These starting calibration settings would reduce the number of experimental tests necessary to complete the calibration campaign aimed to meet the limits imposed by current legislation.

- A parallel work to the evolutions stated above and suitable in any step between them, would be the application of the theoretical optimization to novel concepts such as variable compression ratio, water injection (to decrease the gas temperature, reducing both heat transfer and the impact of the heat capacity ratio variation due to the temperature increment) ... The assessment of the maximum performance, in terms of efficiency and NO_x emissions, under such strategies would provide an estimation of the interest of further investigation on these topics.

Bibliography

Abd-Alla G.H. and Abdalla G.
Using exhaust gas recirculation in internal combustion engines: a review.
Energy Conversion and Management, Vol. 43 n^o 8, pp. 1027–1042, 2002. (cited on p. 22)

Abedin M.J., Masjuki H.H., Kalam M.A., Sanjid A. and Ashraful A.M.
Combustion, performance, and emission characteristics of low heat rejection engine operating on various biodiesels and vegetable oils.
Energy Conversion and Management, Vol. 85, pp. 173–189, Septiembre 2014.
(cited on p. 26)

Achuth M. and Mehta P.S.
Predictions of tumble and turbulence in four-valve pentroof spark ignition engines.
International Journal of Engine Research, Vol. 2 n^o 3, pp. 209–227, Enero 2001.
(cited on p. 23)

Agarwal A.K., Srivastava D.K., Dhar A., Maurya R.K., Shukla P.C. and Singh A.P.
Effect of fuel injection timing and pressure on combustion, emissions and performance characteristics of a single cylinder diesel engine.
Fuel, Vol. 111, pp. 374–383, Septiembre 2013. (cited on p. 20)

Aghdam E.A. and Kabir M.M.
Validation of a blowby model using experimental results in motoring condition with the change of compression ratio and engine speed.
Experimental Thermal and Fluid Science, Vol. 34 n^o 2, pp. 197–209, Febrero 2010.
(cited on p. 56)

Al-Sarkhi A., Jaber J. and Probert S.
Efficiency of a Miller engine.
Applied Energy, Vol. 83, pp. 343–351, 2006. (cited on p. 23)

Alkidas A.C.
Combustion advancements in gasoline engines.
Energy Conversion and Management, Vol. 48 n^o 11, pp. 2751–2761, Noviembre 2007.
(cited on p. 25)

Allen D.J. and Lasecki M.P.
Thermal Management Evolution and Controlled Coolant Flow.
SAE Techinical Paper 2001-01-1732, 2001. (cited on pp. 27, 29)

Andrews G., Ounzain A., Li H., Bell M., Tate J. and Ropkins K.
The Use of a Water/Lube Oil Heat Exchanger and Enhanced Cooling Water Heating to Increase Water and Lube Oil Heating Rates in Passenger Cars for Reduced Fuel Consumption and CO2 Emissions During Cold Start.
SAE Techinical Paper 2007-01-2067, 2007. (cited on p. 28)

Aoyama T., Hattori Y., Mizuta J. and Sato Y.
An Experimental Study on Premixed-Charge Compression Ignition Gasoline Engine.
SAE Techinical Paper 960081, 1996. (cited on p. 25)

Armas O.
Diagnóstico experimental del proceso de combustión en motores Diesel de inyección directa.
Servicio de Publicaciones UPV, ISBN 84-7721-772-X, Valencia, 1999.
(cited on pp. 9, 44, 52)

Arrègle J., López J.J., Guardiola C. and Monin C.
Sensitivity study of a NOx estimation model for on-board applications.
SAE Technical Paper 2008-01-0640, 2008. (cited on pp. 60, 175, 178)

Badami M., Mallamo F., Millo F. and Rossi E.E.
Influence of Multiple Injection Strategies on Emissions , Combustion Noise and BSFC of a DI Common Rail Diesel Engine.
SAE Technical Paper 2002-01-0503, 2002. (cited on p. 20)

Bao R., Avila V. and Baxter J.
Effect of 48 V Mild Hybrid System Layout on Powertrain System Efficiency and Its Potential of Fuel Economy Improvement.
WCX 17: SAE World Congress Experience, mar 2017. (cited on p. 3)

Beck N.J. and Uyehara O.A.
Factors That Affect BSFC and Emissions for Diesel Engines : Part II Experimental Confirmation of Concepts Presented in Part I.
SAE Techinical Paper 870344, 1987. (cited on p. 25)

Bedoya I.D., Saxena S., Cadavid F.J., Dibble R.W. and Wissink M.
Experimental evaluation of strategies to increase the operating range of a biogas-fueled HCCI engine for power generation.
Applied Energy, Vol. 97, pp. 618–629, Septiembre 2012. (cited on p. 25)

Belarte E.
Estudio del proceso de combustión premezclada controlada por la reactividad del combustible en un motor de encendido por compresión.
Doctoral Thesis, Universitat Politècnica de València, 2015. (cited on p. 26)

Benajes J., Martín J., García A., Villalta D. and Warey A.
In-cylinder soot radiation heat transfer in direct-injection diesel engines.
Energy Conversion and Management, Vol. 106, pp. 414–427, 2015. (cited on p. 54)

Benajes J., Martín J., García A., Villalta D. and Warey A.
Swirl ratio and post injection strategies to improve late cycle diffusion combustion in a light-duty diesel engine.
Applied Thermal Engineering, Vol. 123, pp. 365–376, 2017. (cited on pp. v, 50, 124)

Benajes J., Martín J., Novella R. and Thein K.
Understanding the performance of the multiple injection gasoline partially premixed combustion concept implemented in a 2-Stroke high speed direct injection compression ignition engine.
Applied Energy, Vol. 161, pp. 465–475, jan 2016. (cited on pp. 22, 23, 25)

Benajes J., Molina S., García A. and Monsalve-Serrano J.
Effects of direct injection timing and blending ratio on RCCI combustion with different low reactivity fuels.
Energy Conversion and Management, Vol. 99, pp. 193–209, jul 2015. (cited on p. 26)

Benajes J., Molina S., García A. and Monsalve-Serrano J.
Effects of low reactivity fuel characteristics and blending ratio on low load RCCI (reactivity controlled compression ignition) performance and emissions in a heavy-duty diesel engine.
Energy, Vol. 90, pp. 1261–1271, oct 2015. (cited on p. 26)

Benajes J., Molina S., Novella R. and De Lima D.
Implementation of the Partially Premixed Combustion concept in a 2-stroke HSDI diesel engine fueled with gasoline.
Applied Energy, Vol. 122, pp. 94–111, jun 2014. (cited on p. 25)

Benajes J., Novella R., De Lima D., Tribotté P., Quechon N., Obernesser P. and Dugue V.
Analysis of the combustion process, pollutant emissions and efficiency of an innovative 2-stroke HSDI engine designed for automotive applications.
Applied Thermal Engineering, Vol. 58 n^o 1-2, pp. 181–193, Septiembre 2013.
(cited on p. 22)

Benajes J., Olmeda P., Martín J., Blanco-Cavero D. and Warey A.
Evaluation of swirl effect on the Global Energy Balance of a HSDI Diesel engine.
Energy, Vol. 122, pp. 168–181, 2017. (cited on pp. 9, 23, 32, 125)

Benajes J., Olmeda P., Martín J. and Carreño R.
A new methodology for uncertainties characterization in combustion diagnosis and thermodynamic modelling.
Applied Thermal Engineering, Vol. 71, pp. 389–399, 2014. (cited on p. 52)

Benajes J., Pastor J.V., García A. and Monsalve-Serrano J.
An experimental investigation on the influence of piston bowl geometry on RCCI performance and emissions in a heavy-duty engine.
Energy Conversion and Management, Vol. 103, pp. 1019–1030, oct 2015. (cited on p. 26)

Benajes J., Pastor J.V., García A. and Monsalve-Serrano J.
The potential of RCCI concept to meet EURO VI NOx limitation and ultra-low soot emissions in a heavy-duty engine over the whole engine map.
Fuel, Vol. 159, pp. 952–961, nov 2015. (cited on p. 26)

Bendu H. and Murugan S.
Homogeneous charge compression ignition (HCCI) combustion: Mixture preparation and control strategies in diesel engines.
Renewable and Sustainable Energy Reviews, Vol. 38, pp. 732–746, Octubre 2014.
(cited on p. 25)

Bermúdez V., Lujan J.M., Pla B. and Linares W.G.
Effects of low pressure exhaust gas recirculation on regulated and unregulated gaseous emissions during NEDC in a light-duty diesel engine.
Energy, Vol. 36 n^o 9, pp. 5655–5665, 2011. (cited on p. 46)

Boulahlib M.S., Boukebbab S., Gaci F. and Kholai O.
Experimental Study of Energy Balance for Air-Cooled DI Diesel Engines Operating in Hot Climates.
SAE Techinical Paper 2009-01-1974, 2009. (cited on pp. 30, 32)

Bourhis G., Chauvin J., Gautrot X. and de Francqueville L.
LP EGR and IGR Compromise on a GDI Engine at Middle Load.
SAE Int. J. Engines, Vol. 6 n^o 1, pp. 67–77, 2013. (cited on p. 22)

Bowman C.T.
Kinetics of pollutant formation and destruction in combustion.
Progress in Energy and Combustion Science, Vol. 1 n^o 1, pp. 33 – 45, 1975.
(cited on p. 60)

Bression G., Soleri D., Savy S., Dehoux S., Azoulay D., Hamouda H., Doradoux L., Guerrassi N. and Lawrence N.
A Study of Methods to Lower HC and CO Emissions in Diesel HCCI.
SAE Int. J. Fuels Lubr., Vol. 1 n^o 1, pp. 37–49, 2009. (cited on pp. 22, 23)

Broatch A., Martín J., García A., Blanco-Cavero D., Warey A. and Domenech V.
Application of a zero-dimensional model to assess the effect of swirl on indicated efficiency.
International Journal of Engine Research, pp. 1–12, 2018. (cited on pp. 82, 129)

Broatch A., Olmeda P., García A. and Salvador-Iborra J.
Impact of swirl on in-cylinder heat transfer in a light-duty diesel engine.
Energy, Vol. 119, pp. 1010–1023, 2017. (cited on p. 46)

Bryzik W. and Kamo R.
TACOM/Cummins Adiabatic Engine Program.
SAE Transactions, Vol. 92, pp. 1063–1087, 1983. (cited on p. 27)

Canakci M.
Combustion characteristics of a DI-HCCI gasoline engine running at different boost pressures.
Fuel, Vol. 96, pp. 546–555, Junio 2012. (cited on p. 21)

Carreño R.
A comprehensive methodology to analyse the Global Energy Balance in Reciprocating Internal Combustion Engines.
Doctoral Thesis, 2016. (cited on pp. v, 10, 28, 31, 44, 52, 53, 54, 55, 56, 57, 127, 128, 140)

Castilla C., Elias G., Rückert V., Braga A. and Molina R.
A review of prechamber ignition systems as lean combustion technology for SI engines.
Applied Thermal Engineering, Vol. 128, pp. 107–120, 2018. (cited on p. 20)

Caton J.A.
Operating Characteristics of a Spark-Ignition Engine Using the Second Law of Thermodynamics : Effects of Speed and Load.
SAE Techinical Paper 2000-01-0952, 2000. (cited on pp. 30, 31, 32)

Cavazzuti M.
Optimization Methods: From Theory to Design.
Springer, Berlin, Heidelberg, 2013. (cited on p. 151)

Çengel Y.A. and Boles M.A.
Thermodynamics: An Engineering Approach.
Cengel series in engineering thermal-fluid sciences. McGraw-Hill, 2011. (cited on p. 72)

Chan S.H.
Performance and emissions characteristics of a partially insulated gasoline engine.
International Journal of Thermal Sciences, Vol. 40 n^o 3, pp. 255–261, Marzo 2001.
(cited on p. 26)

Chapman I.
The end of Peak Oil? Why this topic is still relevant despite recent denials.
Energy Policy, Vol. 64, pp. 93–101, 2014. (cited on p. 2)

Chastain J.H. and Wagner J.R.
Advanced Thermal Management for Internal Combustion Engines - Valve Design , Component Testing and Block Redesign.
SAE Techinical Paper 2006-01-1232, Vol. 1 n^o 1, pp. –, 2006. (cited on p. 27)

Chen L., Sun F. and Wu C.
Influence of heat transfer law on the performance of a Carnot engine.
Applied Thermal Engineering, Vol. 17 n^o 3, 1997. (cited on p. 74)

Ciniviz M., Hasimoglu C., Sahin F. and Salman M.S.
Impact of thermal barrier coating application on the performance and emissions of a turbocharged diesel engine.
Proceedings of the Institution of Mechanical Engineers, Part D: Journal of Automobile Engineering, Vol. 222 n^o 12, pp. 2447–2455, 2008. (cited on p. 27)

Costa M., Sementa P., Sorge U., Catapano F., Marseglia G. and Vaglieco B.
Split Injection in a GDI Engine Under Knock Conditions: An Experimental and Numerical Investigation.
SAE Technical Paper, 2015. (cited on p. 20)

Curzon F. L. and Ahlborn B.
Efficiency of a Carnot engine at maximum power output.
American Journal of Physics, Vol. 43 n^o 1, pp. 22–24, 1975. (cited on p. 74)

Davies R., Foulger G., Bindley A. and Styles P.
Induced seismicity and hydraulic fracturing for the recovery of hydrocarbons.
Marine and Petroleum Geology, Vol. 45, pp. 171–185, aug 2013. (cited on p. 3)

De Bellis V.
Performance optimization of a spark-ignition turbocharged VVA engine under knock limited operation.
Applied Energy, Vol. 164, pp. 162–174, feb 2016. (cited on p. 21)

Deb K., Agrawal S., Pratap A. and Meyarivan T.
A Fast Elitist Non-Dominated Sorting Genetic Algorithm for Multi-Objective Optimization : NSGA-II.
Lecture Notes in Computer Science, Vol. 1917, 2000. (cited on p. 65)

Dec J.E. and Yang Y.
Boosted HCCI for High Power without Engine Knock and with Ultra-Low NOx Emissions - using Conventional Gasoline.
SAE Int. J. Engines, Vol. 3 n^o 1, pp. 750–767, 2010. (cited on p. 25)

Degraeuwe B.
Contribution to the thermal management of DI Diesel engines.
Doctoral Thesis, Universidad Politécnica de Valencia, 2007. (cited on p. 9)

Degraeuwe B. and Weiss M.
Does the New European Driving Cycle (NEDC) really fail to capture the NOX emissions of diesel cars in Europe?
Environmental Pollution, Vol. 222 n^o X, pp. 234–241, 2017. (cited on p. 5)

Dempsey A.B., Walker N.R. and Reitz R.D.
Effect of Piston Bowl Geometry on Dual Fuel Reactivity Controlled Compression Ignition (RCCI) in a Light-Duty Engine Operated with Gasoline/Diesel and Methanol/Diesel.
SAE Int. J. Engines, Vol. 6 n^o 1, pp. 78–100, 2013. (cited on p. 26)

Desantes J.M., Benajes J., Molina S. and González C.A.
The modification of the fuel injection rate in heavy-duty diesel engines. Part 1: Effects on engine performance and emissions.
Applied Thermal Engineering, Vol. 24 n^o 17-18, pp. 2701–2714, Diciembre 2004.
(cited on p. 20)

Desantes J.M., Benajes J., Molina S. and González C.A.
The modification of the fuel injection rate in heavy-duty diesel engines. Part 2: Effects on combustion.
Applied Thermal Engineering, Vol. 24 n^o 17-18, pp. 2715–2726, Diciembre 2004.
(cited on p. 20)

Desantes J.M., López J.J., Redón P. and Arrégle J.
Evaluation of the thermal NO formation mechanism under low temperature diesel combustion conditions.
International Journal of Engine Research, Vol. 13 n^o 6, pp. 531–539, 2012.
(cited on p. 61)

Ding C., Roberts L., Fain D., Ramesh A., Shaver G., McCarthy Jr J., Ruth M., Koeberlein E., Holloway E. and Nielsen D.
Fuel efficient exhaust thermal management for compression ignition engines during idle via cylinder deactivation and flexible valve actuation.
International Journal of Engine Research, Vol. 17 n^o 6, pp. 619–630, 2016.
(cited on p. 21)

Dings J.
Mind the gap! Why official car fuel enconomy figures don't match up reality.
Transport and Environment, pp. 1–47, 2013. (cited on p. 5)

Dogde L.G., Simescu S., Neely G.D., Maymar M.J., Dickey D.W. and Savonen C.L.
Effect of Small Holes and High Injection Pressures on Diesel Engine Combustion.
SAE Technical Paper 2002-01-0494, 2002. (cited on p. 19)

Durgun O. and Şahin Z.
Theoretical investigation of heat balance in direct injection (DI) diesel engines for neat diesel fuel and gasoline fumigation.
Energy Conversion and Management, Vol. 50 n^o 1, pp. 43–51, Enero 2009.
(cited on pp. 30, 32)

Ebrahimi R.
Performance of an irreversible Diesel cycle under variable stroke length and compression ratio.
Journal of American Science, Vol. 6 n^o 1, pp. 58–64, 2010. (cited on p. 79)

Edwards K.D., Wagner R. and Briggs T.
Investigating Potential Light-duty Efficiency Improvements through Simulation of Turbo-compounding and Waste-heat Recovery Systems.
SAE Techinical Paper 2010-01-2209, 2010. (cited on p. 30)

Edwards K.D., Wagner R. and Graves R.L.
Identification of Potential Efficiency Opportunities in Internal Combustion Engines Using a Detailed Thermodynamic Analysis of Engine Simulation Results.
SAE Technical Paper 2008-01-0293, 2008. (cited on p. 30)

Elgowainy A., Burnham A., Wang M., Molburg J. and Rousseau A.
Well-To-Wheels Energy Use and Greenhouse Gas Emissions of Plug-in Hybrid Electric Vehicles.
SAE International Journal of Fuels and Lubricants, Vol. 2 n^o 1, pp. 627–644, apr 2009.
(cited on p. 4)

Eriksson L. and Sivertsson M.
Computing Optimal Heat Release Rates in Combustion Engines.
SAE International Journal of Engines, Vol. 8 n^o 3, pp. 2015–01–0882, 2015.
(cited on pp. 8, 33)

Eriksson L. and Sivertsson M.
Calculation of Optimal Heat Release Rates under Constrained Conditions.
SAE Int. J. Engines, 2016. (cited on pp. 8, 33)

European Parliament.
Commission regulation (EU) No 64/2012 of 23 January 2012 amending Regulation (EU) No 582/2011 implementing and amending Regulation (EC) No 595/2009 of the European Parliament and of the Council with respect to emissions from heavy duty vehicles (Euro.
Official Journal of the European Union, pp. 1–23, 2012. (cited on p. 5)

European Parliament.
Commision regulation (EU) No 333/2014 OF the European Parliament and of the Council of 11 March 2014 amending Regulation (EC) No 443/2009 to define the modalities for reaching the 2020 target to reduce CO2 emissions from new passenger cars.
Official Journal of the European Union, Vol. 103 n^o 333, pp. 15–21, 2014.
(cited on pp. 5, 18)

Fenimore C.P.
Formation of nitric oxide in premixed hydrocarbon flames.
Symposium (International) on Combustion, Vol. 13 n^o 1, pp. 373 – 380, 1971.
Thirteenth symposium (International) on Combustion. (cited on p. 60)

Flierl R., Lauer F., Breuer M. and Hannibal W.
Cylinder Deactivation with Mechanically Fully Variable Valve Train.
SAE Int. J. Engines, Vol. 5 n^o 2, pp. 207–215, 2012. (cited on p. 21)

Fontaras G., Pistikopoulos P. and Samaras Z.
Experimental evaluation of hybrid vehicle fuel economy and pollutant emissions over real-world simulation driving cycles.
Atmospheric Environment, Vol. 42 n^o 18, pp. 4023–4035, 2008. (cited on p. 4)

Fu J., Liu J., Feng R., Yang Y., Wang L. and Wang Y.
Energy and exergy analysis on gasoline engine based on mapping characteristics experiment.
Applied Energy, Vol. 102, pp. 622–630, Febrero 2013. (cited on pp. 30, 74)

Galloni E., Fontana G. and Staccone S.
Numerical and experimental characterization of knock occurrence in a turbo-charged spark-ignition engine.
Energy Conversion and Management, Vol. 85, pp. 417–424, sep 2014. (cited on p. 21)

Germane G., Wood C. and Hess C.
Lean Combustion in Spark-Ignited Internal Combustion Engines - A Review.
SAE Technical paper 831694, 1983. (cited on p. 20)

Giakoumis E. and Zachiotis A.
Investigation of a Diesel-Engined Vehicle's Performance and Emissions during the WLTC Driving Cycle - Comparison with the NEDC.
Energies, 2017. (cited on p. 5)

Glaude P., Fournet R., Bounaceur R. and Molière M.
Adiabatic flame temperature from biofuels and fossil fuels and derived effect on NOx emissions.
Fuel Processing Technology, Vol. 91 n^o 2, pp. 229–235, 2010. (cited on p. 74)

Goodman P., Galatioto F., Thorpe N., Namdeo A., Davies R. and Bird R.
Investigating the traffic-related environmental impacts of hydraulic-fracturing (fracking) operations.
Environment international, Vol. 89, pp. 248–260, feb 2016. (cited on p. 3)

Guardiola C., Climent H., Pla B. and Reig A.
Optimal Control as a method for Diesel engine efficiency assessment including pressure and NOx constraints.
Applied Thermal Engineering, Vol. 117, pp. 452–461, 2017. (cited on pp. 8, 33, 80)

Guardiola C., López J.J., Martín J. and García-Sarmiento D.
Semiempirical in-cylinder pressure based model for NOX prediction oriented to control applications.
Applied Thermal Engineering, Vol. 31 n^o 16, pp. 3275–3286, 2011.
(cited on pp. 60, 63, 70)

Guardiola C., Martín J., Pla B. and Bares P.
Cycle by cycle NOx model for diesel engine control.
Applied Thermal Engineering, Vol. 110, pp. 1011–1020, 2017. (cited on pp. 60, 61, 63)

Guardiola C., Pla B., García A. and Boronat V.
Optimal heat release shaping in a reactivity controlled compression ignition (RCCI) engine.
Control Theory and Tenchnology, Vol. 15 n^o 2, pp. 117–128, 2017. (cited on p. 33)

Hazar H.
Effects of biodiesel on a low heat loss diesel engine.
Renewable Energy, Vol. 34 n^o 6, pp. 1533–1537, Junio 2009. (cited on p. 26)

He M., Zhang X., Zeng K. and Gao K.
A combined thermodynamic cycle used for waste heat recovery of internal combustion engine.
Energy, Vol. 36 n^o 12, pp. 6821–6829, Diciembre 2011. (cited on p. 30)

Health Effects Institute.
Diesel Exhaust: A Critical Analysis of Emissions, Exposure, and Health Effects.
A Special Report of the Institute's Diesel Working Group, 1995. (cited on p. 2)

Helmers E., Leitão J., Tietge U. and Butler T.
CO_2 -equivalent emissions from European passenger vehicles in the years 1995 - 2015 based on real-world use : Assessing the climate benefit of the European "diesel boom ", url = https://doi.org/10.1016/j.atmosenv.2018.10.039, volume = 198, year = 2019.
Atmospheric Environment, n^o October 2018, pp. 122–132. (cited on pp. 5, 6)

Heuser B., Kremer F., Pischinger S., Rohs H., Holderbaum B. and Körfer T.
An experimental investigation of dual-fuel combustion in a light duty Diesel engine by in-cylinder blending of ethanol and Diesel.
SAE Int. J. Engines, Vol. 9 n^o 1, pp. 11–25, 2015. (cited on p. 26)

Heywood J.B.
Internal Combustion Engines Fundamentals.
McGraw-Hill, ISBN 978-0-07-028637-5, New York, 1988.
(cited on pp. 2, 21, 23, 24, 30, 60, 124)

Hiwase S.D., Moorthy S., Prasad H., Dumpa M. and Metkar R.M.
Multidimensional Modeling of Direct Injection Diesel Engine with Split Multiple Stage Fuel Injections.
Procedia Engineering, Vol. 51, pp. 670–675, Enero 2013. (cited on p. 20)

Hoffmann K., Watowich S. and Berry R.
Optimal paths for thermodynamic systems: The ideal diesel cycle.
Journal of Applied Physics, Vol. 58 n^o 6, pp. 2125–2134, sep 1985. (cited on p. 79)

Hohenberg G.
Definition und Eigenschaften des thermodynamischen Verlustwinkels von Kolbenmaschinen.
Automobil-Industrie, Vol. 4, pp. 15–21, 1976. (cited on p. 57)

Holland J.H.
Adaptation in natural and artificial systems.
University of Michigan Press, Ann Arbor, MI, 1975. (cited on p. 63)

Honardar S., Busch H., Schnorbus T., Severin C., Kolbeck A. and Korfer T.
Exhaust Temperature Management for Diesel Engines Assessment of Engine Concepts and Calibration Strategies with Regard to Fuel Penalty.
SAE Technical Paper, 2011. (cited on p. 29)

Huang R.F., Huang C.W., Chang S.B., Yang H.S., Lin T.W. and Hsu W.Y.
Topological flow evolutions in cylinder of a motored engine during intake and compression strokes.
Journal of Fluids and Structures, Vol. 20 n^o 1, pp. 105–127, Enero 2005. (cited on p. 23)

IEA.
World Energy Outlook 2008.
International Energy Agency, Paris, France, 2014. (cited on pp. v, 3)

Ishibashi Y. and Asai M.
Improving the Exhaust Emissions of Two-Stroke Engines by Applying the Activated Radical Combustion.
SAE Techinical Paper 960742, 1996. (cited on p. 25)

Jaichandar S. and Tamilporai P.
Low Heat Rejection Engines - An Overview.
SAE Technical Paper 2003-01-0405, 2003. (cited on p. 26)

Jamrozik A. and Tutak W.
A study of performance and emissions of SI engine with a two-stage combustion system.
Chemical and Process Engineering - Inzynieria Chemiczna i Procesowa, Vol. 32 n^o 4, pp. 453–471, 2011. (cited on p. 20)

Kalghatgi G.
The outlook for fuels for internal combustion engines.
International Journal of Engine Research, Vol. 15 n^o 4, pp. 383–398, 2014. (cited on p. 1)

Kang H., Ahn H. and Min K.
Smart cooling system of the double loop coolant structure with engine thermal management modeling.
Applied Thermal Engineering, Vol. 79, pp. 124–131, 2015. (cited on p. 29)

Karabektas M.
The effects of turbocharger on the performance and exhaust emissions of a diesel engine fuelled with biodiesel.
Renewable Energy, Vol. 34 n^o 4, pp. 989–993, apr 2009. (cited on p. 21)

Kawaguchi A., Iguma H., Yamashita H., Takada N., Nishikawa N., Yamashita C., Wakisaka Y. and Fukui K.
2016-01-2333 Thermo-Swing Wall Insulation Technology; - A Novel Heat Loss Reduction Approach on Engine Combustion Chamber.
SAE Technical Paper, n^o 2016-01-2333, 2016. (cited on p. 112)

Kawashima J.
Research on a variable swirl intake port for high-speed 4-valve DI diesel engine.
JSAE Review, Vol. 20 n^o 3, pp. 421–424, Julio 1999. (cited on p. 124)

Kimura S., Aoki O., Kitahara Y. and Aiyoshizawa E.
Ultra-Clean Combustion Technology Combining a Low-Temperature and Premixed Combustion Concept for Meeting Future Emission Standards.
SAE Technical Paper 2001-01-0200, 2001. (cited on p. 25)

Kokjohn S.L., Hanson R.M., Splitter D.A. and Reitz R.D.
Fuel reactivity controlled compression ignition (RCCI): a pathway to controlled high-efficiency clean combustion.
International Journal of Engine Research, Vol. 12 n^o 3, pp. 209–226, 2011. (cited on p. 26)

Kokjohn S.L. and Reitz R.D.
Reactivity Controlled Compression Ignition and Conventional Diesel Combustion: A Comparison of Methods to Meet Light-Duty NOx and Fuel Economy Targets.
International Journal of Engine Research, Vol. 0 n^o 0, pp. 1–17, 2013. (cited on p. 26)

Lalanne C.
R Companion to Montgomery's Design and Analysis of Experiments.
John Wiley & and Sons Inc., 2009. (cited on p. 153)

Lapuerta M., Ballesteros R. and Agudelo J.
Effect of the gas state equation on the thermodynamic diagnostic of diesel combustion.
Applied Thermal Engineering, Vol. 26 n^o 14-15, pp. 1492–1499, Octubre 2006.
(cited on p. 53)

Lee Y. and Huh K.Y.
Analysis of different modes of low temperature combustion by ultra-high EGR and modulated kinetics in a heavy duty diesel engine.
Applied Thermal Engineering, Vol. 70 n^o 1, pp. 776–787, 2014. (cited on p. 122)

Li X., Zhou H., Zhao L., Su L., Xu H. and Liu F.
Effect of split injections coupled with swirl on combustion performance in DI diesel engines.
Energy Conversion and Management, Vol. 129, pp. 180–188, 2016. (cited on p. 20)

Lif A. and Holmberg K.
Water-in-diesel emulsions and related systems.
Advances in Colloid and Interface Science, Vol. 123-126 n^o SPEC. ISS., pp. 231–239, 2006.
(cited on p. 26)

Lin Z.
Optimizing and Diversifying the Electric Range of Plug-in Hybrid Electric Vehicles for U.S. Drivers.
SAE International Journal of Alternative Powertrains, Vol. 1 n^o 1, pp. 180–194, apr 2012.
(cited on p. 4)

Macián V., Serrano J.R., Dolz V. and Sánchez J.P.
Methodology to design a bottoming Rankine cycle, as a waste energy recovering system in vehicles. Study in a HDD engine.
Applied Energy, Vol. 104, pp. 758–771, apr 2013. (cited on p. 26)

Maharudrppa-Mallikarjuna J.
Effect of Manifold Orientation on Non-Reacting In-Cylinder Tumble Flows in an IC Engine with Pentroof Piston - An Investigation Using PIV.
SAE Technical Paper 2010-01-0956, 2010. (cited on p. 23)

Malkhede D.N. and Khalane H.
Maximizing Volumetric Efficiency of IC Engine through Intake Manifold Tuning.
SAE Techinical Paper 2015-01-1738, 2015. (cited on p. 21)

Marotta A., Pavlovic J., Ciuffo B., Serra S. and Fontaras G.
Gaseous Emissions from Light-Duty Vehicles: Moving from NEDC to the New WLTP Test Procedure.
Environmental Science and Technology, Vol. 49 n^o 14, pp. 8315–8322, 2015.
(cited on p. 5)

Martín J.
Diagnóstico de la combustión en motores de Diesel de inyección directa.
Reverté, ISBN 978-84-291-4717-9, Barcelona, 2012. (cited on pp. 9, 44, 52, 54, 55, 56)

Masera K. and Hossain A. K.
Biofuels and thermal barrier: A review on compression ignition engine performance, combustion and exhaust gas emission.
Journal of the Energy Institute, In Press, 2018. (cited on p. 122)

Mccracken M E and Abraham J.
Swirl-Spray Interactions in a Diesel Engine.
SAE Technical Paper 2001-01-0996, Vol. 2001 n^o 724, 2001. (cited on p. 136)

Milton G., Blore P., Tufail K., Coates B., Newbigging I., Cooper A. and Shayler P.
CO2 reduction through low cost electrification of the diesel powertrain at 48V.
SAE Technical Paper Series, 2017. (cited on p. 3)

Mingrui W., Thanh-Sa N., Turkson R., Jinping L. and Guanlun G.
Water injection for higher engine performance and lower emissions.
Journal of the Energy Institute, Vol. 90 n^o 2, pp. 285–299, 2017. (cited on p. 26)

Mitchell M.
An introduction to genetic algorithms.
MIT Press, Cambridge, Massachusetts. (cited on p. 63)

Mock P., German J., Bandivadekar A., Riemersma I., Ligterink N. and Lambrecht U.
From laboratory to road. A comparison of official and real-world fuel consumption and CO2 values for cars in Europe and the United States.
International Council on Clean Transportation, n^o May, pp. 77, 2013. (cited on p. 5)

Mock P., Kühlwein J., Tietge U., Franco V., Bandivadekar A. and German J.
The WLTP: How a new test procedure for cars will affect fuel consumption values in the EU.
ICCT White Paper, Vol. 1 n^o 9, pp. 1–20, 2014. (cited on p. 5)

Mohamed-Musthafa M., Sivapirakasam S.P. and Udayakumar M.
Comparative studies on fly ash coated low heat rejection diesel engine on performance and emission characteristics fueled by rice bran and pongamia methyl ester and their blend with diesel.
Energy, Vol. 36 n^o 5, pp. 2343–2351, 2011. (cited on p. 26)

Mohan B., Yang W. and Chou S.K.
Fuel injection strategies for performance improvement and emissions reduction in compression ignition engines - A Review.
Renewable and Sustainable Energy Reviews, Vol. 28, pp. 664–676, 2013.
(cited on pp. 19, 20, 25)

Montgomery D.C.
Design and Analysis of Experiments.
John Wiley & and Sons Inc., 2012. (cited on p. 153)

Moran M.J., Shapiro H.N., Boettner D.D. and Bailey M.B.
Fundamentals of Engineering Thermodynamics, 8th Edition:.
Wiley, 2014. (cited on pp. 72, 73)

Morena J., Vassallo A., Peterson R. C., Gopalakrishan V. and Gao J.
Influence of Swirl Ratio On Combustion System Performance of a 0.4L Single-Cylinder Diesel Engine.
THIESEL 2014 Conference on Thermo-and Fluid Dynamics Processes in Direct Injection Engines, 2014. (cited on p. 136)

Murata Y., Kusaka J., Daisho Y., Kawano D., Suzuki H., Ishii H. and Goto Y.
Miller-PCCI Combustion in an HSDI Diesel Engine with VVT.
SAE International Journal of Engines, Vol. 1 n^o 1, pp. 444–456, 2009. (cited on p. 23)

Murray L., Staley D., Sorch K., Yager C. and Bruno M.
Control and diagnostic systems for a variable capacity engine oil pum and an engine oil pressure sensor.
US Patent, Vol. 2 n^o 12, pp. 1–9, 2014. (cited on p. 29)

Neely G.D., Sasaki S. and Leet J.A.
Experimental Investigation of PCCI-DI Combustion on Emissions in a Light-Duty Diesel Engine.
SAE Techinical Paper 2004-01-0121, 2004. (cited on p. 25)

Nikiforuk A.
Tar sands: Dirty oil and the future of a continent.
Greystone Books Ltd, Barcelona, 2010. (cited on p. 3)

Nitz L.
General Motors' Innovative Hybrid and T̈wo-Mode HybridS̈ystems.
2006 FISITA World Automotive Congress, oct 2006. (cited on p. 4)

Oberdörster G. and Utell M.J.
Ultrafine particles in the urban air: to the respiratory tract–and beyond?
Environmental health perspectives, Vol. 110 n^o 8, pp. A440–A441, 2002. (cited on p. 2)

Oh H. and Bae C.
Effects of the injection timing on spray and combustion characteristics in a spray-guided DISI engine under lean-stratified operation.
Fuel, Vol. 107, pp. 225 – 235, 2013. (cited on p. 20)

Okamoto T. and Uchida N.
New Concept for Overcoming the Trade-Off between Thermal Efficiency, Each Loss and Exhaust Emissions in a Heavy Duty Diesel Engine.
SAE International Journal of Engines, Vol. 9 n^o 2, pp. 2016–01–0729, 2016.
(cited on pp. 33, 80, 174)

Olmeda P, Martín J, Blanco-Cavero D, Warey A and Domenech V.
Effect of in-cylinder swirl on engine efficiency and heat rejection in a light-duty diesel engine.
International Journal of Engine Research, Vol. 18 n^o 1-2, pp. 81–92, 2017.
(cited on p. 122)

Olmeda P., Martin J., Garcia A. and Blanco D.
Evaluation of EGR Effect on the Global Energy Balance of a High Speed DI Diesel Engine.
SAE Papers, Vol. 2016-01-06, 2016. (cited on p. 32)

Osawa K.
Performance of Thin Thermal Barrier Coating on Small Aluminum Block Diesel Engine.
SAE Technical Paper 910461, 1991. (cited on p. 27)

Özcan H. and Söylemez M.S.
Thermal balance of a LPG fuelled, four stroke SI engine with water addition.
Energy Conversion and Management, Vol. 47 n^o 5, pp. 570–581, Marzo 2006.
(cited on p. 26)

Palma A., Del Core D. and Esposito C.
The HCCI Concept and Control , Performed with MultiAir Technology on Gasoline Engines.
SAE Technical Paper 2011-24-0026, 2011. (cited on p. 25)

Pang H.H. and Brace C.J.
Review of engine cooling technologies for modern engines.
Proc. Inst. Mech. Engrs., Vol. 218 n^o 11, pp. 1209–1215, 2004. (cited on p. 29)

Park Y. and Bae C.
Experimental study on the effects of high/low pressure EGR proportion in a passenger car diesel engine.
Applied Energy, Vol. 133, pp. 308–316, Noviembre 2014. (cited on p. 22)

Parlak A.
The effect of heat transfer on performance of the Diesel cycle and exergy of the exhaust gas stream in a LHR Diesel engine at the optimum injection timing.
Energy Conversion and Management, Vol. 46 n^o 2, pp. 167–179, Enero 2005.
(cited on pp. 26, 79)

Parvate-Patil G.B., Hong H. and Gordon B.
An assessment of intake and exhaust philosophies for variable valve timing.
SAE Technical Paper 2003-32-0078, 2003. (cited on p. 21)

Patterson M., Kong S., Hampson G. and Reitz R.
Modeling the Effects of Fuel Injection Characteristics on Diesel Engine Soot and NOx Emissions.
SAE Transactions, Vol. 103, pp. 836–852, 1994. (cited on p. 70)

Payri F. and Desantes J.M.
Motores de combustión interna alternativos.
Reverté, ISBN 978-84-291-4802-2, Barcelona, 2011. (cited on pp. 21, 22, 28, 76)

Payri F., Galindo J., Martín J. and Arnau F.J.
A Simple Model for Predicting the Trapped Mass in a DI Diesel Engine.
SAE Techinical Paper 2007-01-0494, 2007. (cited on p. 54)

Payri F., Margot X., Gil A. and Martín J.
Computational Study of Heat Transfer to the Walls of a DI Diesel Engine.
SAE Technical paper 2005-01-0210, Abril 2005. (cited on pp. 55, 125)

Payri F., Martín J., Garcia A. and Carreño R.
Experimental and Theoretical Analysis of the Energy Balance in a DI Diesel Engine.
SAE Technical Paper 2015-01-1651, 2015. (cited on p. 32)

Payri F., Olmeda P., Martín J. and Carreño R.
A New Tool to Perform Global Energy Balances in DI Diesel Engines.
SAE Int. J. Engines, Vol. 7 n^o 1, pp. 43–59, 2014. (cited on pp. 9, 23, 30, 31, 52, 55, 138)

Payri F., Olmeda P., Martín J. and Carreño R.
Experimental analysis of the global energy balance in a DI diesel engine.
Applied Thermal Engineering, Vol. 89, pp. 545–557, Octubre 2015. (cited on p. 20)

Payri F., Olmeda P., Martín J. and García A.
A complete 0D thermodynamic predictive model for direct injection diesel engines.
Applied Energy, Vol. 88 n^o 12, pp. 4632–4641, Diciembre 2011. (cited on pp. 30, 53)

Pelikan M., Goldberg D. and Cantu-Paz E.
Bayesian Optimization Algorithm, Population Sizing, and Time to Convergence.
Proceedings of the 2Nd Annual Conference on Genetic and Evolutionary Computation, pp. 275–282, 2000. (cited on p. 63)

Piano A., Millo F., Di Nunno D. and Gallone A.
Numerical Assessment of the CO2 Reduction Potential of Variable Valve Actuation on a Light Duty Diesel Engine.
CO2 Reduction for Transportation Systems Conference, n^o Ivc, 2018. (cited on p. 29)

Pickett L.M. and Siebers D.L.
Soot in diesel fuel jets: effects of ambient temperature, ambient density, and injection pressure.
Combustion and Flame, Vol. 138 n^o 1-2, pp. 114–135, Julio 2004. (cited on pp. 19, 25)

Pope C. and Dockery D.
Health Effects of Fine Particulate Air Pollution: Lines that Connect.
Journal of the Air & Waste Management Association, Vol. 56 n^o 6, pp. 709–742, 2006. (cited on p. 2)

Postrzednik S. and Zmudka Z.
Achievement of the charge exchange work diminishing of an internal combustion engine in part load.
Transport Problems, Vol. 7 n^o 1, pp. 63–76, 2012. (cited on p. 80)

Rajashekara K.
Present status and future trends in electric vehicle propulsion technologies.
IEEE Journal of Emerging and Selected Topics in Power Electronics, Vol. 1 n^o 1, pp. 3–10, 2013. (cited on p. 3)

Rakopoulos C.D., Dimaratos A.M., Giakoumis E.G. and Rakopoulos D.C.
Evaluation of the effect of engine, load and turbocharger parameters on transient emissions of diesel engine.
Energy Conversion and Management, Vol. 50 n^o 9, pp. 2381–2393, Septiembre 2009. (cited on p. 21)

Rakopoulos C.D. and Giakoumis E.G.
Second-law analyses applied to internal combustion engines operation.
Progress in Energy and Combustion Science, Vol. 32 n^o 1, pp. 2–47, 2006. (cited on p. 76)

Ramesh A., Gosala D., Allen C., Joshi M., McCarthy J., Farrell L., Koeberlein E. and Shaver G.
Cylinder Deactivation for Increased Engine Efficiency and Aftertreatment Thermal Management in Diesel Engines.
SAE Technical Paper 2018-01-0384, Vol. 1 n^o 1, pp. 1–10, 2018. (cited on pp. 21, 29)

Ramesh A., Shaver G., Allen C., Nayyar S., Gosala D., Parra D. and Koeberlein E.
Utilizing low airflow strategies , including cylinder deactivation , to improve fuel efficiency and aftertreatment thermal management.
International Journal of Engine Research, Vol. 18 n^o 10, pp. 1005–1016, 2017. (cited on p. 21)

Robert Bosch GmbH. Gasoline Systems.
Gasoline Direct Injection. Key technology for greater efficiency and dynamics.
Robert Bosch GmbH, Stuttgart, Germany, 2015. (cited on p. 19)

Roberts A., Brooks R. and Shipway P.
Internal combustion engine cold-start efficiency: A review of the problem, causes and potential solutions.
Energy Conversion and Management, Vol. 82, pp. 327–350, Junio 2014. (cited on p. 28)

Sabathé, L.
Internal Combustion Engine.
United States Patent Office, 1908. (cited on p. 79)

Sahin Z., Tuti M. and Durgun O.
Experimental investigation of the effects of water adding to the intake air on the engine performance and exhaust emissions in a di automotive diesel engine.
Fuel, Vol. 115 n^o x, pp. 884–895, 2014. (cited on p. 26)

Schmidt C.
Beyond a One-Time Scandal. Europe's Ongoing Diesel Pollution Problem.
Environmental Health Perspectives, Vol. 124 n^o 1, pp. 19–22, 2016. (cited on p. 4)

Shibata G., Ishi K., Ushijima H., Shibaike Y., Ogawa H. and Foster D.
Optimization of Heat Release Shape and the Connecting Rod Crank Radius Ratio for Low Engine Noise and High Thermal Efficiency of Premixed Diesel Engine Combustion.
SAE Technical Paper, 2015. (cited on p. 33)

Singh S., Garg A., Gupta A. and Permude A.
Analysis of Thermal Balance of Diesel Engine and Identification of Scope for Waste Heat Recovery.
SAE Techinical Paper 2013-01-2744, 2013. (cited on p. 30)

Smith L.A., Preston W.H., Dowd G., Taylor O. and Wilkinson K.M.
Application of a First Law Heat Balance Method to a Turbocharged Automotive Diesel Engine.
SAE Technical Paper 2009-01-2744, 2009. (cited on pp. 30, 31)

Sobol I.M.
Computaional Methods of Monte Carlo.
Nauka, Moscow, 1973. (cited on pp. 63, 65)

Sorrell S., Speirs J., Bentley R., Miller R. and Thompson E.
Shaping the global oil peak: A review of the evidence on field sizes, reserve growth, decline rates and depletion rates.
Energy, Vol. 37 n^o 1, pp. 709–724, 2012. (cited on p. 3)

Stanglmaier R.H. and Roberts C.E.
(HCCI): Benefits , Compromises , and Future Engine Applications.
SAE Techinical Paper 1999-01-3682, 1999. (cited on p. 25)

Steinparzer F., Nefischer P., Hiemesch D. and Rechberger E.
The New BMW Six-cylinder Top Engine with Innovative Turbocharging Concept.
MTZ worldwide, Vol. 77 n^o 10, pp. 38–45, 2016. (cited on p. 106)

Su T., Chang C., Reitz R., Farrell P., Pierpont A. and Tow T.
Effects of Injection Pressure and Nozzle Geometry on Spray SMD and D.I. Emissions.
SAE Technical Paper 952360, 1995. (cited on p. 19)

Tauzia X. and Maiboom A.
Experimental study of an automotive Diesel engine efficiency when running under stoichiometric conditions.
Applied Energy, Vol. 105, pp. 116–124, Mayo 2013. (cited on p. 32)

Taymaz I.
An experimental study of energy balance in low heat rejection diesel engine.
Energy, Vol. 31 n^o 2-3, pp. 364–371, Febrero 2006. (cited on p. 26)

Teng H.
Waste Heat Recovery Concept to Reduce Fuel Consumption and Heat Rejection from a Diesel Engine.
SAE Int. J. Commer. Veh., Vol. 3 n^o 1, pp. 60–68, 2010. (cited on p. 30)

Teng H., Regner G. and Cowland C.
Waste Heat Recovery of Heavy-Duty Diesel Engines by Organic Rankine Cycle Part I: Hybrid System of Diesel and Rankine Engines.
SAE Technical Paper 2007-01-0537, 2007. (cited on p. 30)

Thirouard M., Knop V. and Pacaud P.
Downsizing or cylinder number reduction in Diesel engines : effect of unit displacement on efficiency and emissions.
In *THIESEL 2012 Conference on Thermo- and Fluid Dynamic Processes in Diesel Engines*, pp. 1–19, 2012. (cited on pp. 9, 32, 76, 82)

Thirouard M, Laget O and Zaccardi J.M.
An Innovative High Efficiency Diesel Combustion Concept with reduced Heat Loss.
In *THIESEL 2016 Conference on Thermo- and Fluid Dynamic Processes in Direct Injection Engines*, pp. 1–16, 2016. (cited on p. 32)

Timmann M., Inderka R. and Eder T.
Development of 48V powertrain systems at Mercedes-Benz.
In *Internationales Stuttgarter Symposium. Proceedings. Springer Vieweg, Wiesbaden*, 2018. (cited on p. 3)

Tinaut F.
Contribución al estudio del proceso de combustión en motores de encendido por compresión de inyección directa.
Doctoral Thesis, Universidad Politécnica de Valencia, 1986. (cited on pp. 9, 52)

Torregrosa A.J., Broatch A., Olmeda P. and Martín J.
A contribution to film coefficient estimation in piston cooling galleries.
Experimental Thermal and Fluid Science, Vol. 34 n^o 2, pp. 142–151, Febrero 2010. (cited on p. 55)

Torregrosa A.J., Broatch A., Olmeda P. and Romero C.
Assessment of the influence of different cooling system configurations on engine warm-up, emissions and fuel consumption.
International Journal of Automotive Technology, Vol. 9 n^o 4, pp. 447–458, 2008. (cited on pp. 27, 28, 29)

Torregrosa A.J., Olmeda P., Degraeuwe B. and Reyes M.
A concise wall temperature model for DI Diesel engines.
Applied Thermal Engineering, Vol. 26 n^o 11-12, pp. 1320–1327, Agosto 2006. (cited on p. 55)

Torregrosa A.J., Olmeda P., Martín J. and Degraeuwe B.
Experiments on the influence of inlet charge and coolant temperature on performance and emissions of a DI Diesel engine.
Experimental Thermal and Fluid Science, Vol. 30 n^o 7, pp. 633–641, 2006. (cited on pp. 28, 44)

Toulson E., Schock H. and Attard W.
A Review of Pre-Chamber Initiated Jet Ignition Combustion Systems.
SAE International Journal of Engines, 2010. (cited on p. 20)

United Nation Environment Programe (UNEP), Global Environmental Alert Service (GEAS).
Gas fracking: can we safely squeeze the rocks?
Environmental Development, Vol. 6, pp. 86–99, apr 2013. (cited on p. 3)

US Energy Information Administration.
U.S. transportation sector energy consumption in 2018, by energy source.
Statista - The Statistics Portal, Statista, 2018. (cited on pp. v, 2)

Uyehara O.A.
Factors that Affect BSFC and Emissions for Diesel Engines : Part 1 - Presentation of Concepts.
SAE Techinical Paper 870343, 1987. (cited on p. 25)

Wagner J., Srinivasan V., Dawson D. and Marotta E.
Smart Thermostat and Coolant Pump Control for Engine Thermal Management Systems.
SAE International, Vol. - n^o 724, 2003. (cited on p. 29)

Wakisaka Y., Inayoshi M., Fukui K., Kosaka H. and Hotta Y.
Reduction of Heat Loss and Improvement of Thermal Efficiency by Application of Temperature Swing Insulation to Direct-Injection Diesel Engines.
SAE Int. J. Engines, 2016. (cited on pp. 27, 71, 110, 122)

Wang C., Xu H., Herreros J.M., Wang J. and Cracknell R.
Impact of fuel and injection system on particle emissions from a GDI engine.
Applied Energy, Vol. 132, pp. 178–191, Noviembre 2014. (cited on p. 25)

Wang X., Huang Z., Zhang W., Kuti O.A. and Nishida K.
Effects of ultra-high injection pressure and micro-hole nozzle on flame structure and soot formation of impinging diesel spray.
Applied Energy, Vol. 88 n^o 5, pp. 1620–1628, Mayo 2011. (cited on p. 19)

Weberbauer F., Rauscher M., Kulzer A., Knopf M. and Bargende M.
Generally applicate split of losses for new combustion concepts.
MTZ worldwide, Vol. 66 n^o 2, pp. 17–19, 2005. (cited on pp. 9, 32, 76, 82)

Wei S., Wang F., Leng X., Liu X. and Ji K.
Numerical analysis on the effect of swirl ratios on swirl chamber combustion system of DI diesel engines.
Energy Conversion and Management, Vol. 75, pp. 184–190, Noviembre 2013. (cited on p. 23)

Weisberg S.
Applied Linear Regressions.
John Wiley & Sons, ISBN 0-471-66379-4, 3rd edition, 2005. (cited on p. 58)

Westman C.
Social Impact Assessment and the Anthropology of the Future in Canada's Tar Sands.
Human Organization, Vol. 72 n^o 2, pp. 111–120, 2013. (cited on p. 3)

Williams F.
Combustion Theory.
The Benjamin/Cummings Publishing Co, ISBN 978-0201407778, 1985. (cited on p. 53)

Wissink M., Splitter D., Dempsey A., Curran S., Kaul B. and Szybist J.
An assessment of thermodynamic merits for current and potential future engine operating strategies.
International Journal of Engine Research, Vol. 18 n^o 1-2, pp. 155–169, 2017. (cited on p. 76)

Wloka J.A., Pflaum S. and Wachtmeister G.
Potential and Challenges of a 3000 Bar Common-Rail Injection System Considering Engine Behavior and Emission Level.
SAE Int. J. Engines, Vol. 3 n^o 1, pp. 801–813, 2010. (cited on p. 19)

Woschni G.
A Universally Applicable Equation for the Instantaneous Heat Transfer Coefficient in the Internal Combustion Engine.
SAE Technical Paper 670931, 1967. (cited on pp. 55, 125)

Woschni G.
Die Berechnung der Wandverluste und der thermischen Belastung der Bauteile von Dieselmotoren.
MTZ, Vol. 31 n^o 12, pp. 491–499, 1970. (cited on p. 55)

Yamaguchi T., Aoyagi Y., Uchida N., Fukunaga A., Kobayashi M., Adachi T. and Hashimoto M.
Fundamental Study of Waste Heat Recovery in the High Boosted 6-cylinder Heavy Duty Diesel Engine.
SAE Int. J. Mater. Manf., Vol. 8 n^o 2, 2015. (cited on p. 30)

Yang Y., Dec J.E., Sjöberg M. and Ji C.
Understanding fuel anti-knock performances in modern SI engines using fundamental HCCI experiments.
Combustion and Flame, Vol. 162 n^o 10, pp. 4008–4015, oct 2015. (cited on p. 21)

Yoon K., Hong J. and Shim J.
A Study on Front End Auxiliary Drive (FEAD) System of 48V Mild Hybrid Engine.
WCX World Congress Experience, apr 2018. (cited on p. 3)

Zeldovich J.
The Oxidation of Nitrogen on Combustion and Explosions.
European Physical Journal A. Hadrons and Nuclei, Vol. 21, pp. 577–628, 1946.
(cited on pp. 60, 70)

Zhang Y., Sagalovich I., De Ojeda W., Ickes A., Wallner T. and Wickman D.
Development of Dual-Fuel Low Temperature Combustion Strategy in a Multi-Cylinder Heavy-Duty Compression Ignition Engine Using Conventional and Alternative Fuels.
SAE International Journal of Engines, Vol. 6 n^o 3, pp. 2013–01–2422, 2013.
(cited on p. 122)

Zhen X., Wang Y., Xu S., Zhu Y., Tao C., Xu T. and Song M.
The engine knock analysis - An overview.
Applied Energy, Vol. 92, pp. 628–636, apr 2012. (cited on p. 21)

Zhou B., Lan X., Xu X. and Liang X.
Numerical model and control strategies for the advanced thermal management system of diesel engine.
Applied Thermal Engineering, Vol. 82, pp. 368–379, Mayo 2015. (cited on p. 27)